



8-2005

Synthesis and Applications of Monolithic HPLC Columns

Chengdu Liang

University of Tennessee - Knoxville

Recommended Citation

Liang, Chengdu, "Synthesis and Applications of Monolithic HPLC Columns." PhD diss., University of Tennessee, 2005.
https://trace.tennessee.edu/utk_graddiss/2233

This Dissertation is brought to you for free and open access by the Graduate School at Trace: Tennessee Research and Creative Exchange. It has been accepted for inclusion in Doctoral Dissertations by an authorized administrator of Trace: Tennessee Research and Creative Exchange. For more information, please contact trace@utk.edu.

To the Graduate Council:

I am submitting herewith a dissertation written by Chengdu Liang entitled "Synthesis and Applications of Monolithic HPLC Columns." I have examined the final electronic copy of this dissertation for form and content and recommend that it be accepted in partial fulfillment of the requirements for the degree of Doctor of Philosophy, with a major in Chemistry.

Georges A Guiochon, Major Professor

We have read this dissertation and recommend its acceptance:

Sheng Dai, Craig E Barnes, Michael J Sepaniak, Bin Hu

Accepted for the Council:

Dixie L. Thompson

Vice Provost and Dean of the Graduate School

(Original signatures are on file with official student records.)

To the Graduate Council:

I am submitting herewith a dissertation written by Chengdu Liang entitled, "Synthesis and applications of monolithic HPLC columns." I have examined the final electronic copy of this dissertation for form and content and recommend that it be accepted in partial fulfillment of the requirements for the degree of Doctor of Philosophy, with a major in Chemistry.

Georges A Guiochon

Major Professor

We have read this dissertation
and recommend its acceptance:

Sheng Dai

Craig E Barnes

Michael J Sepaniak

Bin Hu

Accepted for the Council:

Anne Mayhew

Vice Chancellor and Dean of
Graduate Studies

(Original signatures are on file with official student records.)

Synthesis and applications of monolithic HPLC columns

A Dissertation

Presented for the

Doctor of Philosophy

Degree

The University of Tennessee, Knoxville

Chengdu Liang

August, 2005

Acknowledgements

Many people offered their generous help to the completion of this dissertation, far too many to name, but a few of you deserve singling out. First and foremost, many thanks to Dr Georges Guiochon for guiding me into the research field of chromatography. His advices inspired me to carry out this challenging project. I would like to express my gratitude to my dissertation advisor Dr Sheng Dai for his friendship and mentorship. I would like to thank him for his elaborative instructions in every detail of my research work. I also want to thank Dr Sheng Dai for the opportunity to work and learn in a supportive environment, where I was given the full freedom to develop my research skills. Thanks also to my committee members, Dr Craig Barnes, Dr Michael Sepaniak, and Dr Bin Hu, who spent their precious time on reading and commenting my dissertation.

Many thanks go to the members, past and present, of the Dai group and the Guiochon group. It's been wonderful working with these two groups of great people, who are majoring in two deferent subjects. Special thanks to Dr Shannon Mahurin and Mrs. Michelle Pawel for their language help in Chapter 5, and 7.

Last but not least, a special thanks to my family for their continuous encouragements and spiritual supports during my study in the U.S. Their love is beyond words.

Abstract

Silica and carbon monolithic columns were synthesized and modified for liquid chromatography applications. Column configurations and cladding techniques were investigated in detail. Three novel approaches have been developed for the synthesis of bimodal porous rods. Out of these three methods, gel-casting was adopted for the synthesis of silica monoliths with ordered mesopores and uniform macropores; the use of colloidal templates and dual phase separation has been successfully implemented for the synthesis of carbon monoliths with well-controlled meso- and macro- porosities. The formation of mesopores in carbon materials has been further studied in the microphase separation of block copolymers. Electrochemical modification of carbon monoliths was discovered to be an efficient method for converting covalently bonded functionalities to carbon monoliths. N,N'-diethylaminobenzene has been attached to carbon surface for the separation of proteins and protein digests. The performances of carbon-based monolithic columns were studied intensely through frontal analysis and Van Deemter plot. Temperature and pressure effects were also investigated in carbon-based columns. The density of bonding on the modified carbon monoliths was characterized by thermogravimetric analysis.

CHAPTER 1: INTRODUCTION	1
1.1 <i>The background of chromatography</i>	1
1.2 <i>Components of an HPLC system</i>	3
1.3 <i>The history of particulate columns</i>	5
1.4 <i>The nature of monolithic columns</i>	7
1.5 <i>Development of monolithic columns</i>	9
1.6 <i>The classification of monolithic HPLC columns</i>	11
1.7 <i>Goals of this work</i>	15
CHAPTER 2: CONFIGURATIONS OF MONOLITHIC COLUMNS	18
2.1 <i>New challenges associated with monolithic columns</i>	18
2.2 <i>Polymer-lined stainless steel-tubing encasing</i>	20
2.2.1 <i>Materials for column fabrication</i>	21
2.2.2 <i>General procedure for column encasing</i>	21
2.2.3 <i>Discussion of the preparation procedure</i>	22
2.3 <i>Glass-shrinking encapsulation</i>	24
2.3.1 <i>Setup and shrinking procedure for glass tubing</i>	25
2.3.2 <i>Key points for glass shrinking</i>	26
2.4 <i>Polymerization encapsulation (polymer coating)</i>	27
2.4.1 <i>Materials for polymer coating</i>	27
2.4.2 <i>General procedure for fabrication of polymer-coated monolithic columns</i>	28
2.4.3 <i>Discussion of the polymer-coated column configuration</i>	29
2.5 <i>Multicapillary-array configuration for microbore monolithic columns</i>	29
CHAPTER 3: PREPARATION OF MONOLITHIC SILICA COLUMNS VIA GEL-CASTING	32
3.1 <i>Silica monolithic columns with ordered mesopores and tunable macrochannels</i>	32
3.2 <i>The fabrication of silica monolithic columns</i>	35
3.2.1 <i>Materials and instruments</i>	35
3.2.2 <i>The synthesis of mesoporous silica particles</i>	36
3.2.3 <i>Gel-casting of silica particles into a monolithic rod</i>	36

3.2.4 Fabrication and surface modification of silica columns	37
3.2.5 HPLC application	38
3.3 <i>Results and discussion</i>	38
3.4 <i>Conclusion</i>	43
CHAPTER 4: CARBON MONOLITHIC COLUMNS MADE BY COLLOIDAL TEMPLATES	44
4.1 <i>The background of carbon columns</i>	44
4.1.1 Retention mechanism on carbon	45
4.1.2 Methods for the preparation of carbon stationary phases	49
4.1.2.1 The Guiochon method	49
4.1.2.2 The Unger method	50
4.1.2.3 The Knox method	50
4.1.3 The birth of carbon monolithic column for HPLC	51
4.2 <i>The synthesis and chromatographic evaluation of carbon monolithic columns</i>	53
4.3 <i>Results and discussion</i>	57
4.4 <i>Conclusion</i>	78
4.5 <i>Problems to be solved</i>	80
CHAPTER 5: PHASE SEPARATION FOR THE SYNTHESIS OF CARBON MONOLITHIC COLUMN WITH HIERARCHICAL STRUCTURE	81
5.1 <i>Background of phase separation</i>	81
5.2 <i>Theory of phase separation</i>	84
5.2.1 Thermodynamics of phase separation and Flory-Huggins theory ⁸⁵	84
5.2.2 Thermally induced phase separation ⁸⁹	87
5.2.3 Chemically induced phase separation ⁹³⁻¹⁰²	88
5.3 <i>The dual phase separation in the ternary mixing system</i>	91
5.4 <i>Experimental</i>	92
5.5 <i>Results and discussion</i>	96
5.5.1 The composition of the ternary system	96
5.5.2 Primary phase separation and the control of macropore properties	98

5.5.2.1 The selection of glycol solvents	104
5.5.2.2 Temperature effect	106
5.5.2.3 Catalyst effect and rate	106
5.5.3 Secondary phase separation and mesoporosity	107
5.5.4 The relationship between primary phase separation and secondary phase separation	108
5.5.5 Degassing and the elimination of defects	108
5.6 Conclusion	109
CHAPTER 6: SYNTHESIS OF MESOPOROUS CARBON VIA SELF-ASSEMBLY OF BLOCK COPOLYMERS	111
6.1 Introduction of the synthesis of mesoporous carbon	111
6.2 Experimental	115
6.3 Results and discussion	116
6.4 Conclusion	129
6.5 Future research work	129
CHAPTER 7: SURFACE MODIFIED MONOLITHIC CARBON COLUMNS	130
7.1 The background of the surface modification on carbon phases	130
7.2 Electrochemical modification of carbon surface	131
7.2.1 Electrochemical oxidation of amines	132
7.2.2 Electrochemical oxidation of alcohols	134
7.2.3 Kolbe reaction	134
7.2.4 Electrochemical reduction of diazonium salts	134
7.3 Electrochemical modification of carbon monolith	136
7.4 Experimental	137
7.5 Results and discussion	139
7.5.1 The structure of the monolithic columns	139
7.5.2 The electrochemical modification of monolithic columns	140
7.5.3 The HPLC performance of the electrochemically modified columns	142
7.6 Conclusion	147
CHAPTER 8: CHROMATOGRAPHIC CHARACTERIZATION OF CARBON BASED COLUMNS	149

8.1 Isotherm models.....	150
8.1.1 The langmuir model (L):	150
8.1.2 The antilangmuir model (AL):	151
8.1.3 The bilangmuir model (BL):	152
8.1.4 The quadratic model (Q):	152
8.2 Experimental.....	153
8.2.1 Column preparation.....	153
8.2.2 Column performance.....	153
8.2.3 Frontal analysis (FA) ¹⁶⁹	154
8.2.4 Surface area and porosity measurements.....	155
8.2.5 The measurement of the bonding density of the electrochemically modified carbon column.....	156
8.2.6 Pressure effect on graphitized carbon column.....	157
8.2.7 Reproducibility of columns.....	157
8.3 Results and discussion	157
8.3.1 Column physical parameters	157
8.3.2 Column performance.....	158
8.3.3 The properties of adsorbents obtained through isotherms	171
8.3.3.1 Isotherms on graphitized carbon column	171
8.3.3.2 The isotherms on modified carbon column.....	189
8.3.3.3 The comparison of isotherms between graphitized and modified columns.....	194
8.3.4 Ligand density by TGA-MS.....	197
8.3.5 The reproducibility of monolithic columns.....	199
8.3.6 The pressure effect on the graphitized carbon column.....	202
8.4 Conclusion	208
CHAPTER 9: CONCLUSION	210
REFERENCES	215
VITA.....	228

List of tables

Table 1. Current commercial monolithic stationary phases for HPLC separations.....	10
Table 2 The micro-structure of carbon samples as a function of composition	99
Table 3. Physical parameters of carbon based columns that synthesized by using the monolithic technique described in Chapters 5 and 7.	159
Table 4. Peak symmetry of columns tested by toluene, resorcinol, and 2-tetradecylresorcinol.....	165
Table 5. Fitted Van Deemter equation parameters	166
Table 6. Fitted parameters of isotherms at 30 °C on graphitized carbon column	175
Table 7. The concentrations of inflection points of isotherms on graphitized carbon column at 30 °C. The isotherms are measured with amylbenzene, octylbenzene, tetradecylbenzene.....	178
Table 8. Maximum of surface coverage (Γ_{\max}) of adsorbates on graphitized carbon surface.....	184
Table 9. Fitted parameters of temperature effect on isotherms.	188
Table 10. Fitted parameters of isotherms of toluene, resorcinol, and aniline on modified carbon.....	191
Table 11. Fitted parameters of resorcinol's isotherms on graphitized carbon and modified carbon.....	196
Table 12. k' and HETP measured on six modified carbon columns.	202
Table 13. k' and HETP measured on 2 batches of modified carbon columns.....	203
Table 14. Fitted parameters and calculated molar volume change.....	208

List of figures

Figure 1. The history of packed columns. ³	6
Figure 2. Comparison of particulate and monolithic columns. ⁶	8
Figure 3. CIM disc columns. The discs are a few mm thick.	14
Figure 4. CIM tube preparative columns.	16
Figure 5. Rod columns (left is polymer columns from Isco, right is silica columns from Merck).....	16
Figure 6. Column configuration of polymer-lined stainless steel tubing-encased columns. ²²	20
Figure 7. Setup for the heat shrinking of PTFE tubing onto the porous rod.....	22
Figure 8. Setup of glass shrinking.....	26
Figure 9. A polymer-coated monolithic column.....	28
Figure 10. Capillary array.....	31
Figure 11. TEM images of mesoporous silica particles.....	39
Figure 12. Sintered silica monolith.....	41
Figure 13. The fast separation of phenol and toluene.....	42
Figure 14. The C18 bonded silica phase and the porous graphite carbon phase (courtesy of Thermo Electron Co.).....	45
Figure 15. Scheme of the contact area of planar and non-planar compounds on graphite surface (courtesy of Thermo Electron Co.).....	46
Figure 16. Representation of the interaction of the charged species approaching the carbon surface. ⁶⁴	47

Figure 17. The images of charge and polar molecule reflected by the graphene. ⁶⁰	47
Figure 18. Comparison of methyl and methylene group selectivity on carbon and C18-silica.	48
Figure 19. Structure of the carbon precursor.	52
Figure 20. Schematic representation of the fabrication of column monolithic columns..	59
Figure 21. TEM image of the carbon matrix made with STEM in the ultrahigh resolution mode.....	61
Figure 22 (A). SEM image of the macropore morphology. (B). STEM high resolution SEM image of the mesopores in the carbon skeleton.	62
Figure 23. The nitrogen adsorption/desorption isotherm of the carbon monolith.	63
Figure 24. Raman spectra of the carbon monolith, glassy carbon, and commercial graphite.	65
Figure 25. Powder X-ray diffraction patterns of the carbon monolith and of commercial graphite.	67
Figure 26. Elution of toluene in dichloromethane with and without 1% of n-hexane.....	70
Figure 27. Chromatogram of five alkylbenzenes in a mobile phase made of methanol (30%), Dichloromethane (69%), and n-hexane (1%).	71
Figure 28. Van Deemter plot of the column HETP versus the linear velocity of the mobile phase.	73
Figure 29. Plot of the pressure drop versus the mobile phase velocity (pure hexane as the mobile phase).....	75
Figure 30. General strategy for chemically induced phase separation.	83

Figure 31. Schematic representation of free energy curves.....	84
Figure 32. Phase diagrams of (A) UCST system and (B) LCST system.....	87
Figure 33. Reconstructed phase diagram of chemically induced phase separation as a function of conversion and composition. ⁷⁷	91
Figure 34. Morphologies corresponding to different phase diagram zones. ⁷⁷	92
Figure 35. Schematic representation of the dual separation in a ternary system.....	93
Figure 36. Macropore morphologies and pore sizes. 1) PS32, 2) PSPS11, 3) PS16, 4) PS14, 5)PS15, 6) PS9,7)PS20, 8)PS17.	105
Figure 37. The secondary phase separation and the mesopores (sample PS14).....	107
Figure 38. N ₂ adsorption /desorption isotherm of sample PS14.....	108
Figure 39. Schematic representation of the synthesis protocol used to prepare well defined carbon nanostructure.....	117
Figure 40. FTIR spectrum of PS-P4VP and PS-P4VP/resorcinol complex in the region from 900 to 1650 cm ⁻¹	119
Figure 41. TGA and dTG curves for A) PS-b-P4VP, B) PS-b-P4VP and resorcinol mixture (molar ratio of pyridine groups to resorcinol 1:1), C) resorcinol formaldehyde resin (RFR), and D) PS-b-P4VP and RFR. The top and right axes are the temperature and wt% for the thermogram (TG). The left and bottom axes shows the weight loss rate and time for the derived thermogram (dTG).	121
Figure 42. Electron microscopy images of the carbon film.....	124
Figure 43. The calculation of volume fraction of the mesopores..	125

Figure 44. High resolution transmission electron microscopy image of the carbon wall.	126
Figure 45. Wide angle X-ray diffraction pattern.	127
Figure 46. The Raman spectrum of the carbon film.	128
Figure 47. Electrochemical coupling primary amine on carbon surface.	132
Figure 48. Possible forms of electrochemically attached ethylene diamine on carbon surface: a) single strand; b) ring; c) polymer.	133
Figure 49. Coupling mechanism of the aryl diazonium on the carbon surface	135
Figure 50. A reconstructed 3-D image of the carbon monolith. The image was composed by a series of SEM images, which were taken from sequential depths of carbon sample in the range of 0 to 1000nm.	139
Figure 51. Electrochemical modification of carbon surface.	140
Figure 52. The front, side, and top views of the ligand..	142
Figure 53. Chromatogram of the mixture of 1 aprotinin bovine lung, and 2 ovalbumin..	144
Figure 54. The separation of the cytochrome c digests..	146
Figure 55. Toluene eluted by chloroform and acetonitrile 20/80 at flow rate 1ml/min. k' is 1.2 on glassy carbon, 0.75 on graphitized carbon, and 0.51 on modified carbon.....	160
Figure 56. Resorcinol eluted by methanol and water 85/15 at flow rate 1ml/min. k' is 2.2 on glassy carbon, 1.57 on graphitized carbon, and 3.02 on modified carbon.....	161

Figure 57. 2-tetradecylresorcinol eluted by methanol and water 85/15 at flow rate 1ml/min. k' is 12.5 on glassy carbon, 5.2 on graphitized carbon, and 6.7 on modified carbon.....	162
Figure 58. Van deemter plot of toluene on graphite and modified carbon columns eluted by 20: 80 chloroform and acetonitrile. k' is 0.75 on graphitized carbon, and 0.51 on modified carbon.	167
Figure 59. Van Deemter plot of resorcinol eluted by 15:85 water and methanol. $k'=1.57$ on graphitized carbon, and 3.02 on modified carbon.....	168
Figure 60. Van Deemter plot of 2-tetradecylresorcinol eluted by 15:85 water and methanol. k' is 5.2 on graphitized carbon, and 6.7 on modified carbon.....	169
Figure 61. A typical breakthrough curve. Toluene is eluted on graphitized carbon column at 30 °C by 20:80 chloroform and acetonitrile. k' is 0.75. The time interval of each concentration is 10 minutes.	172
Figure 62. Isotherms of toluene on graphitized carbon eluted by chloroform/acetonitrile 20:80.	173
Figure 63. Isotherms of alkylbenzenes on graphitized carbon column at 30 °C eluted by chloroform/acetonitrile 20:80.	174
Figure 64. Isotherm of amylbenzene on graphitized carbon column at 30 °C eluted by 20: 80 chloroform/acetonitrile.	176
Figure 65. Isotherm of naphthalene on graphitized carbon column at 30 °C eluted by chloroform.....	180

Figure 66. Adsorption density (number of molecules/ nm ²) of alkyl benzenes on graphite column as a function of concentration.	181
Figure 67. Surface coverage of alkylbenzenes on graphite surface as a function of concentration.	183
Figure 68. Isotherm of resorcinol on graphitized carbon column at 30 to 60 °C eluted by 15:85 water/methanol.	185
Figure 69. Isotherm of 2-tetradecylresorcinol and resorcinol on graphitized carbon eluted by 85:15 methanol/water at 30 °C.	187
Figure 70. Isotherms of toluene, resorcinol, aniline on modified carbon column by 85:15 methanol/water at 30 °C. The surface modification is N,N'-diethylbenzene.	190
Figure 71. Curve fitting of the resorcinol isotherm on modified carbon at 30 °C.	192
Figure 72. Curve fitting of the isotherm of aniline on modified carbon.	193
Figure 73. Comparison of isotherms of resorcinol on graphite and modified carbon eluted by methanol/water (85/15) at 30 °C.	195
Figure 74. TGA-MS plot of the modified carbon which is pyrolyzed from room temperature to 600 °C at N ₂ gas flow. The temperature ramp is 10 °C/min.	198
Figure 75. Plot of k' versus column.	200
Figure 76. Plot of HETP versus column.	201
Figure 77. Average k' versus batch.	203
Figure 78. Average HETP versus batch.	204
Figure 79. Plot of k' versus pressure of o-xylene and cyclohexanol eluted by acetonitrile at 303 K on graphitized carbon column.	206

Figure 80. Plot of $\ln k'$ versus pressure of o-xylene and cyclohexanol eluted by acetonitrile at 303 K on graphitized carbon column..... 207

Chapter 1: Introduction

1.1 The background of chromatography

A ultimate goal of modern analytical chemistry is to obtain precise chemical information concerning mixtures. However, no chemical analysis method is truly specific. Consequently, a vital step for most analytical procedures is the separation of analytes. Traditional chemical separations such as distillation, precipitation, crystallization, and extraction have very limited applications to more complicated mixtures such as biochemical mixtures. As a result of the development and maturation of chromatography since the middle of the twentieth century, most complex mixtures can now be easily analyzed via this technique. Chromatography has become a routine method of analytical separation for both academic research and industry.

At the beginning of the twentieth century, the Russian botanist Mikhail Tswett invented and named chromatography. He separated plant pigments by passing solution mixtures through a glass column packed with fine particles of calcium carbonate. The separation of those pigments appeared as colored bands on the column. Tswett named his separation method for the two Greek words “chroma” and “graphein,” which mean “color” and “to write,” respectively.¹ In the past six decades, chromatography has been extensively applied to all branches of science. The 1952 Nobel Prize in chemistry was awarded to A. J. P. Martin and R. L. M. Synge for their contributions to chromatographic separations, which tremendously impacted chemistry-related sciences. More impressively,

between 1937 and 1972, a total of 12 Nobel Prizes were based on work in which chromatography was a key tool.

In all chromatographic separations, the sample is carried by the mobile phase, which may be a gas, a liquid, or a supercritical fluid. The mobile phase is then percolated through an immiscible stationary phase that is fixed on a solid substrate. When the sample passes through the stationary phase, species are retained to varying degrees as a result of the physicochemical interaction between the sample species and the stationary phase. The separation of species appears in the form of bands or zones resulting from various retentions. Chemical information can thus be analyzed qualitatively and/or quantitatively on the basis of these separated zones.

Based on the physical means by which the stationary phase and mobile phase are brought into contact, chromatography can be classified as planar or column.² In planar chromatography the stationary phase is supported on a flat plate or a piece of paper, while the mobile phase is usually driven by capillary force, gravity, or an electric field. In a few cases, the mobile phase is forced under pressure, for example, in overpressure planar chromatography. When a tube holds the stationary phase, the chromatographic method is referred to as column chromatography. In column chromatography, the mobile phase is driven by pressure, gravity, or an electric field.

Because of its astonishing separation power, column chromatography has become the most frequently practiced means of analytical separation. Three types of mobile phases are used in column chromatography: liquids, gases, and supercritical fluids.

Among these three types, liquids are the most frequently used. Therefore, liquid chromatography is the predominant technique used in modern analytical separations.

Early liquid chromatography was operated in glass columns, and the mobile phase was driven by gravity. To ensure a reasonable flow rate, the column was packed with large particles in the 150 to 200 μm range. Such packing yielded poor results with long separation times, often several hours. Beginning in the late 1960s, small particles were packed in a steel tube, which was subjected to high pressure. Such a system dramatically improved the separation power of column chromatography; in the early years, “HPLC” stood for “high pressure liquid chromatography”. With the use of pressure, particles as small as 3 to 10 μm are commonly used as stationary phases. Separation can thus be done in a high-performance mode, which means high resolution and short analysis time. Therefore, these newer procedures are termed “high-performance liquid chromatography” to distinguish them from the earliest methods. By and large, liquid chromatography is currently performed as high-performance liquid chromatography.

1.2 Components of an HPLC system

An HPLC system consists of five key components: a pumping system, an injection system, a column system, detectors, and data acquisition and system-controlling software.

The function of the pumping system is to drive the mobile phase through the column by overcoming the hydraulic resistance of the fine-particle-packed stationary phase. The basic requirements for the HPLC pumping system are (1) the generation of

pressures up to 1200 bar, (2) steady output, (3) adjustable flow rates in the range of 0.1 to 10 mL/min, (4) high reproducibility in flow rates, and (5) corrosion resistance.

The injection system is the inlet for samples. The way in which the sample is introduced into the column greatly affects the precision and reproducibility of the entire HPLC system. The most widely used injection system is based on sampling loops. The sampling size is predetermined by the loop fixed in the injection valve. Most chromatographic systems are equipped with a set of interchangeable loops by which a sample size in the range of 5 to 500 μl can be injected.

The detector provides the chemical information regarding separated bands. The signal from the detector provides the fundamental information for the quantitative and/or qualitative analysis of the sample. Traditional analytical techniques such as UV/Vis, IR, and MS have been widely utilized as detecting systems.










The column is the heart of HPLC. Innovations in HPLC are most often boosted by the development of new column technologies. All the diversities of the HPLC system are based on either the chemistry or the morphology of the packing materials. A detailed introduction of column technology is given in the next section.

The software offers automatic operation of the HPLC system, including the control of the pumping system, the data acquired by the detector, and basic analysis of the data. The computerization of the HPLC systems provides robotic operations and reliable data analysis. Its ease of operation accounts for the broad adoption of HPLC as a daily tool in various branches of science.

1.3 The history of particulate columns

The history of HPLC is actually the history of column innovation. From the slow early process to the sophisticated mature fast high-resolution separation, the ever-growing needs of various branches of science are the driving force in the development of columns. These needs are the following: (1) gains in productivity, (2) improvement in quality, (3) lowered cost of analysis, and (4) biological analysis. First, in the early years of HPLC, separations were believed to be a very slow and insensitive process. A routine HPLC separation could take several hours. In order to achieve high productivity, short, fast columns have been developed. Second, reproducible columns have been developed to improve reproducibility of separations. Efforts have been made to improve the recovery of the sample for the analysis of biological compounds. Third, durable columns have been embraced by the industry for the purpose of cost reduction. Narrow-bore and capillary columns have been developed to reduce the use of solvents. Fourth, the huge demand for separations has been boosted by the rapid development of biological analysis, which requires the analysis of complex samples, large molecules, and unstable compounds. Wide-pore, rugged, and biocompatible packing materials have been developed to meet the requirements of bioseparation.

The trend in particle-packed columns is toward the use of more uniform sized and finer particles to pack shorter columns. Shown in Figure 1 is the history of particle-packed columns.³ In the 1950s and earlier, the column was packed with irregular-shaped nonporous particles. In 1967, spherical glass beads were first used as regular-shaped packing material. The late 1960s and early 1970s saw the emergence of HPLC, which

Year(s) of acceptance	Particle size	Most popular nominal size (µm)	Plates/15 cm (approx.)
1950s	 Irregular-Shaped	100	200
1967	 Glass Bead	50 (pellicular)	1000
1972		10	6000
1985		5	12,000
1992		3-3.5	22,000
1998*		1.5*(pellicular)	30,000
1999		5.0 (Poroshell)	8000**
2000		2.5	25,000
2003		1.8	32,500

*Nonporous silica or resins.
**For protein MW 5700.

Figure 1. The history of packed columns.³

uses high-pressure pumps to drive the liquid phases through the column. These pumps made it possible to use fine particle-packed columns. Subsequently, the major development of packed columns has focused on decreasing the particle sizes. Small particles and short columns have dramatically improved the efficiency of HPLC separation. High throughput, high resolution, and fast columns have been developed to maximize the performance of the packed columns.

Though particle-packed columns dominate the major applications, the hydraulic resistance resulting from particulate morphology is deemed to be the limit for the use of particles smaller than 1 microns. The monolithic column, which overcomes the limits of traditional columns imposed by the backpressure, is considered to be the new generation of HPLC columns.⁴

1.4 The nature of monolithic columns

The monolithic column is also referred in the literature as a rod column, a continuous-bed column, continuous packing, or double porous packing materials.⁵ A monolithic column consists of a single piece of porous material without interparticle voids. The mobile phase passes through the macroporous channels within the continuous porous bed. The mass transfer is thus greatly accelerated via the hierarchically porous structure, which is a combination of macropores and mesopores. Figure 2 schematically compares the morphologies of particulate and monolithic columns.⁶

The HPLC column has two kinds of porosity: external and internal. The external porosity of particulate columns is controlled solely by particle size, which is

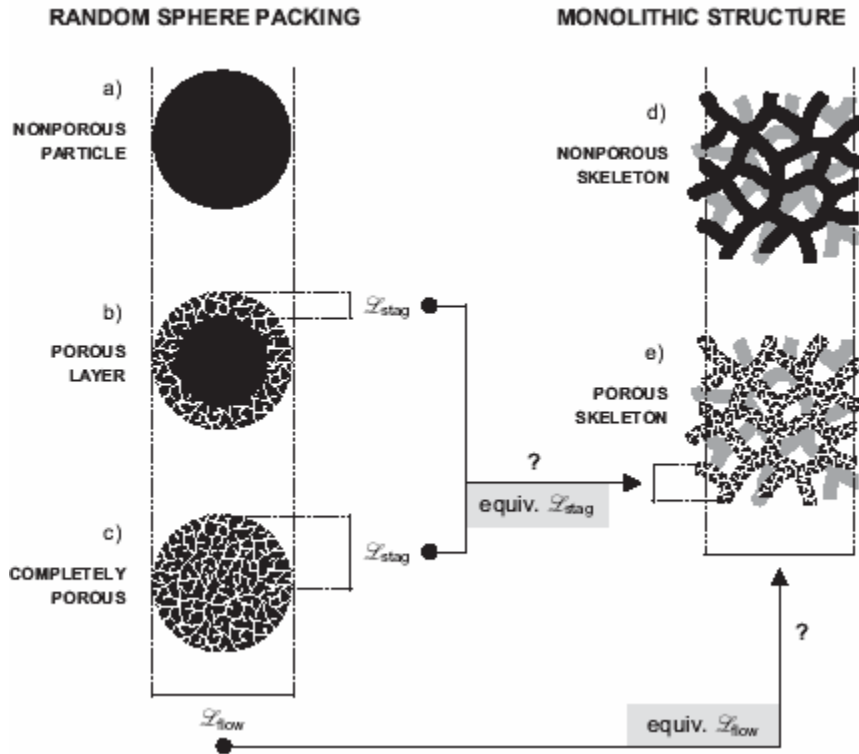


Figure 2. Comparison of particulate and monolithic columns.⁶

an important factor for column efficiency. Column efficiency is related to particle size: the smaller the particle, the higher the column efficiency and backpressure. Thus, improvement in column efficiency is achieved at the price of high pressure. The monolithic column succeeds in controlling external porosity. The efficiency of the monolithic column is determined by domain size, which is the sum of the skeleton and the channel. External porosity can be tuned without affecting the column efficiency by changing the channel size. Therefore, the external porosity can be optimized to produce better hydrodynamics. To maintain the same column efficiency, the monolithic column can be optimized to a much lower backpressure than the particulate column. With the hydrodynamic advantage, the monolithic column can be used for fast, high-resolution,

and high-throughput separations. As mentioned in the above section, the monolithic structure meets the criteria of column improvement.

1.5 Development of monolithic columns

The attempt to produce monolithic stationary phases was initiated in the late 1960s and early 1970s.^{5,7} Extremely swollen polymers and open-pore polyurethane foams have been synthesized for separation purposes. Ross and Jefferson reported the first research on the monolithic column for gas chromatography.⁸ This idea was extended to liquid chromatography by Hansen and Sievers in 1974.⁷ These research efforts were not successful for various reasons. Fifteen years later, Hjerten and his coworkers reinvented the concept.⁹ Polyacrylamide gel was compressed into a rod-shape column for HPLC separation of proteins. Since then research has flourished. Kumakura et al.¹⁰ and Svec's group¹¹ made polymer rods by *in situ* polymerization. The research into silica-based monolithic columns began in 1979, when Pretorius and his coworkers reported on methods for the preparation of silica foam by emulsion and blowing.¹² The successful preparation of silica rods was accomplished by Nakanishi and Soga in 1991.¹³ Porous rods have been prepared in a mold via a sol-gel process. The silica surface has been modified as a reverse-phase chromatographic column. Twenty years of research in the area of monolithic columns has led to the development of various commercial products, some of which are listed in Table 1.

Table 1. Current commercial monolithic stationary phases for HPLC separations.

Product	Shape	Producer	Chemistry	Separation mode
CIM disk	Disc	BIA Separations	Modified polymethacrylate or polystyrene copolymers	Ion exchange, hydrophobic interaction, reverse phase, bioaffinity
CB silica plate	Disc	Conchrom	Modified silica	Reverse phase, normal phase
SepraSorb	Disc	Sepragen	Modified cellulose	Ion exchange
CIM tube	Tube	BIA Separations	Modified polymethacrylate	Ion exchange
UNO	Cylinder	BioRad	Polyacrylamide- based copolymers	Ion exchange
Swift	Cylinder	ISCO	Modified polymethacrylate or polystyrene copolymers	Ion exchange, reverse phase
Chromolith	Cylinder	Merck	Modified silica	Reverse phase
Monoliths	Cylinder	LC Packings	Polystyrene copolymer	Reverse phase

1.6 The classification of monolithic HPLC columns

Based on function, monolithic HPLC columns can be classified as separating, guard, capillary and microbore, fast, and preparative columns. The separating column is the main type used to carry out various separation tasks. Column properties are determined by the chemistry of the column material and the surface functionalities. The separating column is the essence of HPLC columns, and most research on monolithic columns is focused on separating columns. The guard column serves as a protective column to prolong the lifetime and usefulness of the separation column. The basic functions of the guard column are (1) to block the entrance of particles that may clog the separation column, (2) to remove interferences that cause baseline drift, and (3) to prevent the precipitation of compounds in the separation column. The guard column is usually sacrificed to prolong the lifetime of the separating column. Capillary and microbore columns are designed for the separation of small-volume analysis. Capillary columns have a diameter ranging in size from several microns to several hundreds of microns. Microbore and small-bore columns have diameters of 1 to 2 mm. The use of capillary and microbore columns decreases the use of solvents, which is cost-efficient. However, these columns require the miniaturization of other parts of the HPLC system, such as the injection, connecting tubing, and the detection. Because the decreased column size reduces column load capacity, the injection of the sample is decreased to match column capacity. The connecting tubing should be reduced to minimize extracolumn volume. The miniaturization of the detection is most challenging. The traditional UV/Vis cell has to decrease in size to nanoliter range; however, the small detection cell

compromises the sensitivity of UV/Vis. The emergence of the MS detector can solve the problem but adds the cost of instrumentation. Fast columns are columns of very short length. The monolithic structure makes it possible for a high flow rate to be applied to the system without a significant loss of column efficiency. The primary reason to use the fast column is to improve the output of the instrument (evaluated by the amount of analysis per unit instrument time). Preparatory columns are used for the massive separation or purification of some compounds that are difficult or impossible to purify by traditional methods such as distillation, crystallization, and extraction. Large column diameters are required to achieve a reasonable column capacity for production-scale separation.

Based on the separation mechanism, monolithic columns have been produced as reverse phase, normal phase, affinity, chiral, and ion-exchange chromatography columns. Because of the relatively short history of monolithic columns compared to that of particle-packed columns, the monolithic column has not yet been developed for all branches of HPLC. The plain silica monolithic rod had been reported preliminarily as a normal phase column.¹⁴ The polymer-based and C18-grafted columns are usually used as reverse-phase chromatography columns.¹⁴⁻¹⁷ The surface modification of the monolithic materials can convert various functionalities to the column surface. Affinity,¹⁸ chiral,¹⁹⁻²¹ and ion-exchange²⁰ columns have been reported.

Based on the nature of column materials, silica, polymer, and carbon monolithic columns have been developed. The first polymer-based monolithic HPLC columns were reported by Hansen and Seivers in the 1970s.⁷ After 20 years of work by many groups, the first commercial product emerged in 1990.¹¹ Although the monolithic structure offers

advantages, polymer monolithic columns are restricted by the lack of mesopores. Thus the surface area is much lower than that of porous-particle-packed columns. Moreover, the micropores inherent in the polymer monolith dramatically limit the application of polymer monoliths. The real success of the monolithic column has been realized by Nakanishi and his associates. Bimodal porous silica rods have been made via a sol-gel process. Silica rods have been encapsulated by using heat-shrinkable polymer. Merck commercialized the PEEK-tubing-encased silica columns under the trademark Chromolith. The carbon monolithic column was not reported by this group until last year.²² The synthesis and applications of carbon monolithic columns are a part of this thesis. Carbon monolithic columns are designed to solve the separation problems that are difficult to resolve via silica and polymer columns. For example, a carbon column can separate polar compounds and structural isomers that cannot be resolved by polymer or C18 columns. The rigid carbon monolith is inert to any solvent, acid, or base, which enables the column to operate under any condition that the instrument can withstand. The conductivity of the carbon monolith opens the door to potential applications in electrochemically modulated liquid chromatography (EMLC).²²

Based on the modulation of separation, monolithic columns can be operated under the traditional HPLC concept, which controls separations by changing the mobile phase, or under the EMLC condition,²³⁻²⁶ which uses an external electric field to modulate the adsorption/desorption properties of the stationary phase. The early EMLC concept has been demonstrated on carbon-particle-packed columns. However, the low electric conductivity of the particle-packed column results in an unreasonably slow response time

of the EMLC column to changes in the electric field. Consequently, electrical homogeneity over the separation bed cannot be reached during an acceptable time period. The electrical heterogeneity is a significant weakness of the EMLC. The complexity of the particle-packed column is another factor accounting for the limited EMLC research. Highly conductive carbonaceous monoliths not only simplify the EMLC column configuration, but also offer swift electric response to the alternating external electric field. The research into carbon monolithic columns is therefore of strategic importance in EMLC.

Based on the configuration of the column, monolithic columns have been made into discs, tubes, and cylinders.⁴ The convertive interaction media (CIM) disc columns are presented in Figure 3. The color of the disc ring represent the chemistry of the column. The thin disc column has a lower pressure drop than the rod columns. Ultrafast separation has been performed with these discs; however, their are relatively lower than that of traditional columns. Preparative monolithic columns have been made up to a capacity of



Figure 3. CIM disc columns. The discs are a few mm thick.

8 L in tubular column configurations. Figure 4 shows the CIM tube made by BIA separations. The separation is carried by the radial flow from the outside of the tube toward the center.

The most common configuration of monolithic columns is rod shaped. The Merck Chromolith and ISCO Swift columns have been made into a cylindrical shape via molded fabrication or *in situ* polymerization. Rod columns are encased by glass, stainless steel (Figure 5, left), and PEEK tubing (Figure 5, right).

1.7 Goals of this work

Guiochon recently claimed, “The invention and development of monolithic columns is a major technological change in column technology, indeed the first original breakthrough to have occurred in this area ever since Tswett invented chromatography, a century ago.”²⁷ This new generation of HPLC column, the monolithic column, has a briefer history than that of traditional columns; as a consequence, there are far fewer varieties of monolithic columns than particulate columns. The fluid profile and hydrodynamics of monolithic columns are fairly well understood. However, the studies of column materials, column configuration, and surface modification are inadequate to support new developments in monolithic columns. The study of monolithic columns has the potential to lead to a breakthrough for the ever-growing needs of high-throughput separation. However, current research is



Figure 4. CIM tube preparative columns.



Figure 5. Rod columns (left is polymer columns from Isco, right is silica columns from Merck).

still insufficient to meet these needs. In light of this knowledge, we have planned and conducted this research into the synthesis and applications of monolithic columns to promote understanding of the fundamentals of monolithic columns. We have learned from the body of research that the use of an appropriate column configuration is the only way to ensure the implementation of this research in a laboratory with limited mechanical processing capabilities. Therefore, in Chapter 2, configurations of monolithic columns are introduced in detail. Such configurations have great importance for the completion of this study, even though these designs incorporate more principles of engineering than chemistry. Subsequent chapters detail the synthetic methods and applications of monolithic columns made by gel-casting of silica (Chapter 3), colloidal template synthesis of hierarchically porous carbon monoliths (Chapter 4), and phase separation in the synthesis of carbon columns (Chapter 5). For a more complete presentation of the merits of monolithic columns, the following aspects of research have also been explored: the fine adjustment of mesopores (Chapter 6), and a novel approach for column modification (Chapter 7). The characterization of the carbon-based columns is discussed in Chapter 8. Chapter 9 describes the conclusions of this study.

Chapter 2: Configurations of monolithic columns

2.1 New challenges associated with monolithic columns

Because the monolithic column uses a continuous rod as the separation media, the column does not require any frits. However, the new technique requires a special encasing method to convert the monolithic media into a column.²⁸ The shrinking of the monolithic media during condensing of the column precursors is an unavoidable phenomenon for most polymerization reactions. The shrinkage causes a gap between the column wall and the porous rod, dramatically reducing column performance because the mobile phase leaks from the gap instead of flowing through the porous media.⁵ In the early development stage of the monolithic column, the shrinking of the porous rod created problems for the column chemist and delayed the emergence of the practicable monolithic column for many years. In order to overcome the problem, extra efforts must be taken in suppressing the shrinkage or by using a shrinkable material to encapsulate the media.^{15, 17} These efforts have resulted in new column configurations. Although the configuration of monolithic columns is beyond the research scope of a column chemist, the fabrication of a successful column inevitably involves such issues. One cannot conduct HPLC evaluation of monolithic material without appropriate encasing methods. Thus, in this thesis, the configuration of the monolithic column is singled out as the first problem to be solved.

Based on cladding material, the column configuration can be classified into three types. The first type is the column encapsulated in the heat-shrinkable material.

Presynthesized porous rods are encased by shrinking chemically inert materials onto the rod surface. Such materials should not be swollen by common HPLC solvents. PTFE is the first heat-shrinkable tubing reported to be an encasing material.²⁹ However, because PTFE is a soft material, it is not able to withstand the high pressure utilized in the HPLC system.³⁰ A Z-model (Waters Corporation, Milford MA) was used as the external pressurizing device to offset the hydraulic pressure difference between the inner and outer sides of the tubing. Using the Z-model adds to the complexity of the HPLC system. There is an extra cost for the purchase and operation of the pressurizing device; moreover, Waters Corporation cut off the supply of the Z-model devices several years ago. Therefore, using the pressurizing device is not a feasible option for most column chemists. Merck introduced the breakthrough of the heat-shrinkable-material-clad column made by via the use of the shrink-on PEEK tubing, which led to the commercial success of its Chromolith column. The PEEK tubing can be shrunk only in a very narrow temperature window, usually ± 1 °C. The shrink temperature depends greatly on the production process for the PEEK tubing, which varies from batch to batch. It is not easy to apply the PEEK tubing to the monolithic rod in a chemistry lab. Besides the numerous technical difficulties, a commercial source of heat-shrinkable PEEK tubing is not available to most column chemists. A few polymer companies take customized orders, but prices are rarely affordable. Moreover, most research labs have very limited mechanical processing capabilities. Although the need for practicable design of column configuration for a research lab is not recognized by the industry, it is nevertheless very important in carrying out preliminary research. In order to evaluate HPLC performance of novel

monolithic materials, four prototype column configurations have been designed and implemented in our research.

2.2 Polymer-lined stainless steel-tubing encasing

This encasing method uses hard polymer glue, such as epoxy, to fill the gap between the porous rod and the stainless steel tubing. In order to prevent the glue from penetrating into the porous rod, a piece of heat-shrinkable tube was applied to the rod before it was glued into the stainless steel tubing. Stainless steel tubing enforces the strength of the column. Figure 6A provides a schematic configuration of the monolithic column. The center is the porous rod. The layers surrounding it are composed of heat-shrinkable tubing, polymer glue, and stainless steel tubing. Figure 6 B shows silica rods and finalized columns.

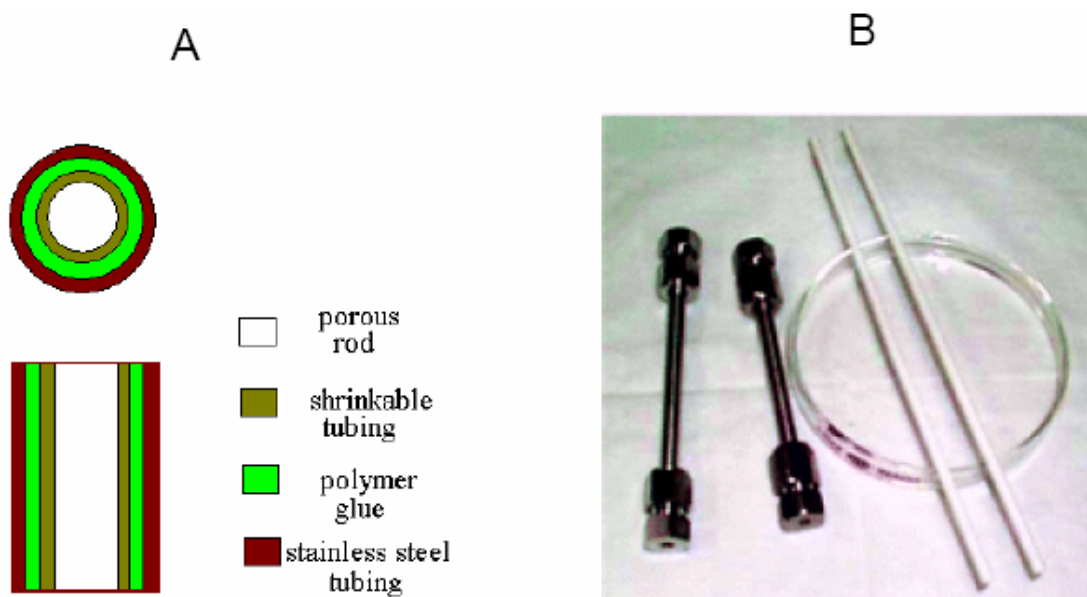


Figure 6. Column configuration of polymer-lined stainless steel tubing-encased columns.²²

2.2.1 Materials for column fabrication

The materials used for the fabrication of the polymer-lined stainless steel-encased monolithic column are ¼ in. 403 stainless steel tubing (purchased from Alltech Inc.), ¼ and 1/16 in. reduce unions (obtained from Supeco Inc.), PTFE and PTFE/FEP heat-shrinkable ¼ and 1/8 in. tubing of ID with shrink ratio of 2 to 1 (from Zeus Co.), and two-component epoxy glue (Miller-Stephenson Chemical Co.).

2.2.2 General procedure for column encasing

A piece of porous rod slightly longer than the targeted column length was thoroughly dried in a vacuum oven at 150 °C. If, for example, the designed column length is 10 cm, the starting rod should be at least 11 cm long. The rod OD varies from 1 to 3 mm depending on the preparative procedure used. A piece of heat-shrinkable tubing was shrunk onto the porous rod using heat guns, according to the setup in Figure 7, or by using a furnace preheated to 360 °C. The polymer tubing shrank during the cooling of the tube and encapsulated the rod after the temperature dropped back to room temperature. The two components of the epoxy glue were mixed and degassed under vacuum conditions. The encapsulated rod was then slid into a precut stainless steel tube. The stainless steel tubing was wrapped by a piece of aluminum foil, leaving one end open. The void in the stainless steel tube was then filled with the glue mixture and permitted to settle for 2 days to allow the hardening of the glue. All materials outside the stainless steel tube were scratched off after the glue cured. A razor saw was used to cut off the encapsulated rod ends that protruded from the stainless steel tube. The cut ends were polished with sandpaper, first with 200 mesh, then 600 mesh, and finished with 1200

TOP VIEW - ROLLER IN LATHE

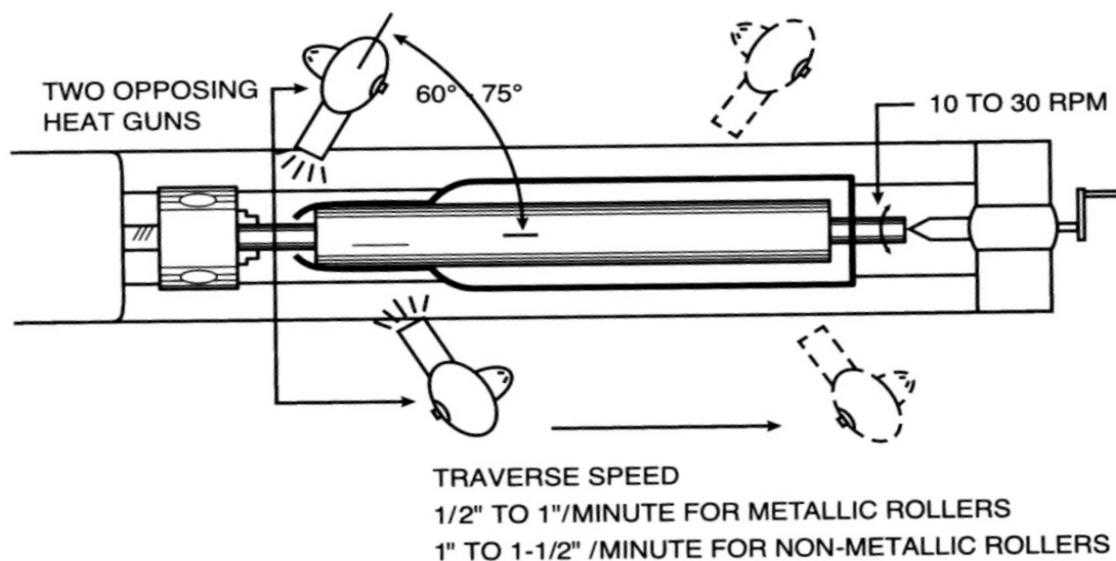


Figure 7. Setup for the heat shrinking of PTFE tubing onto the porous rod.

mesh. Two reducing unions were screwed onto the stainless steel tubing ends and then connected to a pump. Solvent was pumped at a high rate of flow through the rod from one end to wash the rod debris off the opposite end of the tube. The flow direction was then reversed to clean the other end of the rod. The column was then ready for use or on-line modification.

2.2.3 Discussion of the preparation procedure

The heat shrinking of the polymer tube onto the porous rod is the critical step in the successful preparation of a monolithic column. The PTFE heat-shrinkable tube shrinks at a temperature higher than 360 °C. At this temperature, the organic/inorganic hybrid and the organic polymer decompose or react with the oxygen; thus, only silica and

carbon rods can be encased using this procedure. The rods should be dried thoroughly; if there is any moisture inside the rod, the heating of one end of the rod will vaporize and drive the moisture along the rod. The moisture is then condensed into water drops at the unheated part of the rod. When the heat source is moved along the rod, the condensed water drops will not evaporate fast enough to provide room for the shrinking tube; consequently, some drops of water are encapsulated between the rod and polymer tube. These water drops result in bubbles inside the column. A dramatic decrease in column efficiency was always observed when the encased rod was not sufficiently dry before encasing.

The dual-shrinking PTFE/PFE tubing offers better encasing than the PTFE tubing. The dual-shrinking PTFE/PFE tubing consists of two layers. The outer layer, the PTFE tubing, shrinks at temperatures above 360 °C. The inner layer, the PFE tubing, melts at the PTFE shrinking temperature. The molten PFE coats onto porous rod and forms a tight binding layer between the shrunken PTFE tubing and the monolith. The PFE layer also fills in defects on the porous rod surface. The voids from the defects are then eliminated. Using the dual-shrinking tubing ensures a tight and void-free cover layer. However, there is some concern about the penetration of the molten PFE layer into the porous rod, which may go too far into the rod and block the channels inside the rod. To avoid this possibility, the heat-shrinking process should be accomplished in a short period of time. Thus, oven heating is not a suitable process for the shrinking of the dual-shrinking tubing. The thin-walled, low-shrink-ratio (2 to 1) tubing has a thinner layer of PFE than does the thick-walled, high-shrink-ratio (4 to 1) tubing.

The glue selection is based on the following factors: (1) it should offer tight sealing between the stainless steel tubing and the heat-shrinkable tubing, and the curing of the glue should be solvent free and without any shrinkage; (2) after curing, the glue should be mechanically strong enough to sustain the system pressure that was produced during the use of the column; (3) it should have chemical resistance to the common HPLC solvents because the ends of the column are exposed to HPLC solvent, and the glue should be sufficiently tough to prevent damage to the column ends caused by the solvents. Slow-curing epoxy glue meets the above requirements. The mixing of two components of the glue produces numerous air bubbles so, in order to avoid any possible weak contact points between the cured glue and the polymer tubing, the air bubbles were driven away under vacuum.

Polishing the tube ends yields reproducible results. Column efficiency is also greatly affected by the smoothness of the column ends. The final polish with 1200 mesh sandpaper yields a coarseness close to the porous nature of the rod. Therefore, the ends of the column are relatively “flattened.” Polishing with sandpaper with mesh greater than 1200, or with alumina polishing powder, yields the same results as the 1200 mesh sandpaper. Thus, it is not necessary to use a finer polisher than 1200 mesh sandpaper.

2.3 Glass-shrinking encapsulation

In some cases, when strong solvents such as toluene, dichloromethane, and THF are used for the elution from the carbonaceous stationary phase, the heat-shrinkable tubing can become swollen. In such cases, glass tubing offers better resistance to organic solvents than heat-shrinkable tubing. The glass-shrinking encapsulation is designed for

columns using strong organic solvents. In other cases, the use of a glass-encased column allows the researchers to visualize the column. Thus, the separation can be studied *in situ* by actually seeing the separation process along the column. The visualized column is invaluable for modeling the separation process.

2.3.1 Setup and shrinking procedure for glass tubing

Technically, the heat shrinking of the glass tube is more difficult than shrinking the polytubing due to the higher process temperature and the need for an additional vacuum line or compression apparatus. Here, a vacuum line is used to force the glass shrinking onto the rod at the soft temperature of the glass tubing. Shown in Figure 8 is the setup used in our experiments. A Pyrex glass tube contained the porous rod and was then connected to a vacuum line. If the rod were carbon, which can be oxidized by the heated air, the tube would be purged with nitrogen three times to drive the oxygen away. The vacuum line was maintained at 200 micron Hg during the shrinking of the glass tube. A vertical tubular furnace was preheated to 500 °C. The glass tube was then inserted into the vertical furnace from the upper inlet and was moved down toward the bottom of the vertical furnace when the glass tube started to shrink. The movement of the glass tube was maintained at a constant speed as the glass shrank continuously from the bottom end up the length of the porous rod. After the shrinking, the glass-tube-encapsulated rod was allowed to cool to room temperature. The remainder of the fabrication steps for the monolithic column was the same as those for the polymer-lined stainless steel tubing-encased column.

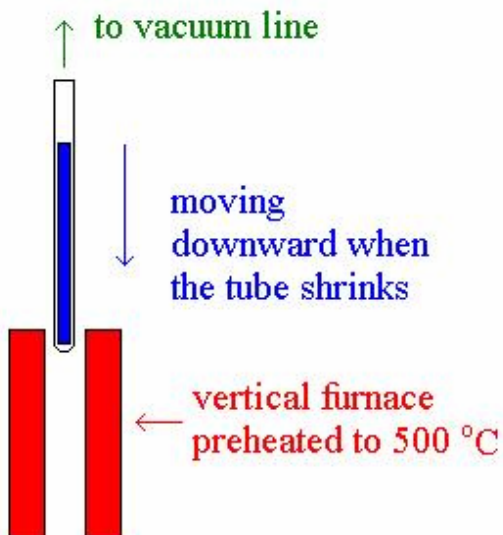


Figure 8. Setup of glass shrinking.

2.3.2 Key points for glass shrinking

The advantages of glass encapsulation over those of the heat-shrinkable polymer tubing are its transparency and its insensitivity to solvents. Thus, this configuration is used only for special cases such those using as strong organic solvents or in visualization studies. When using glass encapsulation, the following points should be taken into account: (1) due to the high temperature required by the shrinking of the glass tube, this configuration can be applied only to the thermally stable stationary phase; (2) the modification of column chemistry can be done only after the encapsulation; (3) the column cannot be used at the basic mobile phase with pH higher than 10 because of the reaction of the glass with the base. Moreover, because the glass is fragile, care should be taken in all fabrication steps to avoid breaking the glass tube.

2.4 Polymerization encapsulation (polymer coating)

Because of the thermal decomposition of the organic compound, the heat-shrinking encapsulation is not applicable to polymer and hybrid rods. When the rod has been modified before the encapsulation, the heat treatment can also damage the organic functionalities that play an important role in the variation of the column chemistry. The damage to the organic parts of the column raw materials can be avoided by using a polymer coating. This idea is inspired by the dual-shrinkable tubing, which has a meltable PFE layer acting as polymer coating during the shrinking process. Two configurations have been designed for the polymer-coating columns. One configuration is similar to the polymer-lined stainless steel tubing-encased column. The only difference is that the heat-shrinkable tube is replaced by a polymer coating. The other configuration is pure polymer-encased columns, which use two polymeric layers acting as a coating layer and a pressure-sustaining layer, respectively. Figure 9 is a photo of the polymer-coated carbon monolithic column.

2.4.1 Materials for polymer coating

The coating polymer was a 5-minute curing epoxy purchased from ITW Devcon Inc. The encasing polymer was a slow-curing epoxy polymer purchased from Miller-Stephenson Chemical Co. The end-fitting nuts were unscrewed from a used Chromolith column.



Figure 9. A polymer-coated monolithic column.

2.4.2 General procedure for fabrication of polymer-coated monolithic columns

A monolithic rod was coated with premixed 5-minute curing epoxy glue. The coating was then cured at 80 °C for 5 minutes. The coated rod was put into a mold with a slow-curing epoxy glue and cured at room temperature for 48 hours. After the removal of the mold, the ends of the polymer-encased rod were polished by the same procedure used in section 2.2.2. Afterward, the ends were manually tapped to M 8 fine threads. Two end fittings from a Merck Chromolith column were screwed onto the ends for the conduction of the mobile phase stream.

2.4.3 Discussion of the polymer-coated column configuration

The advantage of polymer coating is in avoiding heat treatment that may damage the chemical modification of the porous rod. The polymer coating configuration makes it possible to modify the rod before encasing. The disadvantage of this configuration is that the coating polymer more or less penetrates into pores inside the rod. The penetration of coating decreases the permeability of the monolithic column. Using fast-curing viscous epoxy can minimize penetration. Because this fast-curing epoxy has limited mechanical strength, a second layer of slow-curing epoxy was used to enforce the mechanical strength of the coated rod.

Fast-curing epoxy has only moderate chemical resistance to HPLC solvents. Therefore, the polymer-coating configuration can be used only for selected solvents such as water, acetonitrile, and methanol. The penetrated polymer also causes a wall effect that decreases overall column efficiency.

2.5 Multicapillary-array configuration for microbore monolithic columns

The commercial success of the silica-based monolithic column is represented by two series of products. One is the standard 4.6 mm ID column and the other is the capillary column. However, there are no microbore columns, which are the product series between the standard-sized column and the capillary column. The multicapillary-array configuration is designed as a replacement for microbore monolithic columns.

The 4.6 mm ID column is made through the encapsulation of a presynthesized rod by using heat-shrinkable PEEK tubing. The capillary column is made by *in situ* gelation of the silica precursor mixture, which has the same chemical composition as the standard

monolithic column. Due to the tiny size of the capillary, the gelled silica monolith sticks to the capillary wall without an obvious gap. For instance, if the capillary size is 20 μm , the shrinkage ratio of the gelation is 10%. Therefore, the absolute shrinkage of the gelled silica is only 2 μm , which is less than the pore size of the silica monolith, and no obvious gap forms inside the monolithic capillary column. Microbore columns have an ID in the range from 100 μm to 1 mm. Because the monolithic rod is fragile, it is very difficult to make a rod sized from 100 μm to 1 mm. It is not possible to gel the silica monolith *in situ* without creating a gap between the column wall and the monolith. For example, if the column ID is 0.5 mm and the shrinkage ratio is 10%, the absolute shrinkage is 50 μm , which is obviously larger than the pore size. Consequently, a gap will form between the column wall and the monolith.

For the purpose of making the microbore columns, we use the capillary-array rod as a column-encasing material. The gelation of the silica precursor is performed inside each individual capillary with an ID of 10 μm . As shown in Figure 10, the variance of the capillary size is tightly controlled within 2%. All 4000 capillaries are parallel to one another without entanglement. This configuration offers the advantages of the capillary monolithic column without creating gaps between the monolith and column wall. The high column pressure can be handled by the capillary configuration, so no enhancement of the mechanic strength is required. Because of the large number of capillaries, the 10- μm -ID capillary-array column is equal to a microbore column with an ID of 0.632 mm.

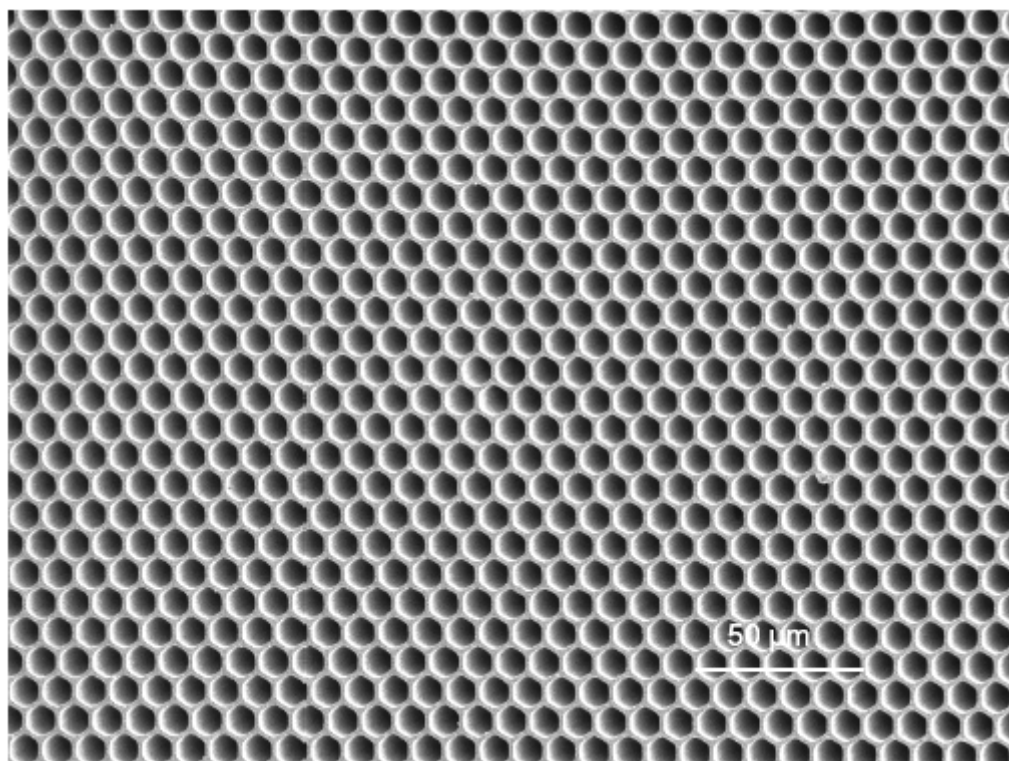


Figure 10. Capillary array.

Chapter 3: Preparation of monolithic silica columns via gel-casting

3.1 Silica monolithic columns with ordered mesopores and tunable macrochannels

Gel-casting of silica particles is a method developed in our lab for the preparation of silica monolithic columns with a hierarchically porous structure of ordered mesopores and tunable macrochannels.^{31, 32} To the best of our knowledge, this is the first report of the synthesis of the ordered mesoporous silica monolithic column.

Research in ordered mesoporous silica flourished in 1992 when researchers at Mobil Research and Development Corporation published a breakthrough report on the synthesis of surfactant-templated ordered mesoporous silica.³³ During a decade of intensive research in synthetic methods by many research groups all over the world, a variety of mesoporous silica with uniform pore sizes have been synthesized through a sophisticated selection of surfactants and reaction conditions. This versatile surfactant template methodology initiated an era of investigations of mesoporous materials in various branches of science. A number of silica materials, such as M41S,³³ FSM-16,^{34, 35} HMS,^{36, 37} MSU-x,³⁸ and SBA-x,^{39, 40} have been successfully used as supports for catalyst and separation, as well as template hosts for the synthesis of nano-scale particles, wires and ordered nonsiliceous porous materials.

Although ordered mesoporous materials have also been used in the HPLC stationary phase, for a variety of reasons the earlier applications of these mesoporous materials in HPLC were not attractive. The critical problem associated with the HPLC applications of the mesoporous materials is the limited mechanical strength of the very

thin wall structures, which makes it difficult for them to sustain the high pressures involved in HPLC systems.⁴¹ Some thick-walled ordered mesoporous silica have been made since the birth of SBA series silica; however, their irregular shape makes them non-attracting for HPLC packing. Recently, several successful applications have been reported when such porous materials are prepared with a spherical morphology of narrow size distribution. Unger et al. prepared spherical MCM-41, MCM-48, and HMS type particles by a modified Stober synthesis.^{42, 43} Acid-prepared mesoporous spheres (APMS) and their HPLC applications were first reported by Landry et al.⁴⁴ Zhao and Stucky and their associates synthesized SBA-15 spheres, using cetyltrimethylammonium bromide (CTAB) as a cosolvent,^{45, 46} while Boissiere et al. developed a two-step procedure to control the particle size of the MSU-1 spheres by simply adjusting the ratio of the fluoride catalyst to silica.⁴⁷ All these applications demonstrated that uniform mesoporous silicas are superior HPLC supports.

In spite of these successes achieved in preparing spherical mesoporous beads for HPLC packing, the efficiency of the particle-packed HPLC column is limited by a necessary compromise between particle size and pressure drop. Due to the high hydraulic resistance of the fine-particles packed column, the silica beads are required to have a significant mechanical strength. However, because of they are highly porous, mesoporous silica spheres are usually not strong enough for fine-particle packing. Hence, the HPLC application of mesoporous silica sphere is still limited. The latest studies in HPLC columns showed that a monolithic column could overcome the pressure drop of particle packed columns. Knox first recognized the intriguing advantage of monolithic columns

early in 1972.⁴⁸ Monolithic columns could provide efficiency nearly equal to conventional particle-packed columns with hydraulic resistance an order of magnitude lower. Recently, our group proposed a theoretical model of the structure of monolithic stationary phases that allows the derivation of relationships between the characteristics of the mass transfer kinetics inside the networks of macro- and mesopores and the first two moments of low concentration bands obtained with monolithic columns.⁴⁹ Silica-based monolithic columns were first reported by Nakanishi and Soga in 1991^{13, 50} and then commercialized by Merck KGaA. Monolithic silica columns have a bimodal pore structure, including networks of macropores and mesopores. The properties of mesopores are critical for achieving separations. There is as yet no reported development of specific mesopore morphologies for monolithic silica columns.

Generally, mesoporous silica is obtained as a precipitate from a mixture of surfactant and silicon-source solutions. The resulting product is in the form of fine particles. Although several groups of researchers have attempted to produce monolithic mesoporous silica,^{51, 52} the synthesis of large size crack-free mesoporous silica monoliths with ordered structure is still a challenge. Moreover, mesoporous silica of solely mesoporous structure is not suitable for HPLC. An additional macropore or channel network is required for allowing a stream of mobile phase to percolate with low hydraulic resistance. Monolithic silica columns with a bimodal pore structure (i.e., mesopores and macropores) demonstrated that a hierarchical porous structure is effective in resolving problems involving pore size and mass transfer kinetics. Though the phase-separation method developed by Nakanishi et al.^{13, 50} can synthesize bimodal monolithic columns

with narrow size distributions of mesopores, this method is not suitable for the synthesis of monolithic columns with well-defined mesopore structure, such as those of hexagonal-structured MCM-41 and SBA-15 and cubic-structured MCM-48 and SBA-16.

Gel-casting is a ceramic fabrication method developed at Oak Ridge National Laboratory in the 1990s. It has recently been used to create hierarchical zeolite structures with designed shape.³¹ We found that gel-casting is a suitable technique for the conversion of particulate mesoporous silica materials into large dimensional pre-designed objects without losing the mesoporous structure of the silica.³² In order to combine the excellent homogeneity of ordered mesoporous silica with the super hydraulic dynamics of a monolithic structure, we converted the ordered porous silica particles into monolithic columns via gel-casting.

3.2 The fabrication of silica monolithic columns

3.2.1 Materials and instruments

Materials: acrylamide, *N,N'*-methylene-bisacrylamide, ammonium persulfate ($(\text{NH}_4)_2\text{S}_2\text{O}_8$), pyridine, phenol, toluene, acetonitrile, and HPLC water were purchased from Aldrich. Pluronic surfactant P123 was donated by BASF Corp. Tetraethoxysilane (TEOS), octadecyldimethylchlorosilane, and trimethylchlorosilane were purchased from Gelest. All chemicals were used as received. Materials for the fabrication of the monolithic column are described in section 2.2.2.

Instruments: Philip XL-30 field emission scanning electron microscopy was used for the structure characterization of the monolith. HD 2000 scanning and transmission electron microscopy was employed for imaging the mesoporous silica particles. A BET

system from Micrometrics Co was used for the measurement of the mesopores' size distribution and surface area. The HPLC test was performed by a HP 1100 system (Agilent Technologies, Palo Alto, CA).

3.2.2 The synthesis of mesoporous silica particles

The mesoporous silica was synthesized by a method slightly modified from the original report.³⁹ 5 g of Pluronic P123 was dissolved in 200ml 1.6M HCl solution and stirred at 35 °C. 10.6 g of TEOS was then added into the surfactant solution and stirred at 35 °C. The silica started to precipitate out after 30 minutes. After the reaction was kept at 35 °C for 20 hours, the temperature of the flask was then gradually raised to 80 °C and was kept at this temperature overnight. The silica particles were recovered by filtration. The raw particles were washed with DI water and dried in a vacuum oven at 80 °C. The dried particles were calcined in a furnace with a temperature ramp from room temperature to 500 °C at the rate 2 °C/min. The temperature was kept at 500 °C for 10 hrs to ensure the complete removal of surfactant.

3.2.3 Gel-casting of silica particles into a monolithic rod

The calcined silica powder was ground and sieved into 10 µm particles. These particles were suspended in a solution of monomer acrylamide, cross-linker *N,N'*-methylene-bisacrylamide, and the initiator, ammonium persulfate (NH₄)₂S₂O₈. The weight ratio of monomer, cross-linker, initiator and water was 5: 0.5: 0.05: 100. The suspension was sonicated for 10 minutes to ensure a homogeneous mixture. A 4.0 mm ID glass tube containing the suspension was centrifuged at 1000 to 2000 rpm for 5 minutes. The centrifugal force packed the silica particles at the bottom of the tube and left a clear

binder solution in the upper layer. Replacing the upper layer of solution with the suspension and repeating the centrifugation several times easily achieved a column of desired length. The silica-packed glass tube was then capped, put into an oven, and cured at 50°C for 1 hour. The monomer and cross-linker were polymerized into an elastic hydrogel. The hydrogel was hardened by removing the cap from the tube and retaining the tube overnight in the oven at 50°C. The cylindrical rod was dried thoroughly in a vacuum oven at 60°C for 2 days. The dry rod was removed from the glass tube and sintered at 700°C for 10 hours. After sintering, the silica particles formed a hard rod with an OD of 3.8 mm.

The polymer network was totally burned up during the sintering procedure. The monolithic column was chemically bonded by refluxing in a toluene solution of octadecyldimethylchlorosilane and equivalent pyridine for 10 hours. Afterward, the bonded-phase column was end-capped by adding 1 ml of trimethylchlorosilane to the toluene solution for 2 hours of additional reflux. The modified rod was washed thoroughly with copious ethanol and dried overnight in a vacuum oven at 60°C.

3.2.4 Fabrication and surface modification of silica columns

A complete column was made by encapsulating the silica rod with a piece of heat shrinkable tubing, using the configuration of polymer-lined stainless steel tubing encasing. A general procedure was described in section 2.2.2. A monolithic column with 3.8 mm ID and a length of 50 mm was tested as a fast HPLC column.

3.2.5 HPLC application

A Hewlett-Packard (Palo Alto, CA, USA) HP 1100 LC system was used to evaluate column performance. This system has a binary pump, an online degasser, an autosampler, a variable wavelength UV detector, a column thermostat, a data station, and a HP PC workstation with a Windows NT operating system. The instrument control and data acquisition were performed using Chemstation software (Rev A 05.03). The column temperature was maintained at 25 °C by the column thermostat. The mobile phase is a mixture of acetonitrile and water. Pure solvents were mixed and delivered through the binary pump. The ratio of these solvents was adjusted by Chemstation software. The column was washed by first pumping pure water and then pure acetonitrile through until a stable baseline of the detector was achieved. A 10 µl phenol and toluene mixture was injected as probe to evaluate the column. The mobile phase was the 30/70 mixture of water/acetonitrile. The column was tested at three flow rates of 0.5, 1.0, and 5.0 ml/min.

3.3 Results and discussion

The calcined silica has a hexagonal porous structure. Shown in Figure 11 are TEM images of the SBA-15 mesoporous silica. The left image reveals a highly ordered honeycomb structure of the ends of the cylindrical pores. In the right image the cylindrical pores are parallel to each other.

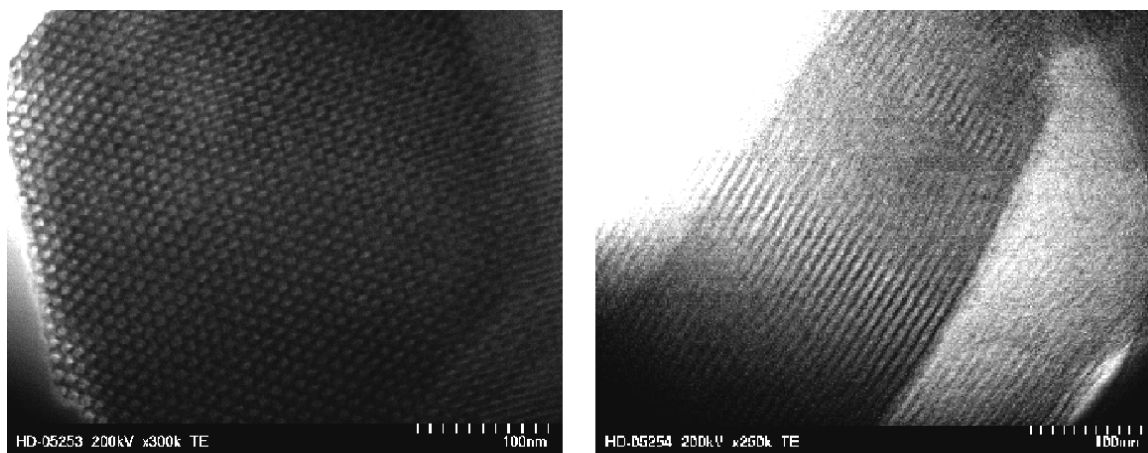


Figure 11. TEM images of mesoporous silica particles.

All organic binders have been burned off during the sintering of the silica particles. The sintering of silica particles causes the interparticular dehydration that eventually binds the silica particles into a monolith. The sintering of the porous particles usually destroys the pore structure to some degree. In this study we minimized the sinter effect on the pore structure by using a temperature of 700 °C, which is the low threshold of the sintering process of these particles.

The BET nitrogen adsorption/desorption test showed that the mesopore diameter undergoes only slight shrinkage, from 8.1 nm to 7.5 nm, after the gel-casting treatment. The initial adsorption volume decreased by a factor of two, and the surface area significantly dropped from 831 m²/g to 535 m²/g. The decrease of the initial adsorption volume indicates that the micropore volume shrunk during the sintering process.

No significant change has been found after the particles have been sintered into a monolithic column, according to the comparison of the TEM images taken before and

after sintering. This observation confirms that the slight shrinking of the mesopore has not changed the meso structure of the silica. Recalling the surface area change measured by BET, one can conclude that the decrease of surface area is mainly attributed to the diminishing of micropores.

Several studies claimed that the wall of SBA-15 is microporous. The formation of the micropore is believed to be due to the thermal decomposition of the surfactant, which is embedded in the silicate wall. The existence of micropores is usually a serious problem for HPLC application because of the peak tailing caused by micropores. Because sintering eliminated the micropores, the HPLC test on this sintered column showed symmetric peaks without obvious peak tailing.

The texture of the sintered silica column was examined by SEM. The sintered rod has a rope-shaped grain texture, as shown in Figure 12. The rope shaped grains have an average diameter of 200 nm and a length of 10 μm .

The overall porosity of the silica monolith is estimated by the injection of an irretentive compound. The injection uracil shows the column to have a porosity of 80.7%, which is attributed to its combination of macropores and mesopores. The size and porosity of the mesopores are controlled by the synthetic method of the silica particles. So far, silica particles with mesopore sizes ranging from 2 nm to 30 nm have been reported. These particles offer a large number of variations in the synthesis of monolithic silica column with various mesoporosity.

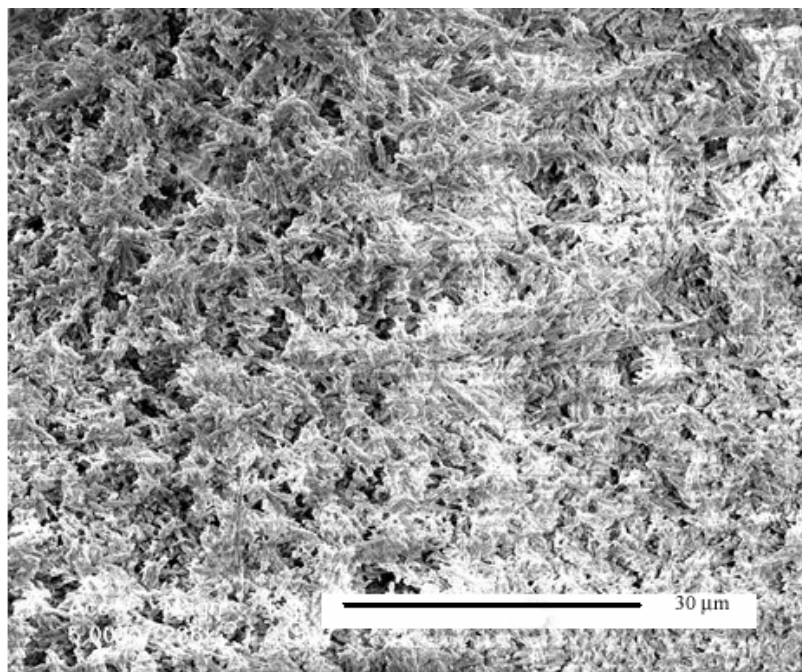


Figure 12. Sintered silica monolith.

Macroporous channels are formed by interparticle voids. The average size of the macropores can be adjusted by using silica particles of different sizes. Typically, sintering of 10 μm SBA-15 particles results in a monolithic column with an average macrochannel size of 5 μm .

This column showed good resolution with extremely low hydraulic resistance and also afforded rapid separations. Figure 13 shows an application for the separation of phenol/toluene at flow rates of 0.5, 1.0, and 5.0 ml/min. When the column was operated at a flow rate of 5 ml/min with a mobile phase of acetonitrile/ water (7:3), phenol and toluene were completely resolved within 0.4 minute. The pressure drop corresponding to the flow rate of 5 ml/min was only 87 bars.

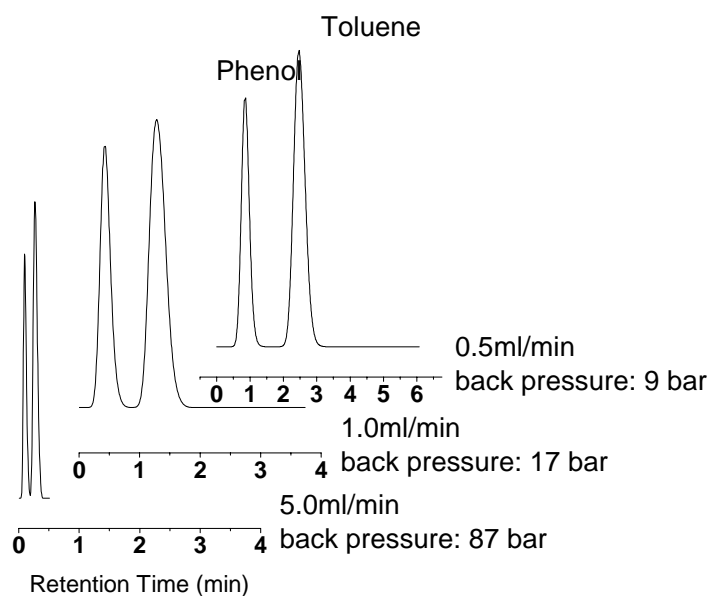


Figure 13. The fast separation of phenol and toluene.

Obviously, the high porosity (80.7% measured by chromatography) of the column contributes to its low hydraulic resistance. The hydraulic resistances of the monolithic columns were related to the sizes of the silica colloid precursors and to their macropore structure. With large macropores, the column can have a low hydraulic resistance that allows a fast stream of mobile phase to carry the analytes through the column. So, fast separation can be achieved by sintering large particles into monolith column. But the gain of fast separation always sacrifices column resolution due to the large domain size of the sintered monolithic column that uses large particles as starting material.

3.4 Conclusion

In conclusion, we report here a general procedure for the synthesis of monolithic silica columns with a bimodal pore structure. Both the macropore and the mesopore modes are adjustable. Monolith columns with a large diversity of mesopore morphology were readily prepared using various silica precursors. The total porosity and hydraulic resistance of the column were easily tailored by gel-casting silica colloids of various sizes. Our procedure also demonstrated that gel-casting is a convenient method for the synthesis of hierarchically structured silica with designed shape. Gel-casting of various silica precursors made it possible to fine-tune the design of monolithic silica columns.

Chapter 4: Carbon monolithic columns made by colloidal templates

4.1 The background of carbon columns

The major obstacle to a wider use of silica-based rod columns is their limited resistance to hydrolysis, which restricts their operation to a relatively narrow pH range.⁵³ Although polymer columns could overcome this limitation, the swelling of polymer beds in the presence of organic solvents results in poor hydraulic performance. As an alternative to beds made of silica gel and organic polymers, carbon-based adsorbents offer the advantage of being free from both hydrolysis instability and swelling problems. Carbon adsorbents were suggested in the past as packing materials able to solve these two problems.²²

In 1976, Colin and Guiochon recognized the intriguing properties of graphitized carbon and began a systematic investigation of its use in liquid chromatography.⁵⁴⁻⁵⁸ Later, several groups made significant contributions to this area.⁵⁹⁻⁶⁶ However, early results obtained with the most popular carbon materials, e.g. carbon blacks, active carbons, glassy carbons, and various cokes, were not encouraging due to the combination of weak mechanical strength, poor control of the pore-size distribution, an irregular particle shape, and an important surface concentration of mineral and oxygen impurities.^{54, 59, 65, 67-72} In 1979 Knox and Gilbert patented a method of control of the size and shape of graphitized carbon particles.⁷² They impregnated porous silica beads with a phenolic resin, pyrolyzed the resin in an inert atmosphere, and dissolved the silica with an alkali, obtaining spherical porous particles of glassy carbon. Unfortunately, this carbon

material has micropores and exhibits poor LC performance with compounds having an alkyl chain of more than two carbon atoms. Better chromatographic performance was obtained by graphitizing porous glassy carbon.^{60, 69} This product is still commercially available from Thermo Electron Corp.

4.1.1 Retention mechanism on carbon

Transmission electron microscopy shows that porous graphitized carbon (PGC) consists of interwoven ribbons of carbon. The ribbon consists of graphene sheets 3.4 angstrom apart. A comparison of the C18 silica phase and the PGC phase is shown in Figure 14. As opposed to the C18 silica phase, the carbon phase has a flat planar surface without any surface group. The retention of analytes on PGC carbon depends on a combination of dispersive and charge-induced interactions.⁶⁰

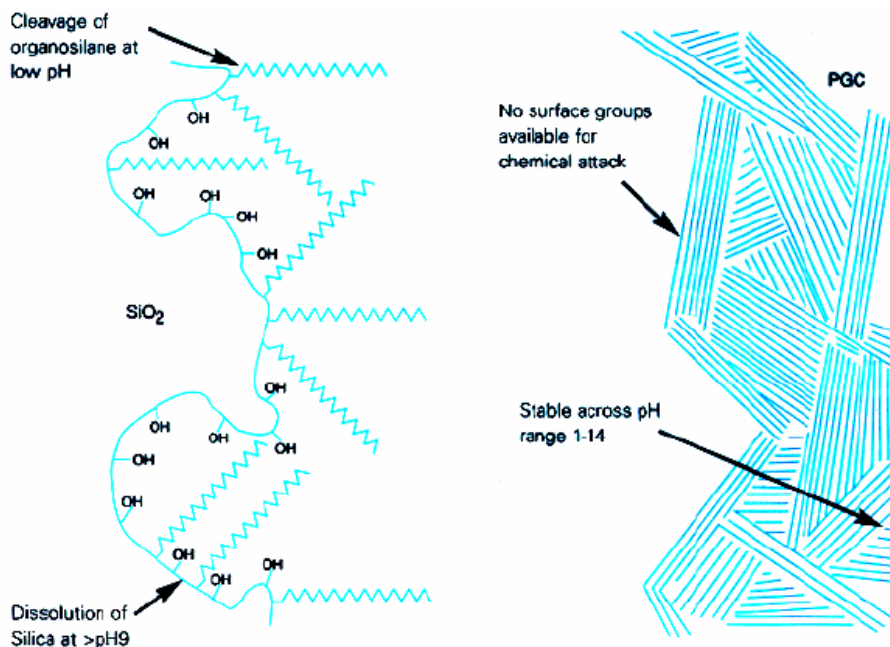


Figure 14. The C18 bonded silica phase and the porous graphitize carbon phase

(courtesy of Thermo Electron Co.).

Dispersive interactions occur in all stationary phases. Compared to the flexible C18 chain, the carbon surface is very stiff. Thus the strength of the dispersive interactions of analytes on graphitized carbon is largely dependent on the molecular area in contact with the carbon surface and the orientation of functional groups of the analyte. Figure 15 schematically represents the contact of planar and non-planar molecules on the carbon surface.

The charge-induced interaction is unique to the carbon stationary. As shown in Figure 16, the mechanism is quite straightforward. When a polar molecule with a permanent dipole approaches the carbon surface, the charge induces the dipole of the graphite by distorting the electron distribution of the graphite surface. Thus a negative image of the polar molecule will reflect on the other side of the graphene (Figure 17).^{60, 64}

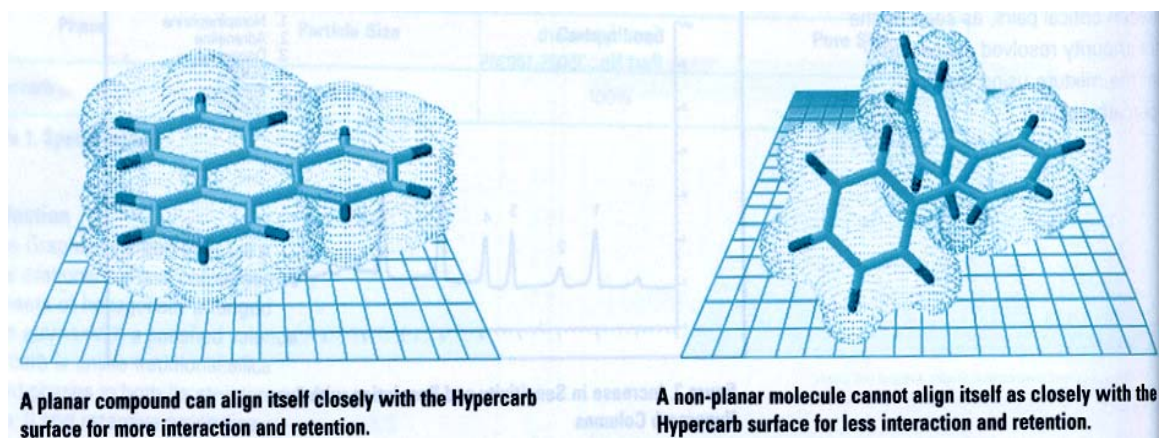


Figure 15. Scheme of the contact area of planar and non-planar compounds on graphite surface (courtesy of Thermo Electron Co.).

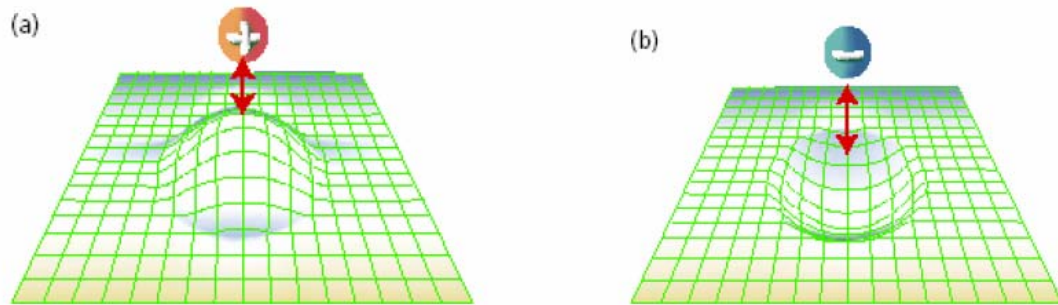


Figure 16. Representation of the interaction of the charged species approaching the carbon surface.⁶⁴

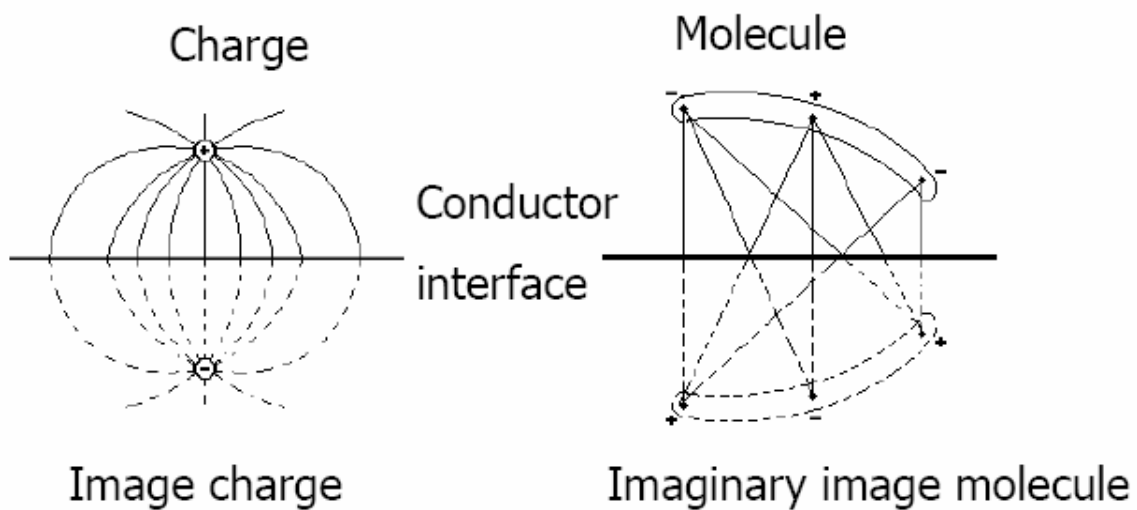


Figure 17. The images of charge and polar molecule reflected by the graphene.⁶⁰

The induced negative charge image interacts with the real molecule through the electrostatic force. The adsorption energy contributed by charge-induced interactions is given the equation 4.1.

$$U = \frac{1}{4\pi\epsilon_0} \sum \left(\frac{q_i q_j}{r_{ij}} \right) \quad 4.1$$

Where, q_i and q_j are the charge of the polar groups and their “electric images”; r_{ij} is the distance between two interacted charge centers; ϵ_0 is the dielectric constant, which is a property of the solvent. Thus, the charge-induced interaction is determined by both the charge profile of the molecule and the dielectric constant of the mobile phase.

The combined effect of the dispersive interactions and charge-induced interactions gives rise to a unique retention pattern of the graphitized carbon. By the virtue of this retention pattern, the carbon can easily differentiate between the closely related structures of compounds that are very difficult to resolve by C18 stationary phases. This is shown in Figure 18.⁶¹

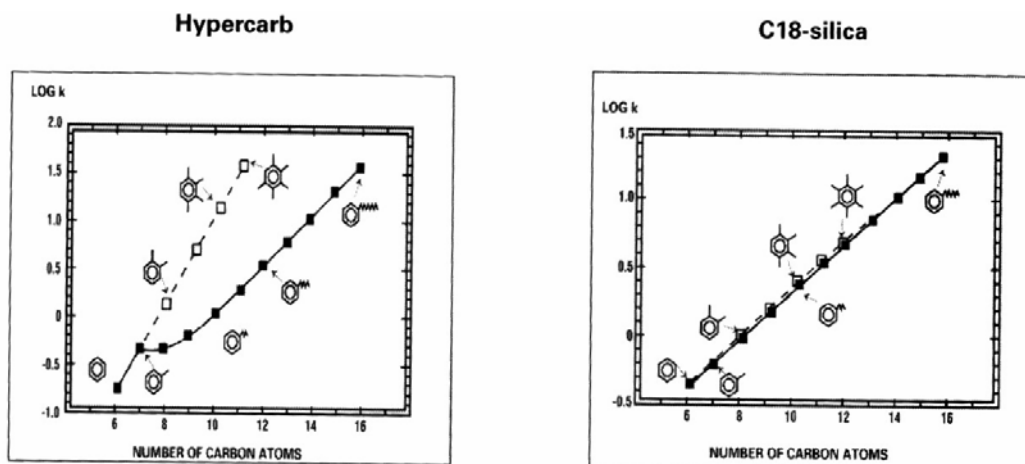


Figure 18. Comparison of methyl and methylene group selectivity on carbon and C18-silica.

4.1.2 Methods for the preparation of carbon stationary phases

The use of carbon stationary phase in liquid chromatography has historically proven to be the most difficult stationary phase to prepare. Since 1976 when Colin and Guiochon made the first attempt at packing a carbon column, many groups devoted their efforts to preparing carbon stationary phase in over two decades.⁵⁴⁻⁵⁶ Several methods have been reported for the synthesis of successful chromatographic carbon materials. These methods were reviewed in several comprehensive reviews.^{60, 62, 64}

4.1.2.1 The Guiochon method

The Guiochon method is the first method that has been reported for liquid chromatographic utilization of the carbon black stationary phase. Before being used in liquid chromatography, carbon black has been successfully utilized in gas chromatography by DiCorcia and Liberti and has been marketed by Supelco Ltd under the trade name of Carbo-pack.⁶⁰ Carbon black consists of graphitic nanocrystalline and amorphous carbon. The fragile nature of this material makes it unsuitable for the HPLC system. Colin and Guiochon deposited pyrolytical carbon onto carbon black agglomerate to make large particles with sufficient surface area and mechanical strength for HPLC applications.⁵⁴⁻⁵⁸ The deposition of pyrolytical carbon was carried out at 1200K using benzene as precursor. The mechanical strength and surface area depends on the amount of deposited carbon. During long deposition time a thick layer of carbon was deposited. The mechanical strength was thus greatly enhanced, but the surface area decreased with the increased thickness of pyrolytical carbon. The alkanes were found to be better precursors for the deposition of carbon than benzene. With carefully chosen experimental

conditions, they can make carbon particles with moderate surface areas and mechanically strong enough to sustain the system pressure under the HPLC operation. The surface impurity has been removed either by hydrogenation at 1300K or thermal treatment at 3000 to 3300K. The removal of surface impurities on the particles slightly improved their chromatographic performance.

4.1.2.2 The Unger method

Unger et al. used coke and active carbon as raw materials for the production of liquid chromatographic packing materials.^{65, 66} Hard particles can be made of coke and active carbon, but coke and active carbon have significantly greater amounts of impurities than carbon black. The impurities form heterogeneous and polar surfaces of coke and active carbon. These heterogeneous surfaces are not suitable for separation unless the impurities have been removed by boiling in HCl solution for 12 hours, followed by heat treatment at 3027 K. After the removal of impurities, the particle size and shape were retained, but the surface area was dropped significantly to a few square meters per gram. These particles were still micropore. Due to the small surface area and micropores, the chromatographic performance of these particles was not attractive.

4.1.2.3 The Knox method

In 1979 Knox and Gilbert invented porous glassy carbon by impregnating a porous silica particle with phenolic resin, followed by the carbonization and removal of the silica.⁵⁹ The resulting hard carbon particles are of spherical shape and highly porous. Unfortunately, these particles are microporous, so the chromatographic performance was poor. However, by heating these particles at over 2000 °C, micropores were eliminated

due to the graphitization of the carbon matrix. These particles then demonstrated good chromatographic behavior, which was similar to the material made by Colin and Guiochon.⁶⁰

The Knox method is reproducible and easily scaled-up. It has been commercialized and marketed under the trade name of Hypercarb. This carbon still is the only pure carbon packing material currently on the market.

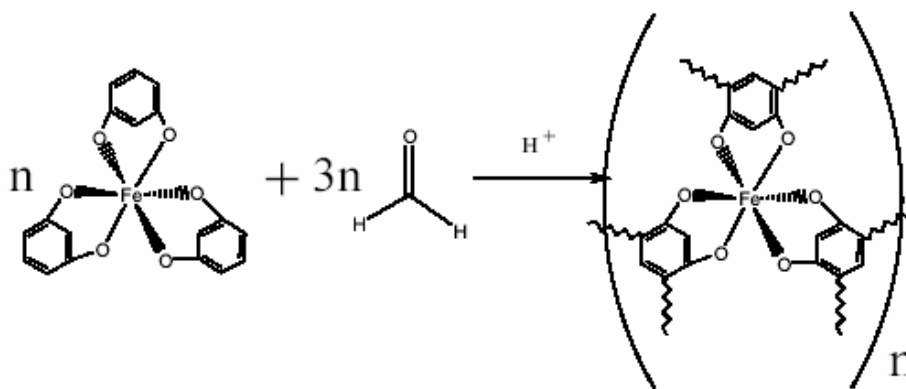
4.1.3 The birth of carbon monolithic column for HPLC

The birth of carbon monolithic column is boosted by the success of silica and polymer monolithic columns. Historically, the difficulty of producing carbon stationary phase lies largely on the synthesis of spherical carbon particles with mesopores. Particulate columns now give way to the monolithic ones. The hurdles encountered in the production of spherical carbon particles are no longer a problem for carbon monolithic columns.

In this work, we report on the preparation of the first monolithic carbon-based column.²² This column was prepared by pyrolyzing a rod made of a copolymer of a resorcinol/iron (III) complex and formaldehyde (Figure 19) in the presence of silica beads. A bimodal pore structure was developed within the column, involving macropores and mesopores. The macropores were tailored by the silica beads, which were sacrificed and turned into flow-through pores upon dissolving these beads in hydrofluoric acid. The mesopores were formed *in situ* as a result of the catalytic pyrolysis of the phenolic resin/iron complex. A full characterization of this rod's pore structure, porosity, and surface area was done by using scanning electron microscopy (SEM), transmission



(a) Resorcinol Fe(III) Complex



(b) Copolymerization of Resorcinol Fe(III) Complex and Formaldehyde.

Figure 19. Structure of the carbon precursor.

electron microscopy (TEM), and BET nitrogen adsorption/desorption. The carbon synthesized has a high graphite index, as checked by both X-ray diffraction (XRD) and Raman spectrum. Later, this carbon rod was encased by polymer lined stainless steel tubing as a monolithic column for HPLC and checked with a series of alkylbenzene compounds. The resulting column possessed the typical properties of monolithic columns, i.e., high efficiency and low hydraulic resistance. The synthetic method described here is a versatile procedure for the production of tailored, bimodal, porous carbon monoliths.

4.2 The synthesis and chromatographic evaluation of carbon monolithic columns

Chemicals: Resorcinol (99.9+%), formaldehyde (37% wt aqueous solution), iron trichloride (99.8%), toluene (99.9%), ethylbenzene (99.9+%), propylbenzene (99.9%), butylbenzene (99.9%), and amylbenzene (99.9%) were obtained from Aldrich (St.Louis, MO). Ethyl alcohol and HPLC solvents were purchased from VWR (West Chester, PA). 10 μm Kromasil silica beads were obtained from Eka Nobel (Bohus, Sweden). Deionized water was homemade. All chemicals were used as received from the manufacturers.

Preparation of the precursor rod: 6 g of silica beads were dispersed in 5 g of an aqueous solution of ethanol (80% ethanol) by ultrasonication. 1.08 g FeCl_3 was then dissolved into the suspension, followed with 2.2 g of resorcinol, dissolved by shaking by hand. The colloid solution turned dark immediately after the addition of resorcinol, indicating the formation of a resorcinol/Fe(III) complex. 2.4 g of an ice-cooled, 37% formaldehyde solution in water was introduced into this mixture, in one step, and shaken again. The mixture was kept in an ice and water bath for 10 minutes and stirred magnetically. After removal from the bath, the mixture was slowly transferred into 5 mm ID glass tubes that were capped when filled. These tubes were then placed in a 70°C hot water bath. The mixture was soon polymerized into a solid rod inside the glass tube. The rod detached from the tube wall because of the shrinking caused by polymerization. The polymer rod aged in the glass tube as it was kept in the hot-water bath overnight. The crack-free phenolic resin/silica rods were removed from the glass tubes by shaking each tube toward its open end. The wet rod was put into the hood for three days in order to evaporate the solvent and, finally, it was thoroughly dried overnight in a vacuum oven at

80 °C. The dried rods were further cured at 135 °C for 4 hours to ensure complete polymerization.

Carbonization and removal of the silica beads and the catalyst: The precursor rods were placed into a cylindrical furnace, purged with N₂ (45 ml/min). A programmed temperature cycle was applied to the furnace. The temperature was first ramped from 135 to 800 °C at 2.5 °C/min, and then kept at 800 °C for 2 hours to ensure complete carbonization. A second temperature ramp took place from 800 to 1250 °C at 10 °C/min. The temperature was kept at a constant 1250 °C for 1 hour. Afterward, the furnace was allowed to cool naturally to ambient temperature. The silica beads and the iron catalyst were removed by concentrated hydrofluoric acid, washed away with copious amounts of distilled water. The porous carbon rod obtained was thoroughly dried under vacuum at 80 °C.

Imaging of the pores and the carbon texture: The surface morphology was examined with a Philip XL30FEG scanning electron microscopy (SEM) at an accelerating voltage of 10 KV. Further examination of the pore morphology and the wall texture was performed with a Hitachi HD-2000 scanning transmission electron microscopy (STEM), with an accelerating voltage of 200 KV and a current of 30 µA. STEM samples were prepared by grinding the carbon monolith in an agate mortar and loading the powder on normal carbon film TEM grids.

Raman microscopy study: Raman spectra were recorded with a Renishaw 2000 Raman microscope equipped with a CCD detector, using an Argon ion laser (514.5 nm excitation wavelength, 5 mW). An objective lens with a magnification of 50 X was used,

both to focus the laser beam and to collect the backscattering radiation. All spectra were recorded with an exposure time of 10 seconds. Each spectrum was the accumulation of three scans. A non-linear, least-square routine provided by the commercial data process software Origin 6.0 (Originlab Corporation) was used to curve-fit the Raman spectra to a Lorentzian function. Values of the band position and the band intensity were derived from the result of this curve-fitting exercise.

X-ray diffraction: X-ray diffraction patterns were measured with a Siemens D5005 X-ray diffractometer with copper K_{α} line (0.1541 nm) as the incident beam. A Gobel mirror was employed as a monochromator. Powder samples were prepared by grinding the monolith with an agate mortar. The sample powder was loaded to a plastic holder and leveled with a glass slide before being mounted on the sample chamber. Because no peaks emerged at angles larger than $2\theta = 60^{\circ}$, the specimens were scanned between 5 and 60° . The scan step-width was set to 0.001° and the scan rate to $0.001^{\circ}/s$. The d_{002} peak was curve-fitted with Origin 6.0 to a Lorentzian function. The peak position and half-maximum peak width were derived from the curve fitting.

BET measurement: Nitrogen absorption/desorption measurements were performed with a Micromeritics Gemini 128. Typically, a piece of 0.05 g carbon monolith was loaded into the apparatus for the measurement. The values of the pore size distribution and the surface area of the sample were derived from the BET isotherm by using the supporting software of the instrument.

Cladding of the rod column and HPLC test: The rod column was clad according to the configuration described in Section 2.2.2. Briefly, the carbon rod was clad in an

oven at 340°C with a section of heat-shrinkable Teflon tubing. The encapsulated carbon rod was then glued into a precut 4.6 mm I.D. stainless steel tube with epoxy glue. The configuration of the column cross-section is illustrated in Fig 6. The column is then ready to be connected to the HPLC system using reduction unions (1/4" to 1/16"). Each monolith column contained a piece of carbon rod of 3.4 mm diameter and 80 mm length. The weight of the carbon rod was 0.164 g.

All chromatography tests were performed with a Hewlett-Packard (Palo Alto, CA, USA) HP 1100 LC system. The whole system consists of a binary pump, an online degasser, an autosampler, a variable wavelength UV detector, a column thermostat, a data station, and a HP PC workstation with a Windows NT operating system. The instrument control and data acquisition were performed using Chemstation software (Rev A 05.03). The column temperature was maintained at 25 °C. For the analysis, pure methanol and dichloromethane were delivered through the binary pump. The ratio of these solvents was adjusted by Chemstation software.

The freshly made columns were washed by flushing them with pure solvents, at 1 ml/min, in the following order: water (5 hours), methanol (2 hours), hexane (2 hours), and dichloromethane (2 hours). The probe compounds were toluene, ethylbenzene, propylbenzene, butylbenzene, and amylbenzene. Each solution contained 0.5 mg of analyte in 1ml of hexane and the injection volume was 10 µl. Hydraulic resistance was evaluated with pure hexane. The system pressure drop was read out and recorded with Chemstation software. The pressure drop caused by the system tubing was measured by eliminating the column and directly connecting the inlet and outlet tubings. The net

pressure drop over the column was calculated by subtracting the system tubing pressure drop from the total recorded pressure drop.

4.3 Results and discussion

Preparation of a porous carbon rod with a bimodal pore distribution: The preparation of carbon monolith involves two major issues:(1) the prevention of cracks and (2) the development of the mesopore structure. The formation of cracks is the most pervasive problem in the preparation of monolithic materials. The drying procedure is most important in the production of large pieces of crack-free, porous monoliths by wet chemistry. Careful attention was paid to all three steps of the synthesis protocol, which could all induce the cracking of the rod. Each step has the potential to cause internal stress leading to the cracking of the rod.

The first step is the aging and drying of the silica/phenolic resin wet rod. After the phenolic resin has been formed and the silica beads are agglomerated within a rod in a glass tube, this rod is aged overnight at 70 °C. During this process, internal stress develops, caused by solvent molecules leaving the resin. This stress tends to crack the wet gel. Aging allows the phenolic resin to form a substantially cross-linked bulk polymer strong enough to overcome this stress. The aging temperature is set below the boiling point of ethanol to avoid the formation of bubbles inside the rod. Hydrogen bonds between silanol groups on the silica surface and hydroxyl groups in the polymer matrix provide strong adhesion of the silica beads to the phenolic resin, making the whole rod hard and strong. The aged wet rod was then dried slowly, at room temperature, inside a hood. These mild drying conditions prevent cracking on the precursor rod.

The second challenge is in the carbonization of the dry precursor rod. The carbonization of phenolic resin generates large amounts of water vapor, carbon monoxide, and hydrogen. These gases must be evacuated to avoid the stress that their expansion causes within the rod. When the rate of increase of the temperature is controlled and kept below $2.5^{\circ}\text{C}/\text{min}$, the formation of gas is slow enough to ensure that the gases escape from the polymer matrix without cracking the rod. Two other important potential sources of cracking, shrinking and thermal expanding, are inoperative here. As is illustrated in Figure 20, the silica templates are closely packed in the dry precursor rod. The resin is located in the voids between silica beads. Consequently, the shrinking, which is caused by carbonization, is localized within the voids among silica beads. This is the reason why no significant overall shrinking is observed during carbonization of the silica embedded precursor rod. The localized shrinking has two positive effects on the preparation of the porous carbon matrix: (1) It provides space for the thermal expansion of the pyrolyzed carbon (note that the linear thermal expansion coefficient of fused silica is $0.36 \times 10^{-6} \text{ K}^{-1}$ at 1000K and of graphite $30 \times 10^{-6} \text{ K}^{-1}$);⁷³ and (2) it enlarges the connecting windows among the silica beads. The second effect contributes significant connectivity to the macropores, which result from the removal of the silica beads. More details are given in the discussion *Porosities of the rod*.

The last challenge is the cladding operation. The carbon rod was wrapped in a piece of heat-shrinkable PTFE tubing. The PTFE tube shrank over the carbon rod when the temperature of the heated tube dropped. A slow cooling of the hot PTFE tube prevents cracking the rod.

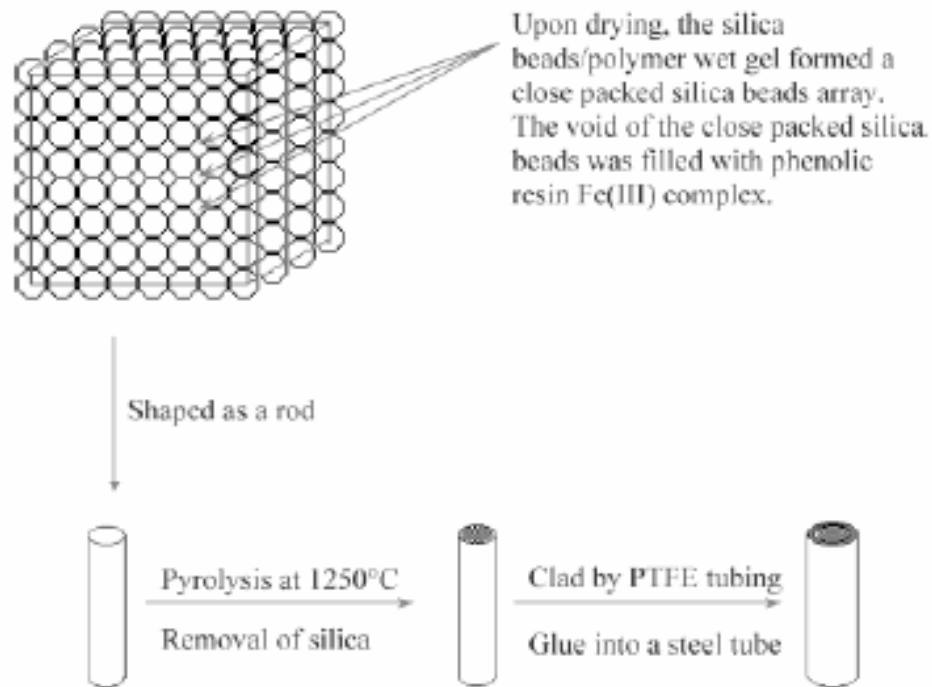


Figure 20. Schematic representation of the fabrication of column monolithic columns.

Porosities of the Rod: As was demonstrated by Nakanishi and his colleagues,^{13, 50} a good monolith for chromatography has a bimodal porous structure. The intriguing properties of monolithic columns are due mainly to this pore combination. The macropore network affords a low hydraulic resistance of the column. The flow-through channels within the monolith offer a more regular shape than those around the particles of a conventional bed; thus, the band dispersion is reduced in monolith columns. To build up regular flow-through channels within the carbon monolith, we used narrow size distribution silica beads. Figure 20 illustrates the basic procedure used for making our porous monolithic columns.

The role and properties of the mesopores in the skeleton of the monolith are the same as those of the mesopores in the particles of conventional beds. They provide a sufficient surface area to ensure retention and separation. However, the glassy carbon that is obtained by pyrolysis of phenolic resins is microporous, which was proven by earlier researchers to be inappropriate for a stationary phase. Knox and his associates eliminated most of the micropores in glassy carbon through graphitization.^{69, 72} Graphitization must be carried out at very high temperatures, about 2400 °C or higher. Such high temperatures are not easy to achieve in a laboratory. Moreover, a temperature treatment this high will drastically diminish the mesoporosity of the glassy carbon; the graphitized carbon rod may no longer have a large enough surface area to achieve separations. To produce mesoporous carbon, catalytic graphitization is often used. It has the potential to yield a product with a high graphite index at a relatively low temperature.

The mesoporosity in the carbon monolith was developed by *in situ* catalytic graphitization. The polymer prepared was a complex of iron, resulting from the polycondensation of the resorcinol/iron complex. The iron ions were reduced to iron atoms during the carbonization. These atoms of iron catalyze the crystallization of glassy carbon. This crystallization of the microporous glassy carbon forms graphite strips in the carbon matrix. These graphite strips are plainly evident in transmission electron microscopy. Figure 21 suggests that the graphite strips are woven in the carbon mass. The inset in Figure 21 clearly reveals the crystalline structure of the graphite strips. During graphitization, the micropores are eliminated, merging gradually into mesopores between the graphite strips. The glassy carbon turns into graphite strips and becomes denser,

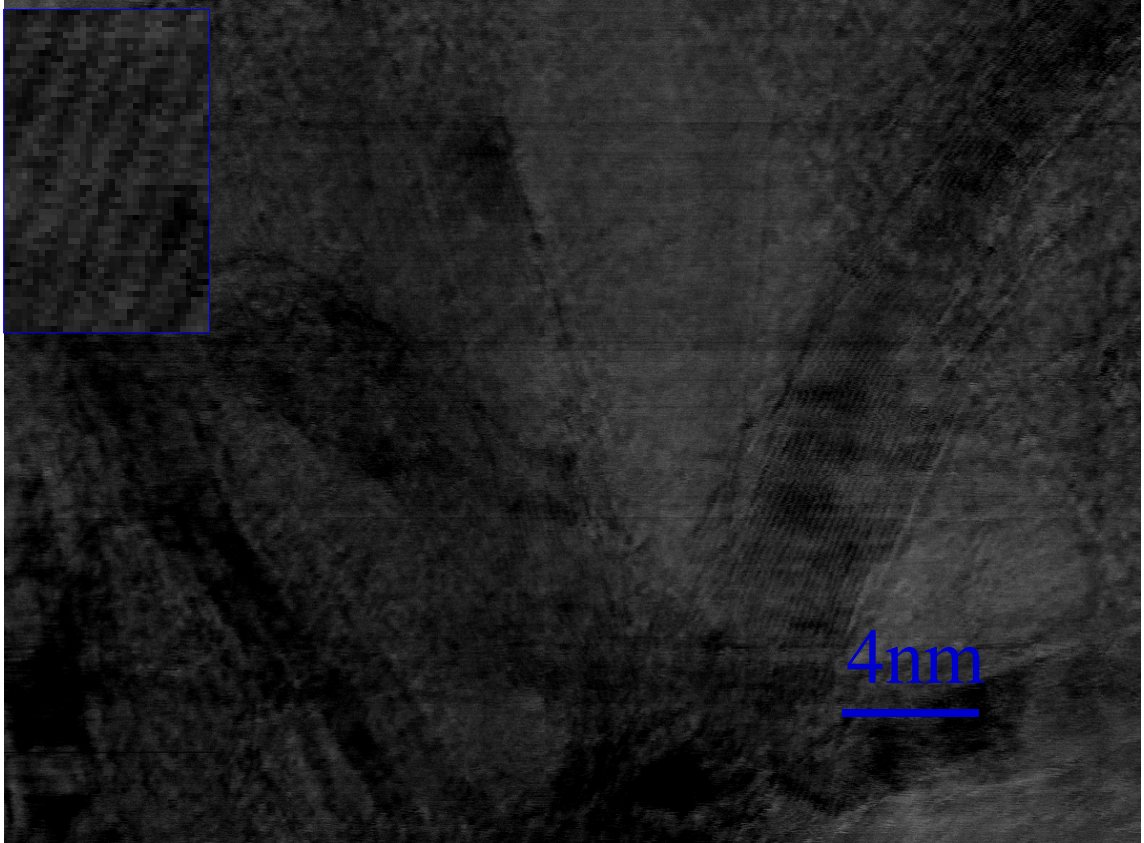


Figure 21. TEM image of the carbon matrix made with STEM in the ultrahigh resolution mode.

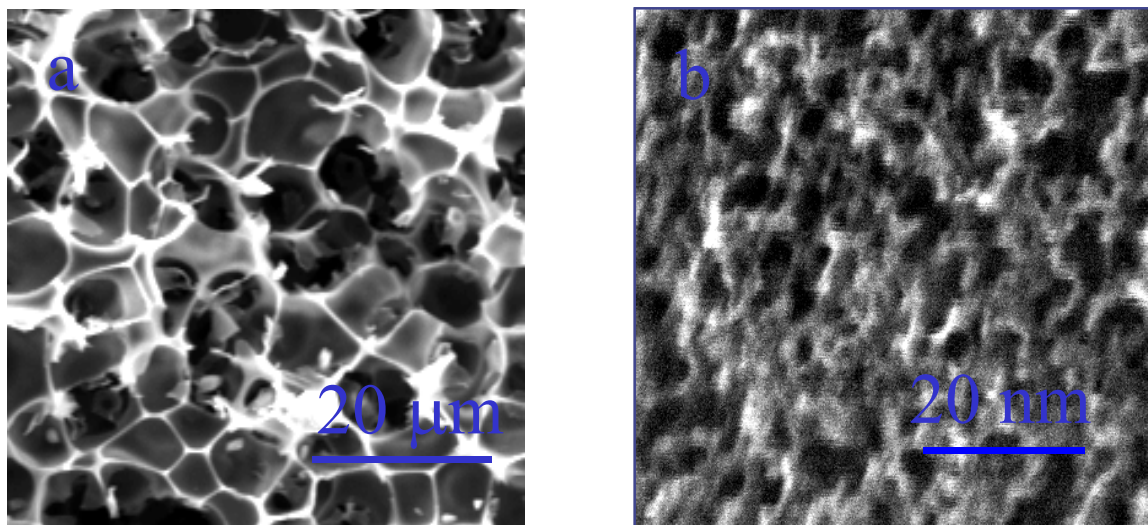


Figure 22 (A). SEM image of the macropore morphology. (B). STEM high resolution SEM image of the mesopores in the carbon skeleton.

causing an increase in the mesoporous volume. Figure 22 shows images of the mesopores and macropores. Figure 22A is a SEM image of the macropores that appears to have diameters between 5 and 10 μm . Figure 22B is a high resolution SEM image of mesopores on a macropore wall, taken by the STEM instrument.

The mesoporosity of the carbon monolith was further examined by measuring the BET nitrogen adsorption/desorption isotherm. Figure 23 shows the isotherm, which does not have the sharp condensation step that characterizes a narrow pore size distribution. The mesopores in the rod have a wide size distribution with irregular pore shapes (Figure 22B). Because the voids between graphite strips cannot be controlled, the pores between graphite strips can have any shape and size. The volume of micropores and mesopores derived from the BET isotherm were 0.0218 ml/g and 0.5229 ml/g respectively. The specific surface area attributed to the micropores and mesopores were 42.33 and 162.94 m^2/g , respectively.

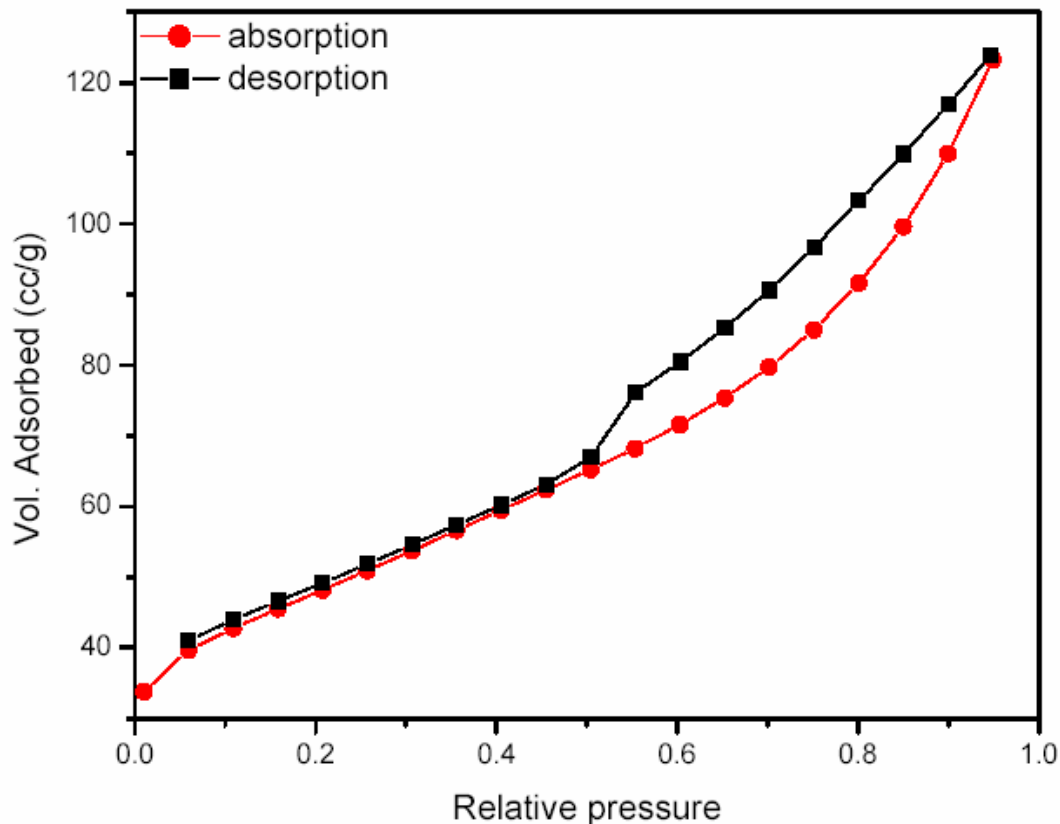


Figure 23. The nitrogen adsorption/desorption isotherm of the carbon monolith.

While the graphitization of the glassy carbon resulted in a significant shrinking of the material, there was no shrinking after carbonization of the precursor rod. In a control experiment, a polymer rod made without imbedded silica beads shrank after carbonization. The incorporation of silica beads seems to prevent shrinking. Assuming densities of 1.8 and 1.0 g/cm³ for the silica beads and the phenolic resin respectively, the approximate volume ratio of silica to polymer was about 1.3, meaning that the silica beads occupied a large fraction of the space in the rod. As suggested in Figure 20, the phenolic resin occupies the voids between the closely packed silica particles. During carbonization, the carbon formed remains in these spaces and shrinking is confined to

them, possibly causing the holes between macropores to open up more. The close-packed structure of the silica beads controls the overall dimension of the rod which is unaffected by the shrinking due to carbonization. Figure 22A shows that the macropores in the carbon monolith are a reproduction of the close-packed silica beads.

Carbon texture characterized by Raman spectra and X-Ray diffraction: Figure 21 reproduces a TEM image that suggests that the carbon monolith is woven by graphite strips. TEM can only reflect local information on the small areas viewed under microscopy. In order to obtain overall information on the carbon monolith, the carbon texture was studied by Raman spectroscopy and X-Ray diffraction. These methods average the signal coming from the whole carbon rod. Figure 24 compares the Raman spectra of the carbon monolith, of glassy carbon, and of commercial graphite. There are, in principle, two vibration modes in the plane of the hexagonal sheets of graphite that are active in Raman: the shear and the stretching modes. The shear mode is difficult to observe due to the broadening of its band caused by the lack of stacking order in graphite.

The stretching mode exhibits a useful peak at $ca. 1548\text{ cm}^{-1}$, which informs on the order of a carbon sample. This peak is called the G-line. In disordered carbon, the G-line is broadened and shifted to 1600 cm^{-1} . The action of broadening and shifting depends on the degree of disorder of a carbon sample. Another line, the D-line at $ca. 1354\text{ cm}^{-1}$, is also present in the spectrum of disordered carbon. This line is attributed to the A_{1g} mode, active in Raman due to the imperfection of the graphite. The ratio of intensities of G- and D-lines varies systematically with the orderliness of the graphite structure. As shown in Figure 24, the intensity ratio of the G- and D-lines is higher in commercial graphite than

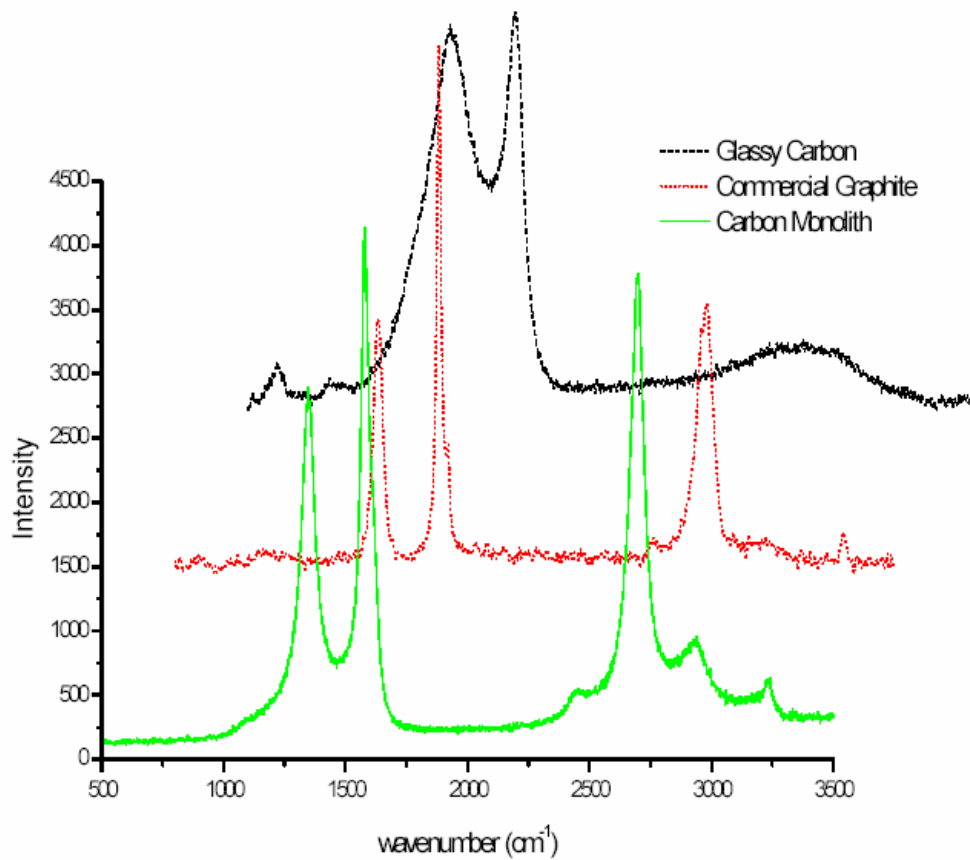


Figure 24. Raman spectra of the carbon monolith, glassy carbon, and commercial graphite.

in monolithic carbon and higher in monolithic carbon than in glassy carbon. The coherence length L_a can be derived from the intensity ratio of these two lines according to the Tuinstra--Koenig relationship.⁷⁴ The L_a value of the monolith is 16.5 nm, smaller than the value for commercial graphite, 31.7 nm. As mentioned above, the information conveyed by Raman spectrum is the average of the signals coming from the carbon illuminated by the laser beam. The carbon monolith is only partially graphitized, so the value derived for L_a is the average for the graphite strips and the glassy carbon grains.

The X-ray diffraction patterns of grounded samples of both commercial graphite and the carbon monolith are shown in Figure 25. The commercial graphite exhibits peaks corresponding to the planes (002), (100), and (004), located at 26.34, 43.01, and 53.86°, respectively. The carbon monolith has a few more peaks, which are attributed to residual metal iron and iron carbide. The (002) peak of the carbon monolith is noticeably broader and lower than that of commercial graphite. Moreover, its position in the carbon monolith is shifted slightly, to 26.05°, indicating that the interplanar d spacing of the carbon monolith is larger than that of commercial graphite. According to Bragg's law, the interplanar spacing is given by $d_{002} = \lambda/\sin\theta$, where λ is the wavelength of the incident X-ray beam. The copper K_α line is 1.541 Å. The calculated interplanar d spacing is 3.418 Å for the monolith and 3.382 Å for commercial graphite. The graphitization index is used to characterize the quantifiable degree of similarity between a carbon material and a perfect single crystal of graphite. The graphitization index is derived from the average interplanar spacing between two successive graphite layers, according to the equation:

$$g_p = \frac{3.440 - d_{002}}{3.440 - 3.354} \quad 4.2$$

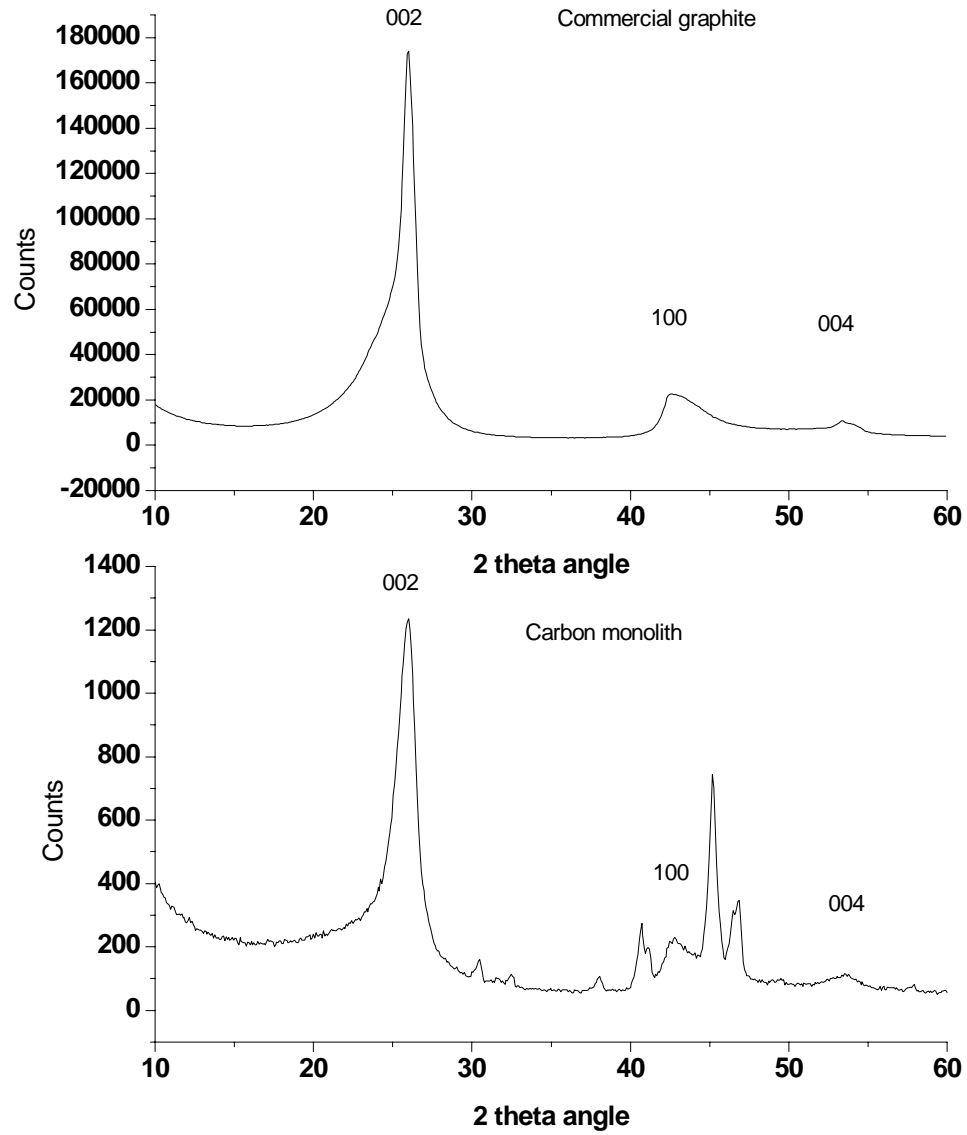


Figure 25. Powder X-ray diffraction patterns of the carbon monolith and of commercial graphite.

Using the d_{002} values reported above, the graphite indices for the carbon rod and for commercial graphite are 0.244 and 0.674, respectively. The low graphite index indicates that the structure of the carbon monolith is far more disorderly than that of commercial graphite.

In addition to its angle position, the width of the (002) peak provides information useful in estimating the average graphite grain size. Based on this peak width, the coherence lengths L_c and L_a can be estimated with the Debye-Scherrer equations:

$$L_c = k \lambda / \beta \cos\theta \quad 4.3$$

$$L_a = 1.84 k \lambda / \beta \cos\theta \quad 4.4$$

where k is the shape coefficient, λ is the wavelength of the incident beam, θ is the Bragg angle, and β the full width at the half maximum (FWHM). Usually, k is set to 1. The L_c and L_a values calculated for the carbon monolith were 10.3 and 19.0 nm, respectively. Note that the L_a value calculated by X-ray diffraction is slightly higher than the L_a value given by Raman. This minor difference arises from a systematic error between these two methods. With a shape coefficient of $k = 0.9$, the L_a would be 17.1 nm, quite close to the Raman value (16.5 nm). On the other hand, Raman microscopy examines only a small superficial area, 2 μm in diameter, which is illuminated by the laser beam, while X-ray diffraction averages the structural information over the whole bulk of the sample.

Chromatographic evaluation: Due to the strong adsorption of analytes on graphite, their elution on carbon columns is achieved with strong solvents. Usually, solvents such as methanol and acetonitrile are weak on graphite; dichloromethane is used most frequently.⁸ The carbon monolithic columns prepared as described above were

tested with pure dichloromethane as the mobile phase. As shown in Figure 26, the elution peak exhibits severe tailing and column efficiency is poor. The possible causes of band broadening and tailing on graphite are micropores, minerals, and halogen-, oxygen- and nitrogen-impurities located on the surface or at the edges of the graphite strips. Heating the carbon rod up to 1600 °C under a hydrogen stream could reduce the halogen-, oxygen-, nitrogen- containing groups on the graphite surface or edges. However, such a treatment did not improve the column performance, ruled out that source of the problem. Iron metal or its compounds may have an effect. Several minor peaks in the X-ray diffraction pattern indicate that the monolithic carbon rod has a small amount of residual iron particles and iron carbide. Since the residual iron particles are embedded in the graphite strips, they do not cause band broadening of the chromatographic peaks. However, the superficial iron carbide cannot be removed by acid washing and may remain on the graphite surface, causing the tailing of chromatographic peaks. Further investigations are planned to evaluate the possible effects of iron carbide on column performance.

A small amount of n-hexane in the mobile phase significantly improves column performance.^{75, 76} Figure 26 compares the peaks of toluene eluted with dichloromethane, with and without 1% of n-hexane. Nearly the same result is obtained with as little as 0.5% of n-hexane. A typical chromatogram for the separation of n-alkylbenzene mixture is shown in Figure 27. The mobile phase was a mixture of 30% methanol, 69% dichloromethane, and 1% n-hexane. The simple explanation is that the carbon rod still contains micropores, due to a partial leaching of iron metal and an incomplete

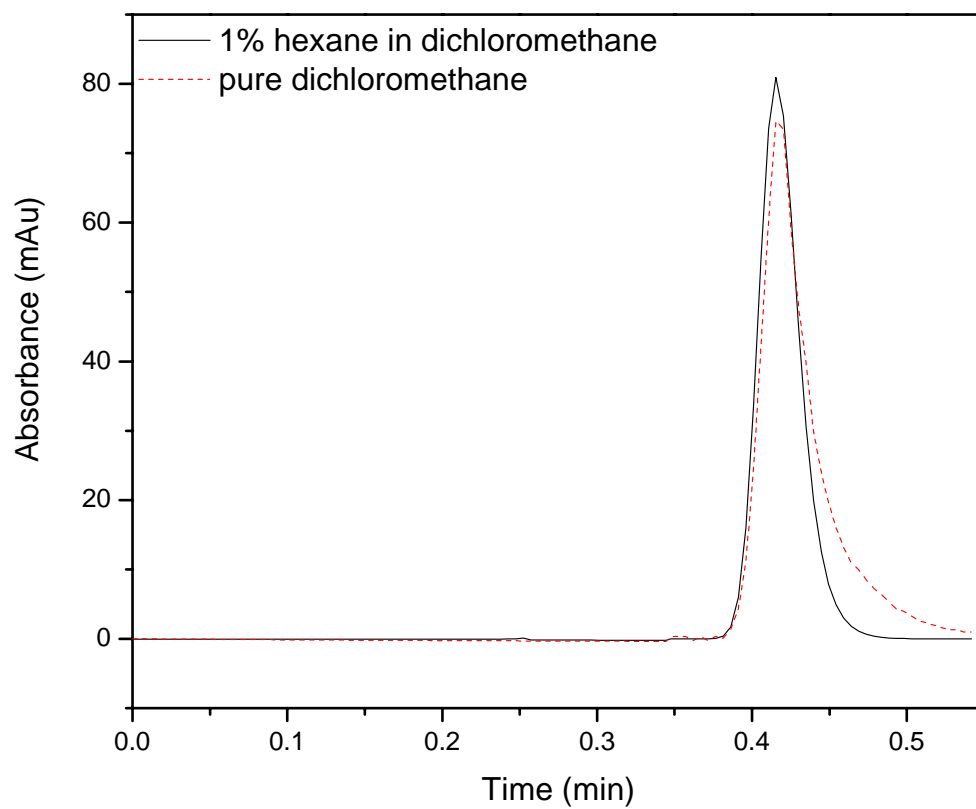


Figure 26. Elution of toluene in dichloromethane with and without 1% of n-hexane.

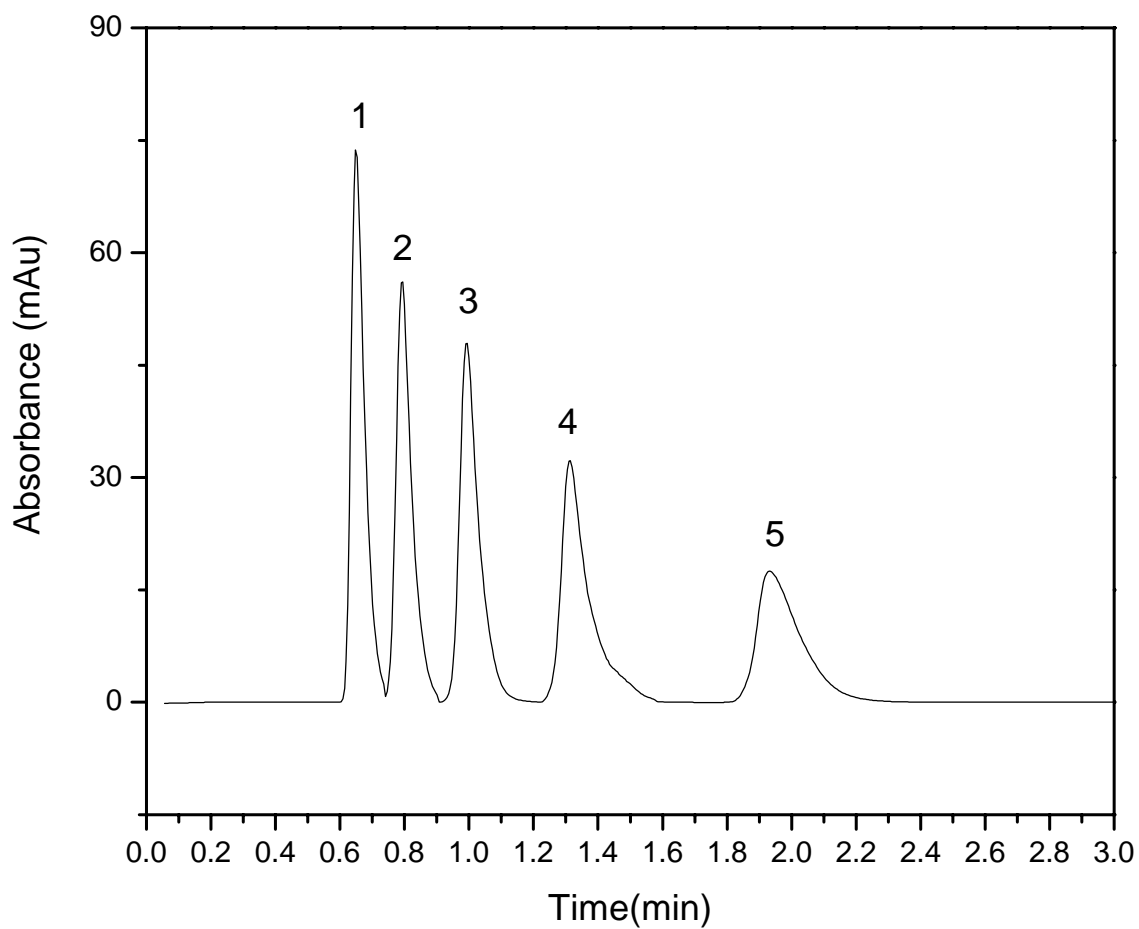


Figure 27. Chromatogram of five alkylbenzenes in a mobile phase made of methanol (30%), Dichloromethane (69%), and n-hexane (1%). The elution order is (1) toluene (k' , 0.10), (2) ethylbenzene (k' , 0.35), (3) propylbenzene (k' 0.72), (4) butylbenzene (k' 1.29), (5) amylbenzene.(k' 2.41).

crystallization of the carbon. Indeed, the BET nitrogen absorption/desorption demonstrated that the carbon monolith has a micropore volume of 0.0218 ml/g and a micropore specific surface area of 42.33 m²/g. Column performance is improved by adding n-hexane because the micropores are completely filled, or nearly so, with the alkane.

Figure 28 shows a plot of the column HETP for toluene in dichloromethane v. the mobile phase velocity. The experimental data were fitted to a simple Van Deemter equation. The best numerical values for A, B, and C were 70.17, 1.69, and 0.73 (length unit, 1 μm). The column had a minimum HEPT of 73.5 μm. The A term, which is the multipath term, is large because the macropore size is large. It is 5 times higher than for the Chromolith Performance (E.M. Merck, Darmstadt, Germany) silica column, a commercial rod column.⁵ The B term is within normal range. The C term is small, a benefit of the monolithic packing. Because the pore structure of monolithic columns provides a better communication between their networks of mesopores and macropores than that in conventional packed columns, mass transfer kinetics tends to be faster in monolithic columns than in particle columns. This may explain the small size of the C term. Thus, column efficiency decreases markedly less with increasing mobile phase velocity in rods than in particle beds, and consequently, monolith columns give better separations at high mobile velocity than particle beds.

Column Porosity: One remarkable property of monolithic columns is their high permeability, which allows their operation at high mobile phase velocity and the achievement of fast analyses. The porosity and permeability of carbon monolith columns

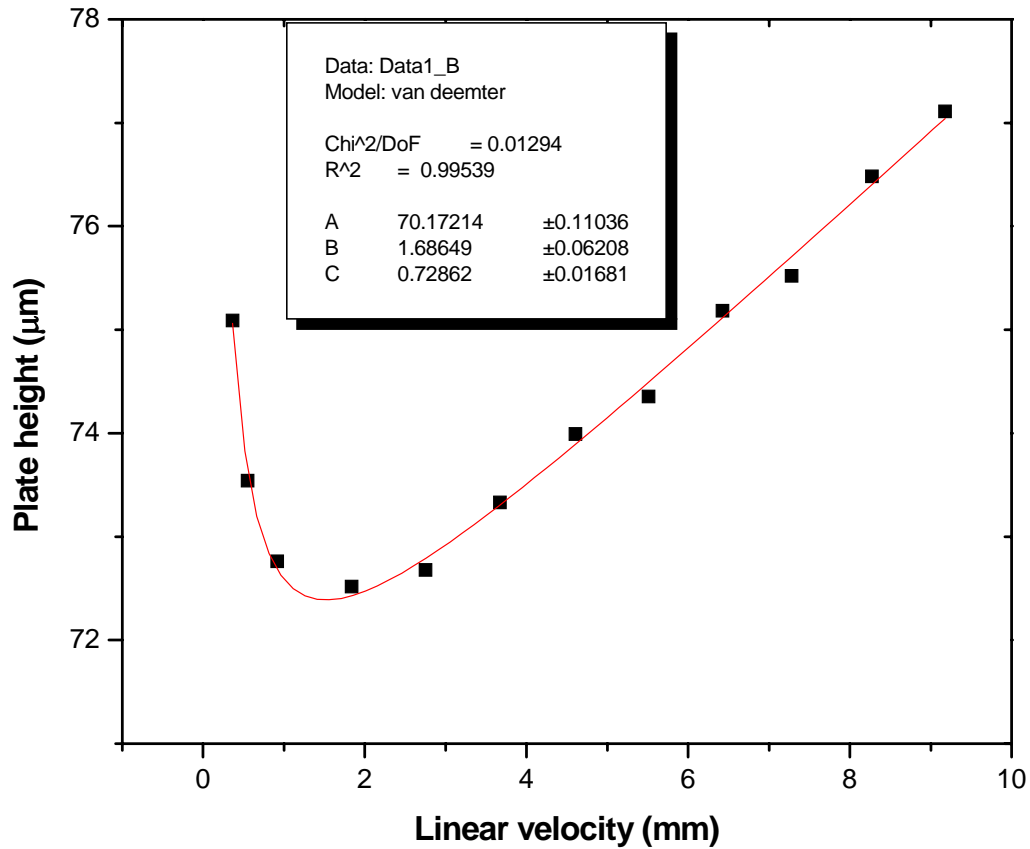


Figure 28. Van Deemter plot of the column HETP versus the linear velocity of the mobile phase. The data were obtained from the elution bands of toluene in 99% dichloromethane and 1% n-hexane (additive). The data were fitted to a simple Van Deemter equation, with A with A = 70.17, B = 1.69, and C = 0.73.

are high, even compared to those of silica monoliths. The lack of a non-retained compound makes it difficult to measure the total porosity directly; however, it can be estimated with reasonable accuracy. The internal porosity of the monolith carbon column has been measured by BET. The micropore and the mesopore volumes are 0.0218 and 0.5229 ml/g, respectively. The density of graphite of *ca.* 2.2 g/cm³ produces an internal porosity of *ca.* 0.545. Adjusting the quantity of silica beads in the initial rod can control the external porosity. A typical 80 x 3.4 mm rod weighs approximately 0.164 g. The total porosity derived from these figures is 0.897, leading to a value of about 0.325 for the external porosity. Merck Chromolith Performance columns have an internal porosity of *ca.* 0.631, an external porosity of *ca.* 0.229, and a total porosity of *ca.* 0.81.⁵

Column Permeability: The permeability of a column is given by the equation:

$$u = \frac{K_0 \Delta p}{\eta L} \quad 4.5$$

where u is the mobile phase flow velocity, K_0 the permeability of the column, Δp the pressure drop, η the viscosity of the mobile phase (0.33×10^{-2} Poise for pure hexane at 25°C), and L the column length. Figure 29 plots the pressure drop v. mobile phase linear velocity, proportional to F_v . Fitting the data to eq. 4.5 gives the value of 1.588×10^{-8} cm² for the specific permeability. The average permeability of six Chromolith Performance columns, measured with three different water/methanol mixtures, was 7.7×10^{-10} cm², or twenty times less. This means that the same flow rate could be obtained with the two types of rod columns, at the same head pressure, but with a mobile phase 20 times more viscous on the carbon rod than on the silica monolith. This is an important advantage because the elution of most analytes on graphitized carbon requires mobile phases that

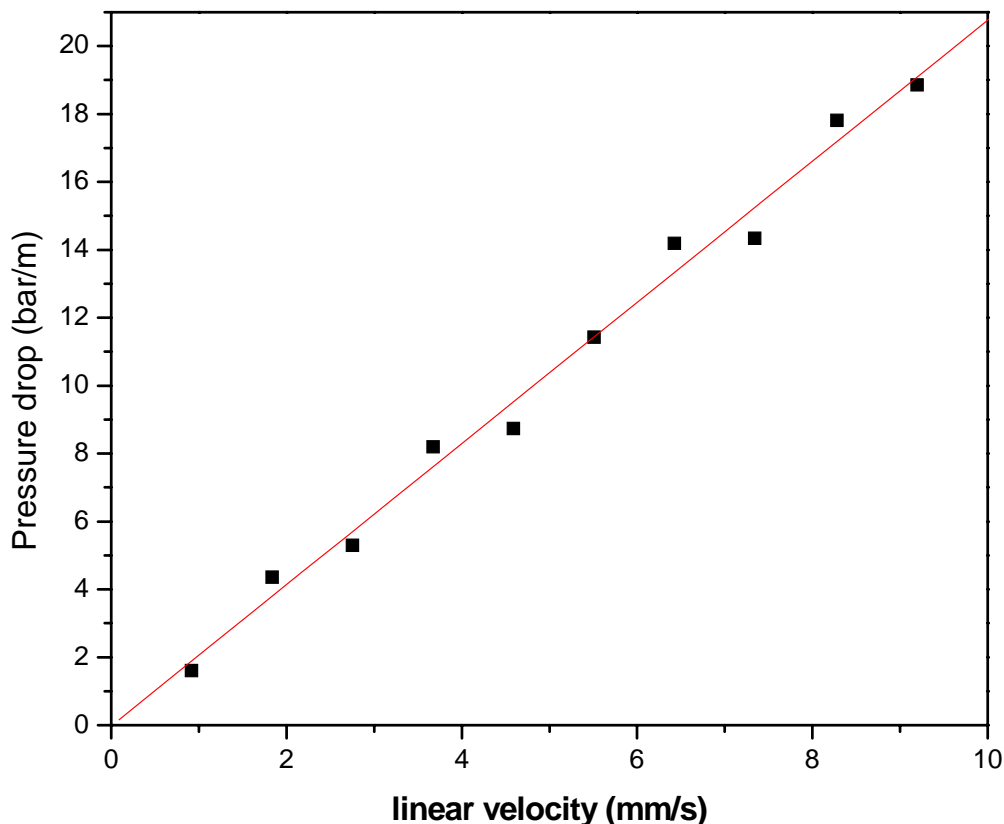


Figure 29. Plot of the pressure drop versus the mobile phase velocity (pure hexane as the mobile phase)

are more strongly polarized and have a higher molecular weight than the conventional eluents used in RPLC.⁷⁰

The bunch-of-capillary model allows a simple comparison of the permeabilities of monolithic and packed columns. This model assumes that the network of channels in packed-bed, or rod columns, is analogous to a bundle of parallel capillary tubes as long as the column. The number and diameter of capillaries in the bundle are specified by the conditions that the column and the bundle have the same void volume and that they deliver the same flow rate under the same inlet pressure. The application of the model

requires some further simplification due to the substantial differences in the constriction and tortuosity of the flow-through channels in the two types of columns. We assume that the constriction and tortuosity of the channels in the rod column are equal to unity. In the packed column, these factors will be taken into account by using the Darcy definition of permeability in porous media, proportional to the square of the packing particles.⁷⁵

Because the length of the column and of each capillary is equal, the equality between the volumes of the bundle and of the column requires the number of capillaries to be given by

$$n = \varepsilon \bullet r_{rod}^2 / r_c^2 \quad 4.6$$

where ε is the external porosity of the rod column, and r_{rod} and r_c are the radius of the carbon rod and the capillary, respectively. The flow rate through a capillary tube is given by the Hagen-Poiseuille equation:

$$F_v = \frac{\pi \Delta p r_c^4}{8L\eta} \quad 4.7$$

Hence, the total flow rate through the bundle of capillaries equivalent to the column is

$$F_v = \frac{\varepsilon \pi \Delta p r_c^2 r_{rod}^2}{8L\eta} \quad 4.8$$

From equation 4.8, we derive the average linear flow velocity of the mobile phase in the bundle of capillaries,

$$u = \frac{F_v}{\pi r_{rod}^2} = \frac{\varepsilon \Delta p r_c^2}{8L\eta} \quad 4.9$$

Combining eqs. 4.5 and 4.9 identifies a simple relationship between column permeability and channel size:

$$K_0 = \varepsilon r_c^2/8 \quad 4.10$$

Column permeability is proportional to its porosity and the square of the average macropore radius. Using the previous values of porosity and permeability for these columns, this equation furnishes values of 1.7 and 7.53 μm for the channel diameters of the Chromolith Performance silica monolithic column and for our carbon monolithic columns, respectively. Thus, the ratio of the column permeability of the carbon monolith to that of the silica monolith is about 20:1. The calculated channel size of the carbon rod is smaller than 10 μm , which is the diameter of the silica beads used as the templates for the macropores. This difference is due to a “bottleneck” effect caused by the small pore openings. After the silica beads are removed, the resulting spherical voids are connected through small windows that are enlarged during graphitization but remain narrower than the beads. The channel size derived from eq. 4.10 is a weighed average of the contributions of the spherical macropores and the connecting windows.

The A term in the Van Deemter equation keynotes the plate height of the column. Similarly to the particle columns, the A term of the monolithic columns is proportional to the channel size. The Chromolith Performance silica monolithic columns have an average channel size of 1.7 μm and their average A term is about 7.5 μm . Therefore, the ratio of A term to channel size is ca. 4.4. The same calculation has been done for the carbon monolithic columns; the ratio is ca. 9.3, which is 2 times greater than that of the silica monolithic columns. Due to the “bottleneck” effect, the channel irregularity of the carbon monolithic columns is larger than that of the silica monolithic columns. Consequently, the ratio of minimum HETP to channel size of carbon monolithic columns is larger than that

of silica ones by a factor of 2. The regularity of the channels in carbon monolithic columns can be improved either by packing the silica templates closely to enlarge the connecting windows among the spherical voids, or by using uniform silica beads as templates.

To compare a monolith and a conventional packed column, Kele and Guiochon⁵ derived a simple equation relating the capillary diameter and the equivalent particle size:

$$r_c = \sqrt{8k_0}d_p \quad 4.11$$

where k_0 is the permeability coefficient ($k_0 = 0.001$). For a channel diameter of $7.53 \mu\text{m}$, the equivalent particle size would be about $41.8 \mu\text{m}$. This explains why the carbon rod column has such an extremely low pressure drop (see Figure 29).

4.4 Conclusion

We were able to prepare a carbon monolithic column that exhibits useful chromatographic properties. This column is made of a partially graphitized, pyrolyzed phenolic resin. It has a bimodal porous structure. The flow-through channels consist of macropores approximately $10 \mu\text{m}$ in diameter connected through narrower, but quite significant, windows. The result is a column with high permeability, equivalent to that of a bundle of $7.5 \mu\text{m}$ capillary tubes. The pyrolyzed carbon has a total surface area of $205 \text{ m}^2/\text{g}$, ensuring significant retention in spite of high column porosity. Mesopores and micropores contribute to the surface area. The mesopores have a broad size distribution. The small quantity of micropores causes serious band broadening in pure dichloromethane, but the addition of a low concentration of n-hexane to the mobile phase considerably reduces the effect. Good separations of n-alkylbenzenes were achieved with

dichloromethane and methanol as the mobile phase, with 1% n-hexane as an additive. Column efficiency is moderate, with a minimum plate height of 73.5 μm , consistent with the large average size of the flow-through pores. However, the HETP increases slowly with increasing mobile phase velocity, indicating rapid mass transfer kinetics in the mesopores.

These results confirm that the procedure described is promising. The preparation of efficient graphitized carbon columns has been a goal tantalizing several research groups for some time because this adsorbent would effectively complement the stationary phases available in HPLC. The major obstacles were those encountered in this work: the formation of micropores and the preparation of highly efficient columns. Several obvious approaches could be followed to improve on our results. TEM analyses showed graphite strips that result from *in situ* catalytic graphitization of the pyrolyzed resin. The graphite index, however, is only 0.244, indicating partial graphitization. This explains the excessive amount of micropores, which could be reduced by increasing the yield of this last step in preparing of the columns. Using smaller beads would allow the preparation of more efficient, but less permeable, columns.

Finally, recent important advances have been made in electrochemically modulated liquid chromatography. It was proved that various separations can be modulated with the aid of electrochemistry.²³⁻²⁶ Modifications of the surface of the stationary phase in the column can be made online. A carbon monolithic column would provide a surface possessing more homogeneous electric properties than those of a packed column.

4.5 Problems to be solved

Though using silica particles can produce carbon monolithic columns with tunable porosities of both macropores and mesopores, the removal of silica particles is an inefficient process; it will be more expensive to manufacture carbon monolithic than particulate columns. Moreover, the bottleneck effect of spherical macropores is a serious obstacle for connectivity of the macropores. In next chapter, we describe a new method to address these two problems with the fabrication of carbon monolith via phase separation.

Chapter 5: Phase separation for the synthesis of carbon monolithic column with hierarchical structure

A method to produce porous carbon rods by using silica microspheres as templates was described in the previous chapter. The use of silica particles as templates in the synthetic method has an obvious advantage in that the pore sizes of the macropores are predetermined by the selection of the templates. The porosity of the rod is easy to control in this way. However, the removal of the templates is wasteful. The possible residue of templates seriously affects the properties and the reproducibility of the column. As pointed out in the previous chapter, the “bottleneck” effect of the spherical voids weakens the hydrodynamics of the monolithic column. These problems do not occur in silica columns prepared by a different synthetic approach, i.e., phase separation. In this chapter, we explore the utilization of phase separation in the synthesis of hierarchically structured porous carbon rods. The carbon rods synthesized in this process are made from porous polymer rod precursors; the phase separation happens during the preparation of the polymer rod.

5.1 Background of phase separation

Phase separation is a well-established method for the synthesis of macroporous polymers with pore size and distribution in the low μm -range.⁷⁷ To induce phase separation in the polymer system, two basic methods have been developed. One is

thermally induced phase separation (TIPS), and the other is chemically induced phase separation (CIPS).

Thermally induced phase separation is carried out in a polymer solution in which the phase diagram exhibits an upper critical solution temperature. The polymer forms a homogeneous solution when it has been heated to the upper critical solution temperature. The homogeneous solution can be induced to phase separation by thermal quench to fall into the binodal or spinodal line, thus resulting in a two-phase morphology. Depending on the quench rate and the composition, phase separation occurs either through nucleation and growth, or via spinodal decomposition. Complete knowledge of the phase diagram, kinetics, and thermodynamics is required for control of the phase separation system. A good example of the thermally induced phase separation is the synthesis of polystyrene foam.⁷⁸ The solution of polystyrene in cyclohexane was heated to above the upper critical solution temperature and then thermally quenched to produce polystyrene foam with a density as low as 0.02 g/cm^3 .^{78, 79} Due to the limits of thermal exchange, thermal induced phase separation is only suitable for the preparation of thin films, where a fast thermal transfer from the heated solution to the environment can be achieved.

Chemically induced phase separation is also called polymerization induced phase separation.⁸⁰⁻⁸⁴ To carry out the chemically induced phase separation, the reactive precursor(s) is mixed with the non-reactive low molecular weight or oligomeric solvent(s). The selection of the solvent or mixture of solvents is very crucial, as a moderate solvent is required for the reactive precursors to give a homogeneous solution in the initial stage and be an immiscible solvent for the polymerized reactive precursors

to obtain a phase separated final morphology. Unlike the thermally induced phase separation that develops in a very rapid thermal quenching process, chemically induced phase separation is a relatively slow process in which the phase separation develops progressively during the polymerization of the precursor. The growth or cross-linking of the polymer chains results in the immiscibility of the cured polymer and the non-reactive solvents. Consequently, the initial solvent becomes a non-solvent in liquid droplets to form a secondary phase, which eventually forms voids for the cured porous polymer. A general strategy is shown in Figure 30.⁷⁷ The secondary phase should be volatile, extractable, or decomposable to form the voids. The polymer phase should be rigid to hold the pores after the removal of the secondary phase. When the polymer is used as a precursor for the monolithic carbon column, neither the collapse of the pores nor the cracking of the entire bulk material should occur.

The chemically induced phase separation is less understood than thermally induced phase separation due to the theoretical complexity of this method. Nonetheless, chemically induced phase separation has been widely utilized in the preparation of porous polymers in forms from of thin films to large chunks.

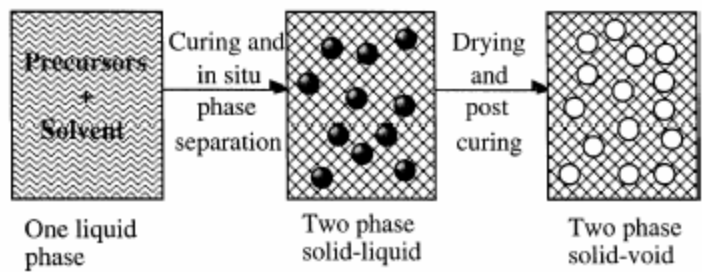


Figure 30. General strategy for chemically induced phase separation.

5.2 Theory of phase separation

The theory of phase separation is based on the thermodynamics of the mixing system. These theoretical guidelines considerably simplify the practice of phase separation. In the following sections, these guidelines are summarized.

5.2.1 Thermodynamics of phase separation and Flory-Huggins theory⁸⁵

Thermodynamically, phase separation results from a change in the free energy of the mixing system, ΔG . Any mixing system falls into one of three types of free energy (ΔG) v. composition (Φ) curves. These three types of free energy curves are presented schematically in Figure 31 as lines a, b, and c.

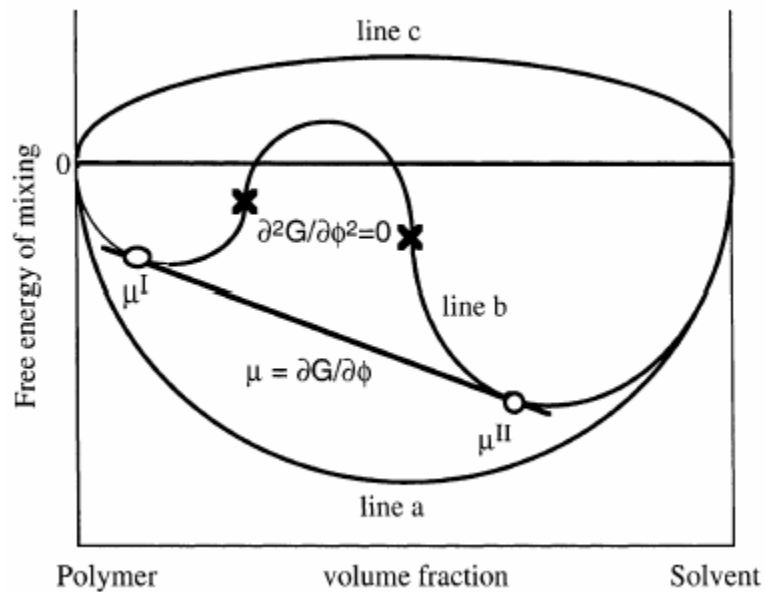


Figure 31. Schematic representation of free energy curves.

When two components are completely miscible, the free energy is negative in the entire composition range, which is indicated by line a. No phase separation occurs in the miscible system. When the components are totally immiscible at any composition ratio, the free energy curve is represented by line c, in which free energy is always positive. In this case the two components always exist in two separated phases. When the free energy curve is between lines a and c, the free energy change has two minima and one maximum and inflection points as shown in line b.

The two inflection points are given by the vanishing of the second derivative of free energy change with respect to the composition ratio as indicated by equation 5.1.

$$\frac{\partial^2 \Delta G}{\partial \phi^2} = 0 \quad 5.1$$

When the composition is between the two inflection points, the homogeneous system spontaneously decomposes into two phases (denoted as phase I and II). The two components decompose in two individual phases through up-hill diffusion against the concentration gradient. This decomposition is known as spinodal decomposition.

At the point of equilibrium, the chemical potentials of each component should be equal at both phases. For example, the potential chemical equilibrium of a polymer/solvent system can be expressed by equations 5.2 and 5.3.

$$u_{pol}^I = u_{pol}^{II} \quad 5.2$$

$$u_{sol}^I = u_{sol}^{II} \quad 5.3$$

When the two points of the free energy curve have a common tangent, the thermodynamic conditions of these two points are equal. The polymer enriched and the

solvent enriched phases can coexist in the system. The portion of the free energy curve between these two points is called the binodal line.

The free energy change is expressed by the Gibbs equation:

$$\Delta G = \Delta H - T\Delta S \quad 5.4$$

Any change in enthalpy or entropy will result in a change in free energy. The changes in enthalpy and entropy in a polymer/solvent system have been calculated independently by Flory and Huggins, using the lattice model.⁸⁵⁻⁸⁹ According to the lattice model, the entropic change of polymer/solvent mixing is given by equation 5.5.

$$\Delta S = -R(n_{pol} \cdot \ln \phi_{pol} + n_{sol} \cdot \ln \phi_{sol}) \quad 5.5$$

where R is the gas constant, n_{pol} and n_{sol} are the molar numbers of polymer and solvent, and ϕ_{pol} and ϕ_{sol} are the volume fraction of the polymer and the solvent. The change in enthalpy is expressed by equation 5.6

$$\Delta H = RT \cdot \chi \cdot n_{sol} \cdot \phi_{pol} \quad 5.6$$

where χ is the interaction parameter, which indicates interactions between the polymer and the solvent molecules. The Flory-Huggins equation 5.7 is the combination of equations 5.5 and 5.6

$$\Delta G = RT(n_{pol} \cdot \ln \phi_{pol} + n_{sol} \cdot \ln \phi_{sol} + \chi \cdot n_{sol} \cdot \phi_{pol}) \quad 5.7$$

According to the Flory-Huggins equation, the free energy change in the polymer/solvent mixing system is dependent on the temperature, composition and interaction between the polymer and solvent.^{90, 91} Using the Flory-Huggins equation, one can reconstruct the phase diagram to represent the phase separation process.

5.2.2 Thermally induced phase separation⁸⁹

Thermally induced phase separation is based on the fact that the interaction parameter χ depends on the temperature T . Within a certain temperature range, χ is proportional to the inverse of T (equation 5.8).

$$\chi = a + \frac{b}{T} \quad 5.8$$

where a and b are two parameters that depend on the nature of the polymer and the solvent. When b is positive, the mixing system has an upper critical solution temperature (UCST). When b is negative, the mixing system is characterized by a lower critical solution temperature (LCST). These two types of phase separation systems are schematically represented in Figures 32 A and B.⁹²

Both systems are widely used in the preparation of porous polymer films. Since the phase separation behavior of these systems depends on the temperature, the thermal exchange rate is crucial for the final morphology. In practice, since it is impossible to

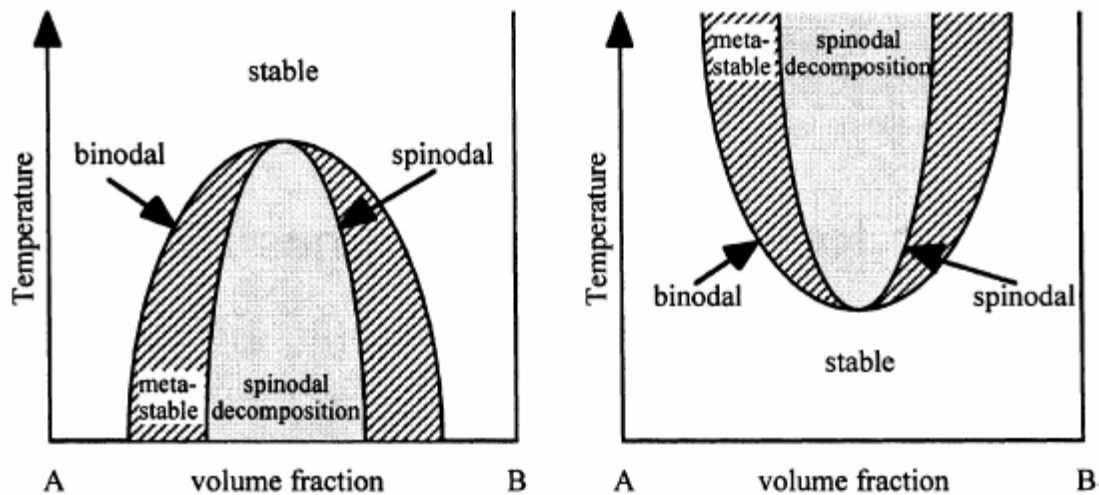


Figure 32. Phase diagrams of (A) UCST system and (B) LCST system.

achieve thermal homogeneity in bulk materials with a fast thermal quench rate, thermally induced phase separation is not suitable for the preparation of large chunk materials.

5.2.3 Chemically induced phase separation⁹³⁻¹⁰²

The theoretical treatment of the chemically induced phase separation is much more complex than the thermally induced phase separation. In chemically induced phase separation, entropy decreases when the monomers start to polymerize. Consequently, the molar fraction of the polymer decreases rapidly with the growth of the molecular weight. Hence, entropy changes progressively with the growth of the polymer chain length. The phase separation is induced when the free energy curve becomes a line b type.

The theoretical treatment of chemically induced phase separation is also based on the lattice model, where the volume change has been taken into account. The total volume of the mixing system is denoted as V_T , which is provided by equation 5.9, the sum of the volume of polymer and solution.

$$V_T = n_{pol} \cdot V_{pol} + n_{sol} \cdot V_{sol} \quad 5.9$$

Then the volume fractions of the polymer and solution are:

$$\phi_{pol} = \frac{n_{pol} \cdot V_{pol}}{V_T} \quad 5.10$$

$$\phi_{sol} = \frac{n_{sol} \cdot V_{sol}}{V_T} \quad 5.11$$

Combining equation 5.5 and 5.9 to 5.11 results in entropy change per unit volume ΔS^V .

$$\Delta S^V = \frac{\Delta S}{V_T} = -R \left(\frac{\phi_{pol}}{V_{pol}} \cdot \ln \phi_{pol} + \frac{\phi_{sol}}{V_{sol}} \cdot \ln \phi_{sol} \right) \quad 5.12$$

In the lattice model, the molar volume of the precursor V_0 is used as the reference volume to rationalize the lattice model. By definition,

$$\frac{V_{pol}}{V_0} = \frac{\overline{M}_n}{\overline{M}_{n0}} \quad 5.13$$

where, \overline{M}_n and \overline{M}_{n0} are the average molecular weight of the polymer and monomer. For bifunctional cross-linking systems, the molecular weight is related to the conversion q of the polymerization by equation 5.14.

$$\frac{\overline{M}_n}{\overline{M}_{n0}} = \frac{1}{1 - \frac{4}{3}q} \quad 5.14$$

Combining equation 5.12, 5.13, and 5.14 gives,

$$\Delta S^V = \frac{R}{V_0} \left[\left(1 - \frac{4}{3}q\right) \phi_{pol} \cdot \ln \phi_{pol} + \frac{\phi_{sol} \cdot V_0}{V_{sol}} \cdot \ln \phi_{sol} \right] \quad 5.15$$

After the same treatment in enthalpy, the volume free energy change can be expressed by equation 5.16.

$$\Delta G^V = \frac{\Delta G}{V_T} = \frac{RT}{V_0} \left[\left(1 - \frac{4}{3}q\right) \phi_{pol} \cdot \ln \phi_{pol} + \frac{\phi_{sol} \cdot V_0}{V_{sol}} \cdot \ln \phi_{sol} + \chi \cdot \phi_{pol} \cdot \phi_{sol} \right] \quad 5.16$$

Thus, the free energy change is a function of the conversion of the polymerization q , the temperature T , the composition Φ , and the interaction parameter χ .

The interaction parameter χ depends on the conversion q and the solubility parameter δ . The solubility parameter is contributed by the polar δ_p , hydrogen bond δ_h , and the dispersive force δ_d . The difference between the solubility parameter of the polymer and the solvent can then be expressed as,

$$|\vec{d}| = \sqrt{(\delta_d^{pol} - \delta_d^{sol})^2 + (\delta_p^{pol} - \delta_p^{sol})^2 + (\delta_h^{pol} - \delta_h^{sol})^2} \quad 5.17$$

When the polymerization occurs, the solubility parameter difference $|\vec{d}|$ is a

function of conversion q , which is denoted as $|\vec{d}(q)|$. $\vec{d}(q)$ can be formulated as,

$$|\vec{d}(q)| = \begin{bmatrix} \delta_d^{unreact} + q(\delta_d^{react} - \delta_d^{unreact}) - \delta_d^{sol} \\ \delta_p^{unreact} + q(\delta_p^{react} - \delta_p^{unreact}) - \delta_p^{sol} \\ \delta_h^{unreact} + q(\delta_h^{react} - \delta_h^{unreact}) - \delta_h^{sol} \end{bmatrix} \quad 5.18$$

Assuming the change in the solubility parameter of the polymer is linear with the conversion q , the interaction parameter χ can be expressed as a function of the conversion q :

$$\chi = \frac{V_0}{RT} |\vec{d}(q)|^2 \quad 5.19$$

Substituting the χ in equation 5.16 by equation 5.19 gives

$$\Delta G^V = \frac{\Delta G}{V_T} = \frac{RT}{V_0} \left[\left(1 - \frac{4}{3}q\right) \phi_{pol} \cdot \ln \phi_{pol} + \frac{\phi_{sol} \cdot V_0}{V_{sol}} \cdot \ln \phi_{sol} \right] + |\vec{d}(q)|^2 \cdot \phi_{pol} \cdot \phi_{sol} \quad 5.20$$

The free energy change is a function of temperature T , conversion q , and composition Φ . Equation 5.20 is the fundamental equation of the chemically induced phase separation. In the same way as the thermally induced phase separation, the phase diagram of the phase separation can be reconstructed by using equation 5.20. Shown in Figure 33 is a reconstructed phase diagram of chemically induced phase separation as a function of conversion and composition.

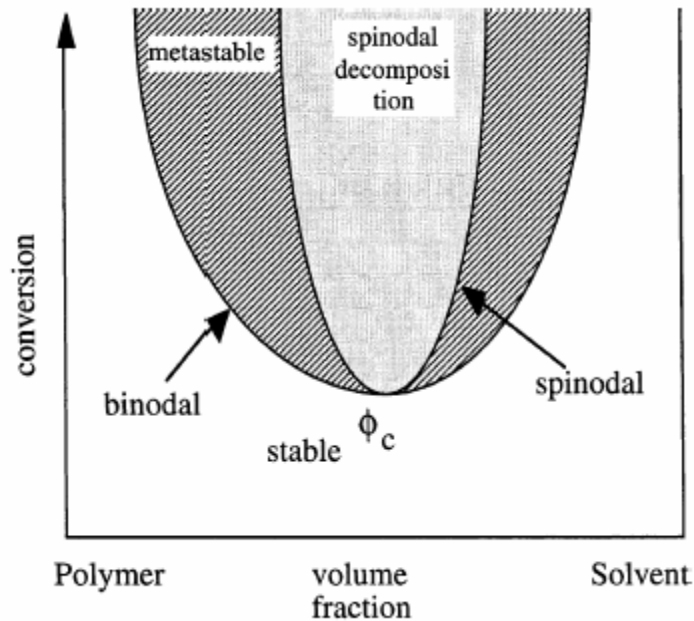


Figure 33. Reconstructed phase diagram of chemically induced phase separation as a function of conversion and composition.⁷⁷

Although in an actual synthetic case the morphology is also affected by the viscosity and the kinetics of the system, the schematically shown phase diagram of the chemically induced phase separation is of particular importance for guiding the morphologic synthesis of porous polymers. Figure 34 shows various strategies of synthesizing different morphologies based on the phase diagram. Spherical particles, co-continuous and isolated pores can be synthesized based on the ratio of the starting materials.

5.3 The dual phase separation in the ternary mixing system

The ternary mixing system is far more complicated than the binary system. Fortunately, the principles of the binary system can be applied to the phase separation of

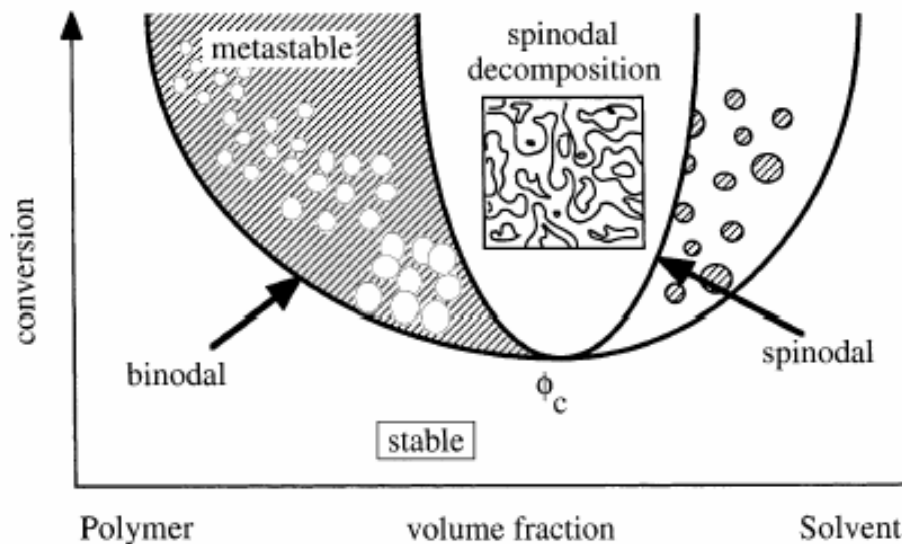


Figure 34. Morphologies corresponding to different phase diagram zones.⁷⁷

any two components of the ternary system. Thus the phase separation in the ternary system can be simplified as two consecutive binary phase separations. By careful selection of the components, two tandem phase separation processes can occur in a ternary system. A complicated hierarchically porous structure can be constructed by using the ternary system. The schematic representation of the dual phase separation in a ternary system is shown in the Figure 35.

5.4 Experimental

Chemicals: Ethylene glycol, diethylene glycol, triethylene glycol, p-toluene sulfonic acid, and furfural alcohol were purchased from Aldrich; Triblock polymer with the commercial name of P123, and P127 were gifts from BASF Corp. Ethanol was purchased from ORNL storage. DI water was obtained from the lab pipeline.

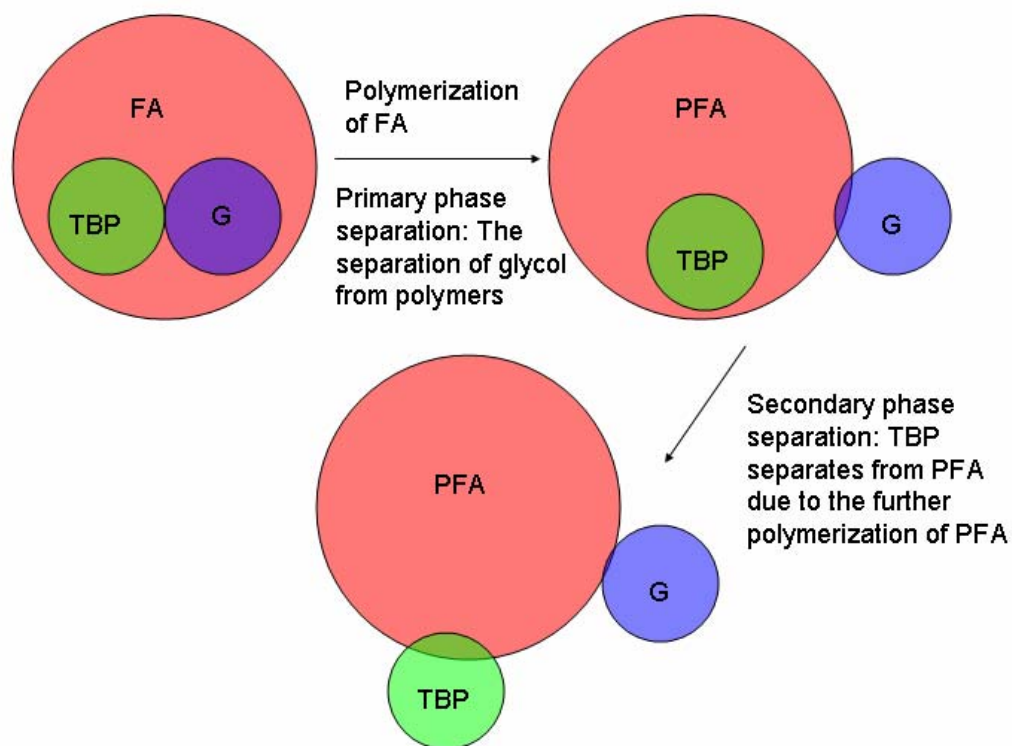


Figure 35. Schematic representation of the dual separation in a ternary system. FA is the furfural alcohol; PFA is the poly(furfural alcohol); TBP is the triblock polymer, which contains three blocks of polymer chains; and G is a glycol solvent.

Instruments: A homemade water bath was employed for the control of the curing temperature of the polymer. The water bath consisted of a water circulator, a water jacket chamber, a heating unit, and a programmable temperature control unit. To achieve precise control of the temperature, the thermometer was calibrated before use, and the sensitivity of the temperature probe was set to 0.1°C. The heating rates were controlled in the range of 0 to 30 °C/hour by a programmable temperature control unit. A Philip XL30FEG scanning electron microscopy (SEM) was used for the characterization of the macroporous morphology. An HD 2000 thin film evaluation system was used for imaging the mesopores. The porosity and surface area was measured by a Micromeritics Gemini 128 system.

The synthesis of polymer rods: The ternary system consists of three main components and a catalyst: furfural alcohol was the reactive monomer; a triblock polymer was used as the secondary phase separation agent; glycol solvent was used as the primary phase separation agent; and *p*-toluene sulfonic acid was the catalyst. Since the morphologies depend on the composition of the starting mixture, a general procedure for the preparation of the polymer rods is specified here. The details of the recipes and their corresponding morphologies are presented in the results and discussion section. In a typical synthesis, 5 g furfural alcohol was mixed with 5 g P123 by magnetic stirring; 0.8 g *p*-toluene sulfonic acid was dissolved in 10 g diethylene glycol. The *p*-toluene sulfonic acid diethylene glycol solution was then added to the furfural alcohol/P123 mixture in three portions. The mixture was then stored overnight at room temperature. The pale yellow color of the starting mixture turned to deep dark brown. The mixture was cast into

a cylindrical tube and was degassed by connecting to the lab vacuum line, which is approximately 30 mmHg. After degassing, the tube was capped and settled in the water bath chamber. The heating was programmed as a heating ramp at 10 °C/hour to 70 °C and then resting at 70 °C for 10 hours. The cured polymer was removed from the tube by opening both ends of the tube and blowing the polymer rod out of the tube via a compressed air line. The polymer rods were washed with DI water and then dried in a vacuum oven at 100 °C.

Carbonization: the polymer rods were placed into a tubular furnace and purged with N₂ (30 ml/min). Each polymer rod was contained in a quartz tube, which is only slightly larger than the rod. The quartz tube prevents the polymer rod from bending during the carbonization. The temperature was ramped to 850 °C at 2°C/min and then kept at 850 °C for 2 hours to ensure complete carbonization. Afterward, the furnace was allowed to cool naturally to ambient temperature. The carbon rods were graphitized in a high temperature furnace at 2800 °C. Unfortunately, graphitization causes serious bending of carbon rods; bent graphitized carbon rods cannot be encased under the conditions of our experiment.

Characterization: SEM images were taken with the Philip XL 30 at 15 kv electron accelerating voltage. A piece of carbon rod was mounted on the SEM sample and held by with a carbon tape. No additional conductive coating was applied to the carbon sample. The STEM images of the mesopores were taken by an HD 2000 thin film evaluation system. A piece of crashed carbon sample was dispersed in acetone solution using an ultrasonic stir. A drop of the suspension was applied to a TEM grid. The grid

was dried in the vacuum oven at 100 °C to completely remove the solvent. The grid was loaded into the HD 2000 system and observed at an electron accelerating voltage of 200 kv. The BET measurement was carried out in a Micromeritics Gemini 128 system. A piece of weighed carbon rod was loaded into a sample tube and N₂ adsorption/desorption at liquid nitrogen temperature was then performed. The software that comes with the instrument calculated the pore size distribution and the surface area.

Cladding: The carbon rods were clad into HPLC columns using the polymer lined stainless steel tube encasing or polymer coating. See Chapters 2 and 4 for the cladding procedure.

HPLC testing is detailed in Chapter 7.

5.5 Results and discussion

5.5.1 The composition of the ternary system

In a ternary system, if one or two components are polymerizable, the polymerization induced phase separation occurs under certain conditions. The phase separation occurs in three types depending on the number of reactive components and the interaction between each component. The three types of phase separation are: (1) one component separated from the homogeneous mixture of the other two components; (2) these three components separated from each other consecutively; (3) the three components separated from each other simultaneously. Type 1 phase can be treated as a binary system. Phase behavior can be predicted by the Flory-Huggins theory. Type 2 phase separation results in hierarchical morphologies in two discrete length scales. A bimodal porous morphology can be achieved using type 2 phase separation at suitable

conditions. Type 3 phase separation produces complicated morphologies in a broad size distribution. A broad pore size distribution is not favorable in the HPLC column. Therefore, type 3 phase separation should be avoided in the synthesis of the porous materials.

If two reactive components co-exist in the ternary system, phase separation is determined by the reaction rates of each component, the interactions between the two polymerized components, and the interaction between the resulting polymer and solvent. The morphologies of the resulting polymer are highly sensitive to the initial composition and the reactivity of the two reactive components. The control of the final morphology is empirical. If there is only one reactive component in the ternary system, the polymerization situation is simpler than the two reactive components system. Although phase separation still occurs in the above three forms, the final morphology of one reactive component system is less sensitive to the reactivity of the reactive component than that of the two reactive components system.

To simplify the ternary system, we use one reactive component to induce the type 2 phase separation in a ternary system. The selection of the components is based on three rules. First, the initial mixture is homogeneous solution. Second, the resulting polymeric structure can be carbonized with carbon yield greater than 30%; although many hierarchically polymeric structures can be produced by phase separation, only a few of them can be carbonized. Third, according to equation 5.16, during the polymerization of the reactive monomer, the component with a small interaction parameter χ separates from the system before the component with a large χ . Consecutive phase separation can only

occur in a system where the interaction parameters of the non-reactive components are significantly different. Fourth, the interaction between the two non-reactive components should be as small as possible to avoid cross interference between the two consecutive phase separations. Fifth, the non-reactive components should be extractable or thermally decomposable.

In this research, furfural alcohol was chosen as the reactive monomer. The poly(furfural alcohol) is a good carbon precursor, retaining the porous structure after the carbonization. The two non-reactive components are glycolic solvents and triblock polymers in the form of $\text{PEO}_x\text{-PPO}_y\text{-PEO}_x$. The glycolic solvents are immiscible with the PEO-PPO-PEO triblock polymers. Thus, the cross interference between the two phase separations is minimized. A homogeneous solution can be achieved by adding the furfural alcohol to the mixture of the glycolic solvents and the triblock polymer. The polymerization is catalyzed by *p*-toluene sulfonic acid; *p*-toluene sulfonic acid is miscible with all three components in the ternary system. The composition and the resulting morphologies are presented in Table 2.

5.5.2 Primary phase separation and the control of macropore properties

The macropores occur during the primary phase separation. In the initial stage, the glycol solvents are immiscible with the triblock polymers. The monomer is a good solvent to both the glycol solvents and the triblock polymers. As presented in Figure 35, the furfural alcohol dissolves the glycol solvent and the triblock polymer at the beginning of the phase separation. In the ternary system, the component with the smallest

Table 2 The micro-structure of carbon samples as a function of composition

Sample #	EG	DEG	TEG	P103	P108	L121	P123	P127	<i>p</i> -TSA	FA	Mac size	Mes size	Morphology
PS1	5.0	-	-	-	-	-	-	-	0.4	5.0	-	-	Spherical particles ~1.5 μ m
PS2	-	5.0	-	-	-	-	-	-	0.4	5.0	-	-	Spherical particles ~1.8 μ m
PS3	-	-	5.0	-	-	-	-	-	0.4	5.0	0.5	-	Co-continuous
PS4	2.5	2.5	-	-	-	-	-	-	0.4	5.0	5.0	-	Coarse co-continuous
PS5	-	2.5	2.5	-	-	-	-	-	0.4	5.0	3.0	-	Co-continuous
PS6	5.0	-	-	2.5	-	-	-	-	0.4	2.5	5.0	0.007	Co-continuous, hierarchical
PS7	5.0	-	-	-	2.5	-	-	-	0.4	2.5	-	0.011	Spherical particles ~1.0 μ m
PS8	5.0	-	-	-	-	2.5	-	-	0.4	2.5	1.2	0.008	Co-continuous, hierarchical
PS9	5.0	-	-	-	-	-	2.5	-	0.4	2.5	2.5	0.010	Co-continuous, hierarchical structure with spherical grains, homogeneous grains ~ 2 μ m

Table 2 Continued

PS10	5.0	-	-	-	-	-	-	2.5	0.4	2.5	-	0.021	Spherical particles ~ 1.5 μm
PS11	-	5.0	-	2.5	-	-	-	-	0.4	2.5	1.5	0.007	Co-continuous, hierarchical
PS12	-	5.0	-	-	2.5	-	-	-	0.4	2.5	-	0.010	Spherical particles ~1.5 μm
PS13	-	5.0	-	-	-	2.5	-	-	0.4	2.5	5.0	0.009	Co-continuous, hierarchical
PS14	-	5.0	-	-	-	-	2.5	-	0.4	2.5	3.0	0.012	Co-continuous, hierarchical
PS15	-	5.0	-	-	-	-	-	2.5	0.4	2.5	5.0	0.015	Co-continuous, hierarchical
PS16	-	-	5.0	2.5	-	-	-	-	0.4	2.5	2.0	0.006	Co-continuous, hierarchical
PS17	-	-	5.0	-	2.5	-	-	-	0.4	2.5	18.5	0.011	Co-continuous, hierarchical
PS18	-	-	5.0	-	-	2.5	-	-	0.4	2.5	2.5	0.009	Co-continuous, hierarchical
PS19	-	-	5.0	-	-	-	2.5	-	0.4	2.5	3.5	0.011	Co-continuous, hierarchical
PS20	-	-	5.0	-	-	-	-	2.5	0.4	2.5	10.0	-	Co-continuous, hierarchical, fine particle grains with average size of ~0.8 μm
PS21	-	-	-	5.0	-	-	-	-	0.4	5	-	-	Fine particles ~0.5 μm

Table 2 Continued

PS22	-	-	-	-	5.0	-	-	-	0.4	5.0	-	-	Fine particles ~0.7 μm
PS23	-	-	-	-	-	5.0	-	-	0.4	5.0	0.1	-	Co-continuous fine porous structure
PS24	-	-	-	-	-	-	5.0	-	0.4	5.0	0.1	-	Co-continuous fine porous structure
PS25	-	-	-	-	-	-	-	5.0	0.4	5.0	-	-	Fine particles ~0.5 μm
PS26	-	5.5	-	-	-	-	2.0	-	0.4	2.5	3.5	0.021	Co-continuous, hierarchical
PS27	-	5.5	-	-	-	-	2.2	-	0.4	2.3	3.5	0.010	Co-continuous, hierarchical
PS28	-	6.0	-	-	-	-	1.5	-	0.4	2.5	-	-	Fail to gel into solid polymer
PS29	-	4.5	-	-	-	-	3.0	-	0.4	2.5	2.8	0.030	Co-continuous, hierarchical
PS30	-	4.0	-	-	-	-	3.5	-	0.4	2.5	-	-	The gel is too soft to handle
PS31	-	5.0	-	-	-	-	2.0	-	0.4	3.0	1.5	0.009	Co-continuous, hierarchical
PS32	-	5.0	-	-	-	-	1.5	-	0.4	3.5	0.8	-	Co-continuous

Table 2 Continued

PS33	-	4.5	-	-	-	-	3.5	-	0.4	2.5	-	-	The gel is too soft to handle
PS34	-	4.0	-	-	-	-	3.0	-	0.4	3.0	2.5	0.015	Co-continuous, hierarchical
PS35	-	4.0	-	-	-	-	2.5	-	0.4	3.5	1.8	0.007	Co-continuous, hierarchical
PS36	-	5.0	-	-	-	-	2.5	-	0.8	2.5	3.0	0.012	Co-continuous, hierarchical
PS37	-	5.0	-	-	-	-	2.5	-	0.2	2.5	3.0	0.012	Co-continuous, hierarchical
PS38	-	5.0	-	-	-	-	2.5	-	0.1	2.5			Fail to gel into solid polymer

Notes: 1) EG: ethylene glycol; DEG: diethylene glycol; TEG: triethylene glycol

2) Triblock polymers have a general formula of $\text{PEO}_x\text{-PPO}_y\text{-PEO}_x$. P103: $x=17, y=56$; P108: $x=129, y=56$; L121: $x=5, y=70$; P123: $x=20, y=70$; P127: $x=106, y=70$.

3) *p*-TSA: *p*-toluene sulfuric acid. FA: furfural alcohol

4) The composition is in grams.

5) Mac size: the average macropore size determined by SEM; Mes size: the average mesopore size measured by STEM.

All pore sizes are presented in the unit of μm .

interaction parameter χ to the polymerizing component is the first separating phase that turns as the primary phase separation. The primary phase separation dominated the entire phase separation in the ternary system. The macropore and average domain size are predetermined by the volume fraction of the primary phase separated component.

The interaction parameter χ is an empirical parameter that can be measured experimentally by light or neutron scattering and osmometry for high dilutions, or inverse gas chromatography near the polymer melt.^{91, 96, 98} In the current mixture, we estimate the interaction parameter by the domain size of spinodal decomposition in the binary system. Samples PS1 to PS3 are the spinodal decomposition of the binary system furfural alcohol in glycol solvent. Samples PS21 to PS25 are the spinodal decomposition of the binary mixture of the furfural alcohol and triblock polymers. The domain sizes in samples PS1 to PS3 are obviously larger than those in samples PS21 to PS25. Therefore, the interaction parameter χ has a larger value in the block polymer mixture than in the glycol solvents. It is evident that the primary phase separation is the glycol solvent separating from the polymer mixture.

The separation process in this ternary system can be described as two consecutive phase separations. The primary phase separation occurs when the conversion q of the furfural alcohol reaches a certain value such that the poly(furfural alcohol) still forms a homogeneous solution with the triblock polymer, but the glycol solvent is no more miscible with the polymers. As a result of the primary phase separation, the ternary system separates into a glycol solvent enriched phase and a polymer mixture rich phase. Afterwards, the poly(furfural alcohol) molecular weight grows with the further

conversion of the furfural alcohol monomer. Consequently, the polymer enriched phase starts to separate into a poly(furfural alcohol) phase and a triblock polymer phase.

Shown in Figure 36 are the morphologies of macropores from various compositions. Macropore sizes from 0.8 to 18 μm can be tailored by a careful selection of the glycol solvents.

5.5.2.1 The selection of glycol solvents

In this study we used three glycol solvents: ethylene glycol, diethylene glycol, and triethylene glycol. Ethylene glycol has the lowest viscosity and smallest interaction parameter with the poly(furfural alcohol). Thus, the primary phase separation of the ethylene glycol from the ternary system has spherical morphologies. The spherical morphologies are most likely to precipitate out of the system through a nucleation and growth mechanism. Although, in a few cases, a co-continuous morphology forms (sample PS9 shown in Figure 36), the skeleton is still composed of spherical grains. Triethylene glycol has the highest viscosity and greatest interaction parameter with the final polymer. Co-continuous morphologies are always present in the triethylene glycol system. However, due to the relatively high viscosity, the triethylene system usually forms large domains, for example, sample PS17. The interaction parameter and the viscosity of diethylene glycol falls between those of ethylene glycol and triethylene glycol; thus, the morphology in the diethylene glycol system is easier to control than in the other two glycol solvent systems.

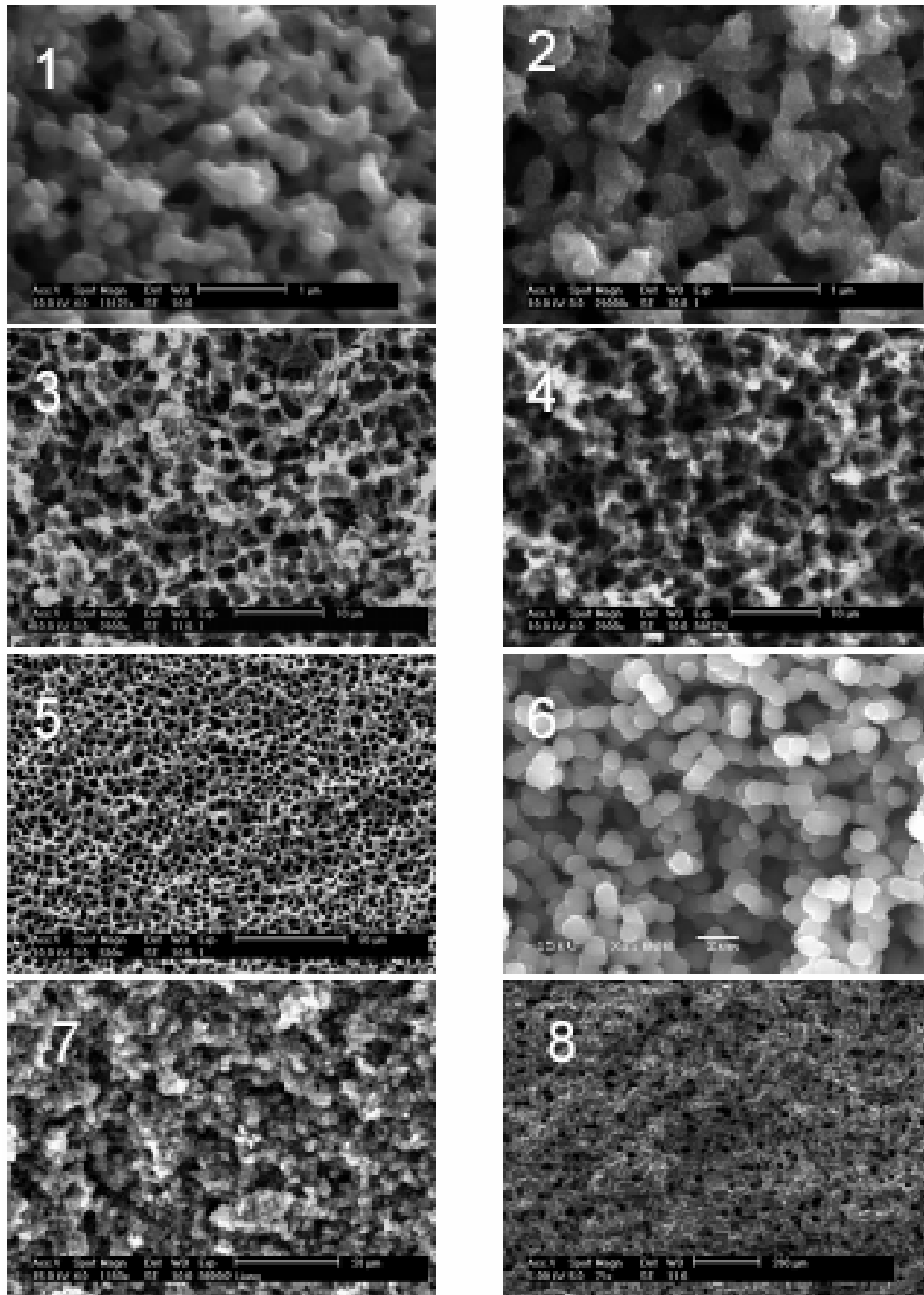


Figure 36. Macropore morphologies and pore sizes. 1) PS32, 2) PSPS11, 3) PS16, 4) PS14, 5) PS15, 6) PS9, 7) PS20, 8) PS17.

5.5.2.2 Temperature effect

Temperature also controls the polymerization of the furfural alcohol. When the temperature of the mixture is less than 50 °C, the polymer cannot grow to sufficient size to form a solid polymeric matrix. This is why, after the mixing and degassing, the mixture must be heated to a sufficient temperature to cure the polymer. In this research, we found that when the curing temperature is higher than 70 °C, the final curing temperature does not affect the morphologies. However, the morphologies are affected by the heating rate. Since the spinodal decomposition line moves as the temperature changes, the final structure results from the dynamic changing of the whole system. In the diethylene glycol system, we found that when the heating rate is slower than 10 °C/hour, the final morphologies are always isolated spherical macropores, and when the heating rate is higher than 30 °C/hour, the final morphologies are co-continuous channels. A radial heterogeneity was found in the sample processed at a heating rate above 40 °C/hour. This radial heterogeneity may be due to the thermal heterogeneity in sample heating. When the heating ramp is too fast to allow thermal equilibrium across the mixture, a temperature gradient may exist in the mixture. This temperature gradient could produce heterogeneous morphologies.

5.5.2.3 Catalyst effect and rate

The catalyst has the least affect on the morphology. When the catalyst concentration is in the range of 2% to 10%, the resulting morphologies are independent of the catalyst concentration. The polymerization rates are proportional to the catalyst concentration. When using high catalyst concentration, the initial exotherm

polymerization reaction may produce too much heat to accelerate the reaction rate beyond control. It is dangerous to use a catalyst concentration higher than 10% due to the uncontrollable exotherm reaction.

5.5.3 Secondary phase separation and mesoporosity

Secondary phase separation occurs in the polymer-enriched phase when the conversion of the monomer is high enough to trigger separation of the triblock polymer from the poly(furfural alcohol). Secondary phase separation produces mainly mesopores in the skeleton. Shown in Figure 37A is the morphology resulting from the secondary phase separation in the polymer phase, while Figure 37B shows the mesopores.

The BET measurement of the carbon rods shows the carbon is microporous (Figure 38). The initial adsorption volume at a relative pressure of 0.1 is 96.6 ml/g, while the final adsorption volume is 127.2 ml/g, indicating that the micropores are the primary contributors to pore volume. No steep adsorption step was found in the isotherm, which suggests that the pore size of the mesopores has a wide size distribution.

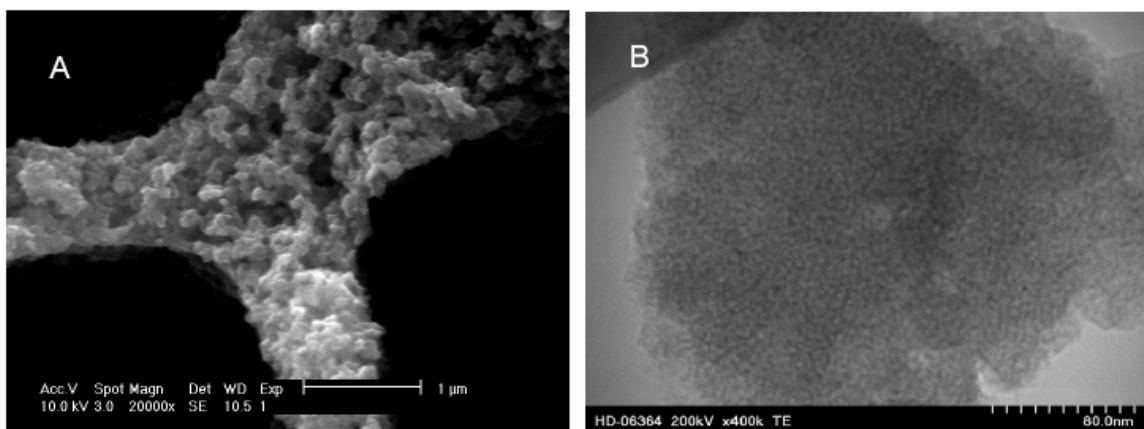


Figure 37. The secondary phase separation and the mesopores (sample PS14).

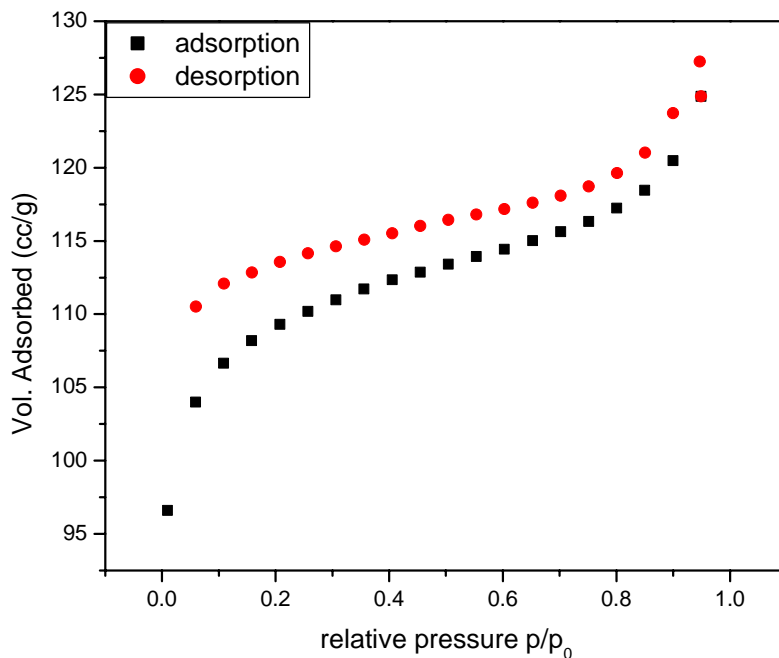


Figure 38. N₂ adsorption /desorption isotherm of sample PS14.

5.5.4 The relationship between primary phase separation and secondary phase separation

Primary phase separation and secondary phase separation in the ternary system are two related processes that influence each other. The final structure results from a combination of the two phase separations. For example, comparison of the samples PS26, PS14, and PS29 shows that decreasing the diethylene glycol fraction results in a decrease in macropore size and an increase in mesopore size.

5.5.5 Degassing and the elimination of defects

Defects in the material are mainly due to air bubbles and impurities such as dust particles from the air or container. The mixing of solvents produces air bubbles in the viscous solution. These air bubbles should be removed before the polymeric rod has been cured. The polymerization of the monomer may also produce air bubbles due to the

decreased air solubility in the polymerization. Therefore, degassing the system before polymerization is crucial for the synthesis of defect free rods. When the reaction mixture was degassed at room temperature in a 30 mmHg vacuum for 30 minutes, the final rods were free of air bubbles. Dust particles are hard to prevent under ordinary laboratory conditions. The amount of dust can be greatly reduced by using particle-free starting chemicals and washing the containers with particle-free water.

5.6 Conclusion

In this research we demonstrated that phase separation is a versatile method for the synthesis of macroporous carbon rods. By using a ternary system, two phase separation processes can be induced to occur consecutively. Hierarchically porous structures are developed by a primary phase separation that produces the macropores followed by a secondary phase separation that mainly produces the mesoporosity of the carbon rods. The porosity and pores sizes of the macropores can be adjusted by using suitable glycol solvents in the concentration range of phase separation. Mesopores result from the secondary phase separation of the triblock polymer from the cured poly(furfural alcohol). The wash-off, or thermal decomposition, of the triblock polymer produces mesopores in the skeleton of the carbon rods. Using triblock polymers in different molecular weights can adjust the mesoporosity of the carbon rod.

According to the pore-forming process, one can conclude that the glycol solvents and triblock polymers act as the porogen of macropores and mesopores, respectively. The ease of removal of the porogen gives this method tremendous advantage in terms of cost-

efficiency and ease of handling. Since all starting materials are hydrocarbons, the carbon in the resulting rods is especially pure.

These carbon rods were carbonized at a relatively low temperature, forming unmistakable micropores. Because the microporous properties of these carbon rods made them unsuitable for the separation of small molecules, future work in this area should include the elimination of the micropores. Traditionally, a high temperature treatment at over 2300 K can significantly reduce the micropores by partially graphitizing the carbon matrix. Surface modification is an alternative method for elimination of the micropores. Since the carbon rods are conductive, electrochemical methods can perform grafting of dense organic ligands. The surface modification of carbon rods is detailed in Chapter 7.

Since the mesopore range is the threshold of spinodal decomposition, the mesoporosity of the resulting carbon is fairly adjustable. The homogeneity of the mesoporosity is also quite a problem. In order to gain further control of mesoporosity, especially the uniformity of the mesopores, new methods should be adopted for the synthesis of carbon materials. The recently developed microphase separation has proven to be a viable method for the tailored synthesis of nanoscale features. In the next chapter, the author describes the fine adjustment of mesopores through microphase separation of block copolymers.

Chapter 6: Synthesis of mesoporous carbon via self-assembly of block copolymers

6.1 Introduction of the synthesis of mesoporous carbon

In any chromatographic separation, the interaction between the stationary phase and analyte plays a key role in separation. The strength of the interaction depends not only on the nature of the ligands, but also on the surface area of the stationary phase. In most situations the surface area is the critical parameter, accounting for column capacity and efficiency. In this chapter we describe a novel method for the fabrication of mesoporous carbon. The carbon can be coated to substrates for provide the high surface area required by HPLC applications.

The external surface and internal surface contribute to the surface area. The external surface is the surface provided by the macropore channel in the monolithic column, or the surface of the microspheres in traditional particulate columns. The external surface in any kind of column is very small. The value of the external surface is usually in the range of a few square meters per gram. The major contribution of the surface area is derived from the mesopores. Mass transportation to and from the mesopores is a diffusion predominating process, so the surface attributed to the mesopores is called the internal surface. By definition, the mesopore region is the pores in the size range between 1.8 and 50 nm. HPLC columns possess mesopores in the range of 5 to 30 nm. The mesopores contribute an internal surface area of 200 to 600 m²/g. The internal surface

provides the contact of the analyte with the surface ligand in molecular level. Hence, the mesopore is very important in the stationary phases.

The synthesis of mesoporous carbon pales by comparison with the synthesis of mesoporous silica, titania and zirconia. Most carbon materials are microporous material, unsuitable for HPLC separation. The activation of carbon materials can enlarge the pore size to the lower mesopore range. Even after enlargement, the pores of the active carbon are still too small to be used in liquid chromatographic columns. Synthetic carbon from the resorcinol/formaldehyde resin (RFR) has been recently reported as mesoporous material.¹⁰³⁻¹⁰⁶ The synthesis of these mesoporous carbon materials requires special drying techniques such as super critical drying and freeze drying.¹⁰⁴⁻¹⁰⁶ These drying techniques are neither easy to handle, nor energy efficient. Also, the scale-up of the synthesis of these mesoporous carbon materials presents numerous problems. In practice, neither the activated carbon, nor the RFR carbon have well-controlled mesopores. The tailoring of the mesopore in carbon is realized by using the template method developed more than thirty years ago.⁷² Even now, the only commercially available liquid chromatographic carbon is synthesized using the template method.

In the last decade the synthesis of ordered mesopores silica has been intensely studied. A variety of ordered mesoporous silica has been synthesized with tailored pore sizes.^{33, 34, 37, 39, 40} The birth of these silica materials made it possible to make ordered mesoporous carbon by replicating ordered mesoporous silica.¹⁰⁷⁻¹¹² The ordered porous carbon materials provide homogeneity to the carbon adsorbent. These ordered porous carbon materials are considered promising materials of separation.¹¹²

So far the synthetic method of ordered mesoporous carbon still inherits the concept of the template method. As mentioned at the end of Chapter 4 and the beginning of Chapter 5, the use of solid template in the synthesis of carbon materials raises a number of problems. Cost and environmental concerns are the main problems associated with the template method.¹⁰³ To solve these problems, the author proposes here a novel synthetic method for ordered mesoporous carbon. This novel synthetic method uses block copolymers (BCPs) as templates for the spatial arrangement of carbon precursors in a well-defined structure. Upon carbonization, the BCPs thermally decompose and are sacrificed as the pores in the resulting carbon. The removal of the solid templates is thus avoided. The absence of template dissolving solved all problems associated with the replicating method. To demonstrate the proposed synthetic method, the author prepared mesoporous carbon film on various substrates. This concept can also be extended to the synthesis of monolithic carbon columns by applying the carbon coating to macroporous monoliths.

The essential element of this proposed synthetic method is the self-assembly of the BCPs. The self-assembly of BCPs has proven to be a versatile approach to the selective organization and nanoscale regulation of the concentration distribution of target molecular species for the fabrication of nanoporous materials.^{113, 114} The mechanism for such organization involves hydrogen bonding,¹¹⁵ ion pairing,¹¹⁶ and/or dative interactions¹¹⁷ between supramolecular assemblies of BCPs and target molecular species. The resulting composites can give rise to various nanostructures according to the structural and phase behaviors of BCPs. The target molecular species are spatially

concentrated in selected microdomains and can eventually serve as nanostructured catalysts,¹¹⁸ spacers,¹¹⁹ or precursors¹²⁰ for the further fabrication of ordered nanostructures. Highly ordered nanoporous materials, such as polymer,¹²⁰ silica,^{40, 121} and organic–inorganic hybrid materials,^{122, 123} have been created through polymerization in the presence of the self-assembled BCPs.

Although BCPs contain high atomic carbon concentrations, ordered nanoporous carbon films have not been successfully fabricated through the direct pyrolysis of self-assembled BCPs.¹²⁴ This inability is because structured BCP compounds with linear structures have very poor carbon yields in carbonization reactions. Furthermore, the survival of the nanostructures during high-temperature pyrolysis (>800°C) is extremely challenging for the self-assembled BCP structures. This deficiency is associated with the structured BCPs, which melt before carbonization reactions. The cross-linking of BCPs can significantly stabilize the self-assembled nanostructures. However, it is still difficult for limited cross-linkage to preserve the pre-organized nanostructures because of the massive loss of carbon via volatile carbon-containing species during pyrolysis.

Highly cross-linked resorcinol formaldehyde resin (RFR) is a well-known carbonization source.^{22, 125} This rigid polymeric carbon precursor can retain preorganized structures during pyrolysis. However, the low solubility of the highly cross-linked RFR in solvents makes it impossible to directly blend RFR with BCPs for the formation of nanostructured RFR. To overcome this limitation, we have developed a stepwise assembly approach to fabricate well-ordered nanoporous carbon films. The essence of this methodology is first to preorganize the resorcinol monomers into a well-ordered

nanostructured film with the assistance of polystyrene-*b*-poly(4-vinylpyridine) (PS-P4VP) self-assembly and solvent-induced structural annealing, which is followed by the *in situ* polymerization of the resorcinol monomers with formaldehyde vapor to form ordered nanostructured RFR. Upon carbonization, the nanostructured RFR is transformed into a highly ordered nanoporous carbon film with the concomitant decomposition of the PS-P4VP template to gaseous species.

6.2 Experimental

Chemicals: PS-P4VP was purchased from Polymer Source. Resorcinol, formaldehyde (37 wt% aqueous solution), and all solvents were purchased from Aldrich.

Instruments: The infrared spectra were taken by using the FTS 3000 (BIO-RAD Inc.). A TGA 2950 system was employed for the thermogravitic analysis (TGA). All TGA measurements were carried out at the temperature ramp of 20 °C/min under N₂. The imaging of the mesopores has been done with a Hitachi HD-2000 scanning transmission electron microscopy (STEM), which was operated at an accelerating voltage of 200 KV and a current of 30 μA. X-ray diffraction patterns were measured with a Siemens D5005 X-ray diffractometer with copper K_α line (0.1541 nm) as the incident beam. Raman spectra were recorded with a Renishaw 2000 Raman microscope equipped with a CCD detector, using an Argon ion laser (514.5 nm excitation wavelength, 5 mW). The carbonization was performed in a tubular furnace that was purged with 100ml/min argon.

Method: 0.1 g of PS-P4VP -- with number average molecular masses (Mn) of PS 11,800g/mol for PS and 11,500g/mol for P4VP, and Mw/Mn of 1.04 for both blocks and 0.0512 g of resorcinol were dissolved in 2 g of DMF. This solution is heated at 100 °C for

4 hours to ensure the formation of hydrogen bonds. After the solution is cooled to room temperature, a drop of solution is cast into a film on a silica plate by spin-coating at 1000 rpm for 2 minutes. The film is afterwards dried in a hood. The dry film, along with two small vials containing DMF and benzene, respectively, are then put into a preheated chamber at 80 °C. The film remains in the sealed chamber for 24 hours to allow the completion of microphase separation via a slow evaporation of the solvents. The microphase separated film is sequentially cured through exposure to formaldehyde gas at 100 °C for 4 hours. The cured film is finally carbonized in nitrogen gas through a temperature ramp of 1 °C/min to 800 °C.

6.3 Results and discussion

The synthesis protocol involves four basic steps: (1) monomer-BCP film casting, (2) structure refining via solvent annealing, (3) polymerization of carbon precursor, and (4) carbonization. Figure 39 schematically illustrates the procedure for the fabrication of ordered porous carbon films.

In step 1, the precursor films can be cast with a solution containing a mixture of PS-P4VP and resorcinol on silica, silicon, glassy carbon, or copper, which is able to withstand the high temperature required by the final carbonization step. Both N,N'-dimethylformamide (DMF) and cyclohexanol are good solvents for PS-P4VP and can be used to cast the precursor films. The concentration of PS-P4VP is in the range of 0.5-10 wt%. The final film structures are not dependent on the casting methods (dip coating and spin coating). The BCP template used in the synthesis has equal lengths of PS and P4VP

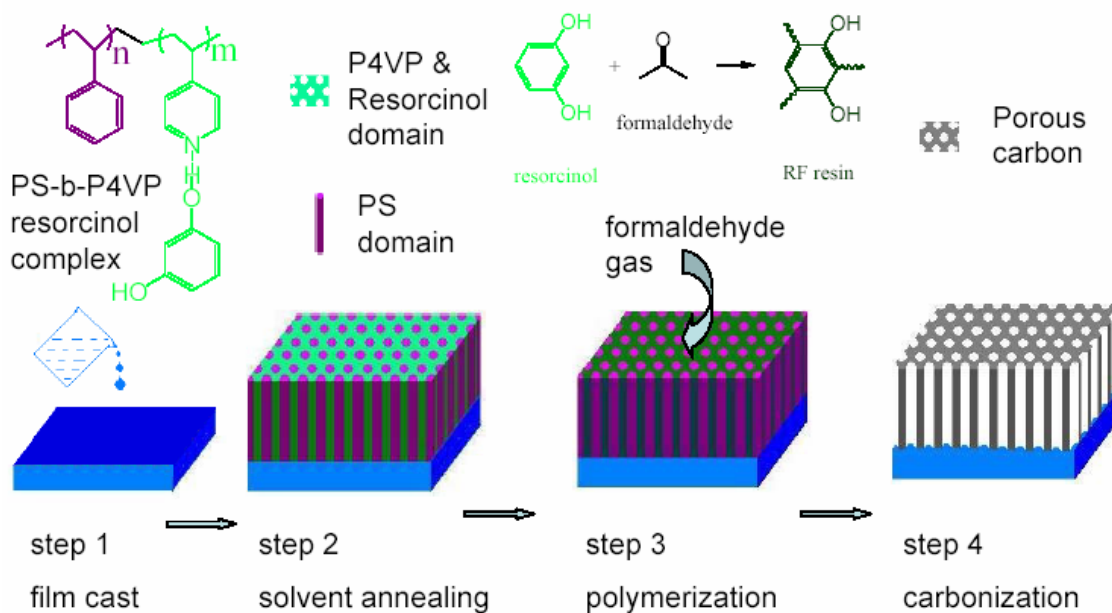


Figure 39. Schematic representation of the synthesis protocol used to prepare well defined carbon nanostructure. Step 1 film casting of PS-P4VP/ resorcinol supramolecular assembly. Step 2, Completion of microphase separation by solvent annealing at 80 °C in DMF/ benzene mixed vapor. The resorcinol is organized in the well defined P4VP domain. Step 3 *in situ* polymerization of resorcinol and formaldehyde by exposing the film to formaldehyde gas. Highly cross-linked RFR is formed within the P4VP domain. Step 4 Pyrolysis of the polymeric film in N₂. Hexagonal carbon channel array is form by sacrificing the block copolymer.

blocks. The bulk material of this PS-P4VP copolymer has a lamellar structure.¹¹³ The self-assembly of PS-P4VP/resorcinol mixture is essentially driven by the hydrogen bond interaction between resorcinol and P4VP block.^{119, 126} This strong hydrogen bond association between the basic P4VP blocks and the acidic resorcinol monomers selectively enriches the resorcinol molecules in the P4VP domain. Accordingly, the volume fraction of the P4VP domain is significantly increased relative to that of the PS domain, resulting in a hexagonal structure.^{113, 119} The PS block in the PS-P4VP/resorcinol complex is the minor component, which forms cylindrical microdomains in the self-assembled film. Figure 40 compares the Fourier transform infrared (FTIR) spectra of PS-P4VP and PS-P4VP/resorcinol mixture (molar ratio of pyridine groups to resorcinol 1:1). As seen in Figure 40, the characteristic stretching modes of the P4VP block at 993, 1415, and 1597 cm^{-1} shift to 1007, 1419, and 1602 cm^{-1} , respectively, for the PS-P4VP/resorcinol mixture. These vibrational frequency shifts are consistent with the interaction between the pyridine groups and the resorcinol molecules via hydrogen bonding.¹²⁶

The second step involves solvent annealing,^{119, 127} which is the key to the formation of highly ordered and well-oriented nanostructures. Russell and his coworkers have reported an efficient method based on solvent annealing for refining self-assembled block copolymer nanostructures.¹²⁷ The controlled evaporation of the solvent results in highly ordered nanostructures oriented normally to substrates. When the as-cast film is annealed in DMF/benzene vapour at 80 °C through a slow evaporation of solvents in a period of 24 hours, the final carbon film has a highly ordered hexagonal structure with all

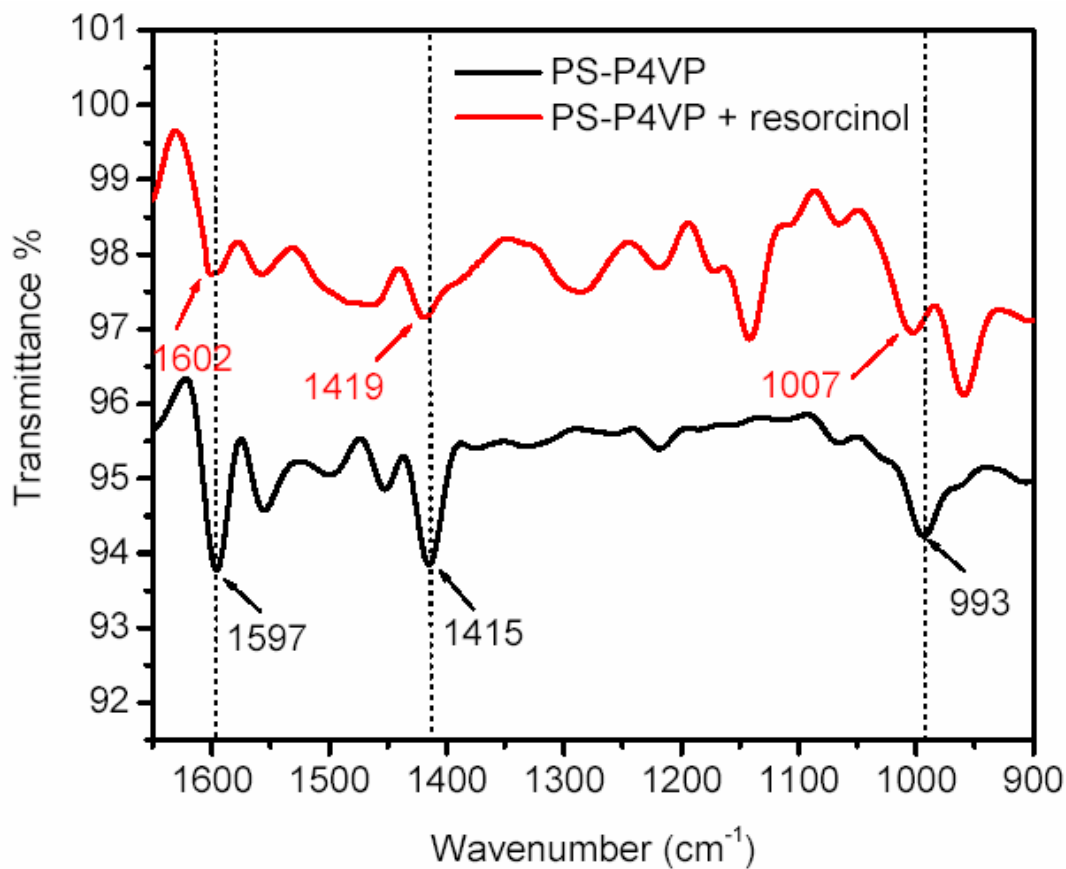


Figure 40. FTIR spectrum of PS-P4VP and PS-P4VP/resorcinol complex in the region from 900 to 1650 cm^{-1} . The characteristic peaks of pyridine ring in PS-P4VP at 993, 1415 and 1597 cm^{-1} shift to 1007, 1419, and 1602 cm^{-1} due to the formation of hydrogen bond with resorcinol.

pores oriented perpendicular to the substrate. DMF is a highly miscible solvent for both the PS block and P4VP block. When the film has swollen in DMF vapor, both blocks have particularly good mobility. With this mobility, the swollen PS and P4VP blocks repel one another and tend to organize into a well-defined structure.¹²⁷ However, the repulsion of these two blocks is damped by DMF, which is highly miscible with both blocks. We found that the addition of benzene vapour intensely accelerates the self-assembly process and significantly enhances the order of the film.¹²⁷ Because benzene is a good solvent only for the PS block, the absorbed benzene vapour is most likely enriched in the PS block domain. Therefore, the repulsion between the PS and P4VP domains is enhanced by benzene. A fast microphase separation is thus achieved in the DMF and benzene mixed vapor.

In step 3, the solvent-annealed nanostructured film above was exposed to formaldehyde vapor to cross-link the resorcinol molecules into a highly cross-linked phenolic resin located in the P4VP domain. The cross-linking was carried out via vapor/solid reactions with minimum perturbation of the self-assembled nanostructures. The reaction rate can be readily controlled by the vapor pressure of formaldehyde.

The final step involves the decomposition of the BCP template to generate ordered nanopores and the carbonization of the nanostructured RFR to form the carbon pore walls. This pyrolysis process was studied using a thermogravimetric analysis (TGA) to continuously measure the mass loss upon heating from room temperature to 800 °C under argon at 20 °C/min. Shown in Figure 41 are the thermograms (TGs) and the derivative thermograms (dTGs) of four samples: (1) PS-P4VP, (2) PS-P4VP and

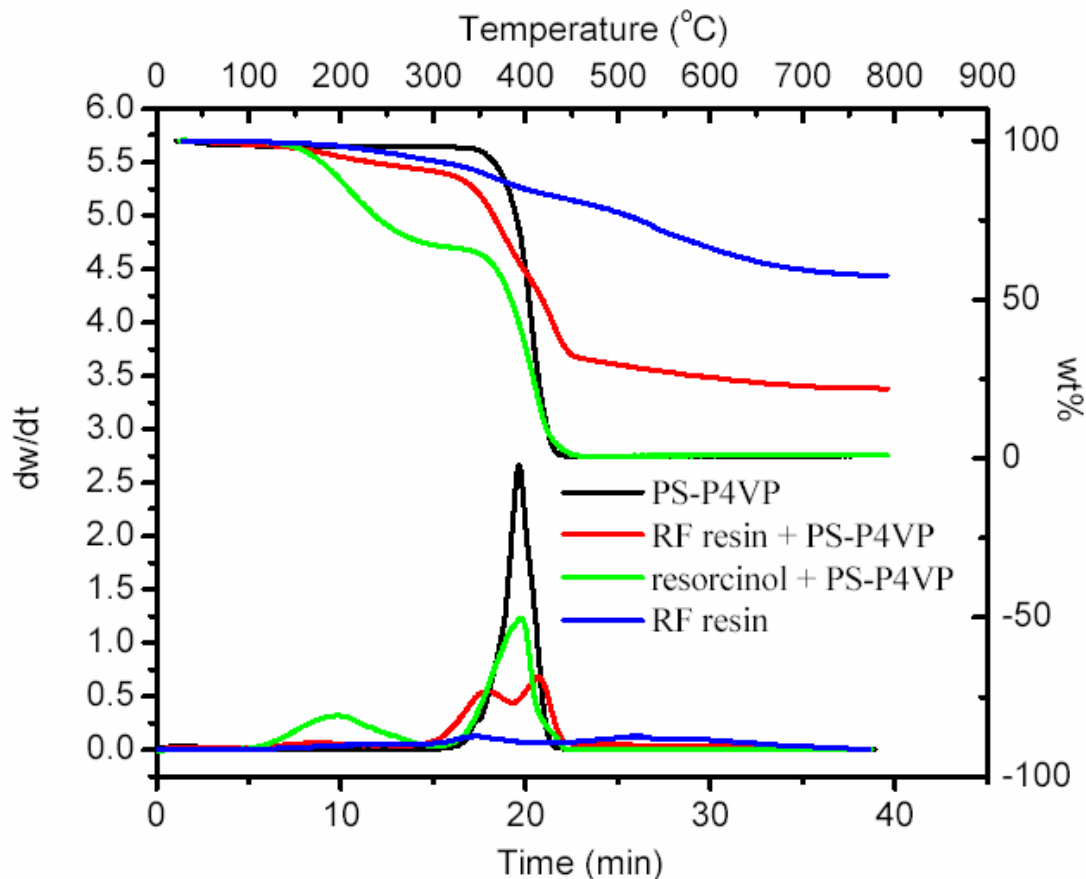


Figure 41. TGA and dTG curves for A) PS-b-P4VP, B) PS-b-P4VP and resorcinol mixture (molar ratio of pyridine groups to resorcinol 1:1), C) resorcinol formaldehyde resin (RFR), and D) PS-b-P4VP and RFR. The top and right axes are the temperature and wt% for the thermogram (TG). The left and bottom axes shows the weight loss rate and time for the derived thermogram (dTG).

resorcinol mixture, (3) RFR, and (4) PS-b-P4VP and RFR. The pure PS-P4VP sample starts to decompose at 328 °C and ends at 430 °C, with only negligible 0.7 wt% residue. Both the decomposition temperature and the reaction rate of the PS and P4VP blocks are too close to resolve in the TG and dTG curves. Therefore, the pyrolysis of PS-P4VP exhibits only one peak in the dTG curve of the pure PS-P4VP sample. The TG curve of the PS-P4VP and resorcinol mixture has two weight-loss stages with corresponding dTG peaks at 195 and 392 °C. The weight loss for the first stage starts at 120 °C, which is only 10 °C above the melt point of resorcinol. The first weight-loss stage ends at 284 °C with the loss of ~34 wt%. The mixture of PS-P4VP and resorcinol has 33.87 wt% of resorcinol. Accordingly, this weight loss in the TG curve indicates that all resorcinol molecules evaporated before the temperature reached 284 °C. The second weight-loss stage of the PS-P4VP/resorcinol mixture starts at 328 °C and ends at 430 °C. This part of the weight loss is attributed to the decomposition of the PS-P4VP copolymer. The TGA curve of the RFR sample exhibits a continuous weight loss from 200 to 750 °C. The carbonization yield for pyrolysis of RFR is 57.59 wt%. The TGA curve of the PS-b-P4VP and RFR sample prepared by cross-linking the PS-P4VP/resorcinol sample via formaldehyde vapor shows a complex pyrolysis behavior. A significant weight loss was found in the range of 200 to 750 °C. The major weight loss occurs from 320 to 430 °C, which is attributed to the decomposition of the PS-P4VP copolymer. The two dTG peaks emerge in this zone, indicating two different decomposition behaviors. Comparing these peaks with the dTG peak of the pure PS-P4VP, it appears that the RFR affects the pyrolysis of the PS-P4VP. Because the RFR is localized in the P4VP domain, the decomposition of the PS domain is

the least affected. The P4VP chain is tangled with the RFR; as a result, the decomposition rate of P4VP may be retarded by RFR due to the interaction between RFR and P4VP. Therefore, the P4VP block may decompose after the PS block. The pyrolysis of the PS-P4VP/RFR mixture yields 22.16% carbon at 800 °C. Taking into account the weight gain in the polymerization with formaldehyde, the weight percentage of the RFR in the PS-P4VP/RFR rises from the 33.87% (resorcinol wt% in PS-P4VP/resorcinol mixture) to 37.34%. Assuming RFR in the P4VP domain has the same carbon yields as the pure RFR (57.59%), the PS-P4VP part only accounts for 1.05 wt% carbon in the final product. Obviously, the RFR is the predominant carbon source of the porous carbon film and the BCP is sacrificed as pores.

A crack-free nanoporous carbon film with thickness of from several tens of nanometers up to $\sim 1 \mu\text{m}$ and size up to 6 cm^2 can be obtained. The nanoporous carbon film strongly adheres to substrates and is homogeneous in thickness. As seen from Figures 42A and D, the nanopores are oriented perpendicular to the film surface. An enlarged Z-contrast image of the carbon film is shown in Figure 42B. The Fourier transform of this Z-contrast image of the film shows a pattern of multiple reflections, which confirms that the film has a highly ordered hexagonal pore array. Based on Figure 42C, the pore diameter is $33.7 \pm 2.5 \text{ nm}$ and the wall thickness is $9.0 \pm 1.1 \text{ nm}$. The volume fraction of the straight channels is ~ 0.565 (see Figure 43 for details). The pore diameter and thickness can be controlled by the volume fractions of PS in BCP and carbon-forming resin, respectively. The cross section of the film scratched from a film substrate is shown in Figure 42D.

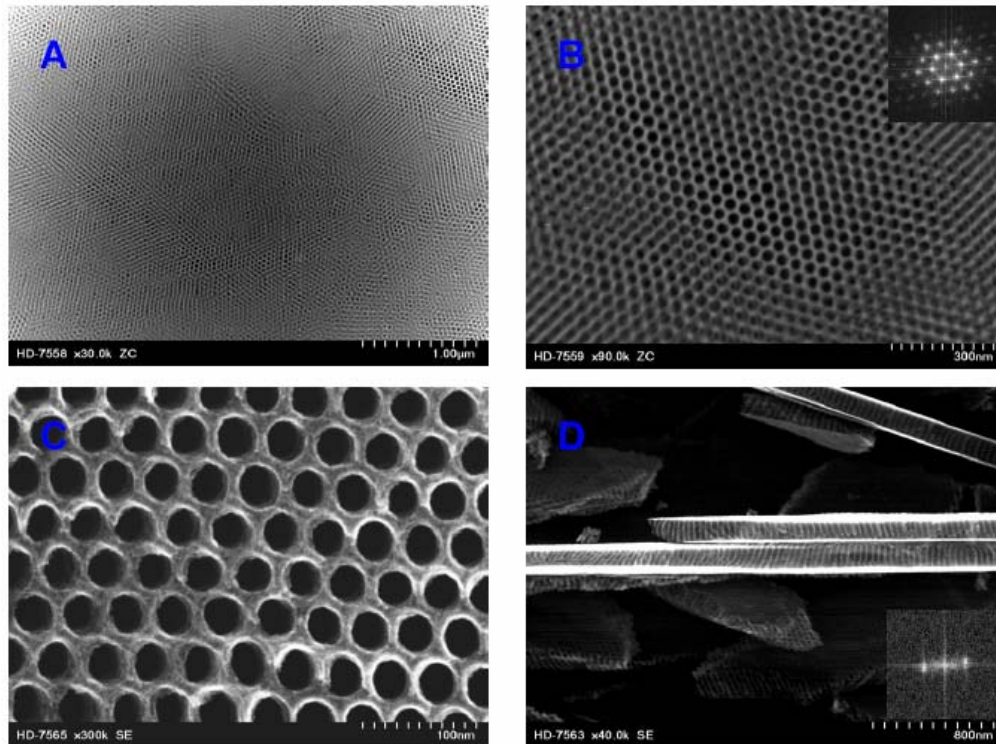


Figure 42. Electron microscopy images of the carbon film. A) A Z contrast image of the large scale homogeneous carbon film in a $4 \times 3 \mu\text{m}$ area. The scale bar is $1 \mu\text{m}$. B) A Z contrast image shows the details of the highly ordered carbon structure. In the inset, a Fourier transform (FT) of the image shows a pattern with multiple reflections, which are characteristic of a highly ordered hexagonal array. C) A high resolution SEM image shows the surface of the carbon film with uniform hexagonal pore array. The pore size is $33.7 \pm 2.5 \text{ nm}$ and wall thickness is $9.0 \pm 1.1 \text{ nm}$. D) A SEM image shows the film cross section, exhibiting all parallel straight channels perpendicular to the film surface. The inset shows the Fourier transform of the cross section image. The FT pattern shows the reflections of the periodic parallel channels.

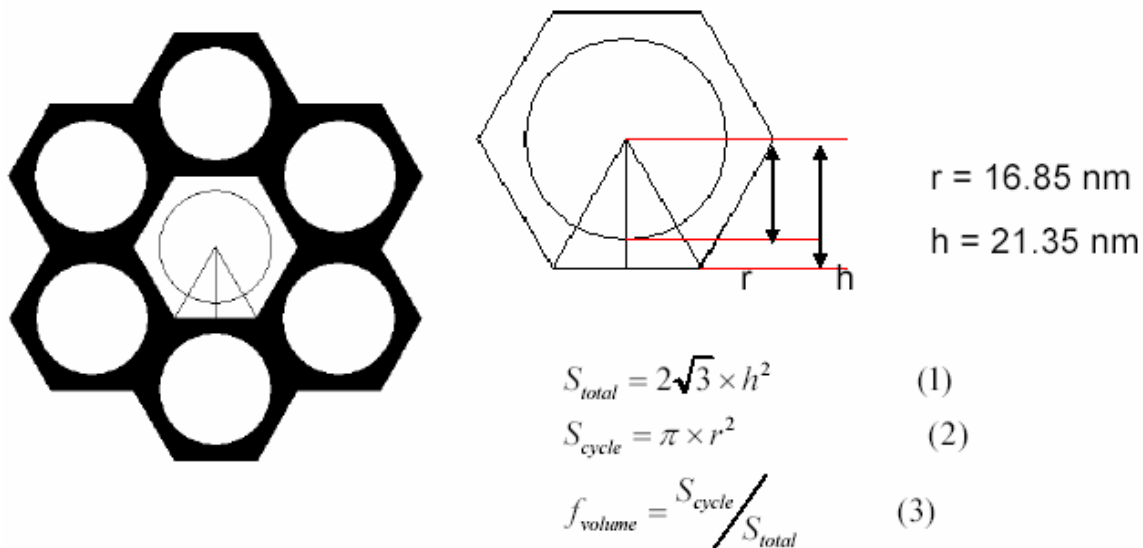


Figure 43. The calculation of volume fraction of the mesopores. The volume fraction of the channel equals to the ratio of cycle area to the total film area. Take an equilateral hexagon unit into account, the total area of the equilateral hexagon (S_{total}), the cycle (S_{cycle}), and the volume fraction of the channel (f_{volume}) are calculated by equation 1, 2 and 3 respectively. With $r = 16.85 \text{ nm}$ (the radius of the channel) and $h = 21.35 \text{ nm}$ (the half center to center distance), $f_{volume}=0.56$.

All straight channels are across the whole film. The inset in the right lower corner is the Fourier transform of the high-resolution SEM image of the film cross section, which reflects parallel periodical channels.

No graphitic structure was found in the high-resolution TEM (HRTEM) mode, suggesting that the wall is amorphous carbon. Wide-angle X-ray diffraction (WAXD) shows broad peaks at 23.6, 43.76, and 80.24 degrees, which are characteristic of amorphous carbon. Raman spectrum shows a broad D band at 1333 cm^{-1} , which overlaps with the G band at 1600 cm^{-1} . Such a broad D band is reminiscent of the glassy carbon texture. The HRTEM image, WAXD pattern, and Raman spectrum are shown in Figure 44 to 46.

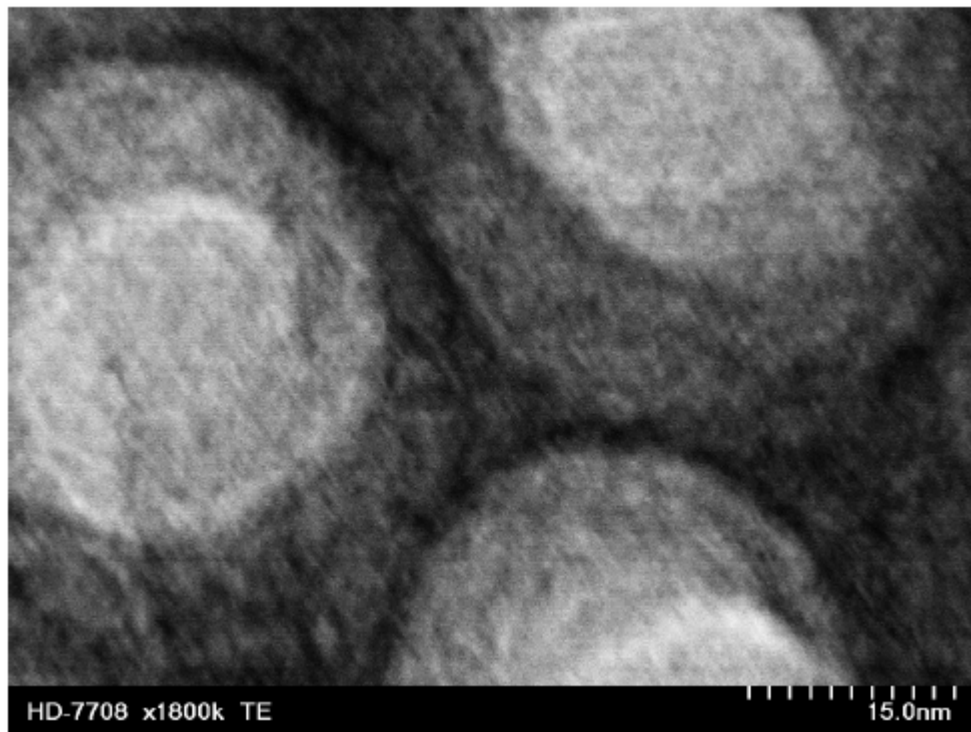


Figure 44. High resolution transmission electron microscopy image of the carbon wall.

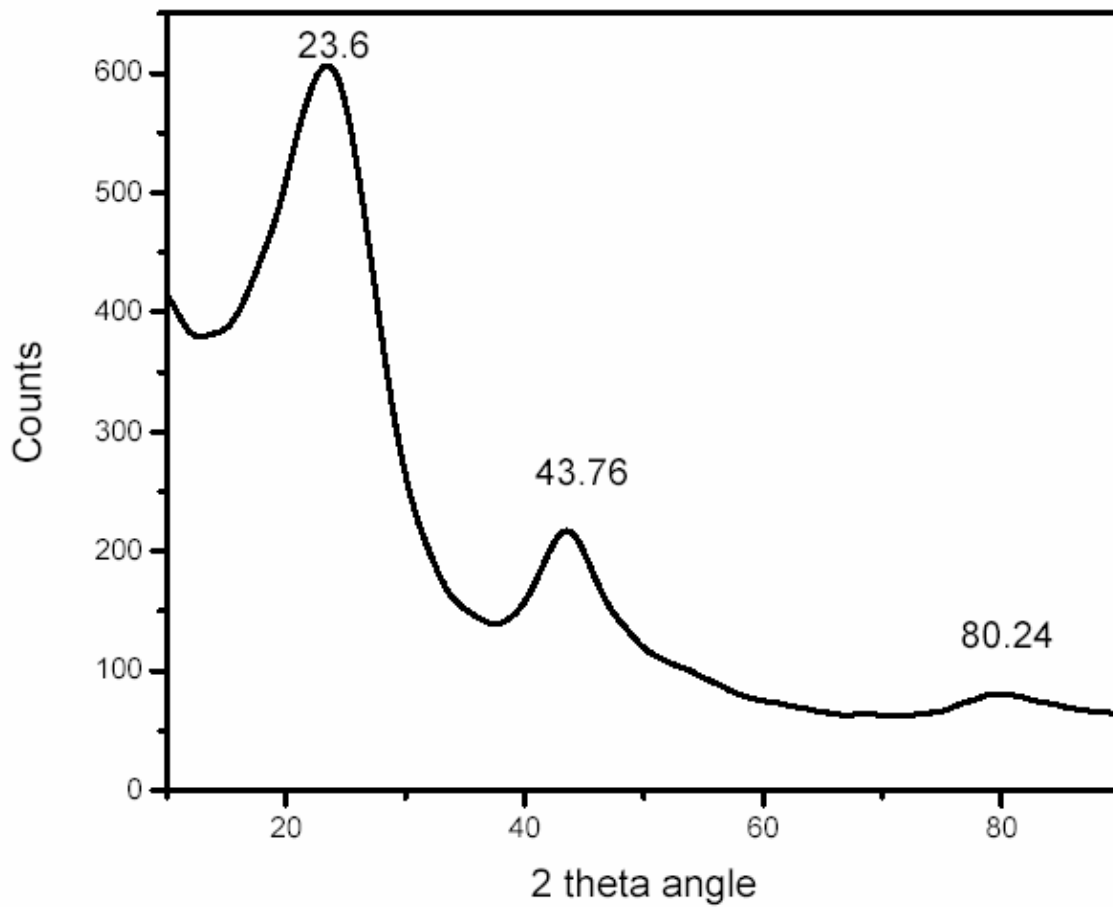


Figure 45. Wide angle X-ray diffraction pattern.

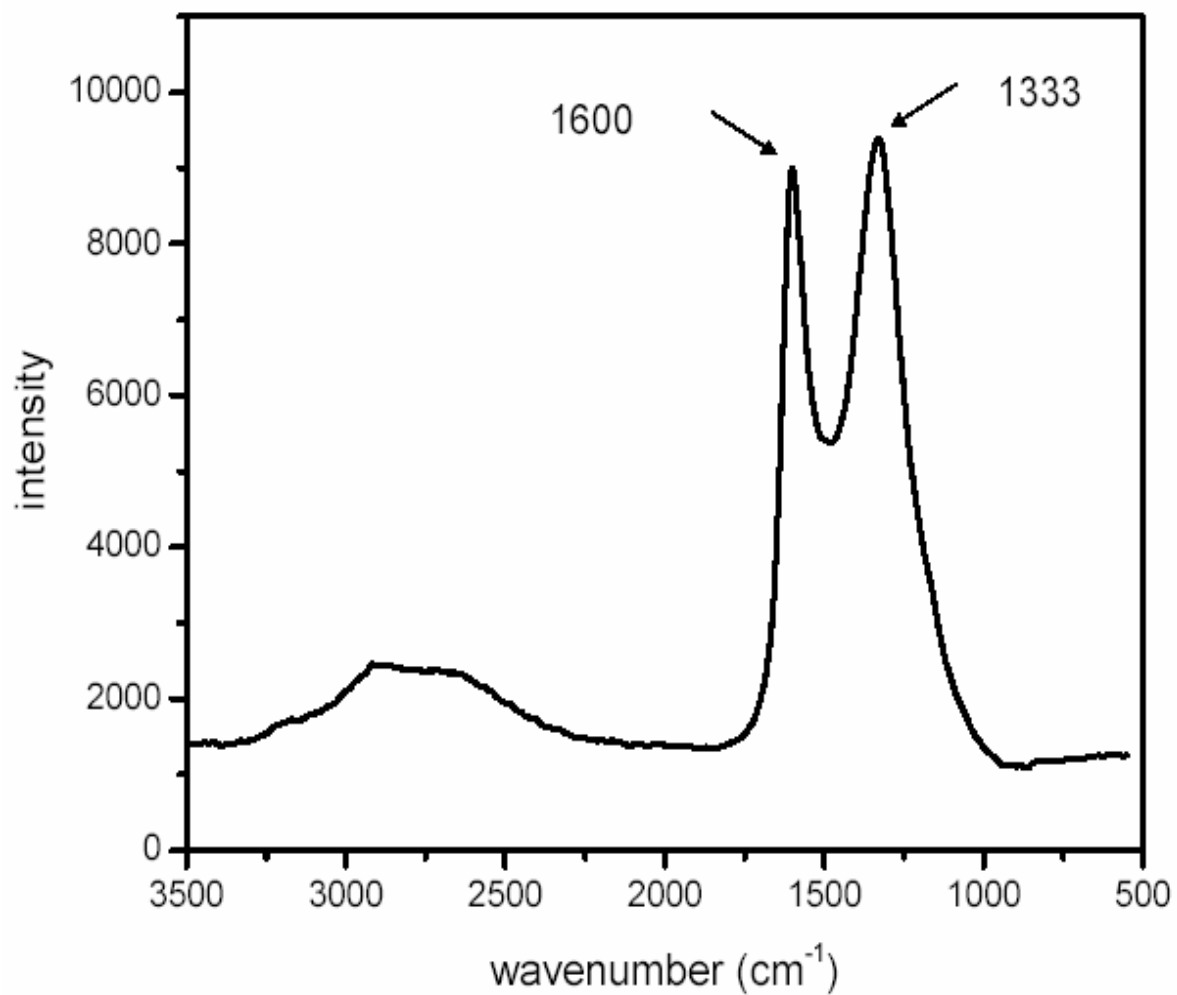


Figure 46. The Raman spectrum of the carbon film.

6.4 Conclusion

In conclusion, a facile methodology based on stepwise self-assembly has been successfully developed to prepare highly ordered and well-oriented mesoporous carbon films through carbonization of the nanostructured phenolic resin and BCP composite. The BCPs play two important roles in the synthesis: (1) directing the formation of phenolic resin nanostructure, and (2) serving as templates for nanopores. The orientation of the ordered carbon nanopores was successfully aligned normal to substrates through a solvent annealing process. The unique structural feature of this oriented nanoporous carbon film highlights opportunities in areas such as separation membranes, chemical sensors, and catalysts.

6.5 Future research work

The current methods demonstrated that mesoporous carbon can be coated onto various substrates. Nevertheless, this coating can be applied to various inorganic macroporous monoliths for the purpose of HPLC application. This carbon film may also find applications in membrane separation and membrane chromatography. The large scale carbon coating on silica plates is also a promising thin layer chromatographic media.

Chapter 7: Surface Modified Monolithic Carbon Columns

7.1 The background of the surface modification on carbon phases

The mature silica chemistry continuously fertilizes the modification of the silica phases. Hundreds of various silica columns have been made via surface modification. These columns cover all branches of liquid chromatography. What is impressive is that the surfaced modified silica columns occupy over 75% of the column market.¹²⁸ The ease of chemical modification on the silica surface is indeed the major reason why the silica phase is so widely used. If the carbon phase cannot be modified, one cannot imagine that the carbon phase can compete with the silica phase in a wide range of applications. To broaden the applicable range of the carbon phases, it is crucial to develop a well-established protocol for the modification of carbon surface.

The carbon columns provide a promising stationary phase alternative the silica columns, which have poor stability. Ironically, chemical inertness makes the carbon surface very difficult to modify. The pioneer works on the modification of carbon phase are mainly focused on physically adsorbed modifiers.¹²⁹⁻¹³¹ However, the ligand that is physically adsorbed on the carbon surface suffers numerous problems of bleaching, reproducibility, and stability.^{130, 131} To develop the covalent bonded phase on the carbon surface is the ultimate goal for the modification of carbon phases. Carr et al. at Pittcon first reported the covalent modification of the carbon phase in 2001. The ligands were bonded to the carbon surface via chemical reduction of the diazonium salts. This method can only convert sub-monolayer ligands onto the carbon surface. The modification occurs

at the edge of the graphene. Thus the modified surface is heterogeneous with alternative surfaces of alky chains and the graphite sheets.¹³² Porter and his associates improved the surface coverage of the ligands. They converted a monolayer of ligands to the carbon surface via electrochemical reduction of diazonium salts in the EMLC system.¹³³ Porter's work demonstrates the feasibility of covalent bonding monolayer ligands on carbon surface. However, the implementation of the EMLC needs a special configuration of columns and additional work on instrumentation. In fact, EMLC has not been well-accepted by chromatographers due to its intrinsic instability. Moreover, the poor conductivity of the fine particle packed column results in a very slow surface modification process.¹³³ Obviously, the electrochemical modification of carbon particles in the micron range cannot be scaled up in industry.

Compared to fine carbon particles, the carbon monolith is highly conductive. Therefore, the electrochemical modification of a carbon monolith is more feasible than that of carbon microspheres. In this chapter, the author investigates the electrochemical modification of monolithic carbon columns. Tertiary amine ligands were covalently bonded to the carbon surface via electrochemical reduction of diazonium salts.¹³⁴ The modified column has been tested as a weak anion exchange chromatographic column for the separation of proteins and protein digests using aqueous mobile phases.

7.2 Electrochemical modification of carbon surface

Compared to silica chemistry, electrochemically assisted covalent modification of carbon surfaces is a relatively recently development. The first report of carbon surface modification via electrochemically generated radicals was made by Pinson and his

colleagues in 1990.¹³⁵ They oxidized a diamine to produce an amine radical that is able to bond covalently to the carbon surface. Since then, a few systems have been developed for the electrochemical modification of carbon surfaces. These systems are summarized below.

7.2.1 Electrochemical oxidation of amines

The electrochemical oxidation of amines on carbon surfaces was reported by Pinson and his colleagues in 1990.¹³⁵ The oxidation of primary amines generates solution radicals that couple to the carbon surface through covalent bonds (see Figure 47). Alkyl chains were bonded to the carbon surface through the imine group. With an appropriate functional group, an approximate monolayer can be achieved with the functionalities standing perpendicular to the glassy carbon surface. Porter et al. also examined secondary and tertiary amines.¹³⁶ They found that although all amines were oxidized on the glassy carbon surface, tertiary amines did not couple to the carbon surface, and secondary amines formed a loose layer with low surface coverage.¹³⁶ Porter's research confirmed that the attaching of an amine to the carbon surface depends on the loss of hydrogen. Tertiary amines have no associated hydrogen. Thus, tertiary amines cannot couple to the carbon surface. Due to the spatial hindrance of the substituted groups, secondary amines

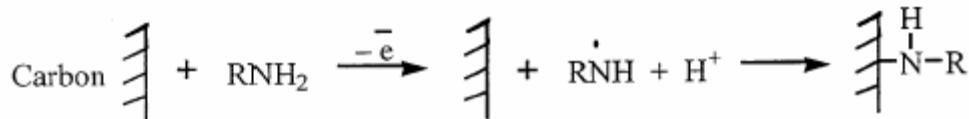


Figure 47. Electrochemical coupling primary amine on carbon surface.

7.2.2 Electrochemical oxidation of alcohols

The oxidation of alkyl alcohols at a high positive potential over 2 V versus SCE forms a self-limiting layer on the carbon surface similar to the oxidation of amines on a glassy carbon surface. The attachment of functionalities was through an ether link.¹³⁸⁻¹⁴⁰ Ohmori and his associates suggested a mechanism through which the oxidation of the carbon forms an aromatic radical, which was attacked by the alcohol via the nucleophilic reaction.

As with the oxidation of amines, the oxidation of alcohols can graft a dense layer only on the glassy carbon. The modification of functionalities on the graphite is heterogeneous and occurs at the edge of the graphene sheet.

7.2.3 Kolbe reaction

The oxidation of arylacetates on both glassy carbon and graphite was investigated by Saveant in an acetonitrile solution.¹⁴¹ A covalently bonded aromatic layer can be grafted to the carbon surface at low potential. The surface coverage on the glassy carbon is three times greater than that on the graphite surface. The modification undergoes a Kolbe reaction generated radical that couples to the carbon surface.

7.2.4 Electrochemical reduction of diazonium salts

The electrochemical reduction of diazonium salts on carbon surface is by far the most investigated method for the electrochemically-assisted modification of carbon surfaces. The modification results in a dense layer of functionalities on both glassy carbon and graphite surfaces. The diazonium salts undergo a one-electron reduction on carbon surface and yield radicals that couple to the carbon surface. The coupling

efficiency of the radical depends on the life span and stability of the radical. The aryl diazonium cation yields a more stable aromatic radical than alkyl groups. Therefore the coupling efficiency of the aryl diazonium cation is much higher than the alkyl diazonium cation. Shown in Figure 49 is the coupling mechanism of the aryl diazonium on the carbon surface that was proposed by Pinson et. al.¹⁴²

The coupling of the aryl group on the carbon surface was favored by both adsorption of the diazonium salts on the carbon surface and by the relatively positive reducing potential of the diazonium that prevents simultaneous reduction of the aryl radical. The coupling of aryl group to the carbon surface occurs on both the glassy carbon surface and the graphite surface. The grafting rate at the edge is faster than that at the basal plane of the graphite sheet. Pinson and Saveant found that not all the radicals coupled to the carbon surface.¹⁴³ The electrochemically generated radical is partially leaked into the solution. According to their research, 84% of the electrochemically generated radical coupled to the glassy carbon, and only 56% of the electrochemically generated radical coupled to the basal plane of the highly ordered pyrolytic graphite (HOPG). Therefore, the modification begins at the edges and moves across the basal

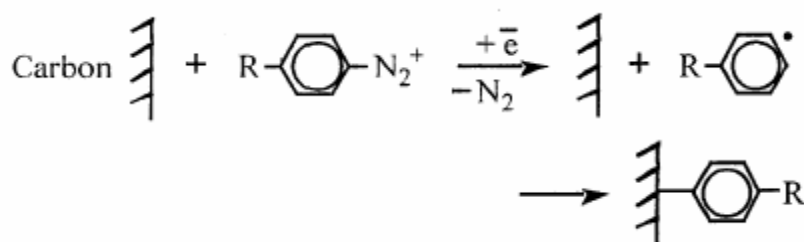


Figure 49. Coupling mechanism of the aryl diazonium on the carbon surface

plane until all surfaces are covered by the ligand. A monolayer of coverage can be achieved with a prolonged deposition time.

7.3 Electrochemical modification of carbon monolith

As we concluded in the previous chapters, the pyrolytic carbon materials are microporous. For most applications in which small pharmaceutical molecules are separated, the presence of micropores in the stationary phase matrix dramatically broadens the bands. Consequently, the column efficiency of the microporous glassy carbon packed column is unsatisfactory. To eliminate the micropores, one can either treat the carbon thermally at temperatures above 2100 °C to graphitize the carbon, or block the micropores through surface modification.

The surface modification of carbon surface has at least two benefits: one is the modification allowing the variation of the adsorption/desorption properties of the carbon surface. Depending on the functionalities, the carbon stationary phase is able to incorporate all the advantages of the silica columns without suffering the pH limitation. The other benefit of surface modification is the elimination of the effect of micropores. The pyrolytic carbon has micropores less than 1 nm that can be blocked by two benzene rings. Numerous researchers in electrochemistry have demonstrated that the covalent coupling of the electrochemically generated radical to the carbon surface starts at the edge of the graphene and at the defects of the carbon matrix. In glassy carbon the defects are micropores that are less than 1 nm. At the beginning of the electrochemical modification, the micropores are blocked by the radicals due to their high reactivity. Thus,

the electrochemical modification of the carbon surface can efficiently eliminate the effect of micropores.

To demonstrate this concept, we modified a tertiary amine to the carbon monolith electrochemically. After the modification, the column was tested as a weak anion exchange column. The separation tests were performed in an aqueous mobile phase by varying the salt concentration of the mobile phase. A protein mixture and a protein-digest tested the column.

7.4 Experimental

Materials: Monolithic carbon rods were prepared by using the method described in Chapter 6. Tris(hydroxymethyl)aminomethane (99.9%), sodium chloride (99.99%), 4-diethylaminobenzenediazonium tetrafluoroborate (99%), tetrabutylammonium tetrafluoroborate (97%), acetonitrile, calcium hydride and hydrochloric acid (37%) were purchased from Aldrich. Aprotinin bovine lung and Ovalbumin were purchased from Sigma. Cytochrome c digest was contributed by Dr. Guiochon's group. The DI water was obtained from the lab pipeline and purified before use by a Millipore lab water system. All chemicals except solvents were used as received. Solvents were dried thoroughly using calcium hydride.

The electrochemical modification of carbon monolith: The electrochemical modification of the carbon surface was carried out using a CH 604 B electroanalysis system (CH Instrument Inc.). Two carbon rods were used as electrodes. One was used as the working electrode and was the target for the modification. The other carbon rod was used as both counter electrode and reference. The electrochemical reaction was

conducted in an anhydrous acetonitrile solution. 4-diethylaminobenzenediazonium tetrafluoroborate and tetrabutylammonium tetrafluoroborate were employed as electrolytes. In a typical run, 30 ml acetonitrile solution containing 0.2 g of tetrabutylammonium tetrafluoroborate and 0.6 g of 4-diethylaminobenzenediazonium tetrafluoroborate was placed in a long tube was fixed with two separated carbon rods. The solution covered 12 cm of the lower ends of the carbon rods. The upper ends of the carbon rods were hooked to the electrochemical system. The electrochemical reduction was carried at -0.8 V for a period of 20 hours.

The fabrication of the HPLC column: The working electrode was washed thoroughly with acetonitrile after the electrochemical modification. The rod was then dried in a vacuum oven at 80 °C. A column was fabricated by using the polymer lined stainless steel tube encasing configuration. The details of the cladding procedure are described in Chapter 2.

The chromatographic test of the modified column: The chromatography tests were performed with a Hewlett-Packard (Palo Alto, CA, USA) HP 1100 LC system. The system consisted of a binary pump, an online degasser, an autosampler, a diode array detector, a column thermostat, a data station, and an HP PC workstation with a Windows NT operating system. The instrument control and data acquisition were performed using Chemstation software (Rev A 05.03). The column temperature was maintained at 25 °C. The mobile phases used were: A, 0.01M Tris buffer (pH 7.4), and B, 1M sodium chloride in A. The online degasser degassed the mobile phases before mixing in the binary pump.

The gradient was controlled through the Chemstation. The flow rate was maintained at 1 ml/min. The data was collected at 230 nm using the diode array detector.

7.5 Results and discussion

7.5.1 The structure of the monolithic columns

Shown in Figure 50 is a reconstructed 3-D image of the carbon monolith after electrochemical modification. The skeleton size of the carbon monolithic was estimated by the SEM images. The main skeleton size is about 500nm and the size of the knot is about 1000nm. The pore size is about 2 micron. The pores are well interconnected through smooth transitions. Such a pore structure accounts for the extremely low hydraulic resistance of the carbon monolithic column.

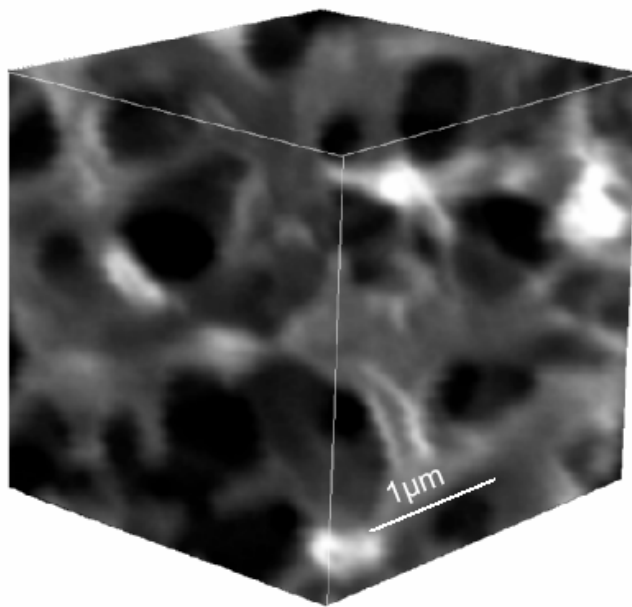


Figure 50. A reconstructed 3-D image of the carbon monolith. The image was composed by a series of SEM images, which were taken from sequential depths of carbon sample in the range of 0 to 1000nm.

7.5.2 The electrochemical modification of monolithic columns

The electrochemical reaction is represented in Figure 51. The electrochemical reduction of the diazonium in anhydrous acetonitrile produces aryl radicals on the electrode surface. When the carbon monolith was employed as the working electrode, the electrochemically generated radicals coupled to the carbon surface through covalent bonding.

Since the carbon monoliths were prepared through a relatively low temperature carbonization procedure, the carbon matrix is microporous glassy carbon. The micropore size is less than 1 nm. All pores are homogeneously distributed over the entire piece of carbon. It is worth noting that the edges of the micropores are carbon atoms with sp^3 hybridization. As demonstrated by many recent researchers, the edge atoms are more electrochemically reactive than the basal plane atoms. Therefore, the chemical modification of the carbon monoliths starts from the edge of the micropores.

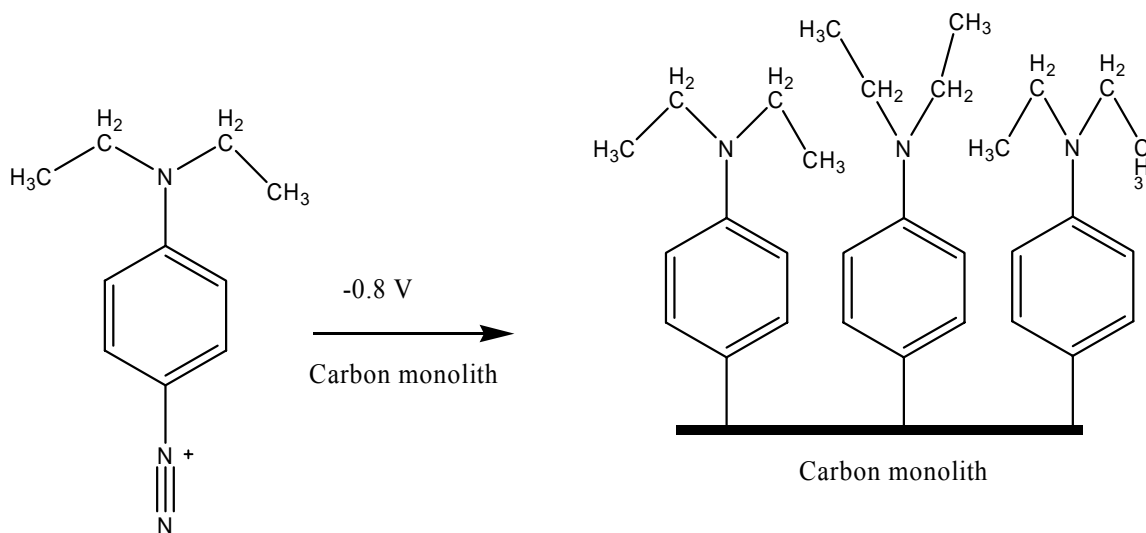


Figure 51. Electrochemical modification of carbon surface.

Shown in Figure 52 are the front, side, and top views of the chemical structure of the electrochemically grafted ligand. The ligand is 7.875 Å high, 5.621 Å long, and 4.398 Å wide. Thus, the grafting of this ligand at the edge of the micropores can efficiently block the openings of the micropores. Therefore, the chemical modification can eliminate the micropores believed to be the main cause of peak broadening in the glassy carbon columns. Indeed, when the unmodified carbon column was injected with 10 µl sample of toluene in acetonitrile (10mg/L) no peak was eluted through the column due to the extreme adsorption of the analytes to the micropores. After modification, the chromatographic performance is reasonably effective.

The micropores were blocked in the early stage of modification. A column modified for 30 min at -0.8 V is able to achieve moderate chromatographic performance with relatively broad peak compared to a column after a long period of electrochemical modification. Columns that have been electrochemically modified 20 hours or longer exhibit no difference in the chromatographic performances. Therefore, we conclude that 20 hours is long enough to ensure the completion of the surface modification for the glassy carbon rods.

Theoretically, the glassy carbon surface is reactively heterogeneous. The edge of the micropores and the defects in the basal plane are believed to be more reactive than the basal plane carbon. These relatively active sites are favored at the beginning of the reaction. After the coupling of the ligands to these relatively reactive sites, these sites become nonconductive. Thus, further growth of the modification layer is limited by the poor electric conductivity of the modifier. After the ligands cover the more reactive edge

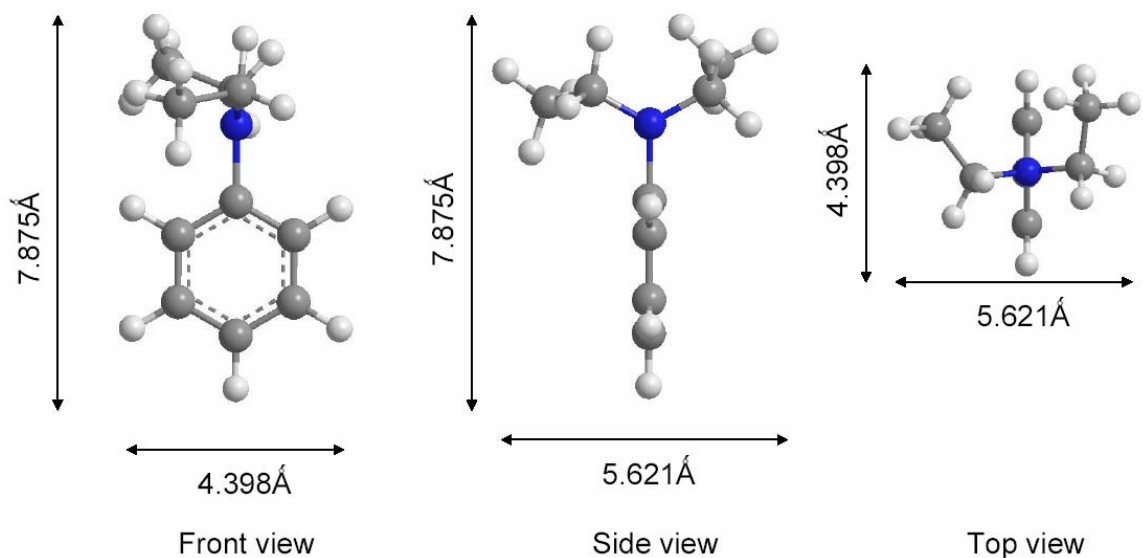


Figure 52. The front, side, and top views of the ligand. This ligand is 7.875 Å high, 5.621 Å long, and 4.398 Å wide.

and defects sites, the coupling on the less reactive basal plane carbon begins to dominate the surface modification process. The electrochemical reaction does not cease until the last electro-conductive site is coupled by the electrochemically generated radical. Consequently, the entire carbon surface is covered by the ligand at the end of the electrochemical modification. Since the modification is limited by the conductivity of the surface, the thickness of the surface modifier is limited by its poor conductivity. Thus, a homogeneous monolayer is achieved by modifying nonconductive ligands onto the carbon surface.

7.5.3 The HPLC performance of the electrochemically modified columns.

Although aryldiazonium salt has been demonstrated to be a universal modifier for carbon surfaces, the lack of appropriate commercially available diazonium salts is the

major obstacle in carbon surface modification. In this study, we found that the 4-diethylaminobenzenediazonium tetrafluoroborate is a relatively cheap diazonium salt available from stable commercial sources. This diazonium salt converts a tertiary amine to the carbon surface. This tertiary amine is terminated with two ethyl groups. The diethyl tertiary amine has been used as a weak anion exchanger (WAX) in the practice of many silica or polymer based columns.^{129, 144-146} Therefore, we expected the modified column to perform ion exchange chromatography.

In order to probe the ion exchange properties of the modified column, two biomolecule mixtures of different molecular weights were tested using the modified carbon monolithic columns. The first mixture was the aprotinin bovine lung and ovalbumin. These two compounds are proteins having molecular weights over 65000 Dalton. The molecular sizes of these two compounds are beyond the mesopore range. Therefore, the retention of these two compounds is governed by the external surface of the monolithic column. Shown in Figure 53 is the chromatogram of aprotinin bovine lung, and ovalbumin. The mobile phases were 0.01 M Tris buffer (pH 7.3) and 1 M sodium chloride in 0.01 M Tris buffer. The aprotinin bovine lung is less charged than the ovalbumin, so it had less retention on the ion exchanger surface.

The second mixture was the cytochrome c digests. The cytochrome c digests are a mixture of peptides and amino acids with molecular weights in the range of several

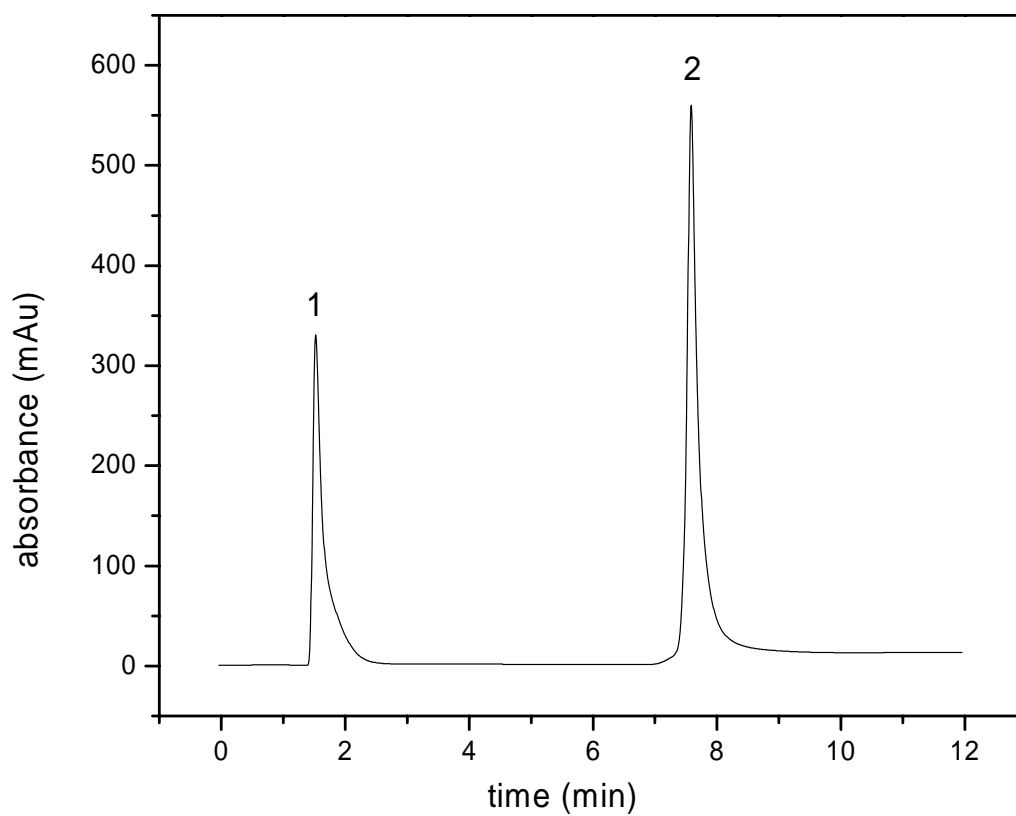


Figure 53. Chromatogram of the mixture of 1 aprotinin bovine lung, and 2 ovalbumin. Mobile phase: A, 0.01 M Tris buffer (pH 7.3); B, 1 M NaCl in A. Injection volume: 10 ul solution that contains 10mg/L of each compound. Gradient: 0-100% B in 10 min. Flow rate: 1ml/min. Column pressure: 20 bar. Detector: UV 230 nm.

hundreds to a few thousands Dalton.(Figure 54) The digests have molecular sizes that are small enough to penetrate into the mesopores. Thus, the retentions of these small molecules are attributed to the interaction of both the internal and external surface of the carbon monolithic column. Only seven peaks appeared in the chromatogram, which indicates that the mixture was not totally resolved under experimental conditions. In the separation of the protein digest, a steeper gradient was required to achieve a good peak shape for the strongly retained compounds. In addition, the peak widths of the protein digest were broader than those of the large protein mixture. The mesopore distribution of the column was measure by BET with N₂ at liquid nitrogen temperature. The BET results indicated a very broad distribution of mesopores. The center of the mesopore size distribution is about 5 nm. This pore size is slightly smaller than those of most commercial columns. Such a mesopore size distribution is not favored in the separation of small molecules. As discussed in Chapter 6, it is necessary to develop a method to produce mesoporous carbon with tunable and more uniform pore size.

The modified column has very low hydraulic resistance. When a column of 10cm long and 2.9mm ID was operated at the linear flow rate of 1mm/s of aqueous mobile phase, the back pressure is only 14 bars. This superior hydrodynamic property is attributed to two facts: 1) the well wetting of the carbon surface after grafting of the amine ligand, and 2) the monolithic structure, which consists of highly connected channels.A control column was made by using an unmodified carbon rod. The control column was connected to the HPLC system and tested using the protein mixture and protein digests. Both probe solutions are firmly retained on the control column. None of

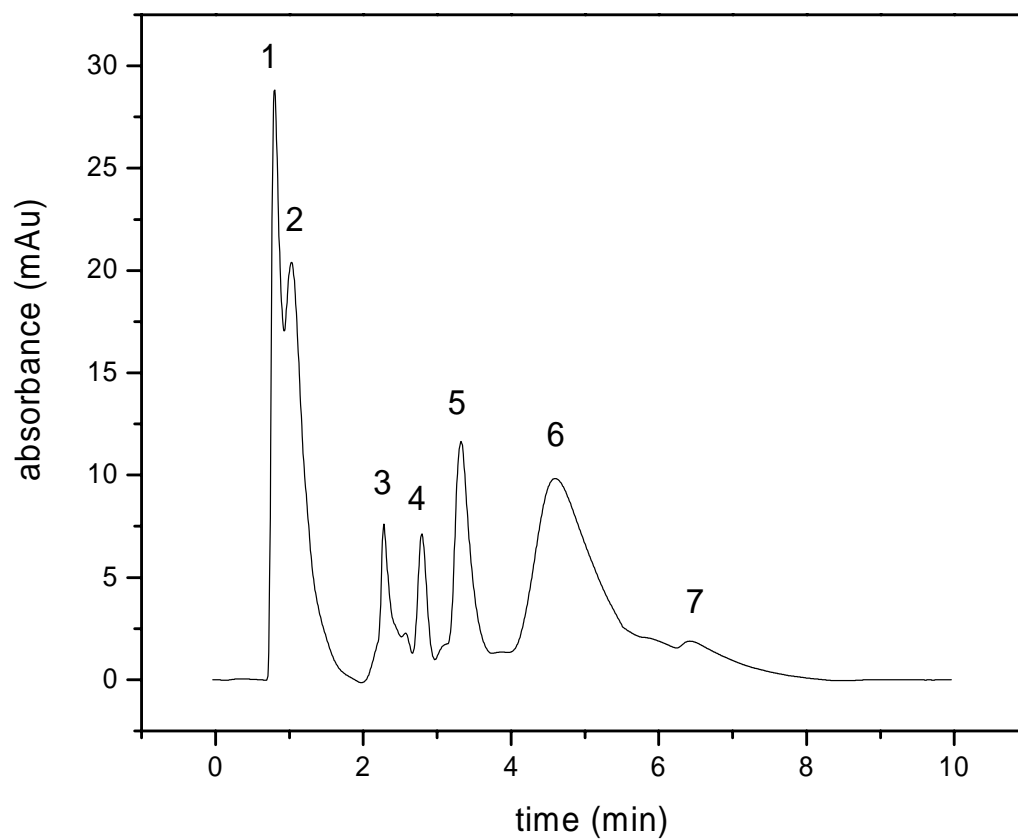


Figure 54. The separation of the cytochrome c digests. Buffer: 0.01 M Tris buffer (pH 7.4). Mobile phase: A, 0.01M Tris buffer; B, 1M NaCl in A. Gradient: 0% B increases to 100% in the first 4 minutes then keep 100% B for 6 minutes. Column ID: 2.9mm. Column length 10cm. Flow rate: 1ml/min.

the compounds are able to elute by using the salt solution in the Tris buffer. The back pressure of the control column is higher than the modified column by a factor of ~ 1.5 when the aqueous solution was used as the mobile phase. This phenomenon confirms that the modified carbon surface is more hydrophilic than virgin carbon.

7.6 Conclusion

This research proves the concept that the carbon surface can be uniformly modified by electrochemical means. The self-limiting nature of the electrochemical reaction ensures the carbon surface will be completely covered with no more than a monolayer of ligand. The properties of the carbon surface were changed after the modification with the ligand. The hydrophobic carbon surface can be converted to hydrophilic surface by electrochemically grafting tertiary amine ligands. The modified carbon surface has the ability to conduct ion exchange chromatography using aqueous mobile phases. The micropores that are inherent in the low temperature glassy carbon can be blocked by the grafted ligands. The blockage of the micropores demonstrates that the electro-modification of carbon surface is an efficient method to convert the glassy carbon into a useful stationary phase material as an alternative to the well-known graphitization method. Indeed, this research demonstrates that the graphitization of carbon is not the only method for the elimination of the micropores in the carbon matrix.

This research also demonstrates that the chromatographic properties of carbon are determined by the properties of the surface modifier. In this research the para- position of the aryldiazonium is tertiary amine. Thus, the chromatographic properties of the carbon monolith are of ion exchange type. Since the para-position of the aryldiazonium can be

substituted by various functional groups that can cover all branches of chromatography, it is safe to predict that the chromatographic properties of the modified carbon surface are not limited to ionic exchange. It is possible to use the carbon monolith as a substitute for silica with the advantage of chemical and physical inertness.

Although theoretically the carbon surface can be converted to meet the requirements of any type of chromatography, the implementation of the conversion is limited by the commercial availability of diazonium salts. Further research efforts are needed to produce a variety of diazonium salts for the purpose of offering more options for carbon surface modification.

Chapter 8: Chromatographic characterization of carbon based columns

The motif of this chapter is the study of the isotherms of a set of compounds that have various chemical properties. The surface properties of the as-synthesized glassy carbon, graphitized carbon, and electrochemically modified carbon have been closely examined by comparing the experimental data with several theoretic isotherm models such as langmuir, bilangmuir, antilangmuir, and quadratic isotherm.^{147, 148} Each isotherm model is based on a specific physicochemical hypothesis. The qualities of the fitting of the isotherm models to the experimental data have been examined by the error level of the fitted parameters. The best fitting model of each isotherm reveals interactions between the adsorbate and adsorbent.¹⁴⁷ By using a set of probing compounds, the surface properties of the adsorbent can be summarized from those isotherms.

The adsorption properties of the graphitized carbon surface have been further investigated by changing the temperature and pressure.¹⁴⁹⁻¹⁶⁰ The temperature effect was examined by single compound adsorption of toluene and resorcinol at 30, 40, 50, 60 °C. The pressure effect was found in the brush type C18 silica columns. The alkyl chain densities of the adsorbents greatly affect the pressure effects. The adsorption on the graphitized carbon surface is assumed to occur on the basal plane of the graphitic surface. Investigation of the pressure effect on flat graphene surface is of great theoretical importance in the fundermental understanding of the question of whether or not the pressure effect occurs on solid surface. In this research, the influence of pressure on the retention facts of Cyclohexanol and o-xylene has been studied with pure acetonitrile

mobile phase at 303 K. A linear relationship between $\ln k'$ and average column pressure has been derived from the experimental data.

The reproducibility of the synthesis method has been evaluated by using 6 columns from 2 batches of synthesis.¹⁶¹⁻¹⁶⁶ Each batch has 3 columns. Column-to-column and batch-to-batch reproducibility have been closely evaluated by the retention factor k and the HETP.

8.1 Isotherm models

In most cases, the quality of the fitting of isotherm models with the experimental data indicates how close the practical adsorption case fits theoretic hypothesis.^{75, 147, 148, 167, 168} In this study, four isotherm models have been considered and fitted with experimental data.

8.1.1 The langmuir model (L):

The langmuir model assumes a homogeneous surface with uniform adsorption energy. If the isotherm fits the langmuir model well, the retention of the adsorbate is uniformly adsorbed on the stationary phase. The ideal adsorption of the langmuir model is forming a monolayer of adsorbate on the adsorbent surface when the saturation of the adsorption is reached.

The formula of the langmuir model is written as:

$$q = \frac{q_s KC}{1 + KC} \quad 8.1$$

where q_s is the specific saturation capacity of the adsorbent and K the equilibrium or binding constant of the compound considered in the phase system studied.

The langmuire model has two parameters, so the fitting equation is written as:

$$y = \frac{P_1 P_2 x}{1 + P_2 x} \quad 8.2$$

where P_1 and P_2 stand for q_s and K respectively.

8.1.2 The antilangmuir model (AL):

The antilangmuir model assumes a strong adsorbate to adsorbate interaction, which reveals the interaction of adsorbate to adsorbent is weaker than the interaction of adsorbate to adsorbate. The adsorption starts from several relatively high energy sites, and then these sites seed the further adsorption. Thus, the adsorption of the adsorbate on the stationary phase surface is heterogeneous. The antilangmuir model fits the concave type isotherms. The formula is similar to the langmuir isotherm with a difference only in the sign of equilibrium constant.

$$q = \frac{q_s KC}{1 - KC} \quad 8.3$$

The fitting equation is written as:

$$y = \frac{P_1 P_2 x}{1 - P_2 x} \quad 8.4$$

Similar to the langmuir model, P_1 and P_2 stand for q_s and K respectively. In the antilangmuir model the q_s and K do not have the same physical meanings as they do in the langmuir model.

8.1.3 The bilangmuir model (BL):

The bilangmuir model assumes a heterogeneous surface of the adsorbent with at least two types of adsorption sites: the strong sites dominate the adsorption; however, the weak sites contribute significantly to the total adsorption.

The bilangmuir model is the sum of two langmuir equations:

$$q = \frac{q_{s,1}K_1C}{1 + K_1C} + \frac{q_{s,2}K_2C}{1 + K_2C} \quad 8.5$$

where $q_{s,1}$ and $q_{s,2}$ are specific saturation capacities of the two types of adsorption sites and K_1 and K_2 are corresponding equilibrium constants.

The bilangmuir model is a four parameter equation, written as:

$$y = \frac{P_1P_2x}{1 + P_2x} + \frac{P_3P_4x}{1 + P_4x} \quad 8.6$$

8.1.4 The quadratic model (Q):

The quadratic model is an empirical formula for complex adsorption/desorption cases. Usually, a number of adsorption sites of various energies contribute to the adsorption. The bilangmuir model is a special case of quadratic model.

The quadratic equation is written as:

$$q = q_s \frac{a_1C + 2a_2C^2}{1 + a_1C + a_2C^2} \quad 8.7$$

This three-parameter equation is fitted with the equation below:

$$y = P_1 \frac{P_2x + 2P_3x^2}{1 + P_2x + P_3x^2} \quad 8.8$$

8.2 Experimental

8.2.1 Column preparation

The monolithic columns were prepared as the procedure described in the previously chapters. The graphitized carbon rods were bent after the glassy carbon rods had been graphitized at 2800 °C. No monolithic graphitized carbon column has been made because of the technical difficulty of cladding the bent rods. The particulate columns of glassy carbon, graphitized carbon, and modified carbon were prepared by particles of these materials in the range of 10 to 25 μm . The particles were prepared by first grinding 5 pieces of 12cm long rods of these materials and then wet sieving the particles through a 25 μm sieve in ethanol. The collected particles were dispersed in 100ml ethanol with the aid of sonication. Afterwards, the suspension were poured into 1L 30:70 chloroform/ethanol mixture and allowed to settle for 1.5 hour to allow the precipitation of the particles. The small particles were sorted by discarding the suspension. The collected precipitation repeated the dispersion/ precipitation cycle for 3 more times. The final collection of the precipitation was dispersed in 30 ml 1:1 chloroform/isopropanol solvent for slurry packing. All particulate columns were slurry-packed at 6000 psi by using a 1:1 mixture of chloroform and isopropanol.^{75, 167}

8.2.2 Column performance

Column performance measurements were conducted at analytic conditions by the injection of various compounds with a typical injection volume of 10 μL . The column performance was evaluated by peak symmetry, retention factor, and column efficiency.¹⁶⁸ The peak symmetries of glassy carbon column, graphitized carbon column, and

electrochemically modified column were compared at identical HPLC condition with a set of probing compounds. A constant flow rate of 1ml/min was used for the evaluation of peak symmetry. The elution of toluene was carried out by 20:80 chloroform/acetonitrile, and resorcinol and tetradecylresorcinol were by 85:15 methanol/water. The retention factor was recorded at the maximum peak position. The Van Deemter plot was measured at various flow rates on the graphitized carbon and modified carbon columns. The linear flow rate tested on the particulate graphitized carbon column was from 0.125 to 2 mm/s, and on the monolithic modified carbon column the rate was from 0.3 to 12 mm/s.

8.2.3 Frontal analysis (FA)¹⁶⁹

The adsorption isotherms were determined by using frontal analysis. One pump of the HPLC instrument was used for delivering the solution of adsorbate and the other pump for delivering the pure mobile phase. A set of sample concentrations was achieved by varying the mixing ratios of solutions delivered by the two pumps. The Chemstation software controlled the mixing ratio and time. At a certain point in time, the column was equilibrated with a solution of concentration C_i , a plateau was recorded corresponding to the equilibrium at the concentration C_i . Then the stream was abruptly replaced by another one with concentration C_b , which is higher than C_i . A breakthrough curve that resulted from the concentration change was then recorded. The concentration change in the stationary phase Δq can be calculated from the equation:

$$\Delta q = \frac{(V_r - V_0)(C_b - C_i)}{V_s} \quad 8.9$$

where, V_r is the retention volume, V_0 is the dead volume of the system, and V_s is the volume of the stationary phase.

The isotherm is determined by measuring a number of successive points, corresponding to various concentration steps. The probing chemicals are 4 alkylbenzenes, which include toluene, amylbenzene, octylbenzene, and tetradecylbenzene, resorcinol, tetradecylresorcinol, naphthalene, and aniline. The selection of mobile phases depends on the compound and the chemistry of the column. All isotherm measurements on the modified carbon were carried out with 15:85 water/methanol. The elution of alkylbenzene on graphitized carbon was conducted by 20:80 chloroform/acetonitrile. The isotherm of naphthalene was done with pure chloroform.

The temperature was controlled by the thermostat that comes with the Agilent 1100 HPLC system. Isotherms of toluene and resorcinol on the graphitized column were measured at 30, 40, 50, and 60 °C. Other isotherms were measured at 30 °C.

The system tubing volume was measured when the column was replaced with a zero dead volume union.

8.2.4 Surface area and porosity measurements

The surface area measurements were conducted with N_2 at liquid nitrogen temperature by using a Micromertic 2750 system. A BET model was employed for the calculation of surface area. The porosity of micropore and mesopore was given by the software that comes with the system. The porosity of micropore and mesopore was used as the internal porosity ϵ_1 of the adsorbent.

The total porosity ε_T was measured by column dead volume; ε_T of each column was measured individually by the injection of non-retained compounds. The measurements of dead volumes of carbon columns were obtained by the injection of a 10 μL water. The modified columns were measured by the injection of 10 μL acetone.

The external porosity ε_E is attributed to the ratio of the macropore volume to the overall column volume. The external porosity of the particulate column depends on the packing density and the average particle size. The external porosity of the monolithic column is generally higher than that of the particulate columns. The macropores or the so called go-through pores are the main source of external porosity. It is easier to calculate the external porosity ε_E by subtracting the internal porosity from the total porosity than the directly measure the ε_E . The calculation is based on equation 8.10.

$$\varepsilon_E = \frac{\varepsilon_T - \varepsilon_I}{1 - \varepsilon_I} \quad 8.10$$

8.2.5 The measurement of the bonding density of the electrochemically modified carbon column

The bonding density of the electrochemically modified carbon was measured by thermogravimetric analysis-mass spectrometry (TGA-MS). The measurement was done with a TA instrument Q-50 system. The heating rate is set at 10 $^{\circ}\text{C}/\text{min}$. The sample was heated in nitrogen environment from room temperature to 600 $^{\circ}\text{C}$. A fraction of the debris that comes from the pyrolysis of the bonded ligand was monitored by the mass spectrograph.

8.2.6 Pressure effect on graphitized carbon column

The pressure effect on the graphitized carbon column was investigated by the elution of the o-xylene and cyclohexanol at various average column pressures. Pure acetonitrile was used as mobile phase. Concentrations of analytes are 10mg/ml of o-xylene and 15mg/ml of cyclohexanol. The injection volume is 10 μ L. Flow rate was kept constant at 1ml/min. The average column pressures were adjusted by adding a piece of PEEK tubing to the outlet of the detector.^{149, 152} The retention factors were recorded at average column pressures of 186, 217, 242, 297, and 321 bars. Each data point of retention factor was averaged over five repeated measurements.

8.2.7 Reproducibility of columns

The reproducibility of the columns was evaluated by retention factors and column efficiencies. The measurements were based on the elution of toluene by 85:15 methanol/water mixture at 1ml/min. The injection volume is 10 μ L. Each measurement was repeated five times. Six monolithic columns from two batches were compared by retention factors and HETPs.

8.3 Results and discussion

8.3.1 Column physical parameters

Nine columns were made from the monolithic carbon rods for the evaluation of the chromatographic use of the hierarchically porous carbon material that has been synthesized via the method described in Chapter 5. These columns have three types of chemistry: the glassy carbon, the graphitized carbon, and the electrochemically modified carbon. Eight monolithic columns were made from two batches of carbon rods, which

were synthesized using identical conditions. Six of the eight monolithic columns were electrochemically modified with diethylbenzene group. The details of the electrochemical modification were discussed in Chapter 7. The remaining 2 monolithic columns are made of as-synthesized glassy carbon.

The glassy carbon rods have been graphitized in helium environment at 2800 °C.

Unfortunately, the graphitized carbon rods were seriously bent after the high temperature treatment. Although the bent monolith can be clad into a monolithic column by some industrial means, we encountered technical difficulties in encapsulating bent rods with any column configuration described in Chapter 2. For the purpose of evaluating the graphitized carbon, the bent rods have been ground into fine particles sized in the range of 10 to 25 microns. The graphitized porous rod was then evaluated in the form of a particulate column. The physical parameters of these columns are tabulated in Table 3.

8.3.2 Column performance

Column performance is tested on three types of columns: the glassy carbon column (column C-50-M-1), the electrochemically modified carbon (column C-50-M-1-DEA), and the graphitized carbon column (column G-50-P). Figures 55 to 57 show chromatograms of the columns with injections of toluene, resorcinol, and 2-tetradecylresorcinol.

The elution of all three compounds on glassy carbon has very broad peaks with only a few tens theoretic plates. Obviously, the glassy carbon is not a suitable material for column adsorbent. The modified carbon column and the graphitized carbon column have good chromatographic performances. The size distribution of macropores, or the content

Table 3. Physical parameters of carbon based columns that synthesized by using the monolithic technique described in Chapters 5 and 7.

Column	I.D. (mm) *	Length (mm)	ϵ_T	ϵ_I	ϵ_E	Specification
C-50-M-1-DEA	3.0	100.2	0.84	0.11	0.82	1. carbon monolithic columns made from carbon rods batch 1 2. all rods were made from 50% of polymer 3. all rods have been electrochemically modified with diethylamine group
C-50-M-2-DEA	3.0	98.1	0.81		0.79	
C-50-M-3-DEA	3.0	99.5	0.82		0.80	
C-50-M-4-DEA	3.0	101.4	0.82	0.12	0.80	carbon monolithic columns made from carbon rods batch 2, which were made by identical synthetic conditions of batch 1
C-50-M-5-DEA	3.0	97.9	0.81		0.79	
C-50-M-6-DEA	3.0	100.6	0.82		0.80	
C-50-M-1	3.0	103.5	0.82	0.15	0.80	carbon rod from batch 1
C-50-M-2	3.0	101.2	0.81	0.15	0.78	carbon rod from batch 2
G-50-P**	4.6	79.6	0.68	0.11	0.63	a packed column by using ground graphitized carbon rods

Note: * I.D. stands for the column internal diameter.
** The column was packed in a piece of manually cut stainless steel tubing. The ends of the tube were polished by using 1200 mesh sandpaper.

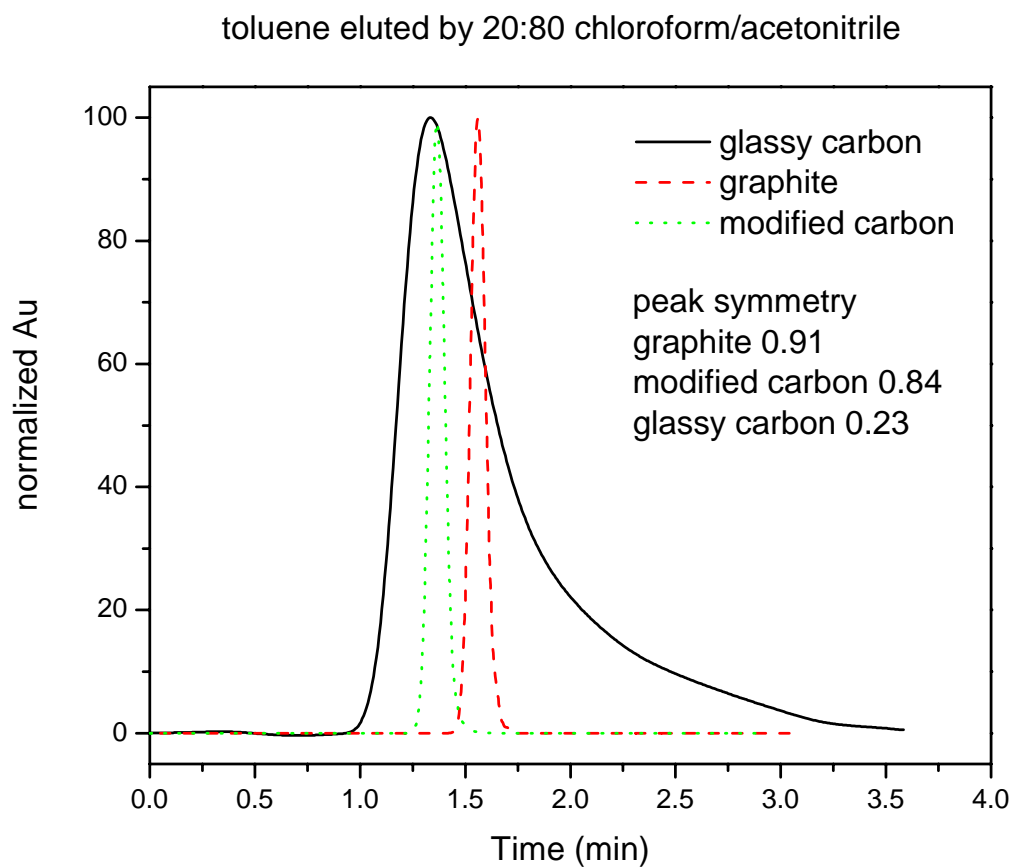


Figure 55. Toluene eluted by chloroform and acetonitrile 20/80 at flow rate 1ml/min.

k' is 1.2 on glassy carbon, 0.75 on graphitized carbon, and 0.51 on modified carbon.

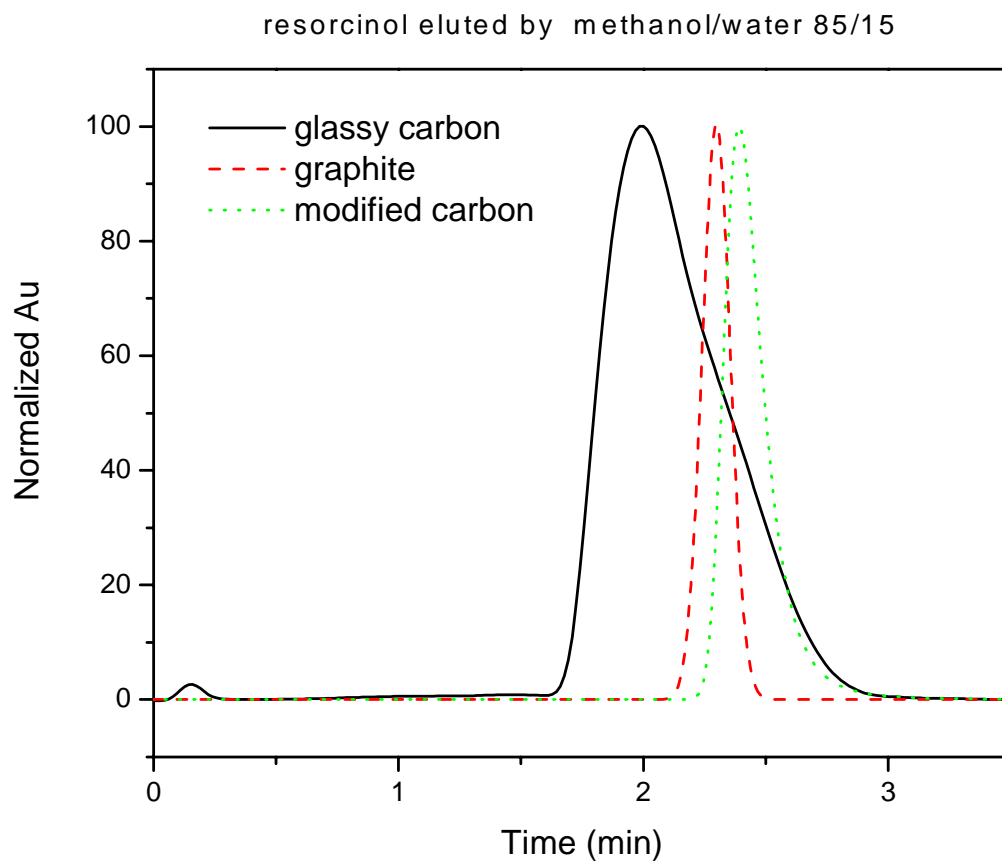


Figure 56. Resorcinol eluted by methanol and water 85/15 at flow rate 1ml/min. k' is 2.2 on glassy carbon, 1.57 on graphitized carbon, and 3.02 on modified carbon.

2-tetradecylresorcinol on glassy carbon/ graphitized carbon/ modified carbon
Mobile phase : methanol/water 85/15

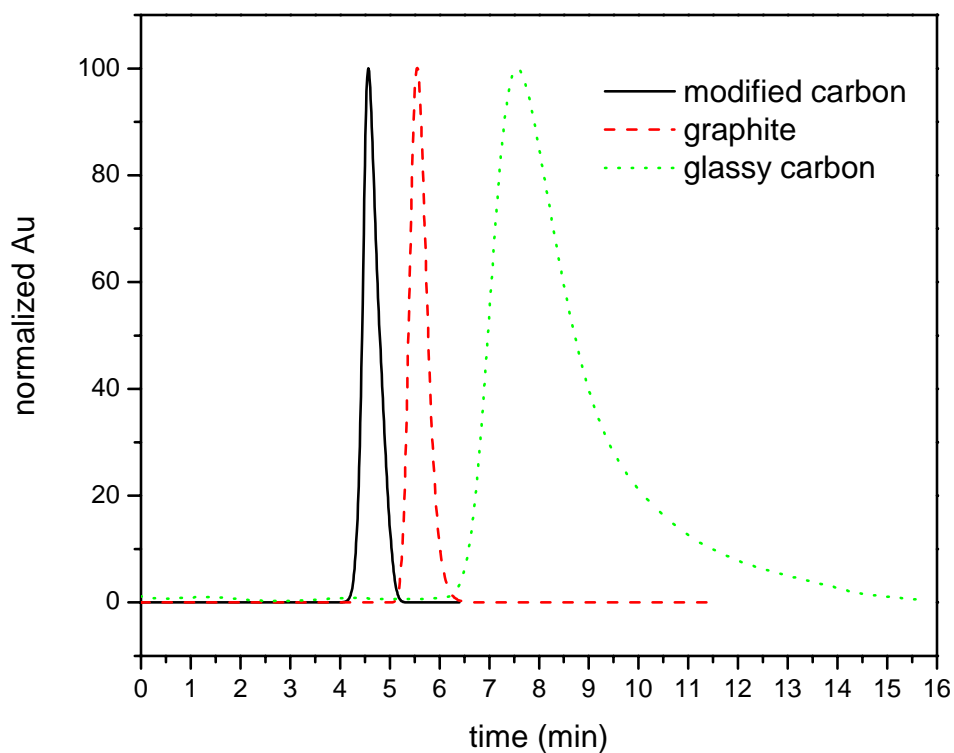


Figure 57. 2-tetradecylresorcinol eluted by methanol and water 85/15 at flow rate 1ml/min. k' is 12.5 on glassy carbon, 5.2 on graphitized carbon, and 6.7 on modified carbon.

of micropores, or both may affect the column performance of the monolithic column. The carbon materials used in this study are from the same source. Since the electrochemical modification of the carbon surface only converts a monolayer of functionalities to the carbon surface, the size distribution of the macropores of the electrochemically modified carbon column is almost identical to that of the glassy carbon column. The influence of macropore size distribution on the column performance can be ruled out. The differences between the modified carbon column and glassy carbon column are located in two aspects. The first aspect is that the volume of micropores in the glassy carbon has been greatly reduced after the modification. The internal porosity of the modified carbon column is 0.148, which is higher than 0.118 the internal porosity value of the modified carbon. The change of surface area gives further evidence of the blockage of micropores after the modification of glassy carbon. The surface area of the glassy carbon column is 215.1 m²/g. When the surface of the glassy carbon has been covered by the modified ligand, the surface area dramatically dropped to 35.2 m²/g. Thus, micropores contribute most of the surface area of glassy carbon. The second aspect is that the surface chemistry of glassy carbon is very different from that of modified carbon. Because of the difference in the surface chemistry, the retention of compounds on glassy carbon differs from that on modified carbon. The surface chemistry of the modified carbon is discussed in depth in Chapter 7. The bonding density of the modified carbon is discussed in Section 8.3.4.

The performance of graphitized carbon column is surprisingly good, though the graphitized carbon column is a packed column. As discussed regarding the modified carbon column, the elimination of micropores may be the major reason for the

improvements of the column performance. The high temperature treatment of glassy carbon causes significant change in the surface area and the volume of micropores. Deriving from the BET measurement, graphitized carbon has a surface area of only 15.7 m²/g. The internal porosity of the graphitized carbon column is 0.11, which is lower than that of the modified carbon. The drawback of the packed graphitized carbon column is the unusually high back pressure. The SEM images of the macropores show that the average macropore size of the graphitized carbon is about 20% less than the glassy carbon. However, the backpressure of the particle column is higher than the monolithic column by a factor of 8. Such a high back pressure is probably due to the irregular particle shape and wide distribution of particle size.

Peak symmetry is also improved by the elimination of micropores. Shown in Table 4 is the peak symmetry data derived from chromatograms in Figures 55 to 57. By definition, the peak symmetry factor is the ratio of the left side peak width to that of the right side at 10% of the peak height. Peak symmetry establishes clear evidence for the surface homogeneity of the carbon materials.¹⁶⁸ The peak symmetry of graphitized carbon is better than that of the modified carbon, and the modified carbon is better than the glassy carbon.

The retention factors on glassy carbon are always higher than those on graphitized carbon and modified carbon, whereas the relative value of retention factors of the compounds on modified carbon and graphitized carbon depends on the properties of the elutes. For example, k' of resorcinol is higher on modified carbon than on graphitized

Table 4. Peak symmetry of columns tested by toluene, resorcinol, and 2-tetradecylresorcinol.

Compound	Peak symmetry of columns		
	Glassy carbon	Modified carbon	Graphitized carbon
toluene	0.23	0.84	0.91
resorcinol	0.42	0.48	100.3
2-tetradecylresorcinol	0.25	0.43	0.65

column, however, the k' of toluene is higher on the graphitized carbon than on the modified carbon. The surface area of glassy carbon is significantly higher than those of graphitized and modified carbons. In addition to that, the surface area of glassy carbon is mainly contributed by micropores, which firmly hold the adsorbate during elution. Therefore, all three compounds have stronger retention on glassy carbon. The surface areas of the graphitized and modified carbons are comparable, so that retention factors of the compounds on these two columns depend on interactions between compounds and column surface chemistries.

The influence of flow rates on the efficiencies of the graphitized carbon column and modified carbon column are tested by toluene, resorcinol, and 2-tetradecylresorcinol. The flow rate on the monolithic column is from 0.3 to 12 mm/s. Because of the high backpressure of the packed graphitized carbon column, the flow rate

on the graphitized carbon column is only from 0.125 to 2 mm/s. Figures 58 to 60 are the Van Deemter plots of toluene, resorcinol and 2-tetradecylresorcinol.

The Van Deemter equation has three terms that given by the equation:

$$H = a + b/u + c \cdot u \quad 8.11$$

The fitting of the experimental data gives values of these three parameters, which are tabulated in Table 5. The Van Deemter plots show that the overall column performance of the graphitized carbon column is better than that of the modified carbon column.

Because the graphitized carbon column is tested in the form of a particulate column with the particles sized in a wide range from 10 to 25 microns, a larger a term is expected of the graphitized carbon column than the a term in the monolithic modified carbon column. However, it is surprising that the a term of the graphitized carbon column is significantly smaller than that of the modified carbon column. This result has two possible causes.

Table 5. Fitted Van Deemter equation parameters

compound	column	Parameters		
		a	B	c
toluene	graphitized	33.24±0.87	2.58±0.14	4.55±0.56
	modified	55.95±0.23	2.31±0.12	0.92±0.03
resorcinol	graphitized	43.27±3.07	3.07±0.51	8.88±1.97
	modified	101.97±0.48	3.80±0.24	0.65±0.06
C14-resorcinol	graphitized	70.67±1.47	1.73±0.24	1.55±0.95
	modified	101.97±1.51	15.51±1.65	1.08±0.23

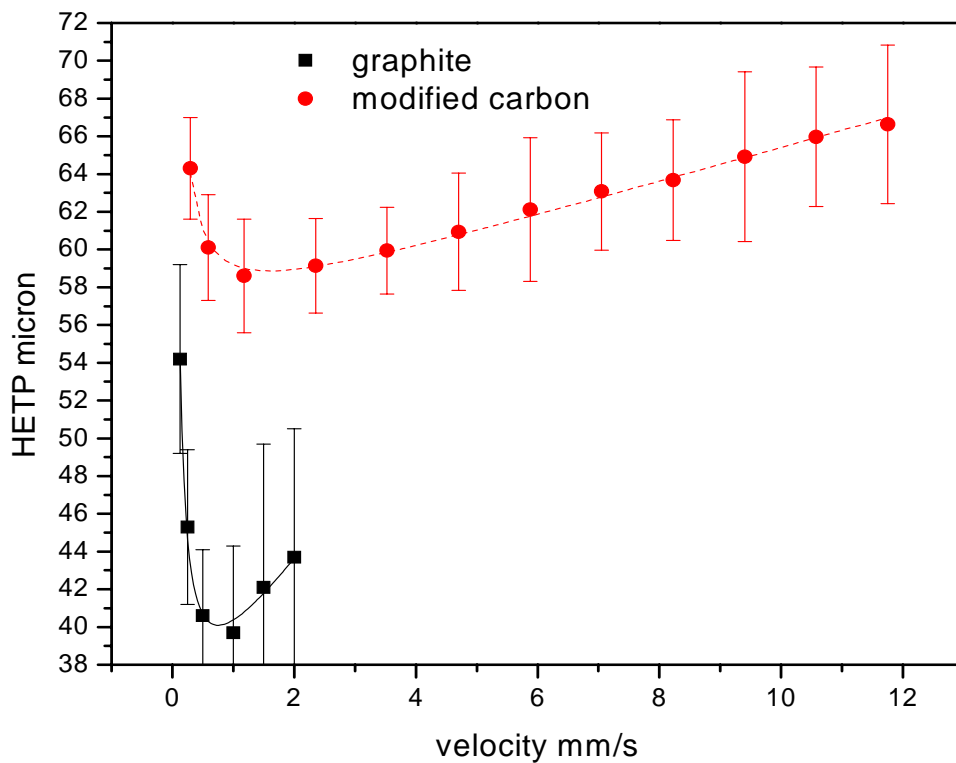


Figure 58. Van deemter plot of toluene on graphite and modified carbon columns eluted by 20: 80 chloroform and acetonitrile. k' is 0.75 on graphitized carbon, and 0.51 on modified carbon.

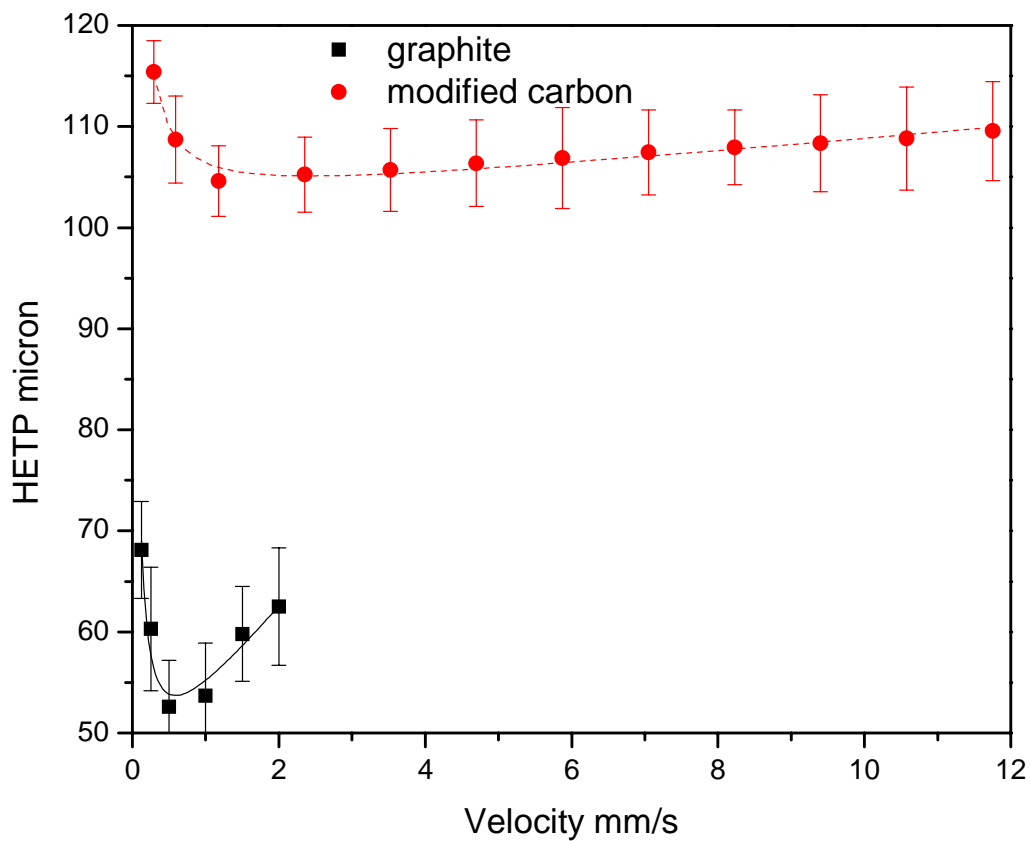


Figure 59. Van Deemter plot of resorcinol eluted by 15:85 water and methanol.

k' =1.57 on graphitized carbon, and 3.02 on modified carbon.

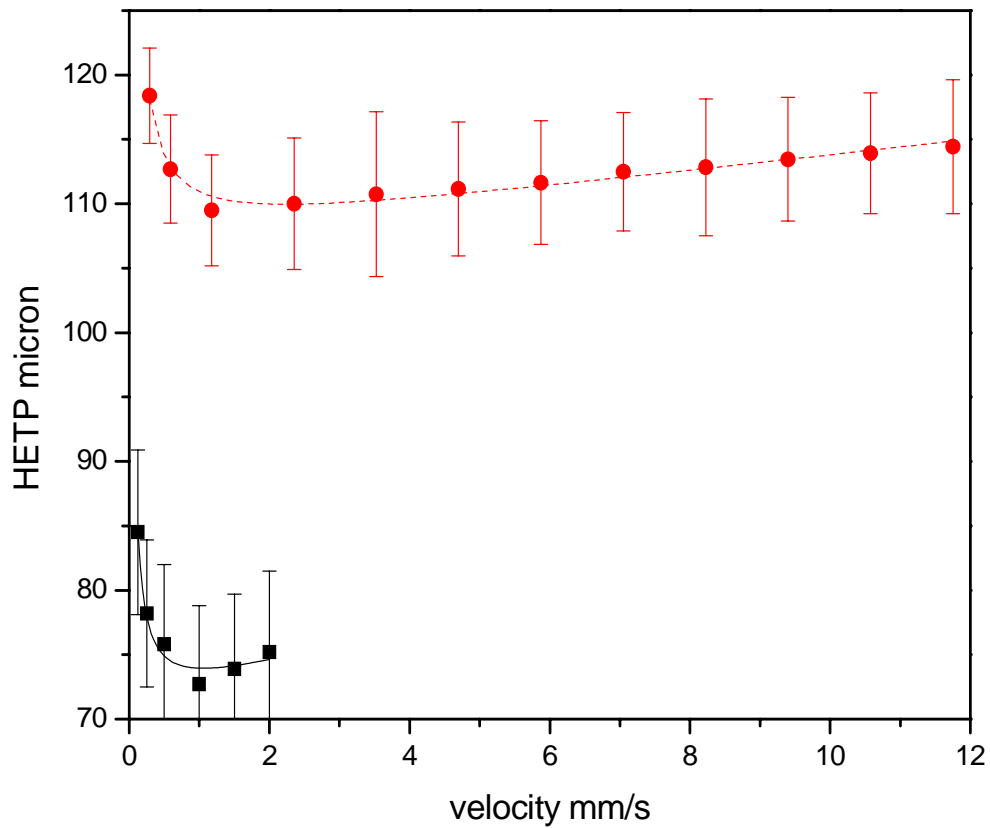


Figure 60. Van Deemter plot of 2-tetradecylresorcinol eluted by 15:85 water and methanol. k' is 5.2 on graphitized carbon, and 6.7 on modified carbon.

One is that the transportation pores in the graphitized carbon column are smaller than those in the monolithic column. The macropores in the graphitized carbon column are acting as transportation pores even though the column is in a packed form. The SEM measurement shows that the average size of macropores in graphitized carbon rods shrunk by 20% from the average size of macropores in their original glassy carbon rods. Therefore, the decreased term in the graphitized carbon column is the result of the decreased size of the macropore. The other possibility is that the porosity of monolithic column is radial heterogeneous. Since the macropores are of irregular shape, the average pore size can only be estimated by the SEM images. The pore size measured by SEM has large error, about 10%. There maybe a kind of radial heterogeneity within 10% that is not detectable by SEM, but 10% of the radial heterogeneity can significantly affect the performance of the monolithic column. The grinding and remixing graphitized carbon particles offsets the radial heterogeneity. Hence, the graphitized carbon has a smaller a term than the modified carbon column. Unfortunately, there is no further evidence to confirm the radial heterogeneity of the monolithic column. A monolithic column of graphitized carbon is very desirable for the testimony of radial heterogeneity. The c term of the modified carbon column is smaller than that of the graphitized carbon column. The c term is a mass transfer coefficient. Usually the c term of the monolithic column is smaller than that of the particulate column. For accelerated separations, the monolithic column has less efficiency loss than the particulate column at high velocities of mobile phase.

8.3.3 The properties of adsorbents obtained through isotherms

Isotherms on graphitized carbon and modified carbon were measured using frontal analysis. A typical staircase type of breakthrough curve is shown in Figure 61. The study of isotherms with a set of compounds on the adsorbent reveals interactions between the adsorbent and adsorbates. Therefore, the surface properties of the adsorbent can be deduced from the isotherm model and the chemistry of probing compounds. In this section, isotherms of alkylbenzenes, naphthalene, resorcinol, and 2-tetradecylresorcinol on the graphitized carbon column have been closely examined and fitted with several models. The isotherms on the modified carbon column were tested by toluene, resorcinol, and aniline. The temperature effect on the graphitized carbon column was carried out with toluene and resorcinol.

8.3.3.1 Isotherms on graphitized carbon column

The isotherm of toluene on graphitized carbon column is upwardly concave. This kind of isotherm is called an antilangmuir type isotherm. Plots in Figure 62 are isotherms of toluene at different temperatures. The best fitting model of these isotherms is the antilangmuir (AL) model using the fitting equation 8.2. The quadratic equation (Q) can also give good fitting with errors only slightly larger than the antilangmuir model. The fitted parameters and errors are listed in Table 6. Isotherms of alkylbenzenes that possess long alkyl chains are S-type isotherm (see Figure 63). The best fitting for this type of isotherm is the quadratic isotherm. The lower part of alkylbenzenes isotherms are concave and the upper part are convex. Figure 64 shows the isotherm of amylbenzene. The two insets in Figure 64 are the plot of the lower and upper parts of the isotherm.

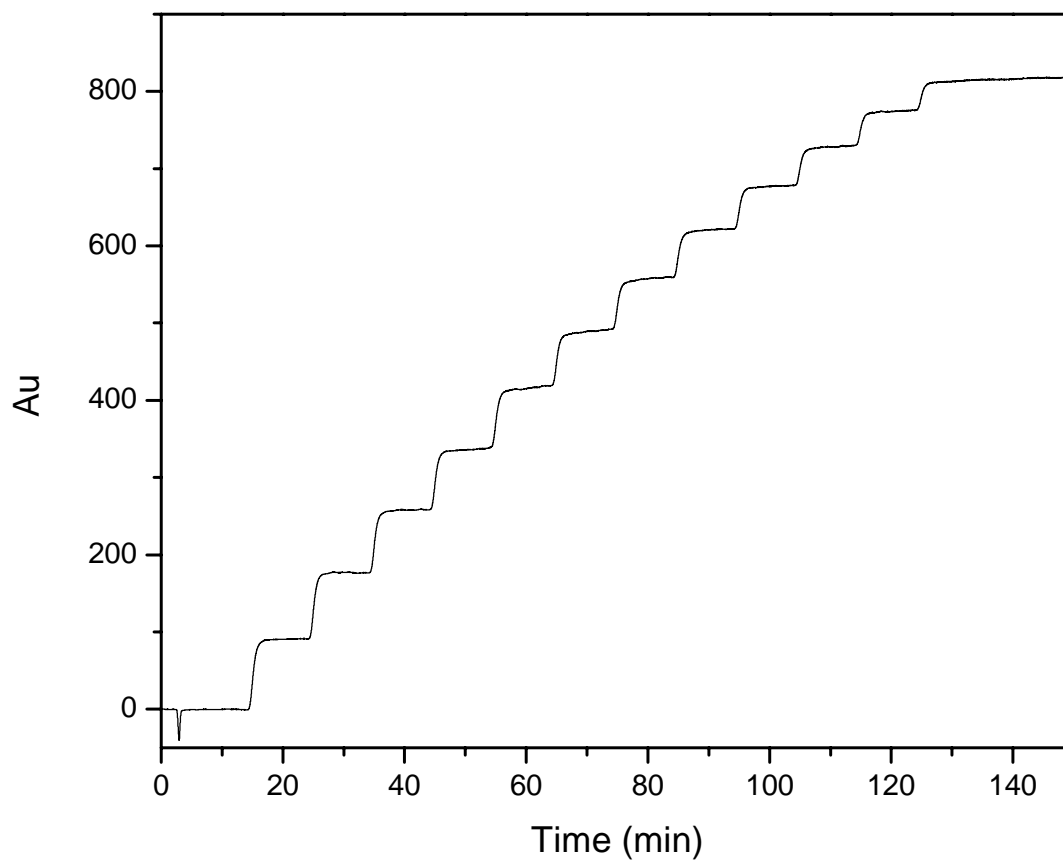


Figure 61. A typical breakthrough curve. Toluene is eluted on graphitized carbon column at 30 °C by 20:80 chloroform and acetonitrile. k' is 0.75. The time interval of each concentration is 10 minutes.

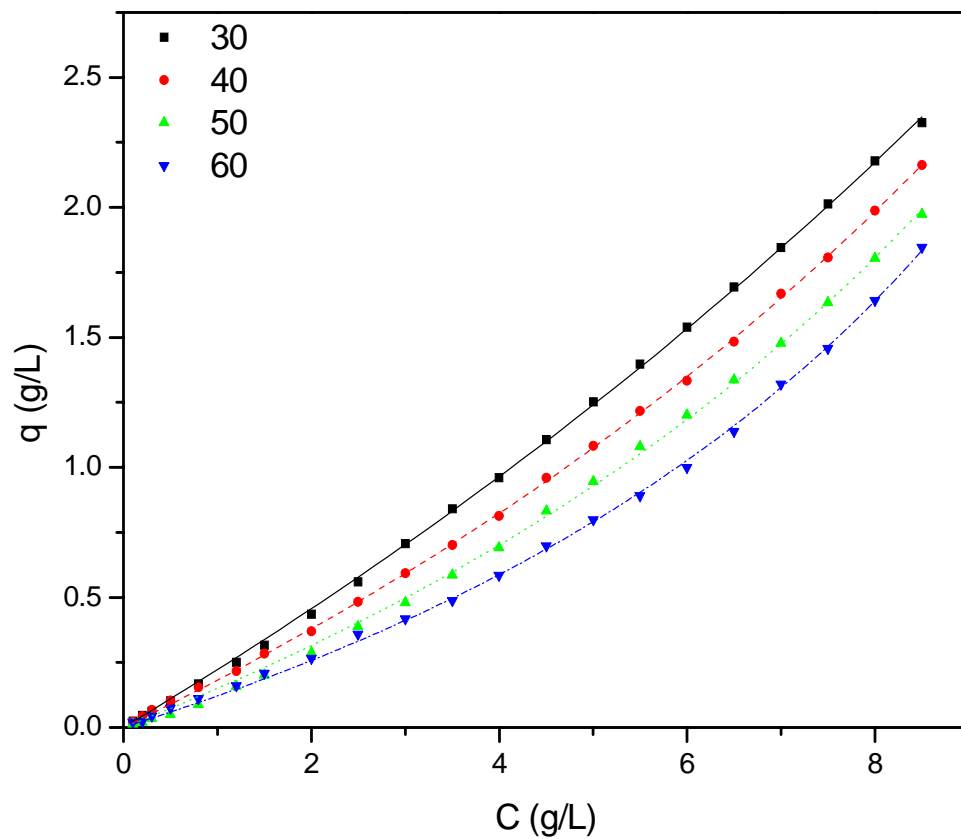


Figure 62. Isotherms of toluene on graphitized carbon eluted by chloroform/acetonitrile 20:80.

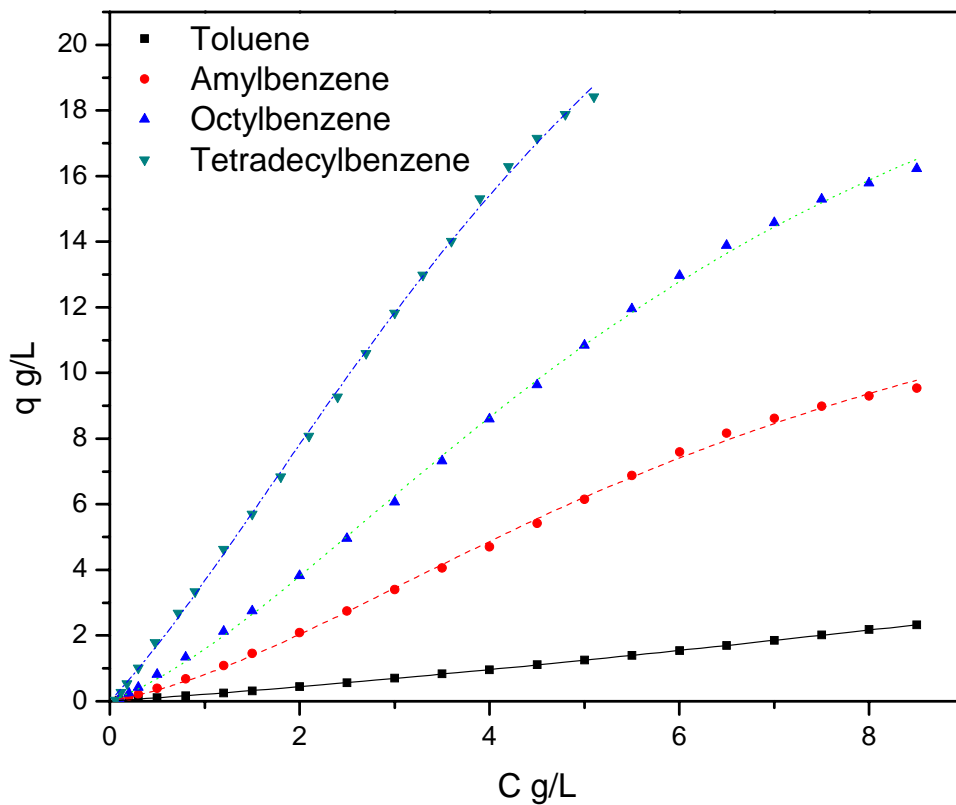


Figure 63. Isotherms of alkylbenzenes on graphitized carbon column at 30 °C eluted by chloroform/acetonitrile 20:80.

Table 6. Fitted parameters of isotherms at 30 °C on graphitized carbon column

Compound	Isotherm model	Parameters		
		P1	P2	P3
toluene	AL	8.56±0.39	0.025±0.001	
	Q	9.74±1.82	0.02031±0.004	0.0009±0.0003
Amylbenzene	Q	8.37±0.44	0.063±0.006	0.021±0.003
Octylbenzene	Q	13.75±0.51	0.081±0.005	0.023±0.002
tetradecylbenzene	Q	20.46±1.40	0.15±0.005	0.030±0.005
Naphthalene	AL	2.88±0.024	0.10±0.004	
	Q	32.35±6.03	0.08±0.01	0.013±0.004
resorcinol 30	L	22.22±0.55	0.02±0.001	
	Q	14.76±321.71	0.030±0.64	0.0001±0.01
C-14 resorcinol	L	50.14±3.24	0.20±0.02	
	Q	1195±7432	0.008±0.05	-0.0004±0.003

isotherm of amylbenzene on graphitized carbon column

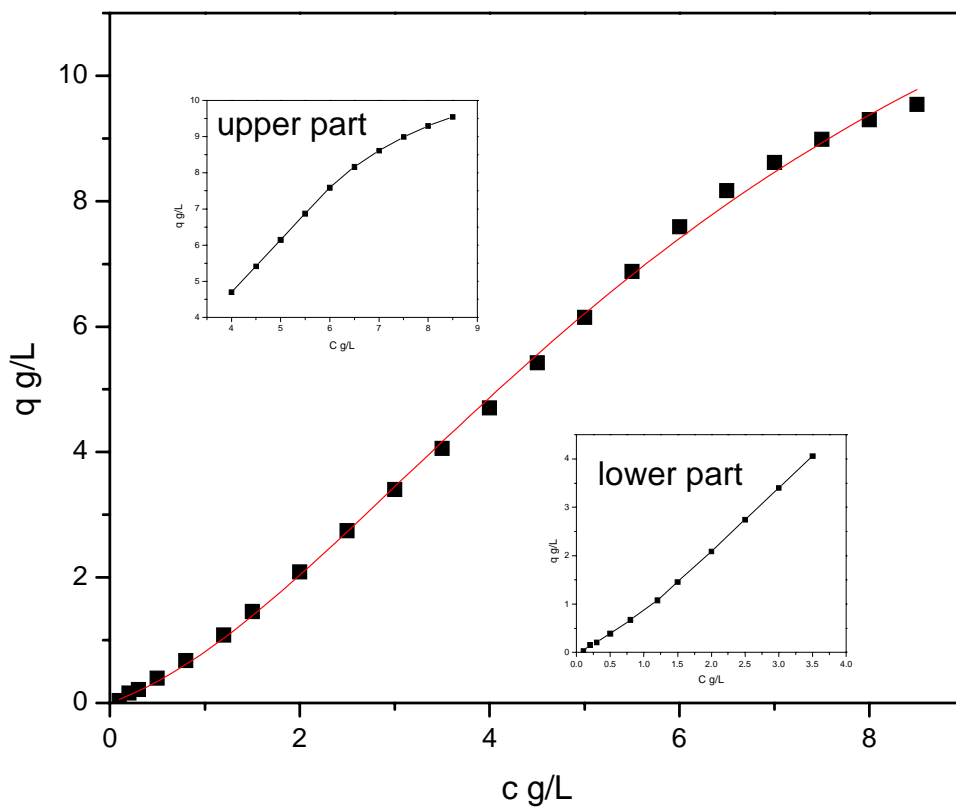


Figure 64. Isotherm of amylbenzene on graphitized carbon column at 30 °C eluted by 20: 80 chloroform/acetonitrile.

Each S-type isotherm has an inflection point. The isotherm of amylbenzene inflects at a concentration of 2.95 g/L, octylbenzene at 2.66 g/L, and tetradecylbenzene at 1.60 g/L. The data indicates the concentration of the inflection point is related to the length of the alkyl chain. The longer the alkyl chain is, the lower the concentration of inflection point. The concentration of inflection points are summarized in Table 7.

Isotherms of alkylbenzenes on graphitized carbon are speculated as heterogeneous adsorption. The antilangmuir fitting of toluene and lower parts alkylbenzenes shows that at diluted concentrations the first several layers of adsorbates have significant adsorbate to adsorbate interaction. At high concentrations isotherms of long chain alkylbenzenes are upwardly convex, which are langmuir types of isotherm. The convex curvatures of the upper part of isotherms indicate that the interactions among the adsorbates are not significant at high concentration. The origin of the S-type isotherms is hypothesized from the molecular structures of the adsorbate. Alkylbenzenes have a flat benzene ring head and a zigzag alkyl chain tail. When the alkylbenzene adsorbed on the graphite surface, the benzene ring lies flat on the graphene basal plane, whereas alkyl chains are randomly adsorbed on the carbon surface or positioned to the solution. The alkyl chains of the adsorbates tangled together and contribute strong adsorbate-to-adsorbate interaction. For the first layer that is adsorbed at low concentration, the adsorbed benzene heads interact with the benzene ring of adsorbates in the solution via π - π interaction. Heterogeneous adsorption thus occurs at the graphite surface. When the adsorbed layers increase to a

Table 7. The concentrations of inflection points of isotherms on graphitized carbon column at 30 °C. The isotherms are measured with amylbenzene, octylbenzene, tetradecylbenzene.

Compound	amylbenzene	octylbenzene	tetradecylbenzene
Concentration of inflection point	2.95 g/L	2.66 g/L	1.60 g/L

certain thickness, the randomly distributed alkyl chains hinder the access of the adsorbates in the solution to the carbon surface. Consequently, the adsorbate-to-adsorbate interaction does not significantly contribute to the adsorption. Therefore, the upper part of the isotherm is upwardly concave with finite adsorption capacity. This point is confirmed by the phenomena that concentrations of inflection points of alkylbenzenes' isotherms depend on the lengths of the alkyl chain. Obviously, the longer the alkyl chain is, the more significant the hindering effect is. The isotherm of toluene is an exception. Because the alkyl chain tail of toluene is only one methyl group, the hindering effect is not observable.

In order to examine the above hypothesis of heterogeneous adsorption on graphitized carbon column, three sets of isotherms were measured, one with naphthalene that eluted by pure chloroform for further evidence to adsorbate-adsorbate interaction, resorcinol that eluted by 15:85 water and methanol mixture for the indirect evidence to adsorbate-adsorbate interaction, and 2-tetradecylresorcinol that eluted by 15:85 water and

methanol mixture for the examine of alkyl chain effect. Naphthalene is a flat molecule with two fused benzene rings. Shown in Figure 65, the isotherm of naphthalene on graphitized carbon is concave upward, a typical antilangmuir type isotherm. Both the antilangmuir model (AL) and quadratic model (Q) give very good fitting to the experimental data (see parameters in Table 6). No inflection point has been found at the accessible concentration range. Adsorbate-to-adsorbate interaction significantly contributes to the adsorption of naphthalene on graphitized carbon surface. This confirms the multilayer adsorption of flat aromatic compounds on graphitized carbon surface.

By definition, the adsorption density is the number of adsorbed molecules per unit of surface area. The adsorption density is denoted as q' . The value of q' is obtained from the isotherm. The q' value can be calculated from the equation:

$$q' = \frac{q \times 6.02 \times 10^{23}}{D_g \times S_a \times M_w} \quad 8.12$$

where the unit of q' is number of molecules per nm^2 ; the unit of q is g/L , D_g is the density of graphite with the value of 1.8 g/cm^3 ; S_a is the surface area of the monolith column with the unit of m^2/g ; M_w is the molecular weight of the adsorbate. Shown in Figure 66, q' of alkyl benzenes on graphitized column surface is plotted as a function of concentration C .

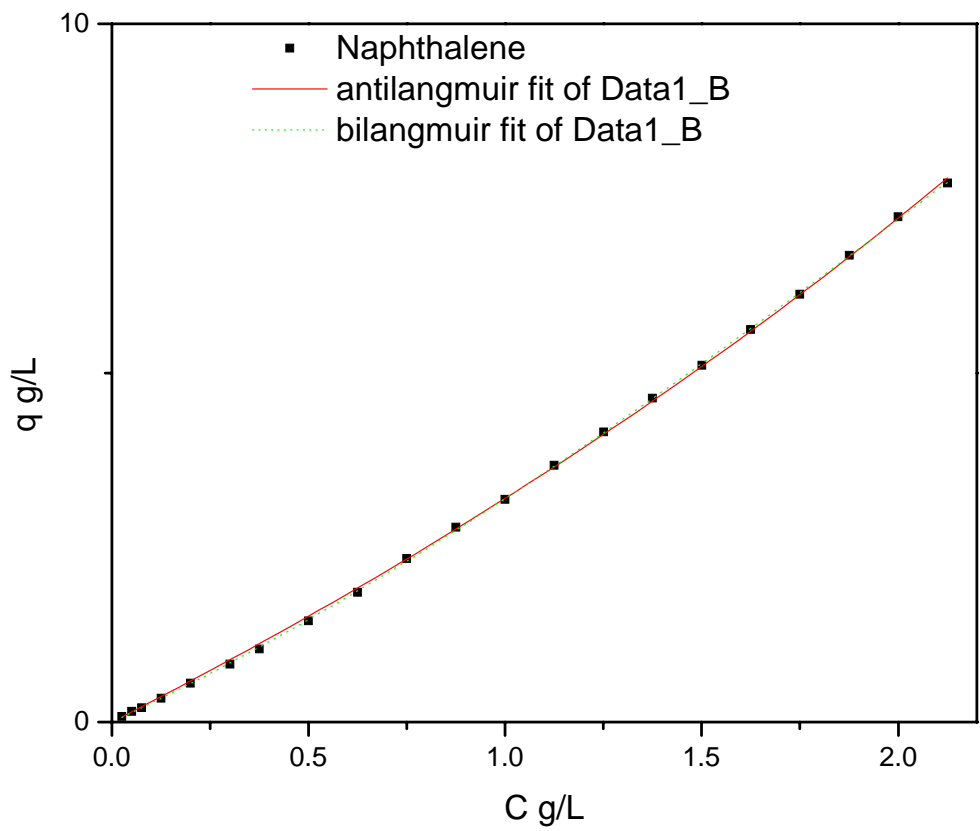


Figure 65. Isotherm of naphthalene on graphitized carbon column at 30 °C eluted by chloroform.

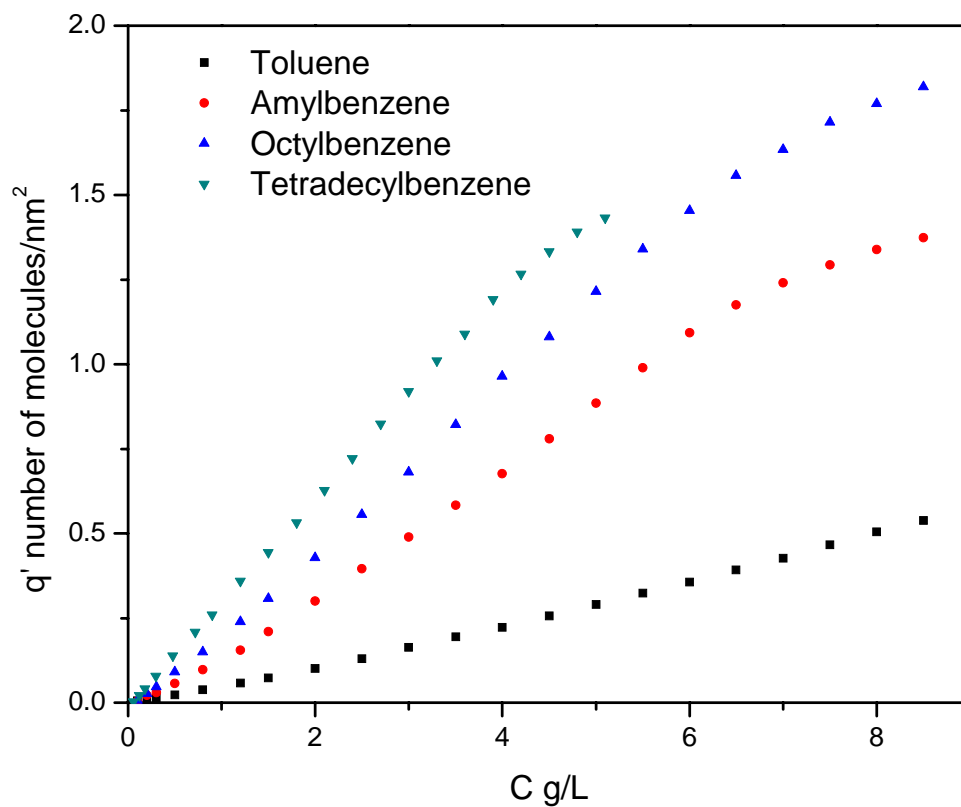


Figure 66. Adsorption density (number of molecules/ nm²) of alkyl benzenes on graphite column as a function of concentration.

Assuming adsorbed molecules are lying flat on the graphite surface, the average surface coverage (Γ) can be estimated by sizes of molecules (S_m) according equation 8.13.

$$\Gamma = \frac{q \times 6.02 \times S_m}{D_g \times S_a \times M_w} \quad 8.13$$

where the unit of S_m is \AA^2 . See Table 8 for molecular size. Γ is dimensionless. If Γ is great than 1, the value indicates the average number of layers covered on the adsorbent surface. Shown in Figure 67 is the plot of surface coverage v. concentration.

When isotherms are fitted with a quadratic model, a theoretic maximum of surface coverage (Γ_{\max}) can be predicted by the fitted q_s . If Γ_{\max} is greater than 1, the adsorbate forms multilayer on graphite surface. If Γ_{\max} is less than 1, the adsorption occurs as two situations: when there is no adsorbate-adsorbate interaction, the isotherm is langmuir type; when there is an adsorbate-to-adsorbate interaction, the molecule forms islands on the adsorbent surface, and the isotherm is S-shaped.

Resorcinol and 2-tetradecylresorcinol were selected as probing compounds to give indirect evidence to the adsorbate-to-adsorbate interaction. Resorcinol has two hydroxyl groups directly connected to the benzene ring. These hydroxyl groups are well solvated by the mixture of 15: 85 water/ methanol. The adsorption of resorcinol to the graphitized carbon surface is always accompanied by solvent molecules that interact with resorcinol through hydrogen bonds. The adsorbate-to-adsorbate interaction among resorcinol molecules is always weakened by the hindering of solvent molecules. Thus, a langmuir type of isotherm is expected. As plotted in Figure 68, isotherms of resorcinol on

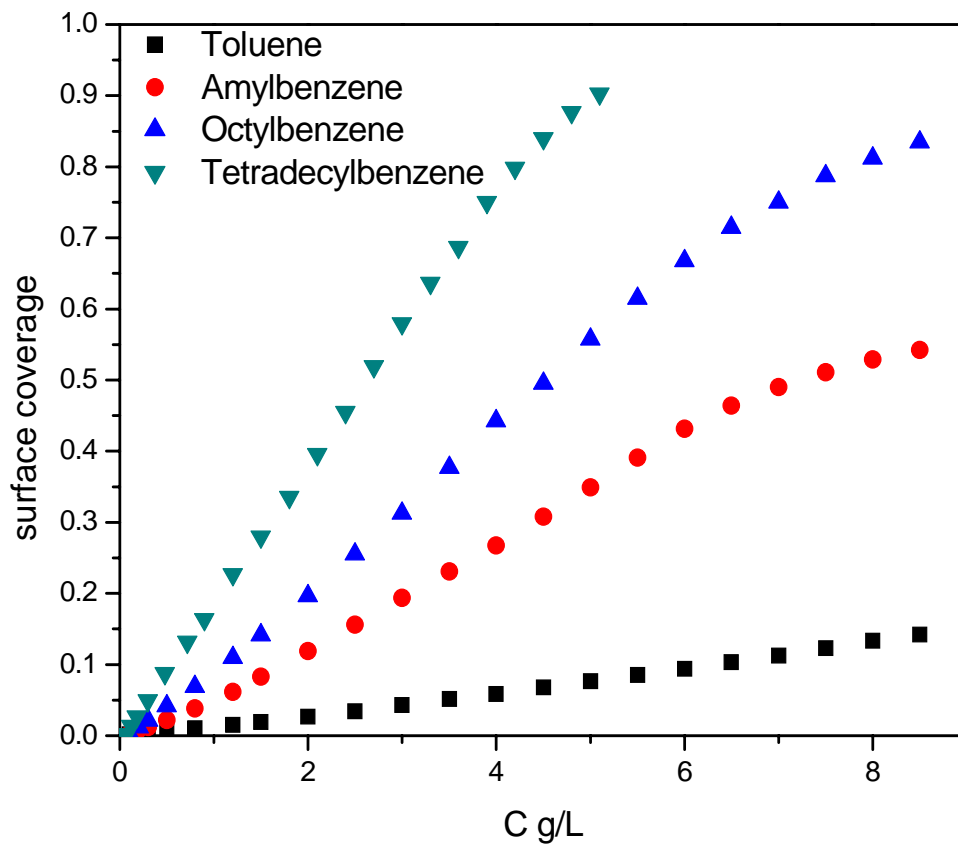


Figure 67. Surface coverage of alkylbenzenes on graphite surface as a function of concentration.

Table 8. Maximum of surface coverage (Γ_{\max}) of adsorbates on graphitized carbon surface. Sizes of molecules are calculated by Chem Office 8.0. The alkyl benzenes are calculated as a flat head of 26.4 \AA^2 and flexible tails with projected areas that vary with the lengths of alkyl chains.

compound	q_s	Size of the molecule $S_m (\text{\AA}^2)$	Molecular weight	Γ_{\max}
toluene	9.74	26.4	92	0.595
amylbenzene	8.37	26.4 (head) 13.1(tail)	148	0.476
octylbenzene	13.75	26.4 (head) 19.5(tail)	190	0.708
tetradecylbenzene	20.46	26.4 (head) 36.6(tail)	274	1.000
naphthalene	32.35	34.5	128	1.857

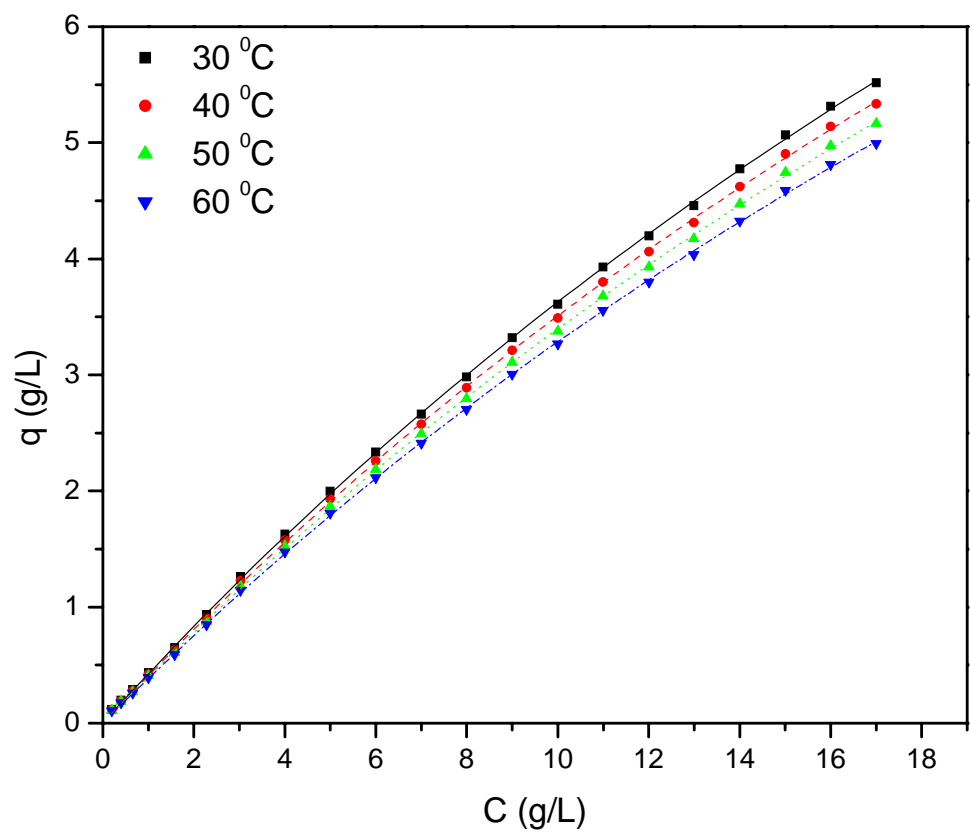


Figure 68. Isotherm of resorcinol on graphitized carbon column at 30 to 60 °C eluted by 15:85 water/methanol.

graphitized carbon are upwardly convex, with finite adsorption capacity. The langmuir model gives excellent fitting to the experimental data.

According to the conclusion of the above discussion, the isotherm of toluene is anantilangmuir type and when the alkyl tail is long enough, the antilangmuir isotherm will become an S-type isotherm. In order to check whether or not the same phenomenon occurs in the resorcinol homologue, the isotherm of 2-tetradecylresorcinol was tested with the identical condition of resorcinol on graphitized carbon column. Figure 69 is the plot of isotherms of resorcinol and 2-tetradecylresorcinol on graphitized carbon column. Obviously, the isotherm of 2-tetradecylresorcinol is a langmuir type isotherm, which is upwardly convex. There is no inflection point in the isotherm curve. The best fitting model for 2-tetradecylresorcinol is still the langmuir model. Thus, the alkyl chain has no influence on the adsorption model of the resorcinol.

The temperature effect on isotherms has been tested on the graphitized carbon column by using toluene, an antilangmuir type isotherms, and resorcinol, a langmuir type isotherm. The plot of isotherms of toluene at 30, 40, 50, and 60 °C is shown in Figure 62. The temperature effect on the resorcinol isotherm is plotted in Figure 68. The fitted parameters were listed in Table 9. The data shows that the amount of the adsorbed analyte decreases with the increase of temperature. For the langmuir model, the parameter P1 is the specific saturation capacity q_s , and the P2 is the equilibrium constant K. Langmuir isotherms of resorcinol on graphitized carbon column have a constant equilibrium constant K with the value of 0.020 ± 0.0006 at various temperatures. The saturation capacity decreases with the increase of temperature.

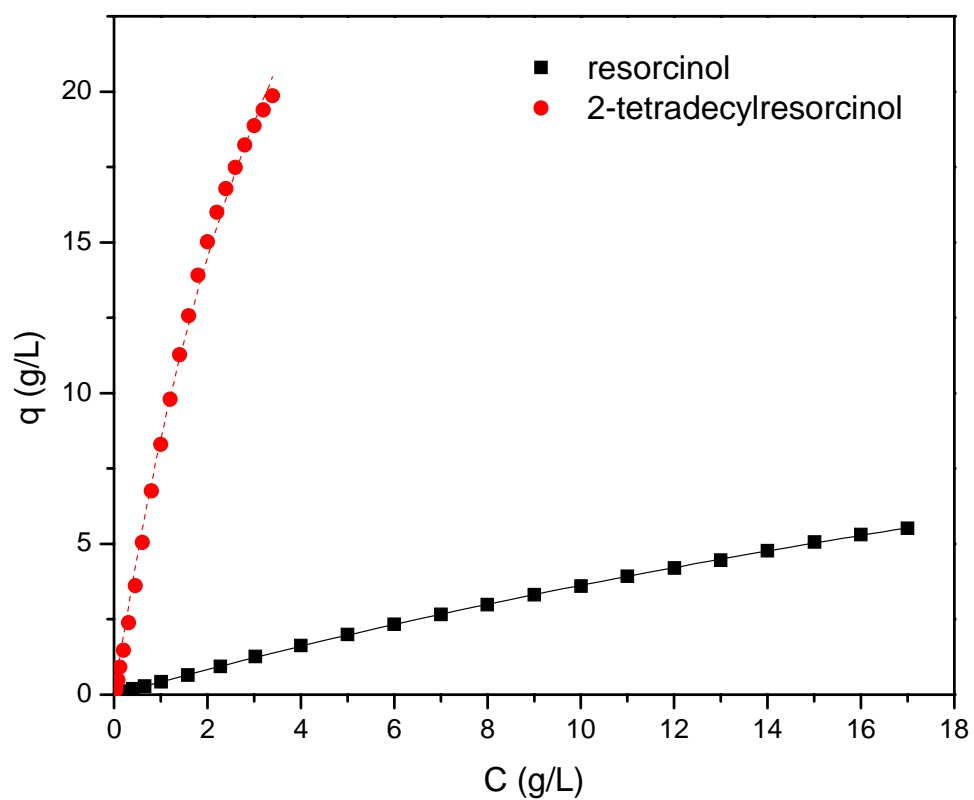


Figure 69. Isotherm of 2-tetradecylresorcinol and resorcinol on graphitized carbon eluted by 85:15 methanol/water at 30 °C.

Table 9. Fitted parameters of temperature effect on isotherms.

Compound temperature	Isotherm model	Parameters		
		P1	P2	P3
toluene 30	AL	8.56±0.39	0.025±0.00096	
	Q	9.74±1.82	0.020±0.0035	0.00085±0.00025
Toluene 40	AL	4.85±0.14	0.036±0.00078	
	Q	11.20±6.91	0.014±0.0079	0.00073±0.00063
Toluene 50	AL	3.14±0.15	0.046±0.0014	
	Q	13.21±5.12	0.0086±0.0031	0.00064±0.00031
Toluene 60	AL	2.075±0.067	0.055±0.0011	
	Q	21.27±56.27	0.0041±0.010	0.00037±0.0011
resorcinol 30	L	22.22±0.55	0.020±0.0006	
	Q	14.76±321.71	0.030±0.64	0.00013±0.012
resorcinol 40	L	21.50±0.53	0.020±0.0006	
	Q	14.22 ± 357.04	0.030 ± 0.74	0.00013 ± 0.014
resorcinol 50	L	20.80±0.51	0.020±0.0006	
	Q	13.76±346.06	0.030±0.75	0.00013±0.014
resorcinol 60	L	20.13±0.50	0.020±0.0006	
	Q	13.31±334.44	0.030±0.74	0.00013±0.014

8.3.3.2 The isotherms on modified carbon column

Isotherms on modified carbon column were tested by resorcinol, toluene, and aniline at 30 °C. Isotherms and best fittings are plotted in Figure 70. The fitted parameters are listed in Table 10.

The isotherm of toluene on modified carbon surface is still an antilangmuir type isotherm. The best fitting of the experimental data is given by the antilangmuir equation. The adsorbate-to-adsorbate interaction significantly contributes to the total adsorption of toluene to the modified carbon surface.

The isotherm of resorcinol on the modified carbon is fitted with langmuir, quadratic, and bilangmuir models. As shown in Figure 71, the best fitting of resorcinol on modified carbon surface is the bilangmuir model. The bilangmuir model assumes that the adsorption is dominated by 2 kinds of adsorption sites. Each type of site has corresponding q_s and K . The bilangmuir fitting gives $q_{s,1}$ is 25.58, K_1 0.02 and $q_{s,2}$ is 1.83, K_2 0.97. This fitting result suggests that the modified carbon surface is heterogeneous. The heterogeneity may due to the insufficient coverage of the carbon surface or micropores that have not been totally blocked by the modified ligand.

The isotherm of aniline on the modified carbon surface is less curved than the isotherm of resorcinol (Figure 72). The best fitting of this isotherm is the quadratic model. As indicated in the isotherm of resorcinol, the adsorption of aniline on the modified carbon surface may be contributed from more than two types of adsorption sites.

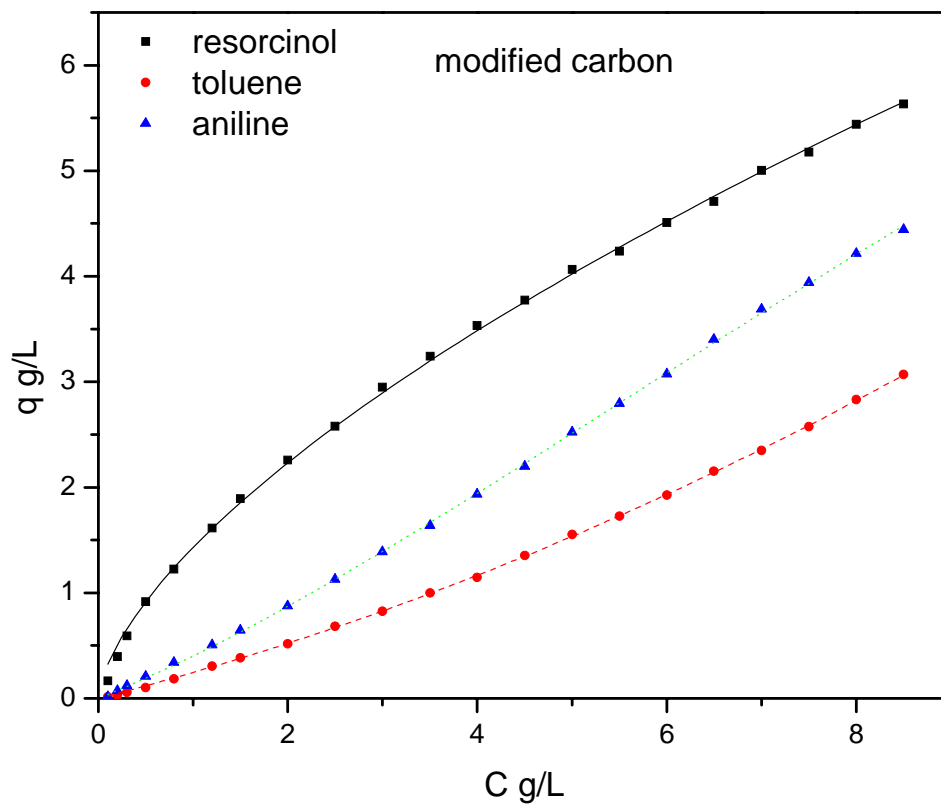


Figure 70. Isotherms of toluene, resorcinol, aniline on modified carbon column by 85:15 methanol/water at 30 °C. The surface modification is N,N'-diethylbenzene.

Table 10. Fitted parameters of isotherms of toluene, resorcinol, and aniline on modified carbon.

Compound	Isotherm model	Parameters			
		P1	P2	P3	P4
Toluene	AL	6.74±0.21	0.037±0.001		
	Q	45.77±44.69	0.0049±0.005	0.0002±0.0002	
Resorcinol	L	9.82±0.46	0.15±0.01		
	Q	6.39±34.04	0.24±1.28	0.007±0.2	
	BL	25.58±8.82	0.0218±0.010 3	1.83±0.31	0.96±0.18
Aniline	L				
	Q	7.91±0.64	0.046±0.003	0.004±0.0006	
	AL	23.44±2.89	0.02±0.002		
	BL	92.57±4718. 4	0.048±0.49	-62.59±4753.65	0.066±0.63

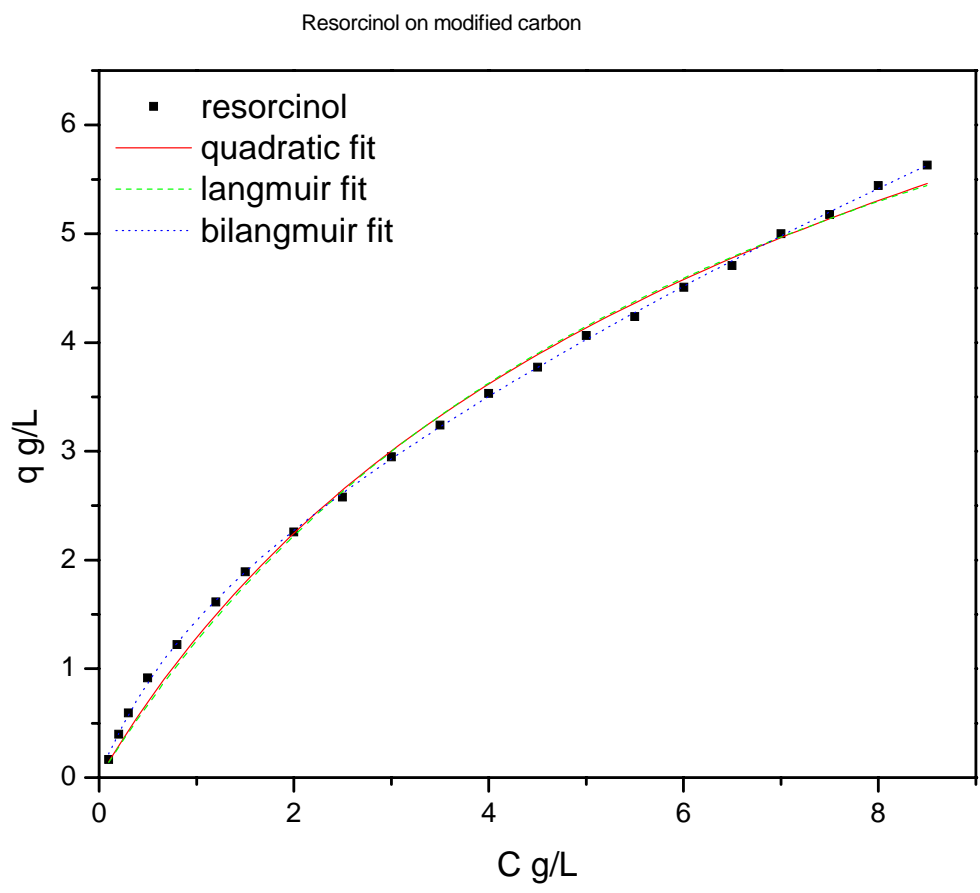


Figure 71. Curve fitting of the resorcinol isotherm on modified carbon at 30 °C.

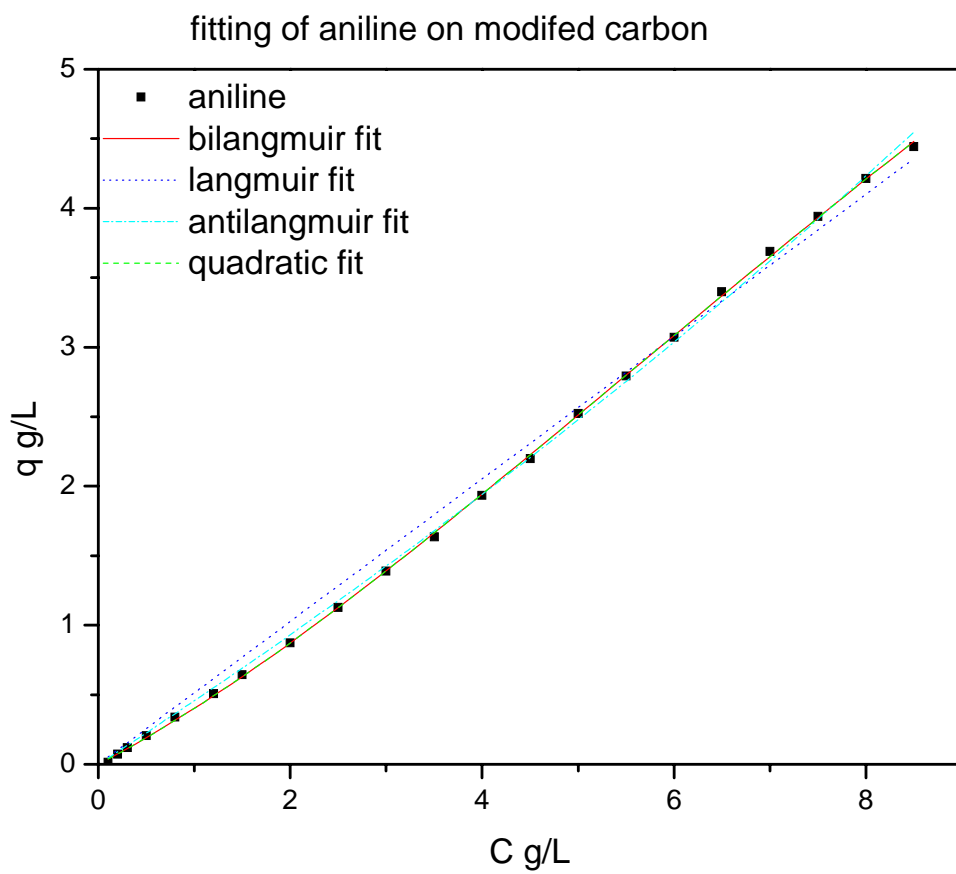


Figure 72. Curve fitting of the isotherm of aniline on modified carbon.

8.3.3.3 The comparison of isotherms between graphitized and modified columns

Isotherms of resorcinol on graphitized carbon column and modified carbon column have been measured at identical conditions (Figure 73). These two isotherms provide the comparison of isotherms on these two types of adsorbents. The fitted parameters are provided in Table 11. According the foregoing discussion, the best isotherm model for resorcinol on graphitized carbon column is the langmuir model, and the best isotherm model for resorcinol on the modified carbon column is the bilangmuir model. The q_s of resorcinol on graphitized carbon is 22.22, and the corresponding K is 0.020. The $q_{s,1}$ value of the bilangmuir fitting of resorcinol on modified carbon is 25.58, and the K_1 is 0.02. The values of these two sets of parameters are very close. This factor suggests that the modified carbon surface has some adsorption sites that are similar to those on the graphitized carbon. The second langmuir term of the bilangmuir fitting of resorcinol on modified carbon has a small $q_{s,2}$ of 1.83 with a larger equilibrium constant K_2 of 0.96. The parameter values of the second langmuir term refers to a stronger adsorption site but with a small site population. It can be concluded that the modified carbon surface has two kind of adsorption sites, one kind of adsorption site is similar to the properties of graphitized carbon surface, the other kind of adsorption site has less population with much higher adsorption energy. The ligand that has been modified the carbon surface is a tertiary amine. Resorcinol is an acidic compound. Therefore, the strong adsorption sites can be assigned to the ligands that anchored on the carbon surface. According to the discussion in Chapter 6, the modification of the carbon surface starts from the edge or defects of the carbon material.

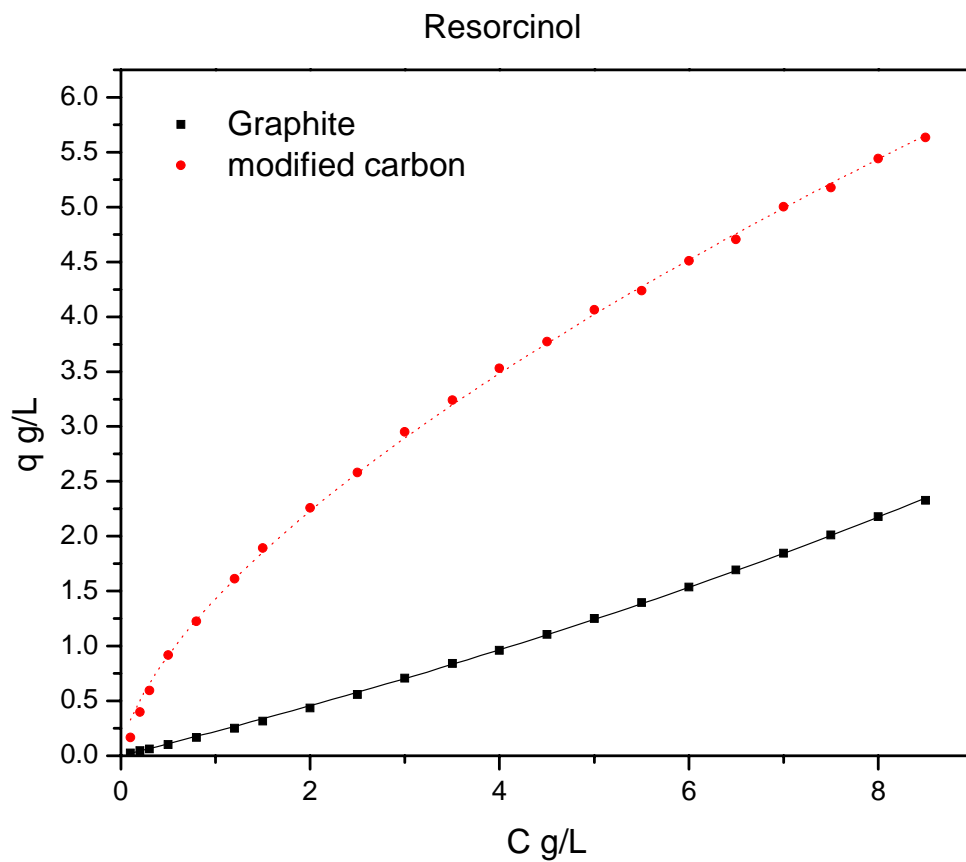


Figure 73. Comparison of isotherms of resorcinol on graphite and modified carbon eluted by methanol/water (85/15) at 30 °C.

Table 11. Fitted parameters of resorcinol's isotherms on graphitized carbon and modified carbon.

Compound	Isotherm model	Parameters			
		P1	P2	P3	P4
Resorcinol on graphite	L	22.22±0.55	0.02±0.0006		
	Q	14.76±321.71	0.03±0.64	0.0001±0.012	
Resorcinol on modified carbon	L	9.82±0.46	0.15±0.012		
	Q	6.39±34.04	0.24±1.28	0.0070±0.17	
	BL	25.58±8.82	0.022±0.010	1.83±0.31	0.97±0.18

The basal plane of the carbon surface is inert than the edge of the graphene. It is possible that the modification of the carbon surface covered only the defect sites and the edge of the graphene. That is to say, the modification only occurs at the pore opening of micropores. The comparison of isotherms on graphitized and modified carbons provides a picture of the micropores on the glassy carbon surface that have been blocked by the modification that becomes the second langmuir type adsorption sites. The carbon surface has not been fully covered by the functionalities.

8.3.4 Ligand density by TGA-MS

The surface area of the glassy carbon before modification is 215.1 m²/g, and it drops to 35.2 m²/g after modification. The change in surface area indicates that the modification blocked micropores. However, there is no further information about surface coverage of the modification. From the discussion on the comparison of isotherms on graphitized and modified carbons, one can conclude that the carbon surface is not fully covered by the functionalities. In order to find out the ligand or bonding density of the modified carbon surface, the modified carbon has been analyzed by TGA-MS. Since the ligand is covalently bonded to the carbon surface, there is no efficient way to break the C-C bond other than pyrolysis.¹⁷⁰ The pyrolysis of the modified carbon releases the bonded ligand. The weight loss gives quantitative result of the ligand density. The MS data monitored the debris of the ligand. Shown in Figure 74 is the TGA-MS plot of the modified carbon sample pyrolyzed in nitrogen at 10 °C/min. Since the pyrolysis involved the rearrangement of the ligand at elevated temperature, the MS data only provides a rough idea of what was emitted from the furnace. The weight loss, along with

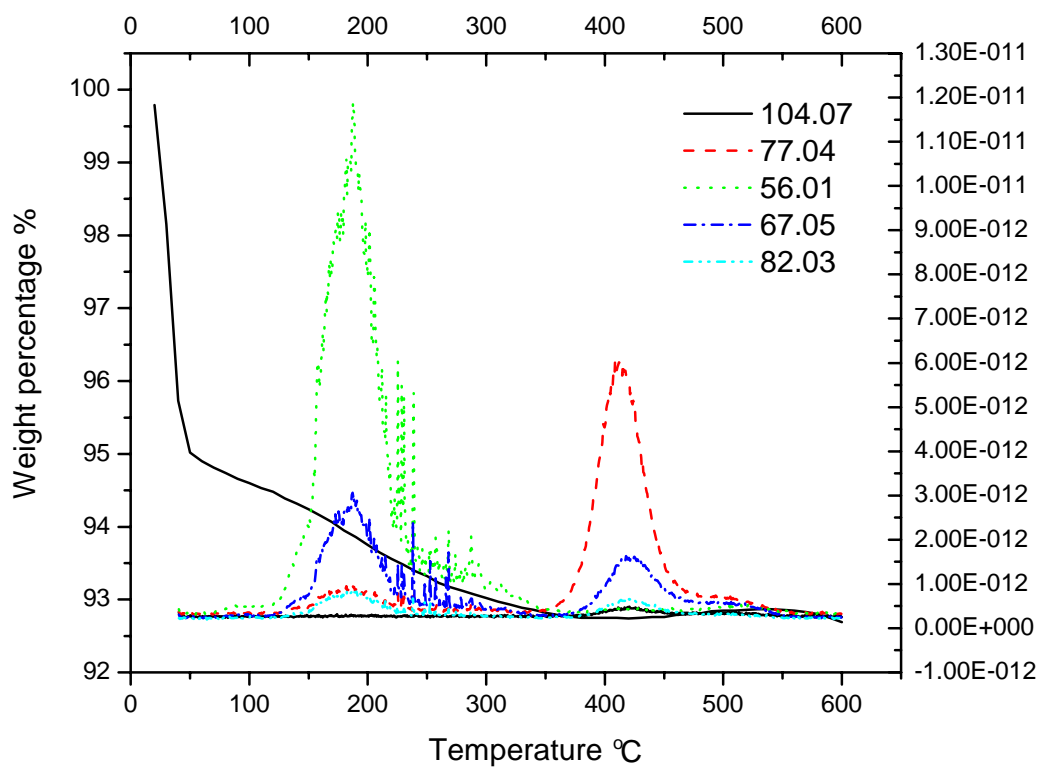


Figure 74. TGA-MS plot of the modified carbon which is pyrolyzed from room temperature to 600 °C at N₂ gas flow. The temperature ramp is 10 °C/min.

the temperature information, provides the weight percentage of the ligand to the sample. Because the weight percentage of the ligand is very small, the weight loss of moisture should be deducted from the total weight loss. The moisture weight should also be subtracted from the total sample weight. The MS data shows the emission of organic moieties starts from 180 °C. Therefore, the weight loss before 180 °C is considered to be water vapor and should be deducted. The calculated weight loss is 2.43%. The surface area of the modified carbon is 35.2 m²/g according to the BET. The ligand density can be calculated by the formula:

$$D_l = \frac{WL \times 0.01}{Mw \bullet Sa} \quad 8.14$$

where, D_l is ligand density mol/m²; WL is relative weight loss percentage; Mw is molecular weight g/mol; Sa is surface area m²/g. Assuming the modification starts from the entrance of micropores, the modification of the ligand does not cover the interior of the micropores. The surface area of the modified carbon other than that of the glassy carbon was used in the calculation of ligand density. Therefore, the value of the Sa is 35.2 m²/g. Mw is 124 g/mol. The calculated ligand density value D_l is 5.57 μmol/ m².

8.3.5 The reproducibility of monolithic columns

The reproducibility of monolithic columns is an important factor evaluating how repeatable the synthesis method is. In this study, 6 columns made from two batches of carbon rods have been compared by the retention factor and the HETP. Each measurement was repeated five times; the final data is the average of the five runs.

Shown in Table 12 are the k' and HETP values that measured six modified columns. The data in Table 12 was presented as two plots in Figures 75 and 76. The average k' over

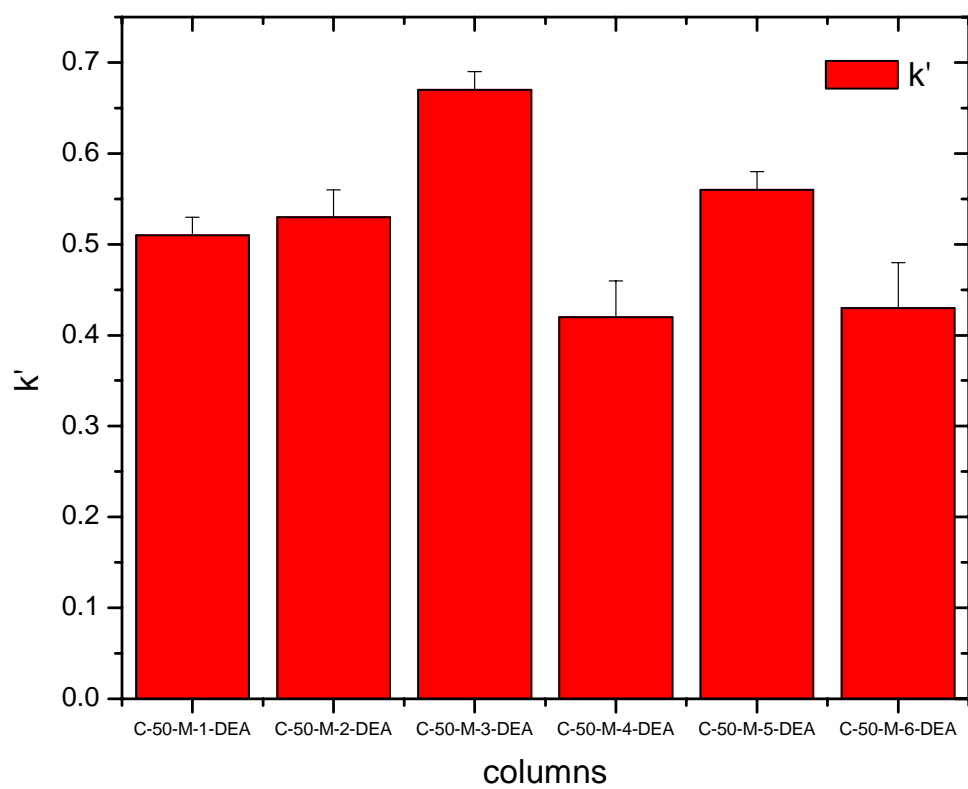


Figure 75. Plot of k' versus column.

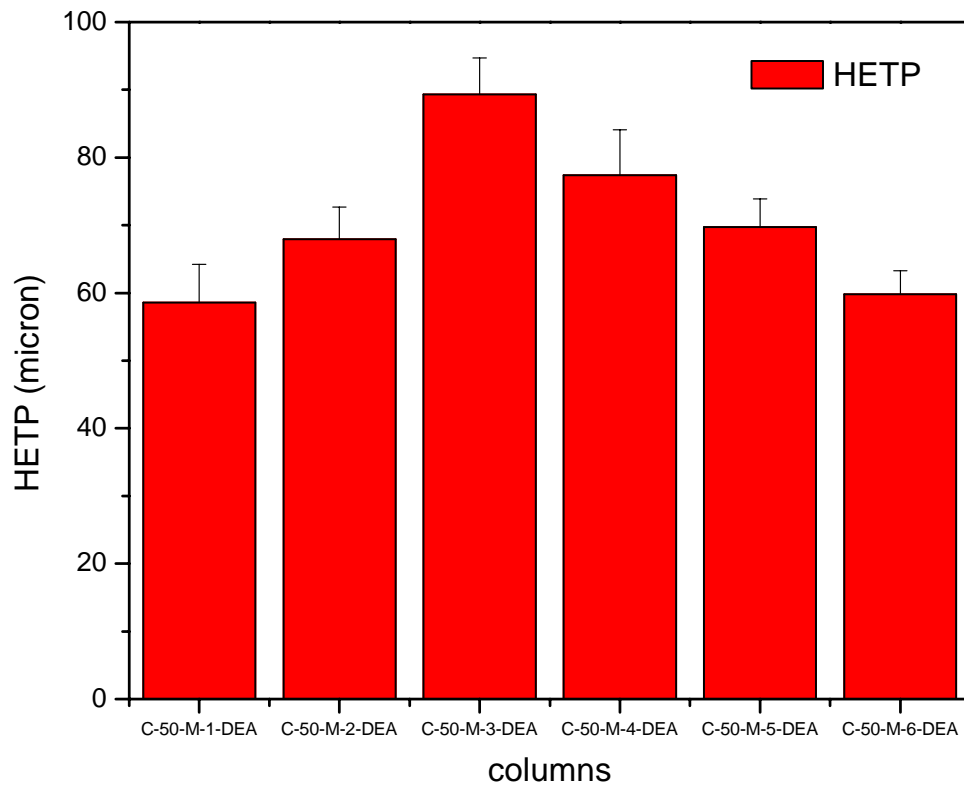


Figure 76. Plot of HETP versus column.

Table 12. k' and HETP measured on six modified carbon columns.

Column ID	k'	k' error	HETP	HETP error
C-50-M-1-DEA	0.51	0.02	58.6	5.6
C-50-M-2-DEA	0.53	0.03	67.9	4.8
C-50-M-3-DEA	0.67	0.02	89.3	5.4
C-50-M-4-DEA	0.42	0.04	77.4	6.7
C-50-M-5-DEA	0.56	0.02	69.7	4.2
C-50-M-6-DEA	0.43	0.05	59.8	3.5

the six columns is 0.52 with a standard deviation 0.09. The average HETP over the six columns is 70.45 microns with a standard deviation 11.52.

The retention factor k' and HETP of each batch is an average of the value of three columns in the same batch. The data of k' and HETP of two batches are listed in Table 13. The plot of k' and HETP versus batch are presented in Figure 77 and 78. The standard deviation of k' between batches is 0.07 and HETP is 2.1. These numbers prove that columns made via the synthesis approach described Chapters 5 and 7 are reproducible.

8.3.6 The pressure effect on the graphitized carbon column

Pressure is often assumed as a negligible factor for the retention of solute in liquid chromatography because of the small compressibility of the mobile and stationary phase.¹⁷¹ The molar volume change of molecules does not significantly affect the retention under moderate pressure of less than 400 bar. With the up-to-date development

Table 13. k' and HETP measured on 2 batches of modified carbon columns.

Batch number	k'	k' error	HETP	HETP error
1	0.57	0.087	71.93	15.74
2	0.47	0.078	68.97	8.82

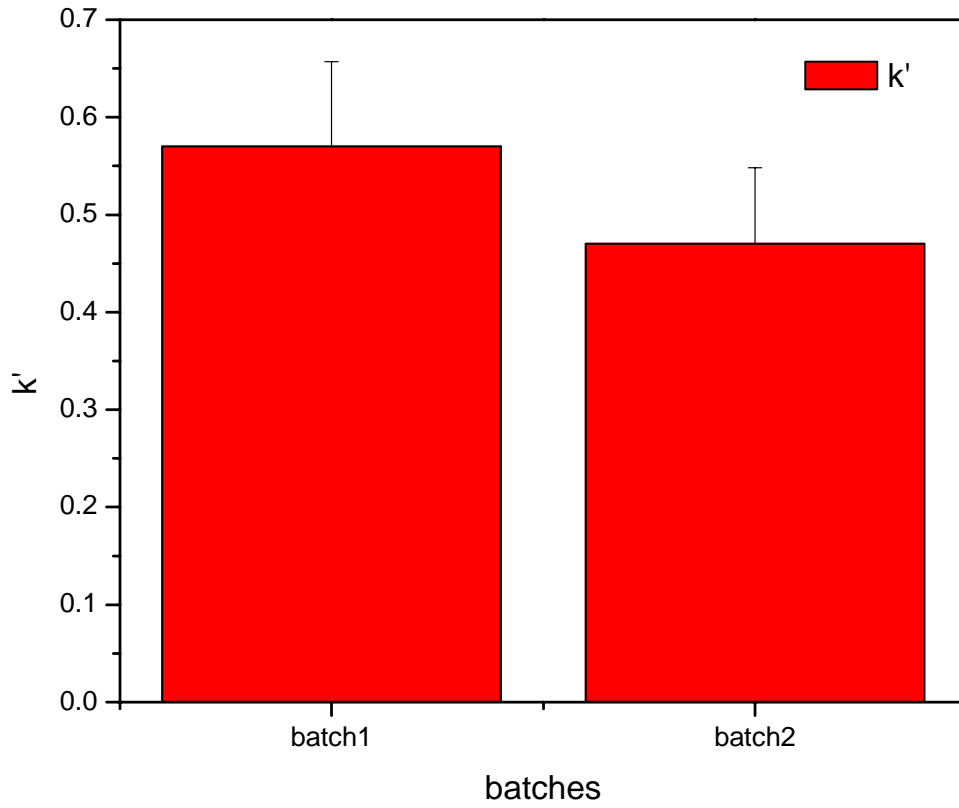


Figure 77. Average k' versus batch.

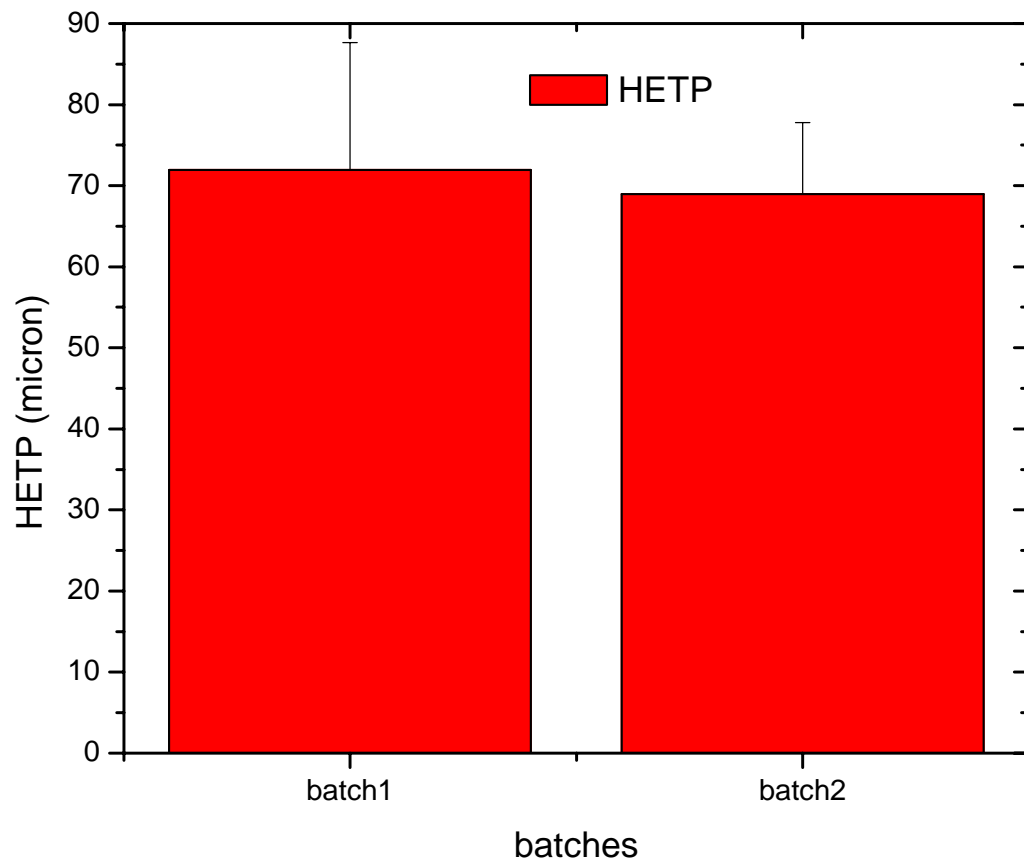


Figure 78. Average HETP versus batch.

of the HPLC technologies, the use of particles as small as 800nm is made possible by delivering mobile phases at ultrahigh pressures up to 1200 bar. Under ultrahigh pressure, the molar volume change may significantly influence the retention of solute. Several groups have theoretically and experimentally studied the pressure effect. Guiochon was the first to point out that at a constant temperature, the natural logarithm of retention factor k has a linear relationship with the applied pressure.¹⁵³ Assuming the phase ratio is constant, the slope of the linear fitting of $\ln k$ versus pressure (P) is given the equation:^{153,}

157, 171

$$\left(\frac{\partial \ln k}{\partial P} \right)_T = \frac{-\Delta V}{RT} \quad 8.15$$

where the k is the retention factor, P is the average column pressure, ΔV is the molar volume change with the unit of $\text{cm}^3 \text{mol}^{-1}$, R is the gas constant with the value of $83.14 \text{ cm}^3 \text{mol}^{-1} \text{K}^{-1} \text{bar}^{-1}$. T is the absolute temperature with the unit of K.

The pressure effect was measured by the elution of *o*-xylene and cyclohexanol on graphitized carbon column with mobile phase of acetonitrile. The recorded retention factors are the average of five identical runs. Figure 79 shows the plot of k' versus pressure of *o*-xylene and cyclohexanol at 303K. Since the $\ln k$ has linear relationship with pressure, the data in Figure 80 were plotted by $\ln k$ versus pressure. The linear fitting was done with the linear equation:

$$\ln k = A + B \cdot P \quad 8.16$$

where A is the interception and B is the slope. If the phase ratio is fixed, A is supposed to be zero. B is given by¹⁵³

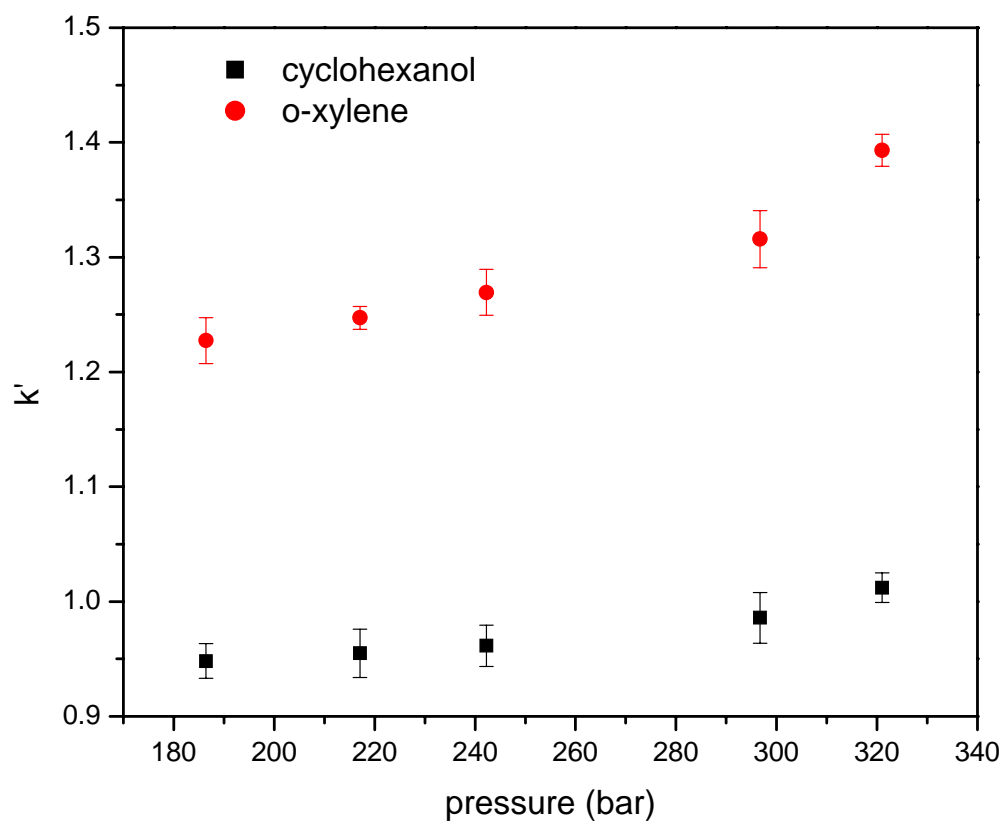


Figure 79. Plot of k' versus pressure of o-xylene and cyclohexanol eluted by acetonitrile at 303 K on graphitized carbon column.

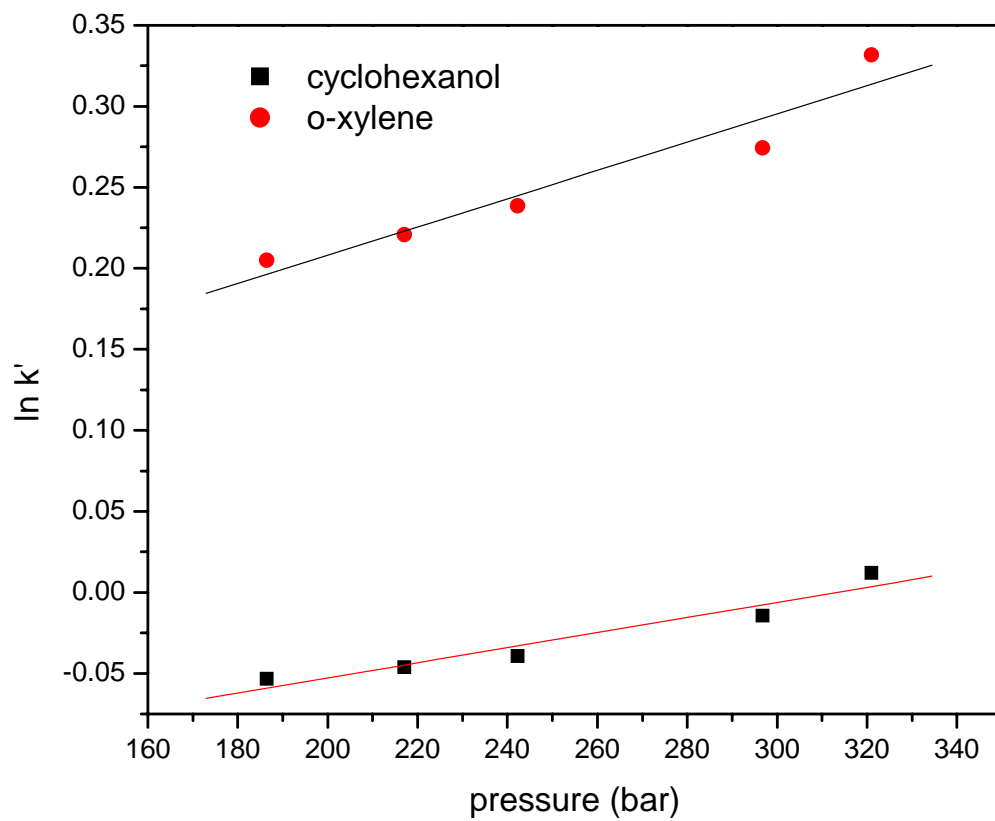


Figure 80. Plot of $\ln k'$ versus pressure of o-xylene and cyclohexanol eluted by acetonitrile at 303 K on graphitized carbon column.

Table 14. Fitted parameters and calculated molar volume change.

compound	A	B	ΔV (cm ³ mol ⁻¹)
o-xylene	0.034±0.037	8.72E-4±1.44E-4	-21.97
cyclohexanol	-0.15±0.018	4.66E-4±7.11E-5	-11.75

$$B = \frac{-\Delta V}{RT} \quad 8.17$$

Thus,

$$-\Delta V = BRT \quad 8.18$$

The linear fitting parameters and the calculated molar volume change are tabulated in Table 14. The results show that obvious pressure effect can be observed on the graphitized carbon column. With the two probing compounds selected in this research, the calculated molar volume change of o-xylene at 303K on graphitized carbon column is -21.97cm³mol⁻¹, and that of cyclohexanol is -11.75 m³mol⁻¹.

8.4 Conclusion

Carbon based stationary phases have been closely examined by isotherm analysis. Graphitized carbon and electrochemically modified carbon are effective materials for HPLC applications. Glassy carbon is not a suitable candidate for stationary phase due to its microporosity. The micropores in glassy carbon can be blocked or eliminated by electrochemical modification or graphitization. The elimination of micropores confers superior chromatographic performance to the carbon material. Graphitized carbon has more homogeneous surface than electrochemically modified carbon. Although

electrochemical modification can efficiently block the micropores, the basal plane of the carbon cannot be fully covered by electrochemical modification. Thus, the modified carbon surface has two kinds of adsorption sites: the naked carbon and the covalently modified ligands. The population of the naked carbon is larger than the population of the ligands. In cases where the modified functionalities have strong adsorption to the adsorbate, for example, the modified amine ligand to the resorcinol, the minority ligands significantly affect to the isotherm. When the functionalities have only weak interaction with the adsorbate, the influence of the minority group is negligible, for example, the toluene eluted on the modified carbon.

The reproducibility of columns is evaluated with two batches of columns. Each batch has three columns. The experimental data shows that the synthesis of the modified carbon column is very reproducible.

The elevated pressure affects the retention factor of adsorbate. The retention factor of o-xylene and cyclohexanol increases with the increase in column pressure.

Several problems need to be solved. The first problem is that the graphitized carbon rods were seriously bent after the high temperature treatment. It is urgent to either find a suitable cladding method for the bent rods, or to prevent bending during graphitization. The surface coverage of the modified carbon surface is the second problem. The performance of the surface modified carbon column can be improved with more densely anchored ligands. The modification of graphitized carbon surface may be the future direction of investigation of carbon based monolithic columns.

Chapter 9: Conclusion

As Guiochon recently claimed, “The invention and development of monolithic columns is a major technological change in column technology, indeed the first original breakthrough to have occurred in this area since Tswett invented chromatography, a century ago.”²⁷ The monolithic column has been recognized as the fourth-generation stationary phase and been well-accepted by both the industrial and academic research communities. Although the research into monolithic columns began in the 1970s, the real success has been achieved only in the last decade. As a result of this success, the Merck Chromolith rod was commercialized in 2000. Since that time, the first commercially available silica monolithic column has greatly expanded the applications of monolithic columns. With such a short history, research into monolithic columns is still in its infancy. Because of the worldwide interest in this research, frequent new achievements have been made in this area. All these achievements have led to intriguing new opportunities for research. Nevertheless, much remains to be done to extend the monolith technique to all areas of traditional particulate columns. To replace the particulate columns with monolithic ones is a long-term and methodical process, which requires the efforts of numerous researchers. The present study is designed to further such research. The main achievements of the research are summarized as follows:

(1) Four novel column configurations have been designed for the purpose of evaluating the chromatographic performances of various monolithic materials. Each configuration is designed to solve problems associated with the encasing of the

monolithic materials. The first type of column configuration is the polymer-lined stainless steel encasing, which offers a versatile method for the evaluation of monolithic materials in a typical research laboratory of limited fabrication capabilities. The second type of column configuration is based on the glass-shrinking techniques that made it possible for researchers to visualize the HPLC column. The glass-encasing technique allows researchers to study the separation process by actually “seeing” the separation in a straightforward way. Due to time constraints and research conditions, we have not yet actually used the glass-encased column in a “real” separation. Nevertheless, this technique has paved the way for modeling the separation in monolithic columns. The third type of column configuration is the polymer encased column. The heat-sensitive materials can be converted to monolithic columns without the kind of heating process that is required by the popular heat-shrinking techniques. The last column configuration is the multicapillary-array monolithic column. This configuration fills the gap between standard-sized and capillary columns. For traditional columns, the microbore columns bridge the gap between standard-sized and capillary columns. Because of the shrinking and brittle nature of the monolithic column, it is impossible to make microbore silica monolithic columns. However, the multicapillary-array monolithic column has the potential to be the counterpart of the microbore particulate column.

(2) The gel-casting method has been introduced for the synthesis of silica monoliths. It is well known that the sizes of the mesopores and macropores are interrelated if the silica monolith has been made via the phase-separation procedure; that is, one cannot tailor the porosity of the mesopore without changing that of the

macropores, and vice versa. We have successfully separated the synthesis of the mesopore and the macropore into two independent procedures. Thus, the gel-casting method allows one to synthesize silica monoliths with independently tunable mesoporosity and macroporosity. Moreover, the silica monolith made by gel casting has more uniform pores than the one made by phase separation.

(3) Graphitized carbon has superior chemical and physical stability compared with silica. In practice, graphitized carbon columns have been widely used to solve the separation problems that are difficult to achieve using columns made of silica or polymers. In this research, we pioneered the synthesis of monolithic carbon columns. The carbon monolith was tailored by using silica microspheres as templates for the macropores. The mesopores result from the removal of the graphitization catalysts that are *in situ* produced iron particles. The research into catalyzed graphitization of carbon monoliths has illustrated the methodology of using colloids as templates for monolithic columns.

(4) The phase-separation method has been successfully applied to the synthesis of carbon monolithic columns. Based on the composition of the starting material, various pore sizes can be developed into the carbon monolith. The pore-forming agents are decomposable at the carbonization step. This method eliminates the removal of templates, which is regarded as a wasteful process. Carbon rods made by this method use inexpensive starting material and employ a simple process. Thus, the fabrication cost of the carbon monolith via phase separation is very low compared with that of carbon particulate columns. The mesopore is tailored using block copolymers as pore-forming

agents. Highly ordered uniform porous carbon materials are made via a solution-based procedure. The lengths of the chains contained in the block polymers strictly control the pore size. A solvent-annealing process further refines the regularity and uniformity. Herein, we developed the first methodology for the synthesis of ordered mesoporous carbon by using thermal-decomposable structure-directing agents. In this method, uniform carbon coating can be applied to any thermal-stable substrate. By coating the mesoporous carbon onto the carbon monolithic, we are able to control the macroporosity and mesoporosity on a case-specific basis.

(5) Electrochemically assisted modification of carbon surfaces has been applied to the grafting of functionalities onto the carbon monolithic column. The advantage of electrochemical modification is the self-limiting nature of the electrochemical reaction. The self-limiting growth of the surface modifier ensures the creation of a monolayer. Various functionalities can be grafted onto the carbon surface by using the para-substituted aryldiazonium salts. Theoretically, all kinds of functionalities can be grafted onto the carbon surface, creating the possibility of substituting carbon columns for silica columns in most applications by offering better hydrothermal and pH stabilities. The surface modification blocks the openings of the micropores on the glassy carbon surface, which ensures a good chromatographic performance of the monolithic column. Historically, because of the intrinsic micropores, glassy carbon has never been proven to be a good stationary phase. So far, graphitization is the only method that has been reported for the elimination of the micropores. In fact, graphitization is one of the major contributors to the high cost of the carbon stationary phase. Electrochemical modification

offers an alternative approach for the elimination of micropores and is much cheaper than graphitization. It is quite apparent that electrochemical-assisted surface modification of the carbon rod paves the way for using glassy carbon as a general material for monolithic columns.

In a summary, this research is devoted to the development of monolithic columns, the fourth generation of chromatographic columns. Our studies suggest that it is only a matter of time before the monolithic technique will be extended to every separation application and becomes competitive with traditional means.

References

References:

1. Skoog, D. A.; Holler, F. J.; Nieman, T. A., *Principles of instrumental analysis*. fifth edition ed.; Harcourt Brace & Company: 2001; 'Vol.' p.
2. Giddings, J. C., *Unified Separation Science*. ed.; 1991; 'Vol.' p 320 pp.
3. Majors, R. E., A review of HPLC column packing technology. *American Laboratory* **2003**, 35, (20), 46-+.
4. Svec, F., Porous monoliths: The newest generation of stationary phases for HPLC and related methods. *LC GC Eur.* **2003**, 16, (6A), 24-28.
5. Kele, M.; Guiochon, G., Repeatability and reproducibility of retention data and band profiles on six batches of monolithic columns. *J. Chromatogr. A* **2002**, 960, (1-2), 19-49.
6. Tallarek, U.; Leinweber, F. C.; Seidel-Morgenstern, A., Fluid dynamics in monolithic adsorbents: Phenomenological approach to equivalent particle dimensions. *Chem. Eng. Technol.* **2002**, 25, (12), 1177-1181.
7. Hansen, L. C.; Sievers, R. E., Highly Permeable Open-Pore Polyurethane Columns for Liquid-Chromatography. *Journal of Chromatography* **1974**, 99, (NOV6), 123-133.
8. Ross, W. D.; Jefferso, R. T., In-Situ-Formed Open-Pore Polyurethane as Chromatography Supports. *Journal of Chromatographic Science* **1970**, 8, (7), 386-&.
9. Hjerten, S.; Liao, J. L.; Zhang, R., High-Performance Liquid-Chromatography on Continuous Polymer Beds. *Journal of Chromatography* **1989**, 473, (1), 273-275.
10. Kumakura, M.; Kaetsu, I.; Asami, K.; Suzuki, S., Characteristics of Porous Polymer Composite Columns Prepared by Radiation Cast-Polymerization. *Journal of Materials Science* **1989**, 24, (5), 1809-1813.
11. Svec, F.; Frechet, J. M. J., Continuous Rods of Macroporous Polymer as High-Performance Liquid-Chromatography Separation Media. *Analytical Chemistry* **1992**, 64, (7), 820-822.
12. V. Pretorius, J. C. D., D.H. Desty, *JOURNAL OF HIGH RESOLUTION CHROMATOGRAPHY & CHROMATOGRAPHY COMMUNICATIONS* **1979**, 2, 583.
13. Nakanishi, K.; Soga, N., Phase-Separation in Gelling Silica Organic Polymer-Solution - Systems Containing Poly(Sodium Styrenesulfonate). *Journal of the American Ceramic Society* **1991**, 74, (10), 2518-2530.
14. Minakuchi, H.; Nakanishi, K.; Soga, N.; Ishizuka, N.; Tanaka, N., Octadecylsilylated porous silica rods as separation media for reversed-phase liquid chromatography. *Anal. Chem.* **1996**, 68, (19), 3498-3501.
15. Tanaka, N.; Kimura, H.; Tokuda, D.; Hosoya, K.; Ikegami, T.; Ishizuka, N.; Minakuchi, H.; Nakanishi, K.; Shintani, Y.; Furuno, M.; Cabrera, K., Simple and comprehensive two-dimensional reversed-phase HPLC using monolithic silica columns. *Anal. Chem.* **2004**, 76, (5), 1273-1281.
16. Tolstikov, V. V.; Lommen, A.; Nakanishi, K.; Tanaka, N.; Fiehn, O., Monolithic silica-based capillary reversed-phase liquid chromatography/electrospray mass spectrometry for plant metabolomics. *Anal. Chem.* **2003**, 75, (23), 6737-6740.

17. Tanaka, N.; Kobayashi, H.; Nakanishi, K.; Minakuchi, H.; Ishizuka, N., Monolithic LC columns. *Anal. Chem.* **2001**, 73, (15), 420A-429A.
18. Sun, X. F.; Chai, Z. K., Urea-formaldehyde resin monolith as a new packing material for affinity chromatography. *J. Chromatogr. A* **2002**, 943, (2), 209-218.
19. Kato, M.; Saruwatari, H.; Sakai-Kato, K.; Toyo'oka, T., Silica sol-gel/organic hybrid material for protein encapsulated column of capillary electrochromatography. *J. Chromatogr. A* **2004**, 1044, (1-2), 267-270.
20. Lubda, D.; Lindner, W., Monolithic silica columns with chemically bonded tert-butylcarbamoylquinine chiral anion-exchanger selector as a stationary phase for enantiomer separations. *J. Chromatogr. A* **2004**, 1036, (2), 135-143.
21. Chen, Z.; Nishiyama, T.; Uchiyama, K.; Hobo, T., Electrochromatographic enantioseparation using chiral ligand exchange monolithic sol-gel column. *Anal. Chim. Acta* **2004**, 501, (1), 17-23.
22. Liang, C. D.; Dai, S.; Guiochon, G., A graphitized-carbon monolithic column. *Anal. Chem.* **2003**, 75, (18), 4904-4912.
23. Harnisch, J. A.; Porter, M. D., Electrochemically modulated liquid chromatography: an electrochemical strategy for manipulating chromatographic retention. *Analyst* **2001**, 126, (11), 1841-1849.
24. Ting, E. Y.; Porter, M. D., Column design for electrochemically modulated liquid chromatography. *Anal. Chem.* **1998**, 70, (1), 94-99.
25. Ting, E. Y.; Porter, M. D., Separations of corticosteroids using electrochemically modulated liquid chromatography: Selectivity enhancements at a porous graphitic carbon stationary phase. *Anal. Chem.* **1997**, 69, (4), 675-678.
26. Deinhammer, R. S.; Porter, M. D.; Shimazu, K., Retention Characteristics Of Polypyrrole As A Stationary-Phase For The Electrochemically Modulated Liquid-Chromatographic (Emlc) Separations Of Dansyl Amino-Acids. *J. Electroanal. Chem.* **1995**, 387, (1-2), 35-46.
27. Al-Bokari, M.; Cherrak, D.; Guiochon, G., Determination of the porosities of monolithic columns by inverse size-exclusion chromatography. *J. Chromatogr. A* **2002**, 975, (2), 275-284.
28. Siouffi, A. M., Silica gel-based monoliths prepared by the sol-gel method: facts and figures. *Journal Of Chromatography A* **2003**, 1000, (1-2), 801-818.
29. Tanaka, N.; Nagayama, H.; Kobayashi, H.; Ikegami, T.; Hosoya, K.; Ishizuka, N.; Minakuchi, H.; Nakanishi, K.; Cabrera, K.; Lubda, D., Monolithic silica columns for HPLC, micro-HPLC, and CEC. *Hrc-Journal of High Resolution Chromatography* **2000**, 23, (1), 111-116.
30. Minakuchi, H.; Nakanishi, K.; Soga, N.; Ishizuka, N.; Tanaka, N., Octadecylsilylated porous silica rods as separation media for reversed-phase liquid chromatography. *Analytical Chemistry* **1996**, 68, (19), 3498-3501.
31. Wang, H. T.; Huang, L. M.; Wang, Z. B.; Mitra, A.; Yan, Y. S., Hierarchical zeolite structures with designed shape by gel-casting of colloidal nanocrystal suspensions. *Chemical Communications* **2001**, (15), 1364-1365.

32. Liang, C. D.; Dai, S.; Guiochon, G., Use of gel-casting to prepare HPLC monolithic silica columns with uniform mesopores and tunable macrochannels. *Chemical Communications* **2002**, (22), 2680-2681.
33. Kresge, C. T.; Leonowicz, M. E.; Roth, W. J.; Vartuli, J. C.; Beck, J. S., Ordered Mesoporous Molecular-Sieves Synthesized By A Liquid-Crystal Template Mechanism. *Nature* **1992**, 359, (6397), 710-712.
34. Inagaki, S.; Fukushima, Y.; Kuroda, K., Synthesis Of Highly Ordered Mesoporous Materials From A Layered Polysilicate. *Journal Of The Chemical Society-Chemical Communications* **1993**, (8), 680-682.
35. Yanagisawa, T.; Shimizu, T.; Kuroda, K.; Kato, C., The Preparation Of Alkyltrimethylammonium-Kanemite Complexes And Their Conversion To Microporous Materials. *Bulletin Of The Chemical Society Of Japan* **1990**, 63, (4), 988-992.
36. Tanev, P. T.; Pinnavaia, T. J., A Neutral Templating Route To Mesoporous Molecular-Sieves. *Science* **1995**, 267, (5199), 865-867.
37. Tanev, P. T.; Chibwe, M.; Pinnavaia, T. J., Titanium-Containing Mesoporous Molecular-Sieves For Catalytic-Oxidation Of Aromatic-Compounds. *Nature* **1994**, 368, (6469), 321-323.
38. Bagshaw, S. A.; Prouzet, E.; Pinnavaia, T. J., Templating Of Mesoporous Molecular-Sieves By Nonionic Polyethylene Oxide Surfactants. *Science* **1995**, 269, (5228), 1242-1244.
39. Zhao, D. Y.; Huo, Q. S.; Feng, J. L.; Chmelka, B. F.; Stucky, G. D., Nonionic triblock and star diblock copolymer and oligomeric surfactant syntheses of highly ordered, hydrothermally stable, mesoporous silica structures. *Journal Of The American Chemical Society* **1998**, 120, (24), 6024-6036.
40. Zhao, D. Y.; Feng, J. L.; Huo, Q. S.; Melosh, N.; Fredrickson, G. H.; Chmelka, B. F.; Stucky, G. D., Triblock copolymer syntheses of mesoporous silica with periodic 50 to 300 angstrom pores. *Science* **1998**, 279, (5350), 548-552.
41. Inagaki, S.; Ogata, S.; Goto, Y.; Fukushima, Y., Mesoporous materials derived from layered silicates and the adsorption properties. In *Mesoporous Molecular Sieves 1998*, ed.; 'Ed.'^'Eds.' 1998; 'Vol.' 117, p^pp 65-76.
42. Grun, M.; Unger, K. K.; Matsumoto, A.; Tsutsumi, K., Novel pathways for the preparation of mesoporous MCM-41 materials: control of porosity and morphology. *Microporous And Mesoporous Materials* **1999**, 27, (2-3), 207-216.
43. Buchel, G.; Grun, M.; Unger, K. K.; Matsumoto, A.; Tsutsumi, K., Tailored syntheses of nanostructured silicas: Control of particle morphology, particle size and pore size. *Supramolecular Science* **1998**, 5, (3-4), 253-259.
44. Gallis, K. W.; Araujo, J. T.; Duff, K. J.; Moore, J. G.; Landry, C. C., The use of mesoporous silica in liquid chromatography. *Advanced Materials* **1999**, 11, (17), 1452-1455.
45. Zhao, J. W.; Gao, F.; Fu, Y. L.; Jin, W.; Yang, P. Y.; Zhao, D. Y., Biomolecule separation using large pore mesoporous SBA-15 as a substrate in high performance liquid chromatography. *Chemical Communications* **2002**, (7), 752-753.
46. Zhao, D. Y.; Sun, J. Y.; Li, Q. Z.; Stucky, G. D., Morphological control of highly ordered mesoporous silica SBA-15. *Chemistry Of Materials* **2000**, 12, (2), 275-+.

47. Boissiere, C.; Kummel, M.; Persin, M.; Larbot, A.; Prouzet, E., Spherical MSU-1 mesoporous silica particles tuned for HPLC. *Advanced Functional Materials* **2001**, 11, (2), 129-135.
48. Knox, J. H., *personal communication* **1972**.
49. Miyabe, K.; Guiochon, G., The moment equations of chromatography for monolithic stationary phases. *Journal Of Physical Chemistry B* **2002**, 106, (34), 8898-8909.
50. Nakanishi, K.; Soga, N., Phase-Separation in Silica Sol-Gel System Containing Polyacrylic-Acid.1. Gel Formation Behavior and Effect of Solvent Composition. *Journal of Non-Crystalline Solids* **1992**, 139, (1), 1-13.
51. Melosh, N. A.; Davidson, P.; Feng, P.; Pine, D. J.; Chmelka, B. F., Macroscopic shear alignment of bulk transparent mesostructured silica. *Journal Of The American Chemical Society* **2001**, 123, (6), 1240-1241.
52. Feng, P. Y.; Bu, X. H.; Stucky, G. D.; Pine, D. J., Monolithic mesoporous silica templated by microemulsion liquid crystals. *Journal Of The American Chemical Society* **2000**, 122, (5), 994-995.
53. Nawrocki, J.; Dunlap, C.; McCormick, A.; Carr, P. W., Part I. Chromatography using ultra-stable metal oxide-based stationary phases for HPLC. *Journal Of Chromatography A* **2004**, 1028, (1), 1-30.
54. Colin, H.; Eon, C.; Guiochon, G., Reversed-Phase Liquid-Solid Chromatography on Modified Carbon-Black. *Journal of Chromatography* **1976**, 122, (JUL7), 223-242.
55. Colin, H.; Eon, C.; Guiochon, G., Modified Carbon-Black in High-Performance Liquid-Chromatography. *Journal of Chromatography* **1976**, 119, (APR28), 41-54.
56. Colin, H.; Guiochon, G., Development and Use of Carbon Adsorbents in High-Performance Liquid-Solid Chromatography.1. Carbon-Coated Silica Particles. *Journal of Chromatography* **1976**, 126, (NOV3), 43-62.
57. Colin, H.; Guiochon, G., Development and Use of Carbon Adsorbents in High-Performance Liquid-Solid Chromatography.2. Reproducibility of Carbon Adsorbents and Influence of Graphitization on Their Performance. *Journal of Chromatography* **1977**, 137, (1), 19-33.
58. Colin, H.; Guiochon, G., Deposit of Pyrocarbon on Carbon-Black. *Carbon* **1978**, 16, (2), 145-152.
59. Gilbert, M. T.; Knox, J. H.; Kaur, B., Porous Glassy-Carbon, A New Columns Packing Material For Gas-Chromatography And High-Performance Liquid-Chromatography. *Chromatographia* **1982**, 16, 138-148.
60. Knox, J. H.; Ross, P., Carbon-based packing materials for liquid chromatography - Structure, performance, and retention mechanisms. In *Advances in Chromatography*, Vol 37, ed.; 'Ed.'^'Eds.' 1997; 'Vol.' 37, p^pp 73-119.
61. Kriz, J.; Adamcova, E.; Knox, J. H.; Hora, J., Characterization of Adsorbents by High-Performance Liquid-Chromatography Using Aromatic-Hydrocarbons - Porous Graphite and Its Comparison with Silica-Gel, Alumina, Octadecylsilica and Phenylsilica. *Journal of Chromatography A* **1994**, 663, (2), 151-161.

62. Leboda, R.; Lodyga, A.; Charnas, B., Carbon adsorbents as materials for chromatography II. Liquid chromatography. *Materials Chemistry and Physics* **1998**, *55*, (1), 1-29.
63. Leboda, R.; Lodyga, A.; Gierak, A., Carbon adsorbents as materials for chromatography. I. Gas chromatography. *Materials Chemistry and Physics* **1997**, *51*, (3), 216-232.
64. Ross, P., The role of porous graphitic carbon in HPLC. *Lc Gc North America* **2000**, *18*, (1), 14-+.
65. Unger, K.; Roumeliotis, P.; Mueller, H.; Goetz, H., Novel Porous Carbon Packings in Reversed-Phase High-Performance Liquid-Chromatography. *Journal of Chromatography* **1980**, *202*, (1), 3-14.
66. Unger, K. K., Porous Carbon Packings for Liquid-Chromatography. *Analytical Chemistry* **1983**, *55*, (3), A361-&.
67. Schellinger, A. P.; Mao, Y.; Carr, P. W., Use of DRYLAB to compare octadecylsilane and carbon supports for reversed-phase chromatography of triazine herbicide test solutes. *Analytical And Bioanalytical Chemistry* **2002**, *373*, (7), 587-594.
68. Jackson, P. T.; Carr, P. W., Study of polar and nonpolar substituted benzenes and aromatic isomers on carbon-coated zirconia and alkyl bonded phases. *Journal Of Chromatography A* **2002**, *958*, (1-2), 121-129.
69. Knox, J. H.; Kaur, B.; Millward, G. R., Structure And Performance Of Porous Graphitic Carbon In Liquid-Chromatography. *Journal Of Chromatography* **1986**, *352*, 3-25.
70. Colin, H.; Guiochon, G.; Jandera, P., The Solvent Eluotropic Strength On Carbon Adsorbents. *Chromatographia* **1982**, *15*, (2), 133-139.
71. Ciccioli, P.; Tappa, R.; Dicorcia, A.; Liberti, A., Graphitized Carbon-Black Columns For High-Performance Liquid-Chromatography. *Journal Of Chromatography* **1981**, *206*, (1), 35-42.
72. Knox, J. H.; Gilbert, M. T., *U.K. patent 2,035,282* **1978**.
73. Taylor, R. E., *Thermal Expansion of Solids Volume I-4; ASM International: Ohio*, **1998**, Chapter 1.
74. Tuinstra, F.; Koenig, J. L., Raman Spectrum Of Graphite. *Journal Of Chemical Physics* **1970**, *53*, (3), 1126-&.
75. Diack, M.; Guiochon, G., Adsorption-Isotherms And Overloaded Elution Profiles Of Phenyl-N-Alkanes On Porous Carbon In Liquid-Chromatography. *Langmuir* **1992**, *8*, (6), 1587-1593.
76. Colin, H.; Guiochon, G.; Siouffi, A., Comparison Of Various Systems For The Separation Of Free Sterols By High-Performance Liquid-Chromatography. *Analytical Chemistry* **1979**, *51*, (11), 1661-1666.
77. Kiefer, J.; Hedrick, J. L.; Hilborn, J. G., Macroporous thermosets by chemically induced phase separation. In *Macromolecular Architectures*, ed.; 'Ed.'^'Eds.' 1999; 'Vol.' 147, p^pp 161-247.
78. Lal, J.; Bansil, R., Light-Scattering Study of Kinetics of Spinodal Decomposition in a Polymer-Solution. *Macromolecules* **1991**, *24*, (1), 290-297.

79. Aubert, J. H.; Clough, R. L., Low-Density, Microcellular Polystyrene Foams. *Polymer* **1985**, 26, (13), 2047-2054.
80. Fond, C.; Kiefer, J.; Mendels, D.; Ferrer, J. B.; Kausch, H. H.; Hilborn, J. G., Influence of voids on the stress distribution and deformation behaviour of epoxies under uniaxial deformation. *Journal Of Materials Science* **1998**, 33, (15), 3975-3984.
81. Kiefer, J.; Kausch, H. H.; Hilborn, J. G., Synthesis of solvent-modified epoxies via Chemically Induced Phase Separation: A new approach towards void toughening of epoxies. *Polymer Bulletin* **1997**, 38, (4), 477-483.
82. Kiefer, J.; Hilborn, J. G.; Hedrick, J. L., Chemically induced phase separation: A new technique for the synthesis of macroporous epoxy networks. *Polymer* **1996**, 37, (25), 5715-5725.
83. Kiefer, J.; Hilborn, J. G.; Manson, J. A. E.; Leterrier, Y.; Hedrick, J. L., Macroporous epoxy networks via chemically induced phase separation. *Macromolecules* **1996**, 29, (11), 4158-4160.
84. Pascault, J. P., Rubber-Modified And Thermoplastic-Modified Polymer Networks - Phase-Separation Process Induced By Polymerization And Polycondensation. *Macromolecular Symposia* **1995**, 93, 43-51.
85. Flory, J., *Principles of polymer chemistry* **1953**.
86. Flory, J., *J Chem Phys* **1942**, 10, 51.
87. Flory, P., *J Chem Phys* **1941**, 9, 660.
88. Huggins, M., *J Chem Phys* **1941**, 9, 660.
89. Huggins, M., *J Am Chem Soc* **1942**, 64, 1712.
90. Nakamoto, C.; Kitada, T.; Kato, E., Pressure dependence on the Flory-Huggins interaction parameter of poly(N-isopropylacrylamide) gels. *Polymer Gels And Networks* **1996**, 4, (1), 17-31.
91. Russell, T. P.; Hjelm, R. P.; Seeger, P. A., Temperature-Dependence Of The Interaction Parameter Of Polystyrene And Poly(Methyl Methacrylate). *Macromolecules* **1990**, 23, (3), 890-893.
92. Einaga, Y., Thermodynamics Of Polymer-Solutions And Mixtures. *Progress In Polymer Science* **1994**, 19, (1), 1-28.
93. Londono, J. D.; Wignall, G. D., The Flory-Huggins interaction parameter in blends of polystyrene and poly(p-methylstyrene) by small-angle neutron scattering. *Macromolecules* **1997**, 30, (13), 3821-3824.
94. AlSaigh, Z. Y., The characterization of polymer blends by inverse gas chromatography. *Trends In Polymer Science* **1997**, 5, (3), 97-102.
95. Williams, R. J. J.; Rozenberg, B. A.; Pascault, J. P., Reaction-induced phase separation in modified thermosetting polymers. In *Polymer Analysis - Polymer Physics*, ed.; 'Ed.'^'Eds.' 1997; 'Vol.' 128, p^pp 95-156.
96. Riccardi, C. C.; Borrajo, J.; Williams, R. J. J.; GirardReydet, E.; Sautereau, H.; Pascault, J. P., Thermodynamic analysis of the phase separation in polyetherimide-modified epoxies. *Journal Of Polymer Science Part B-Polymer Physics* **1996**, 34, (2), 349-356.

97. Borrajo, J.; Riccardi, C. C.; Williams, R. J. J.; Cao, Z. Q.; Pascault, J. P., Rubber-Modified Cyanate Esters - Thermodynamic Analysis Of Phase-Separation. *Polymer* **1995**, 36, (18), 3541-3547.
98. Riccardi, C. C.; Borrajo, J.; Williams, R. J. J., Thermodynamic Analysis Of Phase-Separation In Rubber-Modified Thermosetting Polymers - Influence Of The Reactive Polymer Polydispersity. *Polymer* **1994**, 35, (25), 5541-5550.
99. Verchere, D.; Pascault, J. P.; Sautereau, H.; Moschiar, S. M.; Riccardi, C. C.; Williams, R. J. J., Rubber-Modified Epoxies.2. Influence Of The Cure Schedule And Rubber Concentration On The Generated Morphology. *Journal Of Applied Polymer Science* **1991**, 42, (3), 701-716.
100. Moschiar, S. M.; Riccardi, C. C.; Williams, R. J. J.; Verchere, D.; Sautereau, H.; Pascault, J. P., Rubber-Modified Epoxies.3. Analysis Of Experimental Trends Through A Phase-Separation Model. *Journal Of Applied Polymer Science* **1991**, 42, (3), 717-735.
101. Munk, P.; Hattam, P.; Abdelazim, A. A. A.; Du, Q., Thermodynamics Of Miscible Polymer Blends Studied By Inverse Gas-Chromatography. *Makromolekulare Chemie-Macromolecular Symposia* **1990**, 38, 205-220.
102. Vazquez, A.; Rojas, A. J.; Adabbo, H. E.; Borrajo, J.; Williams, R. J. J., Rubber-Modified Thermosets - Prediction Of The Particle-Size Distribution Of Dispersed Domains. *Polymer* **1987**, 28, (7), 1156-1164.
103. Kyotani, T., Control of pore structure in carbon. *Carbon* **2000**, 38, (2), 269-286.
104. Tamon, H.; Ishizaka, H.; Araki, T.; Okazaki, M., Control of mesoporous structure of organic and carbon aerogels. *Carbon* **1998**, 36, (9), 1257-1262.
105. Tamon, H.; Ishizaka, H., Porous characterization of carbon aerogels. *Carbon* **1998**, 36, (9), 1397-1399.
106. Tamon, H.; Ishizaka, H.; Mikami, M.; Okazaki, M., Porous structure of organic and carbon aerogels synthesized by sol-gel polycondensation of resorcinol with formaldehyde. *Carbon* **1997**, 35, (6), 791-796.
107. Kim, T. W.; Park, I. S.; Ryoo, R., A synthetic route to ordered mesoporous carbon materials with graphitic pore walls. *Angewandte Chemie-International Edition* **2003**, 42, (36), 4375-4379.
108. Jun, S.; Choi, M.; Ryu, S.; Lee, H. Y.; Ryoo, R., Ordered mesoporous carbon molecular sieves with functionalized surfaces. In *Nanotechnology In Mesoporous Materials*, ed.; 'Ed.' 'Eds.' 2003; 'Vol.' 146, pp 37-40.
109. Choi, M.; Ryoo, R., Ordered nanoporous polymer-carbon composites. *Nature Materials* **2003**, 2, (7), 473-476.
110. Darmstadt, H.; Roy, C.; Kaliaguine, S.; Choi, S. J.; Ryoo, R., Surface chemistry of ordered mesoporous carbons. *Carbon* **2002**, 40, (14), 2673-2683.
111. Lee, J. S.; Joo, S. H.; Ryoo, R., Synthesis of mesoporous silicas of controlled pore wall thickness and their replication to ordered nanoporous carbons with various pore diameters. *Journal Of The American Chemical Society* **2002**, 124, (7), 1156-1157.
112. Joo, S. H.; Choi, S. J.; Oh, I.; Kwak, J.; Liu, Z.; Terasaki, O.; Ryoo, R., Ordered nanoporous arrays of carbon supporting high dispersions of platinum nanoparticles (vol 412, pg 169, 2001). *Nature* **2001**, 414, (6862), 470-470.

113. Jain, S.; Bates, F. S., On the origins of morphological complexity in block copolymer surfactants. *Science* **2003**, 300, (5618), 460-464.
114. Huang, E.; Rockford, L.; Russell, T. P.; Hawker, C. J., Nanodomain control in copolymer thin films. *Nature* **1998**, 395, (6704), 757-758.
115. Ruokolainen, J.; Mäkinen, R.; Torkkeli, M.; Mäkelä, T.; Serimaa, R.; ten Brinke, G.; Ikkala, O., Switching supramolecular polymeric materials with multiple length scales. *Science* **1998**, 280, (5363), 557-560.
116. Clay, R. T.; Cohen, R. E., Synthesis of metal nanoclusters within microphase-separated diblock copolymers: sodium carboxylate vs carboxylic acid functionalization. *Supramolecular Science* **1998**, 5, (1-2), 41-48.
117. Antonietti, M.; Wenz, E.; Bronstein, L.; Seregina, M., Synthesis and characterization of noble metal colloids in block copolymer micelles. *Advanced Materials* **1995**, 7, (12), 1000-&.
118. Pai, R. A.; Humayun, R.; Schulberg, M. T.; Sengupta, A.; Sun, J. N.; Watkins, J. J., Mesoporous silicates prepared using preorganized templates in supercritical fluids. *Science* **2004**, 303, (5657), 507-510.
119. Sidorenko, A.; Tokarev, I.; Minko, S.; Stamm, M., Ordered reactive nanomembranes/nanotemplates from thin films of block copolymer supramolecular assembly. *Journal Of The American Chemical Society* **2003**, 125, (40), 12211-12216.
120. Jeong, U. Y.; Ryu, D. Y.; Kim, J. K.; Kim, D. H.; Russell, T. P.; Hawker, C. J., Volume contractions induced by crosslinking: A novel route to nanoporous polymer films. *Advanced Materials* **2003**, 15, (15), 1247-+.
121. Feng, X.; Fryxell, G. E.; Wang, L. Q.; Kim, A. Y.; Liu, J.; Kemner, K. M., Functionalized monolayers on ordered mesoporous supports. *Science* **1997**, 276, (5314), 923-926.
122. Zhang, Z. T.; Dai, S., Preparation and characterization of novel inorganic-organic mesoscopic ordered composites with bridges formed by coordination compounds. *Journal Of The American Chemical Society* **2001**, 123, (37), 9204-9205.
123. Lu, Y. F.; Yang, Y.; Sellinger, A.; Lu, M. C.; Huang, J. M.; Fan, H. Y.; Haddad, R.; Lopez, G.; Burns, A. R.; Sasaki, D. Y.; Shelnutt, J.; Brinker, C. J., Self-assembly of mesoscopically ordered chromatic polydiacetylene/silica nanocomposites. *Nature* **2001**, 410, (6831), 913-917.
124. Kowalewski, T.; Tsarevsky, N. V.; Matyjaszewski, K., Nanostructured carbon arrays from block copolymers of polyacrylonitrile. *Journal Of The American Chemical Society* **2002**, 124, (36), 10632-10633.
125. Zakhidov, A. A.; Baughman, R. H.; Iqbal, Z.; Cui, C. X.; Khayrullin, I.; Dantas, S. O.; Marti, I.; Ralchenko, V. G., Carbon structures with three-dimensional periodicity at optical wavelengths. *Science* **1998**, 282, (5390), 897-901.
126. Ikkala, O.; Ruokolainen, J.; Tenbrinke, G.; Torkkeli, M.; Serimaa, R., Mesomorphic State Of Poly(Vinylpyridine)-Dodecylbenzenesulfonic Acid Complexes In Bulk And In Xylene Solution. *Macromolecules* **1995**, 28, (21), 7088-7094.
127. Kim, S. H.; Misner, M. J.; Xu, T.; Kimura, M.; Russell, T. P., Highly oriented and ordered arrays from block copolymers via solvent evaporation. *Advanced Materials* **2004**, 16, (3), 226-+.

128. Majors, R. E., A review of HPLC column packing technology. *Am. Lab.* **2003**, 35, (20), 46-+.
129. Knox, J. H.; Wan, Q. H., Surface modification of porous graphite for ion exchange chromatography. *Chromatographia* **1996**, 42, (1-2), 83-88.
130. Nagashima, H.; Okamoto, T., Determination of inorganic anions by ion chromatography using a graphitized carbon column dynamically coated with cetyltrimethylammonium ions. *Journal Of Chromatography A* **1999**, 855, (1), 261-266.
131. O'Connell, M. P.; Treacy, J.; Merly, C.; Smith, C. M. M.; Glennon, J. D., Selective preconcentration and ion chromatography of trace lead(II) in environmental samples using a porous graphitic carbon column. *Analytical Letters* **1999**, 32, (1), 185-192.
132. Gray, M.; Dennis, G. R.; Wormell, P.; Shalliker, R. A.; Slonecker, P., Two dimensional reversed-phase-reversed-phase separations - Isomeric separations incorporating C-18 and carbon clad zirconia stationary phases. *Journal of Chromatography A* **2002**, 975, (2), 285-297.
133. Harnisch, J. A.; Gazda, D. B.; Anderegg, J. W.; Porter, M. D., Chemical modification of carbonaceous stationary phases by the reduction of diazonium salts. *Analytical Chemistry* **2001**, 73, (16), 3954-3959.
134. Antoniadou, S.; Jannakoudakis, A. D.; Jannakoudakis, P. D.; Theodoridou, E., Anion-Exchange Activity of Electrochemically Bonded Ethylene Diamine on Carbon-Fibers. *Journal of Applied Electrochemistry* **1992**, 22, (11), 1060-1064.
135. Barbier, B.; Pinson, J.; Desarmot, G.; Sanchez, M., Electrochemical Bonding of Amines to Carbon-Fiber Surfaces toward Improved Carbon-Epoxy Composites. *Journal of the Electrochemical Society* **1990**, 137, (6), 1757-1764.
136. Deinhammer, R. S.; Ho, M.; Anderegg, J. W.; Porter, M. D., Electrochemical Oxidation of Amine-Containing Compounds - a Route to the Surface Modification of Glassy-Carbon Electrodes. *Langmuir* **1994**, 10, (4), 1306-1313.
137. Hoekstra, K. J.; Bein, T., Adsorption of zirconium-phosphonate multilayers onto phosphate-derivatized glassy carbon substrates. *Chemistry of Materials* **1996**, 8, (8), 1865-1870.
138. Maeda, H.; Itami, M.; Yamauchi, Y.; Ohmori, H., Surface characterization of glassy carbon electrodes anodized in 1-alkanols by their wettability and capacitance. *Chemical & Pharmaceutical Bulletin* **1996**, 44, (12), 2294-2299.
139. Maeda, H.; Hosoe, M.; Li, T. X.; Itami, M.; Yamauchi, Y.; Ohmori, H., Indirect detection of alkaline earth ions by the voltammetric response of ferricyanide anion at a glassy carbon electrode anodized in 1-octanol. *Chemical & Pharmaceutical Bulletin* **1996**, 44, (3), 559-564.
140. Maeda, H.; Yamauchi, Y.; Hosoe, M.; Li, T. X.; Yamaguchi, E.; Kasamatsu, M.; Ohmori, H., Direct Covalent Modification of Glassy-Carbon Surfaces with 1-Alkanols by Electrochemical Oxidation. *Chemical & Pharmaceutical Bulletin* **1994**, 42, (9), 1870-1873.
141. Andrieux, C. P.; Gonzalez, F.; Saveant, J. M., Derivatization of carbon surfaces by anodic oxidation of arylacetates. Electrochemical manipulation of the grafted films. *Journal of the American Chemical Society* **1997**, 119, (18), 4292-4300.

142. Delamar, M.; Hitmi, R.; Pinson, J.; Saveant, J. M., Covalent Modification of Carbon Surfaces by Grafting of Functionalized Aryl Radicals Produced from Electrochemical Reduction of Diazonium Salts. *Journal of the American Chemical Society* **1992**, 114, (14), 5883-5884.
143. Allongue, P.; Delamar, M.; Desbat, B.; Fagebaume, O.; Hitmi, R.; Pinson, J.; Saveant, J. M., Covalent modification of carbon surfaces by aryl radicals generated from the electrochemical reduction of diazonium salts. *Journal of the American Chemical Society* **1997**, 119, (1), 201-207.
144. Sykora, D.; Svec, F.; Frechet, J. M. J., Separation of oligonucleotides on novel monolithic columns with ion-exchange functional surfaces. *Journal Of Chromatography A* **1999**, 852, (1), 297-304.
145. Tennikov, M. B.; Gazdina, N. V.; Tennikova, T. B.; Svec, F., Effect of porous structure of macroporous polymer supports on resolution in high-performance membrane chromatography of proteins. *Journal Of Chromatography A* **1998**, 798, (1-2), 55-64.
146. Svec, F.; Frechet, J. M. J., Modified Poly(Glycidyl Methacrylate-Co-Ethylene Dimethacrylate) Continuous Rod Columns For Preparative-Scale Ion-Exchange Chromatography Of Proteins. *Journal Of Chromatography A* **1995**, 702, (1-2), 89-95.
147. Cavazzini, A.; Bardin, G.; Kaczmariski, K.; Szabelski, P.; Al-Bokari, M.; Guiochon, G., Adsorption equilibria of butyl- and amylbenzene on monolithic silica-based columns. *Journal Of Chromatography A* **2002**, 957, (2), 111-126.
148. Zhou, D. M.; Kaczmariski, K.; Guiochon, G., Comparison of the binary equilibrium isotherms of the 1-indanol enantiomers on three high-performance liquid chromatography columns of different sizes. *Journal Of Chromatography A* **2003**, 1015, (1-2), 73-87.
149. Szabelski, P.; Cavazzini, A.; Kaczmariski, K.; Liu, X.; Van Horn, J.; Guiochon, G., Experimental studies of pressure/temperature dependence of protein adsorption equilibrium in reversed-phase high-performance liquid chromatography. *Journal Of Chromatography A* **2002**, 950, (1-2), 41-53.
150. Evans, C. E.; Davis, J. A., Effect of pressure-induced ionization, partitioning, and complexation on solute retention in reversed-phase liquid chromatography. *Analytica Chimica Acta* **1999**, 397, (1-3), 163-172.
151. Evans, C. E.; Ringo, M. C.; Ponton, L. M., Pressure as a unifying parameter in chromatographic retention. In *Unified Chromatography*, ed.; 'Ed.'^'Eds.' 2000; 'Vol.' 748, p^pp 30-36.
152. Felinger, A.; Boros, B.; Ohmacht, R., Effect of pressure on retention factors in HPLC using a non-porous stationary phase. *Chromatographia* **2002**, 56, S61-S64.
153. Guiochon, G.; Sepaniak, M. J., Influence Of Pressure On Solute Retention In Liquid-Chromatography. *Journal Of Chromatography* **1992**, 606, (2), 248-250.
154. Hoenigman, S. M.; Evans, C. E., Pressure-induced perturbation in local solvation: Impact on inclusion complexation. *Abstracts Of Papers Of The American Chemical Society* **1997**, 213, 128-COLL.
155. McGuffin, V. L.; Evans, C. E., Influence Of Pressure On Solute Retention In Liquid-Chromatography. *Journal Of Microcolumn Separations* **1991**, 3, (6), 513-520.

156. Ponton, L. M.; Hoenigman, S. M.; Cai, M.; Evans, C. E., Liquid chromatographic separations with mobile phase additives: Influence of pressure on coupled equilibria. *Analytical Chemistry* **2000**, 72, (15), 3581-3589.
157. Ringo, M. C.; Evans, C. E., Pressure-dependent retention and selectivity in reversed-phase liquid chromatographic separations using beta-cyclodextrin stationary phases. *Analytical Chemistry* **1997**, 69, (4), 643-649.
158. Ringo, M. C.; Evans, C. E., Pressure-induced changes in chiral separations in liquid chromatography. *Analytical Chemistry* **1997**, 69, (24), 4964-4971.
159. Ringo, M. C.; Evans, C. E., Effect of mobile-phase composition on pressure-induced shifts in solute retention for LC separations using beta-cyclodextrin stationary phases. *Journal Of Microcolumn Separations* **1998**, 10, (8), 647-652.
160. Szabelski, P.; Cavazzini, A.; Kaczmarek, K.; Van Horn, J.; Guiochon, G., True and apparent temperature dependence of protein adsorption equilibrium in reversed-phase HPLC. *Biotechnology Progress* **2002**, 18, (6), 1306-1317.
161. Kele, M.; Guiochon, G., Repeatability and reproducibility of retention data and band profiles on reversed-phase liquid chromatography columns III. Results obtained with Kromasil C-18 columns. *Journal Of Chromatography A* **1999**, 855, (2), 423-453.
162. Kele, M.; Guiochon, G., Repeatability and reproducibility of retention data and band profiles on reversed-phase liquid chromatography columns I. Experimental protocol. *Journal Of Chromatography A* **1999**, 830, (1), 41-54.
163. Kele, M.; Guiochon, G., Repeatability and reproducibility of retention data and band profiles on reversed-phase liquid chromatography columns - IV. Results obtained with luna C-18 (2) columns. *Journal Of Chromatography A* **2000**, 869, (1-2), 181-209.
164. Kele, M.; Guiochon, G., Repeatability and reproducibility of retention data and band profiles on reversed-phase liquid chromatography columns V. Results obtained with Vydac 218TP C-18 columns. *Journal Of Chromatography A* **2001**, 913, (1-2), 89-112.
165. Kele, M.; Guiochon, G., Repeatability and reproducibility of retention data and band profiles on six batches of monolithic columns. *Journal Of Chromatography A* **2002**, 960, (1-2), 19-49.
166. Felinger, A.; Kele, M.; Guiochon, G., Identification of the factors that influence the reproducibility of chromatographic retention data. *Journal Of Chromatography A* **2001**, 913, (1-2), 23-48.
167. Diack, M.; Guiochon, G., Adsorption-Isotherm And Overloaded Elution Profiles Of Phenyldecane On Porous Carbon In Liquid-Chromatography. *Analytical Chemistry* **1991**, 63, (22), 2608-2613.
168. Dose, E. V.; Jacobson, S.; Guiochon, G., Determination Of Isotherms From Chromatographic Peak Shapes. *Analytical Chemistry* **1991**, 63, (8), 833-839.
169. G. Guiochon, S. G. S., A. Katti, *Fundamentals of Preparative and Nonlinear Chromatography*. ed.; Academic Press, Boston, MA: 1994; 'Vol.' p.
170. Qin, Y. J.; Shi, J. H.; Wu, W.; Li, X. L.; Guo, Z. X.; Zhu, D. B., Concise route to functionalized carbon nanotubes. *Journal Of Physical Chemistry B* **2003**, 107, (47), 12899-12901.

171. McGuffin, V. L.; Chen, S. H., Theoretical and experimental studies of the effect of pressure on solute retention in liquid chromatography. *Analytical Chemistry* **1997**, 69, (5), 930-943.

Vita

Chengdu Liang was born in China in Dec 1973. He grew up in Hunan province China and got his high school diploma from Lianyuan first high school in 1991. He went to Xiangtan University and spent 7 years there for his BS and MS in organic chemistry. He made his first attempt for a PhD degree during 1998 to 2000 at Hunan University China. In the year 2000, he moved to the United States as a visiting scholar, and worked at the University of Tennessee Knoxville and Oak Ridge National Laboratory before he finished his PhD program. In fall 2001 he was enrolled by the department of chemistry at the University of Tennessee Knoxville and resumed his PhD study under the supervision of Dr Georges Guiochon and Dr Sheng Dai. In May 2005, he completed the requirement of PhD degree in chemistry.